Investigation and Design of a New Ankle Rehabilitation System Based on Soft Robotics to Assist Children with Physical Disabilities.

Alberto Gonzalez Vazquez

School of Engineering, Computer and Mathematical Science

A thesis submitted to AUT University
in fulfilment of the requirements for the degree of
Doctor of Philosophy

2024

Supervisors: Dr. Lorenzo Garcia and Dr. Jeff Kilby

Abstract

Ongoing paediatric physical disabilities can result from various causes, including neurological conditions like Cerebral Palsy (CP), strokes, Acquired Brain Injuries (ABI), neuromuscular diseases such as Duchenne Muscular Dystrophy (DMD) and Spinal Muscular Atrophy (SMA), as well as traumatic injuries. Children with physical disabilities often face limitations in performing Activities of Daily Living (ADL) independently, which can impede their typical development. Mobility and exploration are crucial aspects of a child's development, contributing to cognitive, physical, social, and emotional growth.

Rehabilitation plays a vital role in assisting these children in recovering or maintaining functionality, enabling them to interact with their environment, and ultimately improving their quality of life and autonomy. Rehabilitation exoskeletons have gained significant attention for their potential to address mobility challenges in individuals with physical disabilities. They offer advantages such as enabling extensive practice for children with substantial disabilities, reducing the effort required from therapists during exercises, and providing a quantitative assessment of the patient's motor function.

However, most existing rehabilitation exoskeletons rely on electric motors and rigid components for their functionality. Unfortunately, these designs are often cumbersome, heavy, and unsuitable for use outside clinical facilities. To overcome these limitations, researchers in this field are now focusing on the development of Soft Wearable Rehabilitation Robots (SWRRs) that incorporate artificial muscles based on smart materials (AMSMs). AMSM, provide increased compliance, adaptability, comfort, safety, and reduced weight—critical characteristics for SWRRs.

One noteworthy type of AMSM is the Twisted and Coiled Polymer actuator (TCP). TCPs are created by twisting precursor polymer fibres and applying heat treatment. To activate TCPs, an external heat source, such as metallic wires, is employed to induce joule heating, thereby enabling precise electrical control. TCPs offer several advantages, including high-power density, stress tolerance, strain capacity, and linear behaviour with minimal hysteresis. However, they do face certain limitations, such as low operating frequencies and high operating temperatures.

The focus of this thesis is to investigate the feasibility of using TCPs as artificial muscles to power SWRRs designed for children with muscular dystrophy. The research consists of several key components: literature review on paediatric rehabilitation robots design needs and on the biomechanical requirements for SWRR using AMSM. A

characterisation of TCPs with Nichrome wire. A novel approach to enhance the temperature control and working frequency of TCPs is implemented using a Proportional-Integral-Derivative controller applied to long actuators. Finally, a preliminary prototype of a paediatric ankle SWRR based on TCPs was designed and tested on a dummy resembling the leg of a 10-year-old child. The prototype demonstrates the capability to provide a maximum Range of Motion (ROM) of 26° in the plantarflexion direction within 5 seconds, generating a torque of 1 Nm. However, the final frequency of the system was affected by the low response on the cooling phase.

In summary, this thesis research explores the potential of TCPs as artificial muscles to power SWRRs for children with muscular dystrophy. The findings highlight the importance of developing strategies to address cooling phase limitations and further advance the development of effective and efficient rehabilitation technology for paediatric populations.

Contents

List of Figures

List of Tables

Attestation of Authorship

I affirm that the content presented in this submission is entirely my original work. To the best of my knowledge and belief, it does not include any material previously published or authored by another person (except as explicitly acknowledged), nor has a significant portion of it been submitted for the attainment of any other degree or diploma from a university or other institution of higher learning.

.....

Alberto Gonzalez Vazquez

Publications Arising from Doctoral Thesis

Peer-reviewed journal publications and author contributions

Gonzalez-Vazquez, A., Garcia, L., Kilby, J., McNair, P. (2021). Robotic Devices for Paediatric Rehabilitation: A Review of Design Features. Biomedical Engineering Online. DOI: 10.1186/s12938-021-00920-5.

Gonzalez-Vazquez, A., Garcia, L., Kilby, J., McNair, P. (2023). Soft Wearable Rehabilitation Robots with Artificial Muscles based on Smart Materials: A Review. Advance Intelligent Systems. DOI: 10.1002/aisy.202200159.

Gonzalez-Vazquez, A., Garcia, L., Kilby, J. (2023). Improved Performance in Temperature and Speed of TCP Artificial Muscles for Soft Wearables Robots by Length Modification. Smart Materials and Structures. DOI: 10.1088/1361-665x/acded6.

Gonzalez-Vazquez, A., Garcia, L., Kilby, J. (2024). Paediatric Ankle Rehabilitation System based on Twisted and Coiled Polymer Actuators. Smart Materials and Structures. DOI: 10.1088/1361-665X/ad50b0.

Peer-reviewed conferences publications and author contributions

Gonzalez-Vazquez, A., Garcia, L., Kilby, J., Singh, H. (2021). Artificial Muscles Performance based on TCP-NiCr Actuators. 2021 43rd Annual International Conference of the IEEE Engineering in Medicine & Biology Society (EMBC) Oct 31 - Nov 4, 2021. Virtual Conference. http://paperhost.org/proceedings/embs/EMBC21/files/2261.pdf

Co-authors Contribution

As Co-author, I hereby approved and declare that my role in this study and percentage of contribution, as indicated below, is representative of my actual contribution and I hereby give my consent that this work may be published as part of this PhD thesis.

Chapter 2: Robotic Devices for Paediatric Rehabilitation: A Review of Design Features

Author	Contribution	Percentage	Signature
A.G.V.	Concept and design of the study Data Analysis and interpretation Writing	80%	
L.G.	Concept and design of the study Reviewing and editing	10%	
J.K.	Concept and design of the study Reviewing and editing	5%	
P.M.	Reviewing and editing	5%	

Chapter 3: Soft Wearable Rehabilitation Robots with Artificial Muscles based on Smart Materials: A Review

Author	Contribution	Percentage	Signature
A.G.V.	Concept and design of the study Data Analysis and interpretation Writing	80%	
L.G.	Concept and design of the study Reviewing and editing	10%	
J.K.	Concept and design of the study Reviewing and editing	5%	
P.M.	Reviewing and editing	5%	

Chapter 4: Artificial Muscles Performance based on TCP-NiCr Actuators

Author.	Contribution	Percentage	Signature
A.G.V.	Concept and design of the study Data collection Data Analysis and interpretation Writing	80%	
L.G.	Concept and design of the study Reviewing and editing	10%	
J.K.	Concept and design of the study Reviewing and editing	7%	
H.S.	Data collection	3%	

Chapter 5: Improved Performance in Temperature and Speed of TCP Artificial Muscles for Soft Wearables Robots by Length Modification

Author	Contribution	Percentage	Signature
A.G.V.	Concept and design of the study Data collection Data Analysis and interpretation Writing	80%	
L.G.	Concept and design of the study Reviewing and editing	10%	
J.K.	Concept and design of the study Reviewing and editing	10%	

Chapter 6: Paediatric Ankle Rehabilitation System based on Twisted and Coiled Polymer Actuators

Author	Contribution	Percentage	Signature
A.G.V.	Concept and design of the study Data collection Data Analysis and interpretation Writing	80%	
L.G.	Concept and design of the study Reviewing and editing	10%	
J.K.	Concept and design of the study Reviewing and editing	10%	

List of Abbreviations

Abbreviation	Definition
ABI	Acquired Brain Injury
AC	Alternate Current
ADL	Activities of Daily Living
AM	Artificial Muscles
AMSM	Artificial Muscles Based on Smart Materials
ASO	Active Soft Orthotic
CAD	Computer Aided Design
CB	Crus Brace
CP	Cerebral Palsy
DC	Direct Current
DEA	Dielectric Elastomer Actuators
DIP	Distal Interphalangeal
DMD	Duchenne Muscular Dystrophy
DOF	Degrees Of Freedom
EAPs	Electroactive Polymers
EEG	Electroencephalogram
EMG	Electromyogram
EMGe	Electromyogram envelope
FDA	US Food and Drug Administration
FIB	Foot Instep Brace
HASEL	Hydraulically Amplified Self-Healing Electrostatic
HCI	Human Computer Interface
IMU	Inertial Measurement Unit
IPMC	Ionic Polymer-Metal Composites
LLDPE	Low Density Polyethene
MCP	Metacarpophalangeal
NiCr	Nickel Chromium
np	Number of Papers
PID	Proportional-Integral-Derivative
PIP	Proximal Interphalangeal
PRISMA	Preferred Reporting Items for Systematic Reviews and Meta-Analyses
PVC	Polyvinyl Chloride Gel
PWM	Pulse Width Modulation
ROM	Range of Motion
SBH	Sigmoid-Based Hysteresis
SCI	Spinal Cord Injury
SEA	Serial Elastic Actuators
sEMG	Surface Electromyogram
SMA (used in Chapter 2)	Spinal Muscular Atrophy
SMA	Shape Memory Alloy
SMP	Shape Memory Polymers
SWRR	Soft Wearables Rehabilitation Robots
TCP	Twisted and Coiled Polymer
TRA	Thermally Responsive Actuator
WHO	World Health Organization
WRR	Wearables Rehabilitation Robots

Acknowledgements

I am profoundly grateful to my supervisors, Dr. Lorenzo and Dr. Jeff Kilby. Not only for guiding me during this challenging journey called PhD but also for all the support they provide me that goes beyond the academic aspect but also as tutors and friends. They always assisted not only in ensuring the project was going in the right direction but also in making sure as a student, I had the necessities to finish the project.

My heartfelt appreciation goes to my co-author, Professor Peter MacNair, for the feedback and effort in publishing two articles in top journals.

I'm proud to be part of a group on Biodesign Lab where everyone was supportive and friendly, making it more manageable. The discussion on different topics enriches my thesis and career—thanks to Associate Professor David White, Nick van der Geest and Harsimran Singh.

Inside AUT, I need to thank the people on Theralab, Dr. Micheal Gschwendtner, Zindh and Danielle. They have been there since I started this trip. Without your constant distraction, this journey would have been less enjoyable.

Football is an essential part of my life; it helps me through the way to never feel lost in this foreign country that opens the doors to me. All my teammates on Captain Morgan and Ambers Herd, thanks for all the football evenings, especially the aftermath of the match, regardless of whether we lost or won.

I'm grateful to Conacyt for the economic support during the four years of the PhD; this project would not be possible without their support.

Para finalizar a mi familia. A mis padres Horacio y María que siempre creyeron en mi desde un principio y que sin su apoyo incondicional no estaría en donde estoy. Gracias infinitas. A mi hermano Horacio por siempre estar disponible para una platicadita de los temas más random que encontráramos a pesar de la distancia y del trabajo.

GRACIAS A TODOS =)

Chapter 1 : Introduction

1.1 Context

Paediatric physical disabilities can result from various causes, including neurological conditions like Cerebral Palsy (CP) [1], Strokes [2], Acquire Brain Injuries (ABI) [3], neuromuscular diseases such as Duchenne Muscular Dystrophy (DMD) [4] and Spinal Muscular Atrophy [5], as well as traumatic injuries [6]. Children affected by this condition suffer from musculoskeletal problems such as contracture, bony deformities and muscle weakness [7, 8]. These deteriorations lead to limitation of the children to perform activities autonomously hindering their cognitive, physical, social and emotional development [8, 9].

Rehabilitation plays a pivotal role in aiding children's recovery or maintaining functionality, enhancing their quality of life and autonomy. Timely access to rehabilitation is particularly critical during the developmental stage, where gait patterns and motor abilities are still flexible, aiming to mitigate the risk of escalating disability [10]. Additionally, initiating therapies before the onset of symptoms proves most effective [9]. Common approaches for managing the deterioration of the musculoskeletal system and enhancing physical ability involve passive orthoses, surgical interventions, and physiotherapy [11, 12].

Physiotherapists play a crucial role in the management of physiotherapy, taking charge of prescribing, monitoring, and guiding exercises for children with physical disabilities. This approach aims to prevent a sedentary or immobile lifestyle. The extensively researched aspect of physiotherapy involves direct interventions, such as intensive stretching and strengthening exercises for upper or lower limb motor skills, facilitated by physiotherapists [8]. However, these interventions are often labour-intensive, pose safety concerns, or are challenging to execute [13].

Conventional physiotherapy's effectiveness relies heavily on the experience of the physiotherapist, making it difficult to meet the demands of high-intensity and repetitive training. Achieving optimal consistency and repeatability between rehabilitation sessions becomes challenging [14, 15]. To address these issues, there is a growing interest in rehabilitation robots for use in the rehabilitation process [16, 17]. These robots serve two primary purposes: assisting disabled individuals in their Activities of Daily Living (ADLs) and aiding them in rehabilitation therapy exercises [18, 19].

The introduction of robot-assisted rehabilitation therapy presents a novel strategy for addressing the rehabilitation needs of children with neuromuscular diseases [20].This approach involves the utilization of mechatronic devices that autonomously facilitate highly repetitive and task-specific guided movements [21, 22]. The integration of robots into rehabilitation therapies offers distinct advantages compared to traditional methods, including enabling massed practice for children with substantial limitations, reducing the effort required by therapists during exercises, and providing valuable patient information for enhanced diagnosis [23-25] .

Assisted-rehabilitation robots can be categorized based on the treated physiological part of the body or their mechanical structure type. Physiological classification typically divides robots into upper and lower limbs [23, 26], with further specificity depending on the affected part, such as hands [18] in the upper limb or ankles [14] in the lower limb.

Mechanical structure classification categorizes robots as end-effectors and exoskeletons [19, 27]. End-effector devices apply forces to the distal segments of limbs, creating a mechanical chain that induces movements in other parts of the limb to generate a specific activity pattern. While their simple structure facilitates adaptation to various patients and uses less complicated control algorithms, they produce complex movements involving the entire limb, making it challenging to target specific body parts[28].

In contrast, robotic exoskeletons are wearable machines that replicate the patient's skeletal structure, moving only the joint where the exoskeleton is worn. This design allows for independent and concurrent control of specific segments of the limb. However, adjusting the robot's sections to match the lengths of the patient's limb segments is essential. Additionally, changes in the centre of rotation during joint motion can cause user discomfort. The complexity of control algorithms also increases with the number of Degrees Of Freedom (DOF) in the robot [29].

While numerous robotic rehabilitation devices for upper and lower limbs have been developed, often reaching a proof-of-concept stage, a notable limitation is that the majority of these robots are designed with adult users in mind [30, 31] . This design focus impedes their applicability to the paediatric population since the robots do not fulfil their needs [32, 33]. Commercially available exoskeletons, for instance, are typically tailored for individuals 150 cm tall and above [34], making them unsuitable for the average 5-year-old child, whose height is around 110 cm [35]. This mismatch in design poses a significant challenge when considering the specific needs and dimensions of paediatric users in the development of robotic rehabilitation technologies.

Furthermore, most current exoskeletons use electric motors and rigid links to perform actuation and often have heavy and bulky designs that are difficult to safely wear outside clinical facilities and can harm the children's weak muscles [20]. Hence, researchers in this area are working to develop Soft Wearable Rehabilitation Robots (SWRRs), featuring soft actuators that are agreeable to the users as they have increased compliance, adaptability, comfort, safety, and less weight[36].

Current SWRRs predominantly rely on cable-driven and fluidic actuators, each with its drawbacks. In cable-driven systems, wires embedded into clothing or tubes are connected to electric motors, requiring external components that compromise portability [33, 37]. On the other hand, fluidic actuation (Hydraulic/Pneumatic) utilizes pressurized fluids, necessitating bulky external pumps and valves [38-40].

Hence, recent research addresses these challenges by exploring new actuator technologies for SWRRs, particularly Artificial Muscles based on Smart Materials (AMSMs). AMSMs are soft actuators with a low Young's modulus, resembling biological tissues (10^4–10^9 Pa), capable of converting various physical stimuli (e.g., light, electricity, heat) into displacement [41-45]. AMSMs, due to their inherent properties, can be shaped and integrated into flexible wearable devices, allowing for lightweight and compact robotic systems with power densities comparable to skeletal muscles [46-50]. This innovative approach aims to enhance the functionality and portability of SWRRs for improved integration into daily life.

In AMSMs for SWRR we can find two main categories, Electroactive Polymers (EAPs) and Thermally Responsive Actuator (TRA). EAPs are polymers that under an electric stimulus can generate mechanical energy. Examples of EAPs are Dielectric Elastomer Actuators (DEAs) [51], Ionic Polymer–Metal Composites (IPMC) [52], and Polyvinyl Chloride (PVC) gels [53]. In the case of TRA the mechanical energy comes after a thermal stimulus is applied. Examples of TRA include Shape-Memory Alloy (SMA) [54], Shape Memory Polymers (SMPs) [55], and Twisted and Coiled Polymer Actuators (TCPs) [56]. Nevertheless, AMSMs for rehabilitation robots are still at the early stage of development. Some drawbacks specific to every smart material (e.g., low speed in TRA and low force generation in EAPs) need to be tackled if they are to become widespread technology utilized in SWRR.

TCPs are Artificial Muscles (AMs) fabricated by inserting a twist in precursor polymer fibre while attaching a dead weight at the end until it forms a coil structure, followed by heat treatment [56]. Activation of TCPs involves applying an external heat source, often through joule heating via metallic wires like Nichrome wires, offering electrical

controllability [57, 58]. In comparison to other AMs, TCPs standout due to their high power density (27 W g−1), high stress (10 MPa), large strain (21%), and linear behaviour with low hysteresis [50]. Nevertheless, they suffer from low frequencies (<1 Hz) and high temperatures (> 100 °C) [50, 59, 60].

In SWRR applications, fulfilling biomechanical requirements such as torque, Range of Motion (ROM), and velocity/frequency is crucial. TCPs actuators have garnered attention in SWRRs due to their ability to provide high forces and strains relevant to torque and ROM. However, there is a need for overall performance improvements as they are not yet optimal for SWRR applications. The primary drawbacks include a frequency response lower than that required for ADLs (< 1 Hz) [61] and working temperatures, with discomfort threshold for humans starting at 65 °C [60]. Addressing these limitations is essential for enhancing the efficacy of TCPs in SWRRs, particularly for applications involving paediatric populations.

To better understand the possibilities and limitation of TCPs in SWRR, is possible to find examples on the upper limb specifically on the hand. Patiño et al.[62] developed a wearable orthotic device for hand rehabilitation featuring individual TCP actuators for each finger. The orthosis consisted of two main components: one fitted to the dorsum of the hand and another for the fingers. Each finger incorporated a silicone tube housing a TCP and a filament strain sensor. The TCP actuators within the finger structure could generate forces of approximately 3 N when a 0.3 A step input was applied.

Sutton et al.[63] developed an assistive wrist orthosis with a single DOF. This device employed 16 TCP actuators made of silver-coated Nylon 6.6 sewing thread. It generated a torque of 0.3 Nm to the wrist joint in the flexion direction within 3.9 seconds. They implemented a Proportional-Integral-Derivative (PID) controller to accurately follow a 0.1 Hz sinusoidal signal with a 10 N amplitude. The prototype was able to track the movement during activation but encountered challenges with slow response times during the relaxation phase.

iGrab [60], an ergonomic orthotic device to assist in finger flexion and extension movements, was designed by Saharan et al. The device featured a combination of 3D-printed components and sewn parts, including artificial tendons routed from the fingers to the wrist. The finger tendons were linked to TCP, which were mounted on a forearm bracelet. Frictionless pulleys optimised TCP actuation, and rubber strips enhanced energy efficiency. When applying a 0.6 A step signal, the fingers reached their maximum displacements within 25 seconds (i.e., the index finger was able to move 40° for the Metacarpophalangeal (MCP) joint, 21° for the Proximal Interphalangeal (PIP) joint, and

11° in the case of the Distal Interphalangeal (DIP) joint), with further improvements observed when using pulsed signals, reducing actuation time to under 5 seconds.

These orthotic devices showcase the use of TCPs for the hand and wrist. However, there are no studies on the feasibility of TCP use on the lower limb for children with physical disabilities. Looking at previous studies, TCPs look like a promising technology for paediatric SWRR. It is essential to design paediatric devices specific for them rather than downsizing existing technology, as it will adequately address their needs from the beginning, avoiding the withdrawal of the technology because it does not fulfil their expectations. TCPs seems promising as they present the advantages of compliance light weight and flexibility, making them quickly adapt to different shapes and sizes. These advantages match the main requirement of children's SWRR of safety, weight and operability. Nevertheless, it is still unclear if the biomechanical requirements are feasible with TCPs for different ADLs. Ankle dorsiflexion is one of the movements required to walk and one of the first to be lost in children with physical disabilities. Hence, this study will focus on the biomechanical requirements of ankle dorsiflexion in children, as it is one of the onsets indicating that children start to lose their walking ability, hindering their autonomy. This research considers the specific characteristics that make them different from adults (e.g., weaker muscles and less attention).

1.2 Thesis rationale

Children with physical disabilities tend to develop weak muscles, impeding they normal development due to their inability to move properly [64]. Walking function in children with physical disabilities declines from childhood into adulthood, which contributes to diminished participation in physical activity [65]. Children with disabilities have greater physical activity requirements to prevent decline in their level of function and to prevent secondary conditions that can result from inactivity [66]. Children with physical disability show kinematic deviations at the hip, knee and ankle leading to gait deviations such as crouch gait, jump gait, and foot droop [67-69].

Foot drop is a common gait impairment derived from these pathologies, which consists of a paralysis or significant weakness of the ankle dorsiflexor muscles [70]. It is characterized by the inability to achieve an adequate dorsiflexion, to obtain a sufficient distance with the ground during the swing phase of gait [69]. As a result, it can lead to inefficient gait compensations, increase falls, greater energy expenditure, and reduced endurance [71]. It is also characterized by an uncontrolled plantarflexion, which leads to foot slap [72].

Most of the ankle's motion occurs primarily in the sagittal plane, with plantar and dorsiflexion occurring predominantly at the tibiotalar joint [73, 74]. The typical values for ROM during the plantar-dorsiflexion movement varies between individuals due to different causes like age [75]. The overall ankle ROM in the sagittal plane is between 65° and 75°, moving from 25° to 30° dorsiflexion through to 40°- 45° of plantarflexion [76, 77]. However, during walking activities, the ROM required in the sagittal plane is reduced to around 25°, moving from 20° dorsiflexion to 5° plantarflexion [75, 78].

Concerning the normal forces that the ankle joint generates in the sagittal plane while walking, the maximum ankle momentum during the dorsiflexion movement is around 0.1 Nm/Kg. In comparison, during the plantarflexion, it can vary from 0.93 Nm/Kg to 1.56 Nm/Kg depending on the age [75, 78] . Another interesting parameter is the joint's stiffness that can be seen as mechanical resistance to passive movement. In this case, the required amount of torque to reach 20° of dorsiflexion is almost 8 Nm. In contrast, for reaching 30° plantarflexion the needed torque is about 0.6 Nm [79, 80].

Early access to rehabilitation is key for children, as therapeutic interventions demonstrate maximum effectiveness when initiated before the onset of symptoms [9]. A comprehensive rehabilitation team, comprising physicians, physical therapists, occupational therapists, speech-language pathologists, and orthotics specialists, collaborates in the rehabilitation process. Conventional therapies aimed at mitigating musculoskeletal deterioration and preserving ambulatory capabilities encompass surgical interventions, physiotherapy, corticosteroid treatments, and the utilization of passive orthoses [67, 81]. Nowadays, there is a growing interest in rehabilitation robots driven by their potential to assist individuals with disabilities in executing physical movements integral to the rehabilitation journey.

This work presents a study in the integration of TCP into paediatric SWRR to evaluate the feasibility of this novel technology. It shows the whole design process from researching the needs of the stakeholders, the current state of soft wearable robots, and the research and improving the TCPs performances to finalize with a prototype, providing a broad understanding on the current state of SWRR based on AMSM giving insights on the limitations and future directions of TCP technology.

1.3 Statement of purpose

This research aims to understand the feasibility of the use of soft robotic on SWRR for children with physical disabilities using TCPs. The work centres around three key research question for their potential to augment the understanding on the area of

paediatric SWRR. In the subsequent sections, it will explore the possibilities of TCPs as the main actuation mean for SWRR trough the following research questions:

1. Why is different to develop paediatric SWRR than normal SWRR?
2. To what extent does the developed proposed TCPs AMSMs produce forces and displacement that can be used to generate the ROM and torques in the sagittal plane that are similar to those needed to move a child's ankle during passive dorsiflexion movement?
3. How a control strategy developed for SWRR performs in generating dorsiflexion movements?
4. Can a feasibility study identify the critical attributes for SWRR that could assist ankle dorsiflexion movement in children's sagittal plane?

As the thesis is explored each question serve as beacon guiding the study into the world of soft robotics for paediatric rehabilitation and its prefund implication for both technology and healthcare.

The first research question aims to understand the distinctions between paediatric and adult SWRR thoroughly. This exploration is crucial for identifying critical differences in requirements essential for the tailored design of SWRR specifically for children. The emphasis on customization is pivotal to mitigating potential challenges, such as the rejection of robotic solutions by the paediatric demographic. Furthermore, recognizing these variances is important for making well-informed decisions in selecting the most suitable AMSM technology.

The second research question delves into the exploration of AMSM technology. Each variant of AMSM possesses unique characteristics, encompassing both advantages and disadvantages. These distinctive features significantly influence the design considerations for paediatric SWRR. The selection of AMSM technology is pivotal, given the diverse forces, strain, and speed characteristics associated with each variant. These attributes play a crucial role in the context of SWRR, impacting the ROM and torque.

The third research question shifts from examining the physical characteristics of AMSM to a more intricate scenario. While skeletal muscles have the inherent ability to contract and generate displacement and forces, a control strategy is essential to replicate the precise motions inherent in children's activities. The control strategy is integral, serving as a core component of any robot. Once the control strategy for the chosen AMSM is comprehended, it can be extrapolated to different body parts or applied to various scenarios.

The final research question delves into assessing the feasibility of TCP technology in paediatric SWRR, building upon the prior investigation into the actuators themselves. Each variant of AMSM presents its unique strengths and limitations suitable for diverse applications. However, comprehending their functionality in driving specific human activities, such as ankle dorsiflexion, serves as a crucial exploration. This investigation provides insights into whether further exploration of the technology is required or if it is feasible to address the disadvantages of AMSM technologies in the design of SWRR. Moreover, this understanding is vital for the development of SWRR tailored explicitly for children, minimizing potential risks when implemented with real patients. Ultimately, the results contribute valuable information for adapting AMSM to SWRR, with potential applications extending to the broader population.

1.4 Thesis methodology

As delineated in the preceding section (1.2), the deficiency in paediatric exoskeletons underscores the inadequacy of current robotic requirements tailored for adult patients. Consequently, the quest for new technologies to enhance children's user experience, particularly in the realm of actuators, becomes imperative. AMSM emerge as a promising solution to address challenges prevailing in the current landscape of rehabilitation robots.

A critical task involves selecting an appropriate AMSM technology for experimentation. This decision hinges not only on the capabilities of AMSMs but also on their ease of production or tunability to meet specific requirements. Considerations of time and cost, acting as constraints, emphasize the importance of that AMSM selection processes as this can introduce substantial delay to research timelines.

Before venturing into human trials, understanding the potential of AMSMs to fulfil user requirements becomes essential. This necessitates a grasp of the manufacturing process and its correlation with the performance TCP, a prominent AMSM in focus. The modification of the manufacturing process is a key facet, ensuring that is possible to acquire the requirements set by the project.

To ensuring the fit of the TCPs for the project after their selection, first a testing on their characteristics of force, strain and response time were made. This was done by applying a step signal and how the TCP respond to it. Whit this data it was possible determine the fitness of the TCPs for SWRR.

The next step was to enhance the TCP behaviour as its main limitations are the generated temperature (can harm the children) and the response time. Hence a control strategy was needed to improve both aspects. The project, in adhering to the principle

of avoiding external components that increase system complexity and weight, explores novel techniques rooted in control mechanisms and physical characteristics of AMSMs. This exploration precedes the design of the initial prototype, laying the foundation for enhanced performance.

Given the involvement of children in the project, a profound ethical commitment becomes imperative. At this juncture of technological development, obtaining validity through a preliminary test that circumvents direct human involvement is feasible. Physical models emulating children were employed to assess the performance of the designed paediatric SWRR for ankle rehabilitation. This design is informed by insights gleaned from AMSM experimentation and physiological data specific to children.

In conclusion, methodological choices were meticulously crafted to conduct ethical research without compromising the validity of data derived from experiments. The results presented signify the culmination of a rigorous research process focused on overcoming challenges and envisioning future technology for paediatric SWRR, ultimately geared towards enhancing the quality of life for children. This contribution stands as a robust addition to the field.

1.5 Thesis organisation

This thesis unfolds as a systematic progression of studies, organized into Chapters that build upon each other, as illustrated in Figure 1.1. Chapters 2-6 have been prepared for publication in distinct quality peer-reviewed journals/conferences and may exhibit some recurring content. Within this thesis each Chapter will be introduced with prefaces, retaining its original published form.

Chapter 2 conducts a comprehensive review of existing scientific literature on paediatric rehabilitation robots. It establishes a context for the design requirements of paediatric SWRR, emphasizing the need for a distinct approach compared to adults. Key components crucial for rehabilitation robots are highlighted, and an analysis of paediatric user needs emphasizes the importance of compliance, lightweight design, and safety—challenges difficult to surpass when employing rigid robotics. The insights gained directly address the first research question.

In Chapter 3, the current state of AMSM is explored through an extensive literature review, leading to the selection of TCP actuators for the paediatric SWRR ankle application due to their high power-to-weight ratio, linearity and strain advantages. Chapter 4 delves into the properties of TCP actuators embedded with Nickel Chromium (NiCr) wire, investigating the impact of the NiCr on strain and generated temperature.

Those factors are crucial to designing SWRR. This investigation directly addresses the second research question.

Chapter 5 marks a shift from characterizing TCP actuators to enhancing their functionality. Recognizing the need for fast and precise movements, the focus turns to implementing a control strategy. This includes exploring the impact of length on speed and temperature. This Chapter sets the path to achieving the goal of research question 3, as speed and precise control are required to generate accurate and helpful dorsiflexion movements.

In Chapter 6, the integration of TCPs into a paediatric ankle SWRR is explored. The Chapter evaluates TCP performance within the context of paediatric SWRR for ankle rehabilitation. The assessment is concentrated explicitly on ROM, torque, and speed, given their critical role in SWRR functionality. The integration of TCPs into the exoskeleton provides valuable insights to address research questions 3 and 4.

Finally, Chapter 7 serves as a synthesis, bringing together the research findings and their implications in the field of AMSM for paediatric SWRRs. This Chapter critically analyses the conclusions derived from the research, providing a comprehensive discussion that situates the entire thesis within a broader context. Additionally, it highlights potential avenues for future research and underscores the current limitations of AMSM. The Chapter demonstrates the ongoing advancements in using AMSM for paediatric SWRRs.

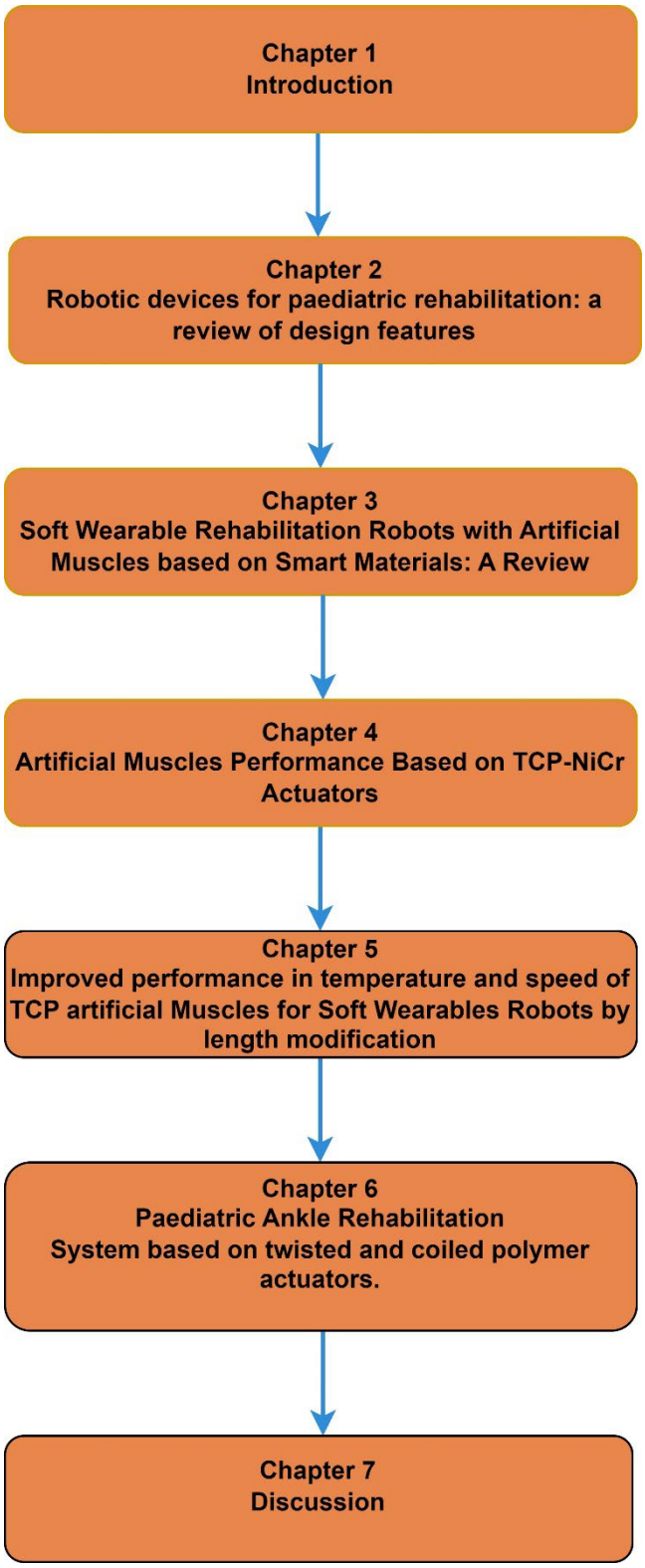

FIGURE 1.1 THESIS STRUCTURE

Chapter 2 : Robotic Devices for Paediatric Rehabilitation: A Review of Design Features.

2.1 Preface

The content of this Chapter is a copy of the article “Robotic Devices for Paediatric Rehabilitation: A Review of Design Features”, published and peer-reviewed in the journal Biomedical Engineering Online [82].

Designing rehabilitation robots tailored to children presents unique challenges due to their distinct needs compared to adults. Despite the availability of various rehabilitation devices, only a limited number are specifically designed for children, resulting in scarce information on paediatric rehabilitation robot design. This Chapter provides a comprehensive review of current paediatric rehabilitation robot technology, examining essential requirements, variations based on diseases and affected body parts, and how these needs are addressed by existing robot technology. The analysis focuses on three main aspects of the robots: actuators, training strategies, and Human-Computer Interfaces (HCIs).

The examination highlights weight, safety, operability, and motivation as crucial factors in the successful design of devices for children. Notably, there is a discernible trend towards developing exoskeletons, allowing assistance with ADLs beyond the rehabilitation setting and fostering broader adoption of the technology. With this evolving focus, the Chapter anticipates a demand for new technologies that can actuate more compliant, lightweight, adaptable, and safe systems, emphasizing the potential role of soft actuators in meeting these requirements.

2.2 Abstract

Children with physical disabilities often have limited performance in ADLs, hindering their physical development, social development and mental health. Therefore, rehabilitation is essential to mitigate the adverse effects of the different causes of physical disabilities and improve independence and quality of life. In the last decade, robotic rehabilitation has shown the potential to augment traditional physical rehabilitation. However, to date, most robotic rehabilitation devices are designed for adult patients who differ in their needs compared to paediatric patients, limiting the devices’ potential because the paediatric patients’ needs are not adequately considered. With this in mind, the current work reviews the existing literature on robotic rehabilitation for children with physical

disabilities, intending to summarise how the rehabilitation robots could fulfil children's needs and inspire researchers to develop new devices. A literature search was conducted utilising the Web of Science, PubMed and Scopus databases. Based on the inclusion-exclusion criteria, 206 publications were included, and 58 robotic devices used by children with a physical disability were identified. Different design factors and the treated conditions using robotic technology were compared.

Through the analyses, it was identified that weight, safety, operability and motivation were crucial factors to the successful design of devices for children. The majority of the current devices were used for lower limb rehabilitation. Neurological disorders, in particular CP, were the most common conditions for which devices were designed. By far, the most common actuator was the electric motor. Usually, the devices present more than one training strategy being the assistive strategy the most used. The admittance/impedance method is the most popular to interface the robot with the children. Currently, there is a trend on developing exoskeletons, as they can assist children with ADLs outside of the rehabilitation setting, propitiating a wider adoption of the technology. With this shift in focus, it appears likely that new technologies to actuate the system (e.g., Serial elastic actuators) and to detect the intention (e.g., physiological signals) of children as they go about their ADLs will be required.

2.3 Introduction

Mobility and exploration are essential in children's development and contribute towards cognitive, physical, social and emotional development. However, children with physical disabilities present limitations when performing activities autonomously, which hinders their typical development [64]. Ongoing paediatric physical disability arose from many different causes, including neurological disorders like CP [8], Stroke [83] and ABI [84], neuromuscular diseases such as DMD [85] and Spinal Muscular Atrophy (SMA) [86], or Traumatic Injuries [87, 88] (Table 2.1).

Rehabilitation is essential to help the children recover or maintain functionality when interacting with their environment, improving the quality of life and autonomy [89, 90]. Furthermore, early access to rehabilitation is critical for children while they are in the stage of development. The gait pattern and motor abilities are still malleable [91], intending to reduce the probability of developing more severe levels of disability [92, 93].

Table 2.1 Incidence or prevalence of conditions that cause physical disabilities in children

Condition	Incidence or prevalence
Cerebral Palsy	Prevalence of 1 per 500 live births [8]
Stroke	Incidence of 1.2 to 13 per 100,000 children per year [83]
Traumatic Brain Injury	Incidence of 691 per 100000 children [87]
Duchenne Muscular Dystrophy	Prevalence of 1 per 5000 live male births [94]
Spinal Muscular Atrophy	Prevalence of 7.8-10 per 100,000 live births [86]

The standard therapies to manage the musculoskeletal system's deterioration and improve and maintain physical ability include passive orthoses, surgery, and physiotherapy [37, 81]. Physiotherapists prescribe, monitor, and guide exercise, which can prevent an unnecessarily sedentary or immobile lifestyle. The most extensively investigated aspect of physiotherapy is the effect of direct interventions on upper or lower limbs. Such interventions often involve intensive stretching and strengthening exercises facilitated by the physiotherapist [8] to improve motor skills. These interventions are often highly labour intensive and can be challenging to perform [13]. Furthermore, the effectiveness of physiotherapy often depends on the experience of the physiotherapist. Thus, it is not easy to achieve optimal consistency and repeatability between rehabilitation sessions [14, 15].

There is a growing interest in robots that can support the patient, the family and the medical professional in a wide range of activities used for the care of people with physical disabilities, for example, companion robots [95, 96], monitoring robots[97] and surgery robots[98], all of them can be considered as healthcare robots.

Healthcare robots can be divided into three main categories, clinical robots, assistive robots and rehabilitation robots [26, 99]. Clinical Robots are focus on supportive care and cure process (e.g. help in surgery and diagnosis) in clinical environments; assistive robots primary function is to provide assistive help either to carers or directly to patients either in a hospital or in a specialist care facility (e.g. patient lifting and to assist in routine services); rehabilitation robots are robots design towards restoring the functionality and mobility of people with physical disabilities, in that case, the recovery of mobility could be achieved by assisting the patient during ADLs (e.g., walking and grasping objects) [13, 33] or with physical training therapy [18, 19, 26, 100, 101], and are the main focus of this study.

Rehabilitation therapy for the recovery of mobility based on robots has been proposed as a new procedure for children with physical disabilities [102]. This Robot-assisted rehabilitation therapy consists of a mechatronic device that provides highly repetitive and task-specific guided movements autonomously [21, 22]. The use of robots in rehabilitation therapies bring advantages over traditional therapies, as they allow

extensive practice in children with substantial disabilities, reduced effort required of therapists during the exercises, and provide a quantitative assessment of the patient's motor function (e.g., quantitative feedback of ROM and strength with each repetition) [23-25, 103, 104].

Rehabilitation robots are often classified by their mechanical structure and are generally divided into end-effectors and exoskeletons [19, 27]. End-effector devices work by applying forces to the distal segments of limbs, creating what is termed a "mechanical chain" that prompts movements of other parts of the limb generating a pattern of specific activity across different joints. If utilised on a single segment and joint, their simple structure makes it easier to adapt them to many patients and needs less complicated control algorithms. However, it is difficult to isolate specific joints since they produce complex movements that involve the whole limb [28].

Contrarily, robotic exoskeletons could be termed "wearable machines" that mirror the patient's skeletal structure; therefore, they only move the joint of the limb where the exoskeleton is worn. This approach allows for independent and concurrent control of specific segments of the limb. However, it is essential to adjust the length of sections of the robot to the lengths of the segments of the patient limb. Moreover, when the joint is in motion, the position of the centre of rotation can change, creating discomfort in the user. Thus, increasing the number of DOF of the robot increases the control algorithm's complexity, weight, mechanical complexity, and power requirements, making it unattainable for home use [14, 29].

Apart from mechanical structure, robots possess essential elements to ensure the systems' reliability and robustness [30]. Actuators, training strategy and the HCI are among these essential elements. The actuators play a crucial role because they determine the torque and movement provided by the robot and influence the total weight and compliance of the system[36, 100]. The training strategy and the HCI are an integral part of the robot-assisted rehabilitation since it determines how the patient interacts with the robot and the type of assistance that the robot can provide. Many authors have analysed these last two characteristics as part of the robot's control [19, 101, 105]. However, control also involves "low level" considerations that are more related to the internal communication of the components (sensors, structures, microcontrollers, actuators, etc.) at a hardware level rather than how the device interacts with the patient [106-110].

Although multiple devices for the robotic rehabilitation of upper and lower limbs have been developed, at least in a proof-of-concept phase [26, 27, 30, 105, 106, 111, 112], most presented robots were designed for adult users, impeding their use on the

paediatric population. For example, commercial exoskeletons are made for a subject 150 cm tall onwards [34], while the average height for a five-year-old child will be around 110 cm [35].

However, to develop technology planned to be used on the paediatric population is not only a matter of reducing the size of the robots. But it should be tailored to their own capabilities and goals that differ from those of the adults. For instance, a simple downscaling of the robots is not enough as the normalised joint torques on adults are greater than those of a child [78, 113], making them potentially dangerous when used on small children. Additionally, in the case of children, as their cognitive abilities are still developing, it could be hard for them to fully understand how the technology work [34, 114]. Hence, it is hard to adapt a robot made for adults to be used by children since the robots do not fulfil the children's needs [32, 33].

Consequently, to address the children's needs adequately, it is essential to include them and other stakeholders (e.g., family members, clinicians, and health care providers) during the development process, providing feedback to identify possible issues of importance [36, 64]. Furthermore, it is essential to focus not only on addressing the impairment or limitation in users' functional abilities but also on other fundamental needs, like accessibility and aesthetics [115], to avoid the user abandoning the rehabilitation device due to frustration [116].

Despite the progressive development of robotic rehabilitation devices, their application to the paediatric population is still scarce. Consequently, the key features to design an optimal robotic rehabilitation device that better enhance children's abilities with physical disabilities have not been well defined yet. Based on this framework, this review aims to address the following questions:(1) What are the design requirements for paediatric rehabilitation robots? (2) How does the current technology contribute to achieving the paediatric design requirements? And (3) How do the paediatric conditions impact the device design?

2.4 Methods

An in-depth literature search was performed to conduct the review, following the search strategy of the Preferred Reporting Items for Systematic Reviews and Meta-Analyses (PRISMA) guidelines [117].

A literature search was conducted to identify literature associated with the topic based on searches in PubMed, Scopus, and Web of Science, using the combination of the following keywords: (pediatric OR kid* OR child*) AND (aid OR assist* OR improve* OR

augment* OR enhance* OR reinforce* OR therap* OR rehabilitation) AND (active ortho* OR exoskeleton* OR wearable robot* OR portable robot* OR robot* suit OR robot*) AND (movement OR motion OR walk* OR gait OR grasp* OR handl*). To make our search as complete as possible, a search through the university library databases was also conducted.

After the preliminary search, the following inclusion and exclusion criteria to narrow the literature search were used. The inclusion criteria were:

- Studies involving robotic devices for robot-assisted rehabilitation therapy
- Studies involving robotic devices for assessment of patients with Physically disabilities,
- Studies involving devices designed for children or utilised with a paediatric population (<18 years old),
- written in English,
- full-text articles.

And the exclusion criteria were:

Studies that only present software solutions or simulations,

- Studies involving passive devices (do not have actuators),
- Studies involving postural change,
- Studies involving only the adult population and
- Studies involving robots that do not replace the movement itself (e.g., wheelchairs).

2.5 Findings

The outcome of this literature review is compiled in the following sections:

- An overview of the literature search,
- the paediatric robotic rehabilitation design requirements,
- an analysis of the type of robots used in paediatric robotic rehabilitation;
- the actuators to drive the robots;
- training strategy of the robots;
- the human-computer-interface of the assistive systems, and
- the treated conditions in children with physical disabilities.

2.5.1 Literature search

Based on the keywords mentioned in the methods section, 1604 publications were found, with:

- 811 publications from Web of Science,
- 547 publications from PubMed,
- 241 from Scopus, and
- 5 from a search on the University library.

First, a check was made for duplicated publications. After this process, the abstracts of 1248 publications were screened, and 301 titles were selected for full-text reading. After carefully applying the inclusion-exclusion criteria to the full read papers, 206 publications were selected. Among the chosen publications, 10 were reviews, 42 only discussed a section of the design process of the rehabilitation robot, 138 presented a clinical application, and 16 included the design process plus a clinical application (Figure 2.1 shows a flow diagram that illustrates the process of the selection of the papers).

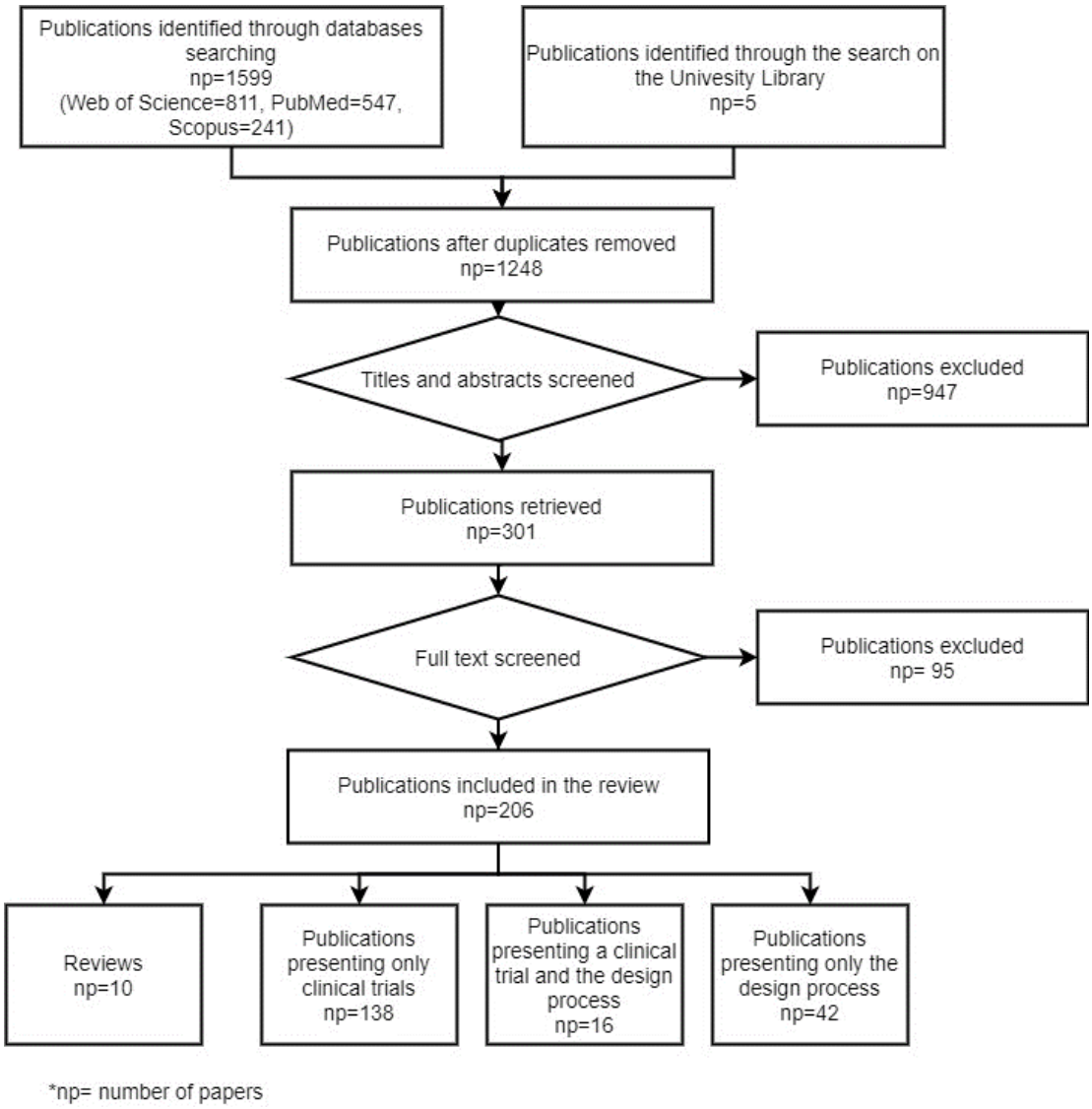

FIGURE 2.1 LITERATURE SEARCH FLOW DIAGRAM

The ten review articles examined a variety of rehabilitation robots for children with physical disabilities. They were focused on children with neurological problems (e.g., CP, ABI, and Stroke) or Spinal Cord Injury (SCI) and only investigated their use as part of physical therapy. In Fasoli et al. [24], Meyer et al. [118], and Bayon et al. [119], the robot assistive therapies for children with CP were examined. Vova et al. [120] reviewed the efficacy of functional electrical stimulation and exoskeletons in gait training to improve motor function and gait pattern in children with CP. Zwicker et al. [121] reviewed the efficiency of robot-assisted treadmill training compared to traditional treadmill training in children with CP. Chen et al. [122] examined the effectiveness of various devices for upper limb robotic therapy on children with CP. The effects of robotic gait training practices in individuals with CP were investigated in Carvalho et al. [102]. Falzarano et al. [90] and Mahamud et al. [123] investigated upper and lower limb rehabilitation devices for neurological diseases. Dannenberg et al. [124] compared different locomotor training, including robotic training, in children with SCI. Compared with the previous reviews, this

work analyses a broader range of aspects of paediatric rehabilitation robots, focused on the design parameters to fulfil the paediatric needs and how the technology and different conditions affect the robot design.

2.5.2 Paediatric robotic rehabilitation design requirements

Fifteen different requirements were identified (Table 2.2). The requirements are based on those proposed by Batavia and Hammer for assistive devices [125] and expanded by proposed requirements for paediatric rehabilitation devices highlighted by Weightman et al. [126], Bützer et al. [33] and Keller et al. [32]. In paediatric rehabilitation, it was apparent that the stakeholder's needs related to operability, weight, safety, and motivation factors were relevant.

In paediatric rehabilitation devices, operability is critical as children are in a continuous development phase during which their bodies, cognitive capabilities and physical abilities (e.g., skill levels) are changing, making them a "heterogeneous population" [34, 127]. Consequently, the device must adapt to different children's abilities and sizes [128].

An important consideration is that the robot's weight could obstruct the movement pattern of the limb and increase the child's energy consumption [129, 130]. Furthermore, due to their musculoskeletal system's immature development, their muscle strength and joint torque generation may not be adequate to assist in the movement being undertaken [131].

Concerning safety, children often cannot adequately assess the hazards of using complex technological devices [114]. Therefore, it is crucial to design safety mechanisms that minimise risky situations. These should be able to be activated remotely by adults with the child [32]. Furthermore, the use of compliant materials with shock-absorbing features (e.g. elastic elements like spring and Bowden cables) would be beneficial [13].

Finally, motivation is crucial because function recovery is not enough to engage children in the rehabilitation process [132]. Consequently, researchers have used strategies to engage children, like aesthetic designs attractive to the children [33, 133] or a virtual environment where they can interact with virtual objects [134, 135].

Table 2.2 Paediatric rehabilitation robots' requirements and examples

Requirement	Definition	Example
Target group	Range of ages and problem of the users	ChARMin covered an age range from 5-18 years old [136].
Mechanical functionality	The device performance, including the controlling level of assistance, the functional workspace, smoothness of movement and robustness.	McDaid designed a gait trainer that allows children to stretch their legs through the entire ROM and support body weight up to 80kG [28].
Weight	Total unsupported or unpowered mass of the device in relation to the user's body weight.	Lerner developed a Bowden cable structure for an ankle exoskeleton with a weight of 1.85KG and placed 65% of the total mass above the waist to minimize the metabolic cost of walking due to the device's weight [130].
Therapeutic benefit	The type of exercise that the rehabilitation system should promote and how this will improve the user quality of life	The paediatric Anklebot provided intensive task-specific sensorimotor therapy to the ankle of children with motor disabilities to promote motor learning [132].
Safety	The potential for the device to harm its user.	IOTA device included a security stop button that immediately halts the servo motors [137].
Comfort	The user can use the device without physical pain or discomfort.	The P-LEG robot used 3D printed braces based on 3D scans of the child's legs to improve the child's comfort [128].
Reliability	The consistency of the device operation in normal operating conditions	Laubscher designed a gait guidance controller to guide the motion of the patient's legs to follow healthy gait patterns to avoid unnatural gait patterns [138].
Operability	The device is easy to control and adaptable to changes in the user's ability and sizes	ATLAS exoskeleton used a slide and tubular regulation size system to adapt to the fast growth of the patients at all stages [139].
Product appeal	User satisfaction with the design, like fit, appearance, and sound of the device	One of the main requirements for PEXO was an appealing design, so the kidPexo version resembles a crocodile [33].
Quality of construction	Typical use and care should cause no damage, distortion, or hinder the expected useful lifetime of the device.	PEXO device did not have electronics in the hand module, making the device water and dustproof [33].
Social acceptability	Matches user needs for discretion or attention to avoid stigmatization	Weightman selected the handgrip of his robot through a questionnaire with different aspects like shape, style, feel, and colour [126].
Motivation	Encompass any aspect of the device considered to motivate the child	ChARMin used an Audio-visual interface with various game-based virtual reality scenarios to motivate the child for active participation [32].
Cost	The financial burden of the initial purchase and ongoing costs of the device	Volpini developed a low-cost robotic gait trainer to be used in developing countries [140].
Easy to maintain/repair	The ease of keeping the device fully operational, including when damaged	P-Legs' brace 3D print fabrication method made it easy to get new braces as the children grow [128].
Portability	The possibility of the device to be transported between location	Cleary developed a smaller version of Pedbot that can be used at home [141].

2.5.3 Type of robots used on paediatric robotic rehabilitation.

Fifty-eight different devices were found that at least had a prototype in action. In tables 2.3-2.7 (Figure 2.2-2.6), the rehabilitation robots are presented chronologically and separated by their mechanical structure (end-effector or exoskeleton) and the anatomical part of the body where they are working (upper limb or lower limb). Furthermore, the

tables summarise the characteristic features of the selected devices. This tabulated summary constitutes the reference for information provided in subsequent sections.

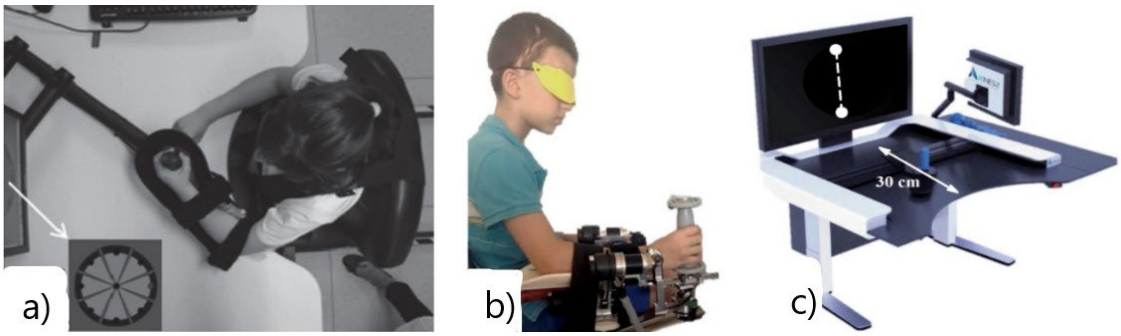

FIGURE 2.2 PICTURE OF UPPER LIMB END-EFFECTORS REHABILITATION ROBOTS A) INMOTION2/ MITMANUS [142], B)WRIST ROBOT [143], C) REAPLAN [144].

Table 2.3 Upper limb end-effectors rehabilitation robots

System (year)	Treated part of the body	DOFs	Actuator	Type of Rehabilitation	Type of training	HCI input	Paediatric Disease (Design for or Treated condition)	Paediatric Design	Stage of the device
Inmotion2/ Mitmanus (BIONIK, Canada) (1998) [145, 146]	Shoulder/ Elbow	2	DC motors	Physical therapy	Passive/ Active/ Assistive	Impedance	Neurological	No	Clinical trial/ Commercial (FDA)
Wrist-Robot (2009) [147, 148]	Forearm/ Wrist	3	DC motors	Physical therapy	Passive/ Active/ Assistive	Impedance	Neurological	No	Clinical trial
NJIT-RAVR (2009) [149, 150]	Shoulder/ Elbow/ Forearm	6	DC motors	Physical therapy	Active/ Assistive/ Resistive	Admittance	Neurological	No	Clinical trial
GNO arm (2009)[151]	Elbow	1	DC motor/ Cable driven	Assistance	Assistive	Finger Movement	DMD	Yes	Feasibility study
AMADEO (Tyromotion, Austria) (2012) [152, 153]	Fingers	5	DC motors	Physical therapy	Passive/ Active/ Assistive	Impedance	Physical disabled children	No	Clinical trial/ Commercial (FDA)
REAplan (AXINESIS, France) (2012) [144, 154]	Shoulder/ Elbow	2	DC motors	Physical therapy	Passive/ Active/ Assistive	Position	Neurological	No	Clinical trial/ Commercial
PASCAL (2013) [155, 156]	Shoulder/ Elbow	3	Dc motors	Physical therapy	Passive/ Active/ Assistive	Velocity	Neurological	Yes	Clinical trial
ReHaptic (2014) [157, 158]	Forearm/ Wrist	2	DC motors	Physical therapy	Passive/ Active/ Assistive/ Resistive	Admittance	Neurological	Yes	Clinical trial
MyPam (2015) [159]	Shoulder/ Elbow	2	Electric motors	Physical therapy	Active/ Assistive	Position	CP	Yes	Feasibility study

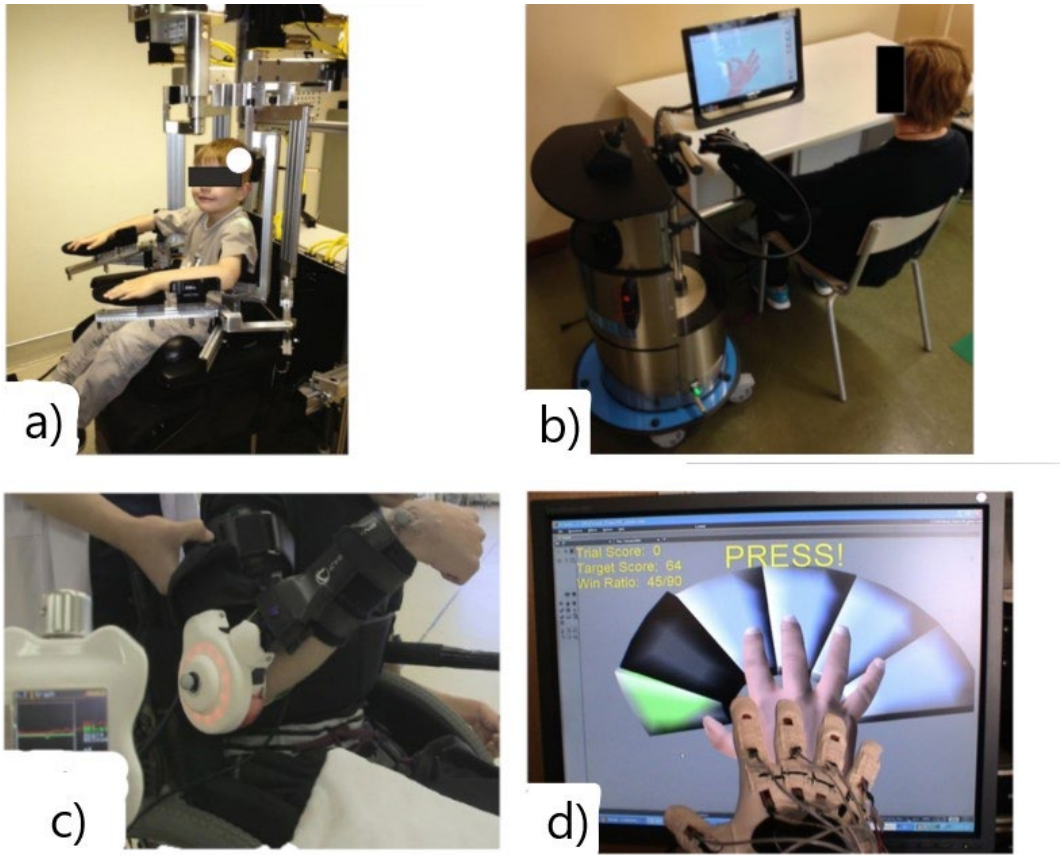

FIGURE 2.3 PICTURE OF UPPER LIMB EXOSKELETONS REHABILITATION ROBOTS A) KINARM [160], B) GLOREHA [161], C) HAL SINGLE JOINT [162], AND D) PNEUGLOVE [163].

Table 2.4 Upper limb exoskeleton rehabilitation robots

System (year)	Treated part of the body	DOFs	Actuator	Type of Rehabilitation	Type of training	HCI input	Paediatric Disease (Design for or Treated condition)	Paediatric Design	Stage of the device
KINARM (KinArm, Canada) (1999) [160, 164]	Shoulder/ Elbow	2	DC motors	Physical therapy	Passive/ Active	-	Neurological	No	Clinical trial/ Commercial
IOTA (2013) [137]	Thumb	2	DC motors/ Cable driven	Physical therapy	Passive/ Active/ Assistive	Movement	Neurological	Yes	Prototype
ChARMin (2014) [32]	Shoulder/ Elbow/ Wrist	6	Electric motors	Physical therapy	Passive/ Active/ Assistive	Movement	Neurological	Yes	Feasibility study
Universidad Nacional de San Juan (2014) [165]	Elbow	1	DC Motor	Physical therapy	Passive/ Assistive	EMG	Injuries	Yes	Clinical trial
Milwaukee University (2014) [166]	Wrist	2 actuated + 2 passives	DC motors/ Cable driven	Physical therapy	Assistive	Position	CP	Yes	Prototype
GLOREHA (2016) (IDROGENET, Italy) [22, 39]	Hand	5	Pneumatic	Physical therapy	Passive/ Active/ Assistive	Movement	Neurological	No	Clinical trial/ Commercial (FDA)
HAL single joint (Cyberdyne, Japan) (2019) [162]	Elbow	1	DC motor	Physical therapy/ Assistance	Assistive	EMG	CP	No	Clinical trial/ Commercial
PEXO (2019) [33]	Hand	2 actuated +1 passive	DC motors/ Cable driven	Physical therapy/ Assistance	Passive/ Assistive	Push buttons or EMG	Neurological	Yes	Feasibility study
PneuGlove (2019) [167]	Hand	5	Pneumatic	Physical therapy	Active/ Assistive/ Resistive	Movement	CP	Yes	Feasibility study
Exohand-2 (Android Technics, Russia) (2020) [168]	Hand	2 each hand	Electric motors	Physical therapy	Assistive	EEG	CP	No	Clinical trial/ Commercial

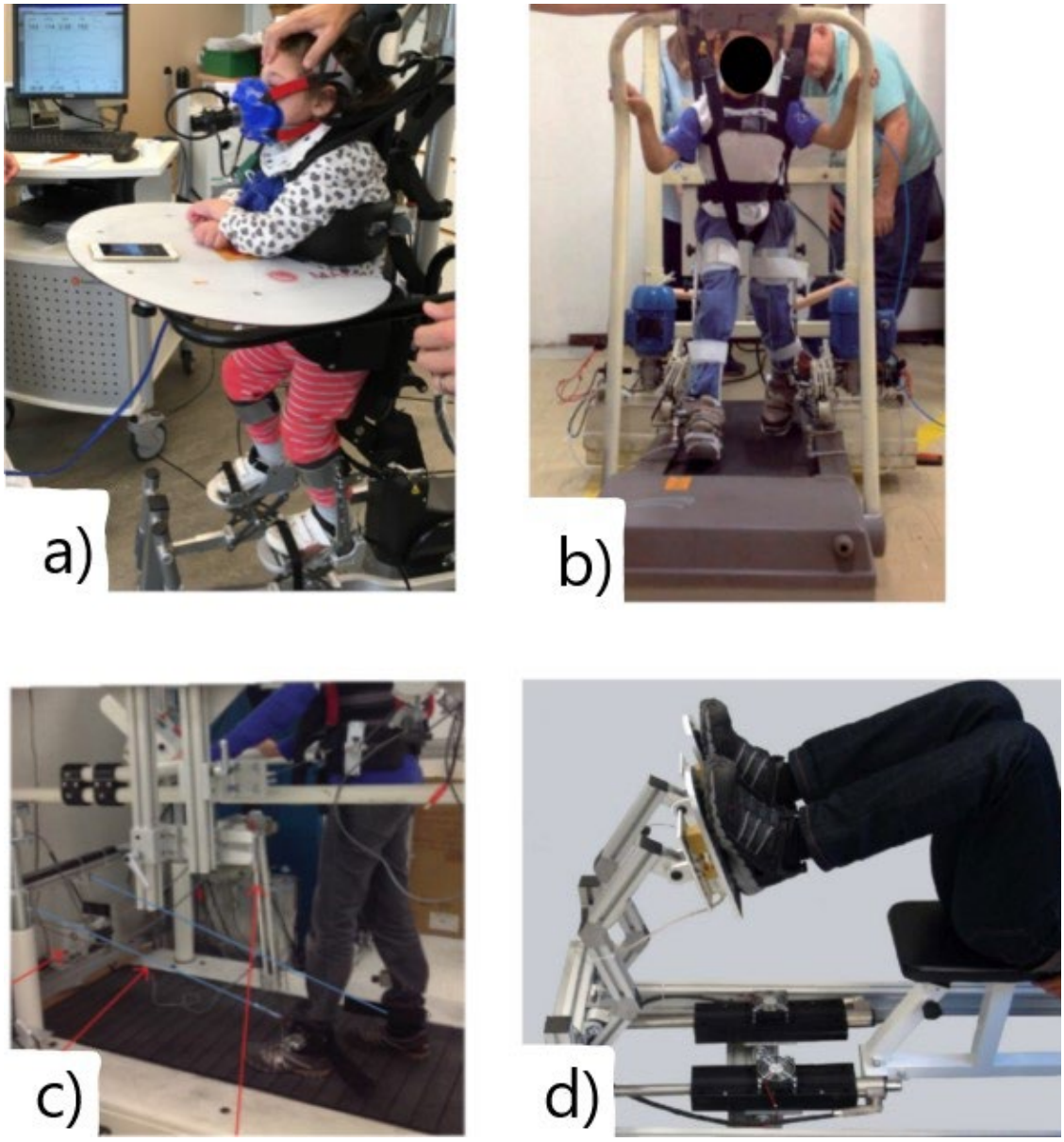

FIGURE 2.4 PICTURE OF LOWER LIMB END-EFFECTORS REHABILITATION ROBOTS, A) INNOWALK [169], B) UFMG [140], C) 3DCALT [170], D) LEG PRESS [171] "REPRINTED FROM BIOMEDICAL SIGNAL PROCESSING AND CONTROL, VOL. 38, F. CHRIF ET AL., CONTROL DESIGN FOR A LOWER-LIMB PAEDIATRIC THERAPY DEVICE USING LINEAR MOTOR TECHNOLOGY, PAGE 121, COPYRIGHT (2017), WITH PERMISSION FROM ELSEVIER."

Table 2.5 Lower limb end-effectors rehabilitation robots

System (year)	Treated part of the body	DOFs	Actuator	Type of Rehabilitation	Type of training	HCI input	Paediatric Disease (Design for or Treated condition)	Paediatric Design	Stage of the device
GAIT trainer GT 1 (REHA-STIM MEDTEC ,Switzerland) (2000) [172, 173]	Hip/ Knee	2	DC Motors	Physical therapy	Passive/ Assistive	Velocity	Neurological	No	Clinical trial/ Commercial
MOTOmed gracile (RECK, Germany) (2000) [174, 175]	Hip/ Knee	2	DC motors	Physical therapy	Passive / Active/ assistive/ Resistive	Velocity	Physical disabled	Yes	Clinical trial/ Commercial (FDA)
IntelliStretch (Rehabtek, USA) (2002) [176, 177]	Ankle	1	DC motor	Physical therapy	Passive/ Active/ Assistive/ Resistive	Velocity and Torque	Neurological	No	Clinical trial/ Commercial (FDA)
Innowalk (Made for Movement, Norway)(2009) [178, 179]	Hip/ Knee	2	Electric motors	Physical therapy	Passive	-	Neuromuscular problems	Yes	Clinical trial/ Commercial
National Taiwan University (2009) [180]	Hip/ Knee	2	DC motors	Physical therapy	Passive	-	CP	Yes	Prototype
3DcaLT (2011) [181, 182]	Hip/ Knee	4	Electric motors/ Cable driven	Physical therapy	Active / Assistive/ Resistive	Motion	CP	No	Clinical trial
Paediatric ICARE (2011) [183, 184]	Hip/ Knee	2	DC motors	Physical therapy	Active/ Assistive/ Resistive	Speed	Neurological	Yes	Feasibility study
Rutger ankle CP system (2011) [185, 186]	Ankle	6	Pneumatic	Physical therapy	Active/ Resistive	-	CP	Yes	Clinical trial
SS-POINT (2013) [187, 188]	Ankle	2	DC motors	Physical therapy	Passive/ Active/ Resistive	-	Neurological	No	Clinical trial
TPAD (2014) [189, 190]	Hip/ Knee	6	AC motors	Physical therapy	Assistive/ Resistive	Motion	CP	No	Clinical trial

Table 2.5 Lower limb end-effectors rehabilitation robots (continued)

Pedbot(2016) [141, 191]	Ankle	3	DC motors	Physical therapy	Active/ Assistive/ Resistive	Position	CP	Yes	Clinical trial
Wyss Institute (2017) [192]	Hip/ Knee	8	DC motors/ Cable driven	Physical therapy	Assistive	Gait segmentation/motion/ force	CP	Yes	Prototype
Pro-Gait (2017) [28]	Hip/ Knee	2	DC motors	Physical therapy	Passive		CP	Yes	Prototype
UFMG (2017) [140]	Hip/ Knee	2	Electric motors	Physical therapy	Passive	-	CP	Yes	Prototype
Leg Press (2017) [171]	Knee	2	Linear electrical motors	Physical therapy	Assistive/ Resistive	Impedance	Neurological	Yes	Prototype

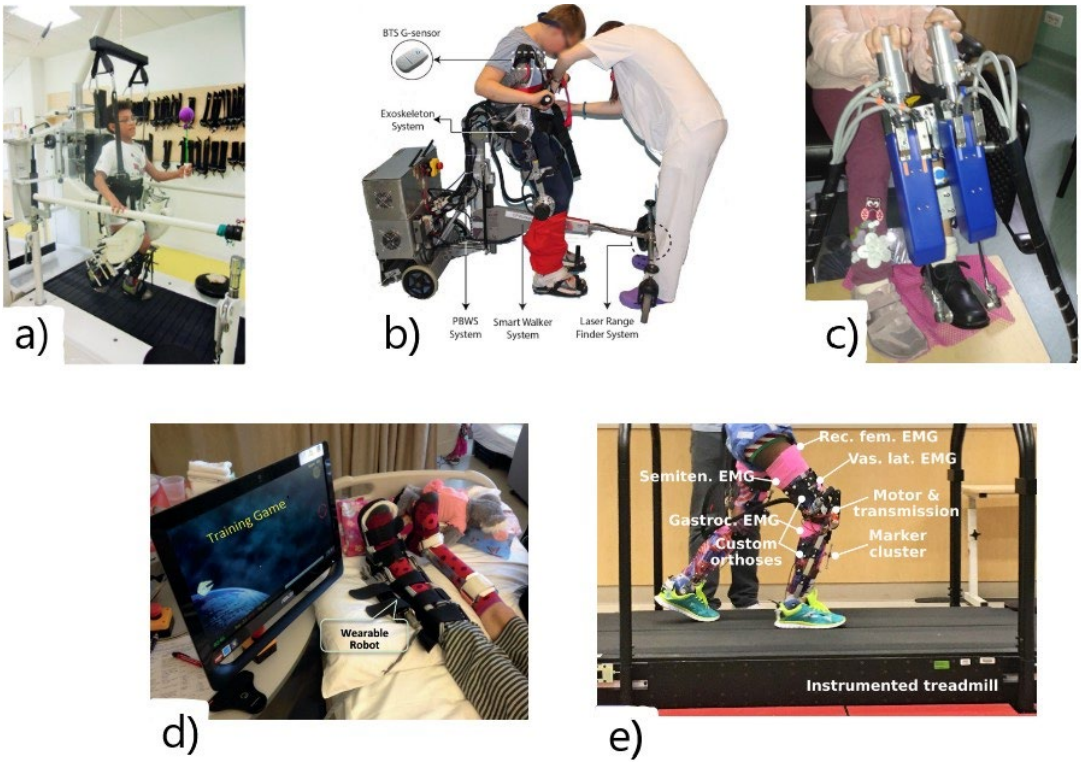

FIGURE 2.5 PICTURE OF LOWER LIMB EXOSKELETONS REHABILITATION ROBOTS, A) LOKOMAT [193], B) CPWALKER [194], C) PEDIANKLEBOT [195], D) WEARABLE ANKLE REHABILITATION ROBOT DEVELOPED BY THE REHABILITATION INSTITUTE OF CHICAGO [196], F) P.REX [197].

Table 2.6 Lower limb exoskeleton rehabilitation robots

System (year)	Treated part of the body	DOFs	Actuator	Type of Rehabilitation	Type of training	HCI input	Paediatric Disease (Design for or Treated condition)	Paediatric Design	Stage of the device
Lokomat (Hokoma, Switzerland) (2007) [198, 199]	Hip/ Knee	4	DC Motors	Physical therapy	Passive/ Active/ Assistive/	Impedance	Neurological	Yes	Clinical trial/ Commercial (FDA)
HAL (Cyberdyne, Japan) (2007) [200, 201]	Hip/ Knee/ Ankle	6	DC Motors	Physical therapy/ Assistance	Assistive	Footswitch EMG	CP	Yes	Clinical trial/ Commercial (FDA)
HWA (Honda, Japan) (2007) [202, 203]	Hip	2	DC Motors	Physical therapy/ Assistance	Assistive	Movement	CP	No	Clinical trial/ Commercial
University of Verona (2011) [204]	Hip	2	Pneumatic	Assistance	Assistive	Footswitch	CP	Yes	Feasibility study
Ekso-GT (ekso Bionics, USA) (2012) [205, 206]	Hip/ Knee	4	DC motors	Physical therapy	Passive/ Assistive	Hip movement	ABI	No	Clinical trial/ Commercial (FDA)
PediAnklebot (2015) [132, 207]	Ankle	2 active+ 1 passive	DC motors	Physical therapy	Active/ Assistive	Impedance	Neurological	Yes	Clinical trial
Walkbot K (P&S Mechanics, South Korea) (2016) [208, 209]	Hip/ Knee/ Ankle	6	AC motors	Physical therapy	Passive/ Assistive/ Active	Impedance	Physical disabled	Yes	Clinical trial/ Commercial (FDA)
Robogait (Bama teknoloji, Turkey) (2017) [210, 211]	Hip/ Knee	4	Electric motors	Physical therapy	Assistive	Force	Physical disabled	No	Clinical trial/ Commercial
WAKE-Up (2017) [13, 212]	Knee/ Ankle	4	SEA	Assistance	Assistive	Footswitch	CP	Yes	Feasibility study
Universidad Pontificia Bolivariana (2017) [213]	Hip/ Knee	4	DC motors	Physical therapy	Passive	-	Physical disabled	Yes	Prototype
CPWalker (2017) [194, 214]	Hip/ Knee	4	DC motors	Physical therapy	Passive/ Active/ Assistive	Impedance/ EEG/ LRF	Neurological	Yes	Clinical trial

Table 2.6 Lower limb exoskeleton rehabilitation robots (continued)

Rehabilitation Institute of Chicago (2017) [196, 215]	Ankle	1	DC motor	Physical therapy	Passive/ Assistive/ Resistive/ Active	Torque/Position	ABI	No	Clinical trial
ATLAS (2017) [216-218]	Hip/ Knee/ Ankle	10	SEA	Assistance	Active/ Assistive/ Passive	Footswitch/ Position/ Force	SMA, SCI	Yes	Clinical trial
P.REX (2017) [197, 219]	Knee	1	DC motor	Physical therapy/ Assistance	Assistive	Footswitch/ Position/ Torque	CP	Yes	Clinical trial
University of Arizona ankle (2018) [130]	Ankle	1	DC motors/ Cable driven	Physical therapy	Assistive/ Resistive	Footswitch/ Torque	CP	Yes	Clinical trial
Tsukuba University (2018) [131]	Knee	2	Electric Brake	Assistance	Assistive	Footswitch	CP	Yes	Feasibility study
Los Olivos University (2018) [220]	Hip / Knee	4	DC motors	Assistance	Assistive	Joystick	DMD	Yes	Prototype
P-Legs (2019) [128]	Hip/ Knee/ Ankle	6	DC motors	Physical therapy/ Assistance	Passive/ Assistive	Impedance	Neurological	Yes	Prototype
ExRoLEG (2019) [221]	Knee	2	Linear actuators	Physical therapy/ Assistance	Assistive	EMG/ limit switch	CP	Yes	Prototype
Cleveland State University (2019) [138, 222]	Hip/ Knee	4	DC motors	Physical therapy/ Assistance	Assistive	Position Velocities	CP	Yes	Prototype
ExoRoboWalker (2019) [223]	Hip/ Knee/ Ankle	6	DC motors	Physical therapy	Passive		CP	Yes	Prototype
Indian Institute of Technology Guwahati (2020) [110]	Hip/ Knee/ Ankle	6	DC motors	Physical therapy	Passive		Physical disabled	Yes	Prototype
Instituto Politécnico Nacional (2020) [17]	Hip/ Knee/ Ankle	6	DC motors	Physical therapy	Assistive	EMG	Physical disabled	Yes	Prototype

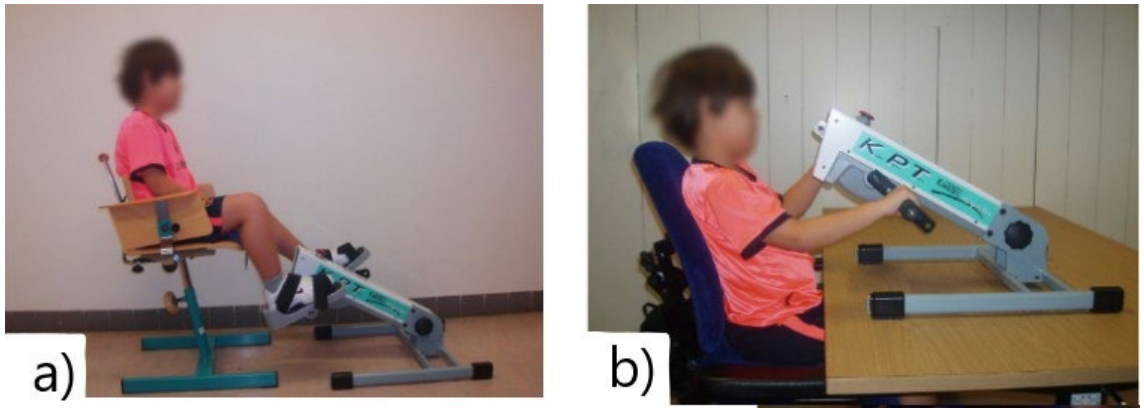

FIGURE 2.6 PICTURE OF KPT CYCLA [224] AN END-EFFECTORS REHABILITATION ROBOT FOR BOTH A) LOWER AND B) UPPER LIMBS.

Table 2.7 End-effectors rehabilitation robots for upper and lower limbs

System (year)	Treated part of the body	DOFs	Actuator	Type of Rehabilitation	Type of training	HCI input	Paediatric Disease (Design for or Treated)	Paediatric Design	Stage of the device
KPT Cycla (Kinetec, France) (2010)[224]	Upper: Shoulder/ Elbow Lower: Hip/ Knee	2	Electrical motor	Physical therapy	Passive/ Active	-	DMD	No	Clinical trial/ Commercial (Discontinued)

In respect of the developmental stage of the devices, the stages were classified into four categories, 1) Commercial in the case the robots are available for its commercialisation; 2) clinical trial when the robot undergo a study where the participants were assigned to groups undergoing similar forms of therapy, but at different intensities, using various devices or undergoing various forms of therapy in a different order, aiming to determine the efficiency of therapy [19]; 3) feasibility study when the experiments conducted with a low number of people, often using the prototype of a device, to evaluate its safety and clinical feasibility without showing the potential benefits of the device [19]; 4) prototypes when the robots had not performed any test that involves people. It can be observed that 18 of them reached the commercialisation phase, but only 9 of them are certified by the US Food and Drug Administration (FDA). However, only 5 of the commercially available devices present a paediatric version of the rehabilitation system. In the case of clinical studies, 34 systems conduct at least one clinical trial, 9 presented a feasibility study, and 15 are in the prototyping phase.

From the 58 devices, it was apparent that the majority (67%) were designed or had been redesigned for children. When it comes to the type of robot, more than half were an exoskeleton type structure. In the past five years, there is a trend (tables 2.3-2.7) for this structure to be more popular with designers than end-effectors for this structure robotic rehabilitation in paediatrics. Additionally, it can be noted that the majority of robots not explicitly designed for children are end-effector devices. In the case of the exoskeletons, the DOFs is related to the number of joints and limbs that are powered. Therefore, it is possible to find exoskeletons with passive DOFs, which means that those joints are not actuated, but allow the free movement of the children´s joint. In contrast, for the end-effectors, the relation of DOFs of the robot and the actuated joints is not linear and depends on the robot's mechanical design.

2.5.4 Actuators

Rehabilitation robots are moved by devices called actuators. Actuators convert a source of energy (e.g., electrical, thermal, pneumatic) into mechanical motion. Commonly rehabilitation assisted robots are powered by electrical actuators. Among the compared systems in tables 2.3-2.7, over 93% of the robots used electric motors as the actuator, and about 7% used pneumatic actuators.

Motor actuator

In robotic-assisted rehabilitation, the most common actuators are electrical motors with a rigid power transmission element such as a harmonic drive, ball-screws, timing belts,

and chains. Unfortunately, their need for transmission negatively affects the back drivability, efficiency, safety, size, and mass [225]. Nevertheless, they were likely chosen since they are efficient and easy to control. Some examples of paediatric robotic rehabilitation devices using electrical motors and rigid transmission are the Pedianklebot that used two brushless dc motors and a Rohlix linear traction device [226], the electric motor with timing belt used in ChARMin [136], or the motor with chain transmission used in P.REX [219].

Some researchers (64) used a cable-driven transmission to replace the rigid transmission for an elastic cable to improve the power to weight ratio and lower the inertia over the treated body segment. Examples include the ankle exoskeleton designed by The University of Arizona [227] or TPAD [190], an end-effector robot for gait rehabilitation that used Bowden cables attached to the hip to generate assistive forces. This change in the transmission brings other advantages like modularity, simple architecture and is convenient for reconfiguration, even though they present some disadvantages being unidirectional and difficult to model and control [189, 225, 228].

Following the concept of adding a flexible element in series with the actuator to improve the electric motors' compliance, Serial Elastic Actuators (SEAs) incorporate an elastic part in series with the electric actuator. This elastic element helps to decrease the actuator's impedance and inertia and increases the back drivability allowing better force control, even though they are limited by a large volume, heavy mass and complicated structure [13, 229]. An example of the use of this technology is the ATLAS exoskeleton [230].

Pneumatic actuators

Some authors considered that the mechanical linkage of the electric actuators is too heavy and can generate resistance at the joints, making them inadequate for rehabilitation applications [39, 131]. Instead of electrical motors, they used pneumatic actuators, consisting of a simple air pressurisation mechanism in an expandable chamber, converting the energy from the compressed air to mechanical motion [14, 50, 231]. Their main advantage is improved back-drivability, and they are often lightweight at the site of actuation, have high power density, and can generate fast movements. They are not without limitations; firstly, poor portability because they need external compressors or fluid tanks as the power source. Secondly, it is challenging to create a good model and control strategy due to their nonlinear response to input pressure [50, 232, 233]. Among the devices analysed that used pneumatic actuators were the Rutgers

ankle platform [185] for CP children and two gloves for hand rehabilitation PneuGlove [167] and Gloreha [22].

Training strategy

Devices for robotic rehabilitation may provide different training strategies depending on the type and severity of the patient's impairment. These can be divided into passive, active, assistive, or resistive[30]. In general, the devices can offer more than one type of training.

In passive training, the force/motion is generated by the robot alone to perform the exercise. The advantage of this training is that patients with minimal muscle activity can receive therapy. For instance, through repetition of a movement, ROM can often be maintained with muscles and joint structures (e.g., ligaments) repeatedly stretched, ultimately maintaining their physiological length. Such movement reduces contractures at joints, which can finally be very useful to caregivers making a notable difference to the ease of transfers (e.g., sitting in a wheelchair to lying in bed). Examples of devices using passive training are Innowalk [179] and Intellistretch [234].

In the active training mode, the patient's muscle can still generate activity on the affected limb. The robot does not help, making the patients perform the exercise by themselves at least partially. The active mode provides data concerning torques and the ROM produced, allowing assessments before and after therapy/surgery. For instance, Kinarm [235] and Lokomat [236] are devices that can perform active training.

For assistive or active-assistive training, the muscles of the affected body part can still be activated. Therefore, the patient can at least partially perform the exercise or movement without the robot. The assistance will be triggered after a particular event is detected through an HCI, allowing the patients to move further with the robot's help. Assistive training is relevant as it involves the active participation of the children. Moreover, it improves the physiological responses needed to maintain and increase muscle strength and length, ultimately leading to improved ROM, in which the muscles provide some of the torque required. Due to these advantages, many designers have produced devices that use this training mode. Examples are Pedianklebot [207] and the wrist-robot [148].

As the name implies, the robot applies a force opposing the desired movement in resistive training, making the task more challenging. Resistive training is used to enhance muscle strength in the treated limb. This type of training was employed in the ankle device developed by the University of Arizona [237] and the upper limb end-effector NJIT-RAVR [238].

2.5.5 Human-computer-interface (HCI)

The term HCI refers to methodologies to identify the user's intent to move in the desired direction from different input sources and translate this intention into a command for the robot to move to facilitate the appropriate actions [239]. The designers who report upon the use of an HCI have primarily developed assistive training. Two main types of HCI inputs were identified: those associated with physical interactions and physiological signals[240]. In this aspect, the devices can rely upon only one signal as the input source or use two or more signals as input to start the desired movement.

The main physical interactions used on HCIs to control such robots are Impedance/admittance, body-powered control, and gait phases detectors. Impedance and admittance control are the two most commonly used HCI. They are based on the relation between position and force rather than controlling either force or position explicitly. Impedance control accepts position or velocity as the input and outputs force or torque, and admittance is the opposite of impedance. Hence force or torque are inputs, and velocity or position the outputs. This method could provide a natural, comfortable, and safe touch interface [239]. Some examples of devices that used this HCI are the NJIT-RAVR [150] and Rehaptic [157] upper limb robots that employed admittance control or the robots for upper and lower limb Inmotion2 [145] and Pedianklebot [207] that applied impedance control.

When the children cannot generate an intention to move with the treated limb, body-powered control is applied. It consists of using the movement of a different body part as the trigger signal to initiate the rehabilitation robot. The main drawback of this approach is that it is hard to control many degrees of freedom due to the activation system's simplicity. An example of this HCI is the Ekso robot, where the activation was made by moving one's body weight laterally and then forward to trigger the assistance [205].

In assisted gait, a favoured approach for HCI is the use of gait phase detection. This technique identifies the different gait phases (heel strike, midstance, toe-off, and the swing phase) to apply forces to assist the children's movement depending on the gait phase. Robots usually perform gait segmentation using Inertial Measurement Units (IMUs) to detect angular velocities of the shank and/or the thigh, or footswitches to detect the foot's ground reaction forces while the child is walking [241]. The main advantage is that splitting the gait cycle into discrete phases provides enhanced consistency and robustness to an inherently variable process and allows lower-level controllers' implementation within each phase. The problem is that gait detection should be characterised for every target group, as the physical disability modifies the gait pattern

[219]. An example of this type of system is the P.REX exoskeleton which utilised a combination of the footswitch and IMUs to detect the different gait phases to provide different levels of assistance within each phase [219].

Alternatively, for HCI based on physiological signals, Electromyograms (EMG) that measure electrical activity in the muscles and Electroencephalograms (EEG), which measure electrical activity in the brain, are the main signals used. They are widely utilised because they can be obtained using non-invasive techniques without the need for medical intervention.

Concerning electromyograms, the primary type is Surface EMG (sEMG), a non-invasive and easy-to-configure procedure in which adhesive electrodes are placed on the skin above the muscle of interest. The benefit of using the EMG signal is that it allows detection of the user's intent before the movement occurs. The electrical activity can be detected even if it is insufficient to generate movement of a joint. However, sEMG can suffer from contamination of the signal by electromagnetic interference, skin perspiration, movement of electrodes and crosstalk artefacts. Also, for each muscle group of interest, a single EMG channel only shows the activation of that group. So, to perform an activity where many muscles fibres are recruited, it is necessary to use multichannel sEMG. Some examples of this technology in paediatric rehabilitation robots are the lower limb exoskeleton HAL [200] and the device for upper elbow rehabilitation of the San Juan National University [165].

The EEG signal is recorded using many small surface electrodes, often configured in a bathing like cap placed over the scalp that detects the underlying electrical signals. The main advantage of the EEG signal is that the physical disability level does not limit it. Even if the patient has lost all their ability to move the limb required for a task, the brain activity thought to be related to the intent to activate the muscles can be recorded. There are two main disadvantages to this system. Firstly, it is unsuitable for children with brain damage as they cannot generate standard brain patterns for limb activation. Secondly, the EEG signal has greater variability within it than the EMG signal, and it is also easily affected by changes in the patient's mood and attention. Examples of the EEG signal using are the CP walker that used this signal as a part of its HCI to help children with a physical disability move their legs (120) and the Exohand-2 that used the EEG signal to interact with the exoskeleton [168].

2.5.6 Treated Conditions

The majority of studies and devices were for children with neurological conditions (np = 183, 89%), CP being the most studied condition (np = 129, 63%). In contrast, other

neurological disorders included ABI and strokes. Significantly few researchers investigated other conditions such as neuromuscular diseases (np = 15, 8%) and traumatic injuries to limbs and the spine (np = 6, 3%). The results obtained from the studies that perform clinical trials or a feasibility study suggests that robotic rehabilitation could benefit children with physical disabilities.

Neurological disorders

Concerning CP, there was evidence of improvement in physical disability using assisted rehabilitation robots. The benefits include an increase in muscle activity [237, 242], endurance for physical activities [182, 243], improvements of balance [179], walking speed [182, 188], the strength of the muscles [244, 245], ROM of the joints [162, 246], upper limb kinematics [247], and manual dexterity [22, 248].

For paediatric ABI, there were reports in the improvement of the walking ability [249], improvement of the lower limb motor performance [196], increase in the ROM of the wrist joint and force increase in the hand [250], improve in motor function, and gait pattern [251, 252].

In children who suffer a stroke, three studies used rehabilitation robots while performing physical therapy. Marini et al. [148] demonstrated an improvement in wrist motion after the robotic therapy, and Bützer et al. [33] showed the possibility of using a wearable hand exoskeleton to assist children during task-oriented training could be helpful for rehabilitation therapies or assist children during ADLs.

Neuromuscular diseases.

The neuromuscular disease presented a different scenario than neurological disorder due to the degeneration of their muscles as the disease progresses, making hard the use of rehabilitation robot due to stiffness in the robot's joints, which can harm children's weak muscles. Hence they require compliant actuation [20, 218]. Jansen et al. [20] found that robotic rehabilitation therapy on upper and lower limbs help prevent functional deterioration in children with DMD. Meanwhile, Ganguly et al. [253], Garcia et al. [254] and Sanz-Merodio et al. [218] showed an improvement in walking ability in children with SMA with the assistance of ATLAS, and the exoskeleton was designed to provide Robotic-assisted gait training for children with SMA. Moreover, Koo et al. [151] reported improved arm mobility in children with DMD while using a robotic arm device.

Traumatic injuries

Even if traumatic injuries are common in the paediatric population, robot rehabilitation has not been applied widely in injuries that differ from those at the head. Only scarce information was found related to these conditions. A study of hands robotic rehabilitation was found, highlighting the possibility of using robotic devices to treat burns [153]. Additionally, a study observed a significant improvement in the arm movement and elbowed angle after physical therapy using an upper-limb exoskeleton for three months in children that suffer a car accident [165]. Finally, another case reported improving walking ability after robotic-assisted gait training in a girl with SCI [255].

2.6 Discussion

It is possible to see that various novel rehabilitation robots have become available to rehabilitation professionals and clients in recent years. And this trend will continue as is possible to incorporate them in activity programs aimed at improving independent function [23-25, 103] where they offer advantages over the traditional rehabilitation therapies, as they reduced the required effort of therapists during the exercises of the therapies, allowed massed practice in children with substantial limitations and provide information of the patient. Furthermore, they have the potential to be used as assistive devices to aid functional performance for users when they are worn. These possibilities will lead to a new variety of ways for assessment and intervention impacting users' abilities, task demands, or the environment to promote functional performance and participation.

The findings of this review indicate that the design and development of robotic technologies for the physical rehabilitation of children is in a preliminary stage of development, as many of the founded devices were designed for adult patients. However, there is a trend toward creating robots specifically for children [13, 32, 33, 254]. Yet less has been done to prove the benefits and constrain of such a system.

Traditionally, rehabilitation robot designers have focused solely on improving physical function [115], which can lead to rejection of the devices as not all the needs of children with disabilities are considered. Thus, to ensure successful adoption of the technology, the rehabilitation robots should cover these needs of the children. Hence, stakeholders' cooperation is essential through their integration within the design and production process by providing feedback. Designers can use this feedback to validate that the robot meets the stakeholder's needs. However, the fulfilment of these needs has strong relationships to the chosen technology, mainly the type of robot, the actuator, the training

strategy and the HCI. Thus, it is essential to know the advantages and disadvantages of the technology.

Type of robot

When it comes to the type of robot, we can see a trend to migrate from end-effector to exoskeletons. However, most of the devices that had performed clinical trials were end-effector robots designed for adults. This relation could be because the end-effector robot works on the distal part of the limb, guiding the children limb through a movement [256]. This property is helpful in the case of operability as it does not require adaptation to match the children limb's size, making it easy to be used by a diverse group of children. Furthermore, the bulky frames over the patient limbs are avoided, helping to reduce the weight that the children need to handle. These advantages come with the problem of the systems requiring bulky and heavy external structures, reducing the device's portability, constraining its use to medical facilities or specific spaces inside a building. Thus, limiting the amount of therapy that the children can have [141]. Additionally, the activity is restricted to a workspace constraining the number of possible movements [28], which could reduce motivation.

On the other hand, exoskeletons work in parallel to the patient limb to perform the activity. Hence, they can be portable devices with the possibility to provide assistive help during ADLs and robotic-assisted rehabilitation therapy in a single device [33]. This advantage will help to provide free movement to enhance the subject's motivation and autonomously practice their movement training for longer periods [13, 214]. Furthermore, as technology advance, this freedom in mobility will help to increase the participation of children with physical disabilities in different social activities [257]. However, as the technology moves from clinical facilities to open spaces and robots interact more closely with the children, designers will face notable challenges (e.g. the irregularities of the surfaces on which one walks and how the robot reacts to perturbations outdoors environment). Consequently, the requirements of weight, comfort, safety, portability and social acceptability for the exoskeletons will be harder to achieve.

Actuators

The paediatric robotic rehabilitation technology is moving from end-effectors to exoskeletons due to their versatility to be used as a rehabilitation tool or an assistive device [33]. Consequently, actuation technology starts to be a critical part of the design as it negative influence the weight and the size of the robot.

For the end-effectors robots, actuators are not as critical as with the exoskeletons because they could be placed in external structures. This advantage makes it possible

to use bulky and heavy actuators like electric motors. However, using electric motors is hard to achieve compliance that is an important property to increase safety as it is needed to avoid opposing forces that can injure the children. In end-effector robots, compliance was achieved using sensors and a control strategy [218] or using a soft material like the Bowden cables [189].

On the other hand, for exoskeletons, the robot design requirements are hard to enhance with the currently used technology. The actuation system components such as motor and rigid elements are designed for industrial applications not to interact with and to be worn by children. However, they are still the standard as they have the advantages of efficiency, are easy to control, and are readably available in the market. Therefore, the choice of the actuation system is crucial to improve the weight, portability and safety of the exoskeleton.

The first exoskeletons relied on electric motors with rigid transmissions, making them bulky and heavy, reducing their compliance as they generate high resistive torque from the metallic links of the exoskeleton. Therefore, making it difficult to move and less safe can cause non-desirable inertial movements [258, 259]. Furthermore, they require external structures to manage the weight of the exoskeleton.

As the rehabilitation robots move from rehabilitation therapies inside a medical facility to assist the children during ADLs, new actuation technology is needed. This challenge led to using SEA actuators and cable transmission since they have the advantage of been intrinsically complaints as they incorporate soft materials, making the device safer.

Using Bowden cables in the transmissions brings other advantages like simple architecture, low weight on the limb's distal part, and easy to reconfigure. This last advantage is significant in paediatric rehabilitation as it allows to change the motor easily depending on the abilities and size of the children [33, 130], even though they present some disadvantages because they become unidirectional and difficult to model and control. Instead, in the case of SEAs, which still require rigid links, they were highlighted on the use for children with neuromuscular diseases, as some children are not only weak on the affected joint but the entire body. Thus the exoskeleton must hold the children, but at the same time being compliant to avoid inertial forces that can harm the weak muscles of the children [218].

Another type of actuator used on the robots was the pneumatic. Their attributes of low weight and easy to manufacture actuators of different shapes and sizes [260, 261] make them a desirable technology in this field. They are easy to adapt to children with various conditions. However, their main constrain is that they are typically connected to external

mechanisms like compressors and pumps cumbersome and noisy. Thus, reducing their portability and appealing making them impractical to use outside clinical facilities.

Table 2.8 General summary of advantages and drawbacks of each actuation technology

Actuation Technology	Advantages	Drawbacks
Electric motors	High Precision Easy to control Readably available in the market	Not compliant Large Size Heavy Noisy
SEA	High Precision Easy to control Compliant Better force control	Large Size Heavy Complex structure
Bowden Cable	Modularity Simple architecture Easy to reconfigure Low weight on the distal part of the limb	Unidirectional Difficult to model and control
Pneumatic	Lightweight Compliant Have high power density Fast actuation Low cost Easy to manufacture in different shapes and sizes	Poor portability because they require external components Difficult to model and control

In table 2.8, the advantages and disadvantages of the current actuator technology are presented. It is possible to notice that there is no perfect actuator technology, so more research in this area is needed. Moreover, In the future will be interesting to see devices that use different soft actuators technologies that are inherent compliant and lightweight, such as the already mention SEAs, pneumatic, and Bowden cables. But also new technologies that are under research to be used on rehabilitation robots, like Shape Memory Alloys [262], DEAs [263], or TCPs [60], as they will reduce the overall weight and increase the compliance. Furthermore, this new technology can be manufactured in different sizes and shapes [46] that could be easily adapted to robots for children of varying height and ability conditions.

Training strategy

In the case of the training strategy, there is no best strategy, but it rather depends on many factors like the abilities and disease that the children have. For example, passive training is suitable for patients with limited mobility; however, when the children are able to generate movements, it tends to decrease children's participation during the exercise, thus reducing the efficiency of the training [264]. That is why most of the research on the training strategy is centred on assistive training, where the children's participation is

needed. This engagement with the therapy increases the motivation of the children to perform the activities, enhancing the benefits from the therapy [265]. Another advantage of assistive training is that it is used together with video games to increase children's motivation and social interaction [159]. In addition, this strategy is required for assistive devices. It needs to provide the required intensity to generate the movement safely, efficiently, and reliably, depending on the applied force by the user [216]. However, there is no clear which is the best strategy to provide assistive movement, where some examples of different assistive strategies are guidance force, path control, and locomotion strategy [32, 159, 214, 265].

Alternatively, some researchers suggest that resistive training could be more beneficial for rehabilitation therapy than an assistive force, as it increases the engagement of the children, which can help drive motor learning [237, 266]. Hence, further research is required on the optimal training strategy to increase the benefits from the rehabilitation therapies.

Human-computer-interface

The HCIs are essential in developing robotic rehabilitation robots, as they are the medium for the interaction between the children and the robot, impacting the functioning of the actuators and training strategies directly. Thus, HICs are a crucial factor for safety and motivation needs, as it is how the children "communicate" their intention to the robot. Consequently, If the HCI is complex to use, it could lead to the rejection of the device [34]. Furthermore, for safety reasons, the HCI must detect the trigger signal properly and discern between intended movements and involuntary movements, as it can generate undesirable responses [29, 267]. For instance, in the case of CP patients presenting increased muscle tone, rapidly occurring muscle spasms, and severe jerks, which can be considered as a deviation of pattern, causing the robot to apply undesired forces to correct for it or turn off the device suddenly [268].

Consequently, selecting the best HCI for every case needs to be evaluated depending on the capabilities of the children. For example, it could be challenging for patients with advanced muscular dystrophy to use EMG and admittance/Impedance interfaces as their muscles progressively deteriorate, turning unable to activate the muscles to generate a movement or a detectable signal [151, 269]. On the other hand, EEG could lead to a better motor function recovery for children with CP as it integrates the central nervous system into rehabilitation therapy [214]. However, this technology could be hard to implement in patients with a cognitive deficit, requiring concentration [168, 270]. For HCIs, it would be interesting to see more devices using physiological signals as they can also evaluate the efficiency of the therapy [214], novel approaches of body-powered

control to address children with limited mobility of limbs [271], and devices that integrate different HCI strategies to make the system more robust and adaptable [128, 216, 272].

Treated Condition

To better understand how the technology can positively impact children's lives, it is essential to analyse how the rehabilitation robot's technology has addressed the different paediatric conditions that can generate physical disability. Because, even If they share in common the deterioration of the musculoskeletal system, each one of the conditions presents certain specific characteristics that need to be considered.

Most of the research has focused on children with neurological conditions, particularly children with CP. However, it seems likely that many of the designed robots that currently work with neurological conditions could also be utilised in traumatic injury scenarios, especially because they have been designed for rehabilitation therapies that can improve common problems across both neurological and traumatic injuries like ROM deficits and a lack of ability to generate muscle force [143, 153]. Contrarily, neuromuscular diseases present a different scenario than neurological disorders and traumatic injuries as the diseases are progressive, making it hard to obtain a permanent improvement on the children's skills. Thus, the designs have been focused on design devices capable of assisting with exercise and helping with the ADLs to maintain specific abilities (e.g. walking) for a longer period of time [239, 257].

Unfortunately, the outcomes proving the efficiency of rehabilitation robot in children is still scarce, as the pieces of evidence are low and weak. Hence, the information coming from these studies should be asses carefully, as there are very few randomised controlled trials, with small sample sizes and variability in children's ability, outcomes measures, treatment protocols, and used devices [102, 122]. Thus, to better understand if the designed robots fulfil the paediatric needs properly by improving their quality of life and physical ability, more studies and robots designed especially for them are needed. Furthermore, more studies with children presenting different conditions from neurological ones are needed, as it can be noticed that the treated condition impacts the requirements design of the rehabilitation robot.

2.7 Limitations

It was apparent that some studies were conducted with participants from a wide range of ages; therefore, it was difficult to target all the articles that include paediatric participants. Another problem was the upper bound on the paediatric population's age as some papers with the term young adults included paediatric participants.

2.8 Conclusion

While robotic rehabilitation is gaining momentum with increasing numbers of devices being produced for adults, there is a lack of well-designed and effective products available for children. Early examples of robots have often been created by scaling downsize to meet the smaller stature of children. Few robots have been specifically designed and produced, with children being the focus of the project/program. It is apparent that children have special needs, and these need to be incorporated into designs early in the development program. And even if the fulfilment of these needs are closely related to the chosen structural and technological components like the actuator, training strategy and HCI, they go beyond them. Consideration must also be given to the aesthetics that appeal to children and the need for the robot's structure to be as unobtrusive as possible. Without such needs being met, no matter how effective the robot works from an engineering perspective, it will not be utilised well by the child.

It is apparent that there is still a lack of understanding of what the most effective therapy is to improve function and quality of life in specific paediatric conditions (e.g., CP or Stroke). Nevertheless, common impairments (e.g. ROM, strength) must be addressed across numerous clinical conditions if patients improve function in everyday tasks. Hence, there is much opportunity for robots to play a role in assisting paediatric rehabilitation. A much more difficult goal to achieve is the development of robots to assist children. At the same time, they do function-related tasks like walking, sitting, lying, and assisting when the child moves from one posture to another. This demand increased complexity throughout the various engineering systems of the robot. After that, a further challenge lies in the robot being able to assist indoors within a relatively safe environment and outdoors where the "lay of the land" is notably different and less predictable. Hence, exploring new technologies to actuate the system and detect children's intentions when they want to move is necessary.

2.9 Chapter Summary

This chapter exposes the transition in paediatric rehabilitation robotics from end-effector robots to wearable counterparts. However, the prevailing rigid robotics paradigm remains, employing stiff and bulky materials unsuitable for seamless interaction with humans. This constraint becomes more pronounced, especially concerning paediatric users, where weight, safety, and adaptability considerations assume heightened significance to their adult counterparts. This divergence in requirements answers research question one of this work. Furthermore, overcoming these challenges with rigid

robots is inherently difficult. Consequently, investigating soft robotics is a compelling strategy to address these challenges, leading to question two.

Chapter 3 : Soft Wearable Rehabilitation Robots with Artificial Muscles based on Smart Materials: A Review.

3.1 Preface

The content of this Chapter is a copy of the article *"Soft Wearable Rehabilitation Robots with Artificial Muscles based on Smart Materials: A Review"*, published and peer-reviewed in the journal Advanced Intelligent Systems [273].

Until now, the current state of soft robotics still relies on actuator technology, involving motors and fluidic actuators that often require large and heavy components. AMSM offer a promising alternative, as they prevent the need for external components. Their merits, including compliance, adaptability, comfort, safety, and reduced weight, align closely with the difficulties of paediatric applications.

After the literature review, which examined the state of AMSM, acknowledging its emerging developmental stage and the absence of a singular technology possessing all requisite characteristics for widespread adoption in SWRRs, the focus narrowed to TRA AMSMs. These include TCP and SMA AMSMs, distinguished by their prominence in generating force, albeit with a compromise on speed. TCPs were selected for further investigation due to additional merits, such as linearity and cost-effectiveness.

The research presented in the thesis also addresses the critical aspect of correlating AMSM capabilities with biomechanical requirements—a significant advancement given the scarcity of information on biomechanical requirements for SWRRs. Examining how these requirements are met through exoskeleton designs is meticulously presented. The Chapter also highlights the principal challenge encountered by AMSMs in SWRR robots. For TCPs, the drawbacks involve high working temperature, limited working speed, and lower strain than human skeletal muscles. Subsequent experimental interventions were performed to improve these deficiencies in TCPs, which were analysed with results in the following Chapters 4 and 5.

3.2 Abstract

Wearables robots have gained attention for the rehabilitation of people with physical disabilities. However, the current technology relay on heavy and bulky actuation components, making it hard to use outside of clinical settings. AMSMs have gained attention for use in SWRR as they present advantages of compliance, are light-weight,

and do not require external components. Nevertheless, they present challenges that remain unresolved, preventing widespread adoption. This work reviews the current state of SWRR with AMSMs. A literature search was conducted utilizing Web of Science and Scopus. Based on the inclusion-exclusion criteria, fifteen devices were found using four different smart materials. This study attempts to provide an insight into the distinct biomechanical requirements, the use of smart materials, their limitations, their designs and possible future research directions, which can provide helpful guidance on the implementation and development of advanced SWRR with AMSMs.

3.3 Introduction

During the last decade, wearable devices such as exoskeletons have gained popularity [274] in different fields, such as the military [275], industry [276] and rehabilitation [277]. In the latter, rehabilitation exoskeletons are used to restore or maintain the functionality and mobility of people with physical disabilities [19]. These are receiving greater attention as the number of people with disabilities affecting physical performance will increase in the following decades as the population ages and individuals live longer with non-communicable conditions (e.g. CP, Stroke, ABI and Muscular Dystrophies) [95, 278, 279].

Most current exoskeletons use electric motors and rigid links to realize actuation and are often have heavy and bulky designs that are difficult to safely wear outside clinical facilities [29]. Hence, researchers in this area are working develop SWRR, featuring soft actuators that are agreeable to the users as they have increased compliance, adaptability, comfort, safety, and less weight [38, 130, 139].

Currently, SWRR relies mainly upon two soft robotic technologies, cable-driven and fluidic actuators. For a cable-driven system, the wire is embedded into clothes or tubes and attached to an anchor point. The other side of the wire is connected to an electric motor to generate the desired movement and force by pulling the cable [33, 37] (Figure 3.1a). Alternatively, in fluidic actuation (Hydraulic/Pneumatic), a pressurized fluid is inserted into a chamber made of highly deformable material to generate a displacement [38-40] (Figure 3.1b). However, these require large and heavy external pumps and valves to compress the fluid [280]. Unfortunately, cable-driven and fluidic actuation require cumbersome components (e.g. electric motors, pumps, and valves) to work, compromising the portability of the systems when used in daily life [36].

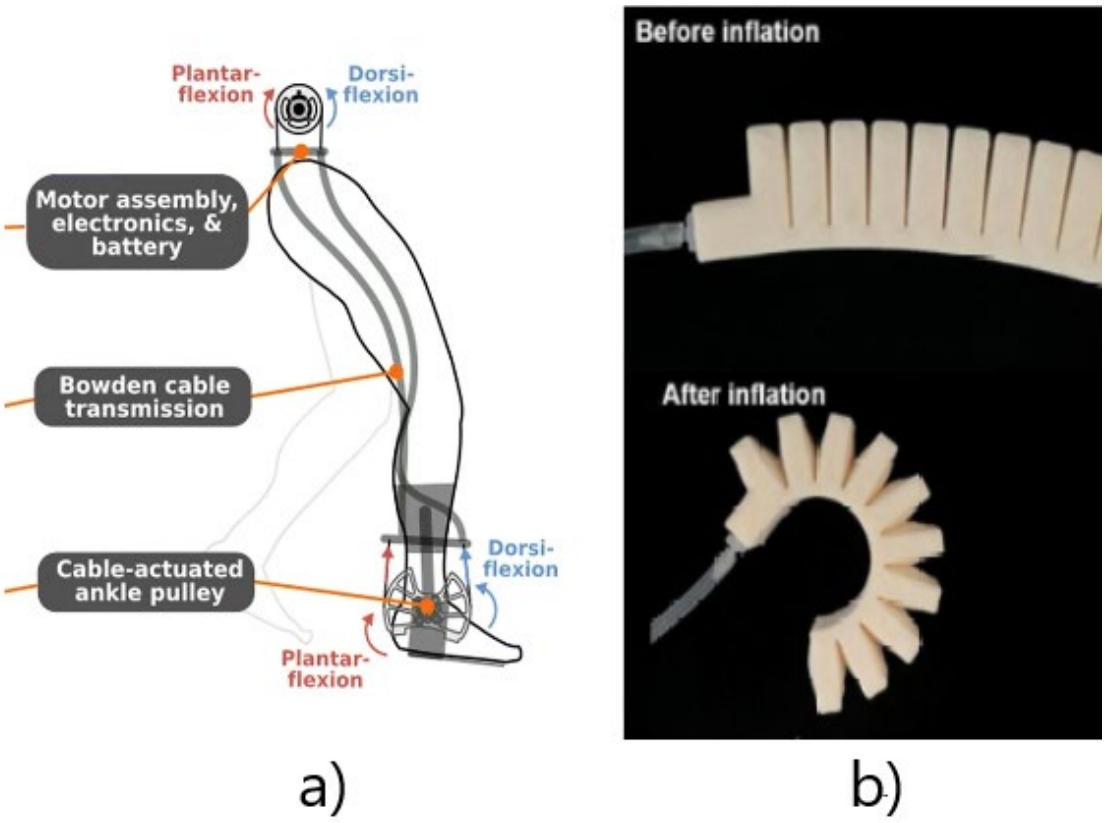

FIGURE 3.1 A) ANKLE FOOT ORTHOSIS CABLE-DRIVEN SYSTEM SCHEMATIC PROVIDING PLANTAR-FLEXION AND DORSIFLEXION ASSISTANCE. REPRODUCED WITH PERMISSION. [37] COPYRIGHT 2019, SPRINGER NATURE. B) PNEUMATIC ACTUATOR BEFORE AND AFTER INFLATION. REPRODUCED WITH PERMISSION. [40] COPYRIGHT 2020, IEEE.

Therefore, in recent years, research has been committed to developing new actuator technologies that can overcome the drawbacks of the current actuators used in SWRR. These technologies include AMSM. AMSM are soft actuators composed primarily of material with a low young modulus similar to that of soft biological materials (10^4-10^9 Pa) that can sense and directly convert physical stimulus (e.g. light, electrical, heat) into physical displacement [41-45]. Some examples of smart materials are SMAs [54], DEAs [51], IPMCs [52], SMPs [55] and TCPs [56]. Due to their inherent properties and manufacturing processes, AMSM can be fabricated in various shapes, allowing them to be embedded into flexible and deformable wearable devices [46-49]. Furthermore, it is possible to fabricate robots with a relatively small weight and volume as they present a power density comparable to the skeletal muscles [50].

Nevertheless, AMSMs for rehabilitation robots are still at the early stage of development. Some drawbacks specific to every smart material (e.g. low speed in SMA and TCPs and low force generation in DEAs and IPMC) need to be tackled if they are to become widespread technology utilized in SWRR [50, 231].

The purpose of this paper was to review SWRR incorporating AMSM; seeks to a) identify the biomechanical requirements for these robots; b) identify the different AMSM technologies utilized; b) identify the AMSM limitations for these robots; c) describe the AMSM enhancement design techniques and d) discuss future trends for development in the field of SWRR based on AMSM.

3.4 Methods

An in-depth literature search was performed, following the search strategy of the Preferred Reporting Items for Systematic Reviews and Meta-Analyses (PRISMA) guidelines [117]. The literature search utilized Scopus and Web of Science databases, using the combination of the following keywords: (Artificial Muscle*) OR (actuat* AND (complian* OR elastic* OR soft)) and (robot* OR wearable OR "active ortho*" OR "active prosthe" OR exoskeleton) and (rehab* OR assistance) not pneumatic*. In order to make our search as complete as possible, a search through the university library databases was also conducted.

To eliminate areas not linked sufficiently with the aims, papers in the following areas were excluded:

- Non-actuated compliant systems
- Non-wearable systems
- Solutions where the soft actuator was relying on electric motors or fluidic systems (e.g., pneumatic and hydraulic) as the source of force generation
- Studies that did not report any mechanical information on the robot
- Studies not related to either assistance or rehabilitation

3.5 Findings

Based on the keywords, 2094 publications were found, with: 1193 publications from Web of Science, 948 publications from Scopus, and 4 from a search on the University library.

First, a check was made for duplicated publications. Thereafter, the abstracts of 1466 publications were screened, and 186 titles were selected for full-text reading. After carefully applying the exclusion criteria to the fully read papers, 36 publications were selected. Among the chosen publications, 8 were reviews, and 28 discussed the development and characteristics of the device (Figure 3.2 shows a flow diagram that illustrates the process of the selection of the papers).

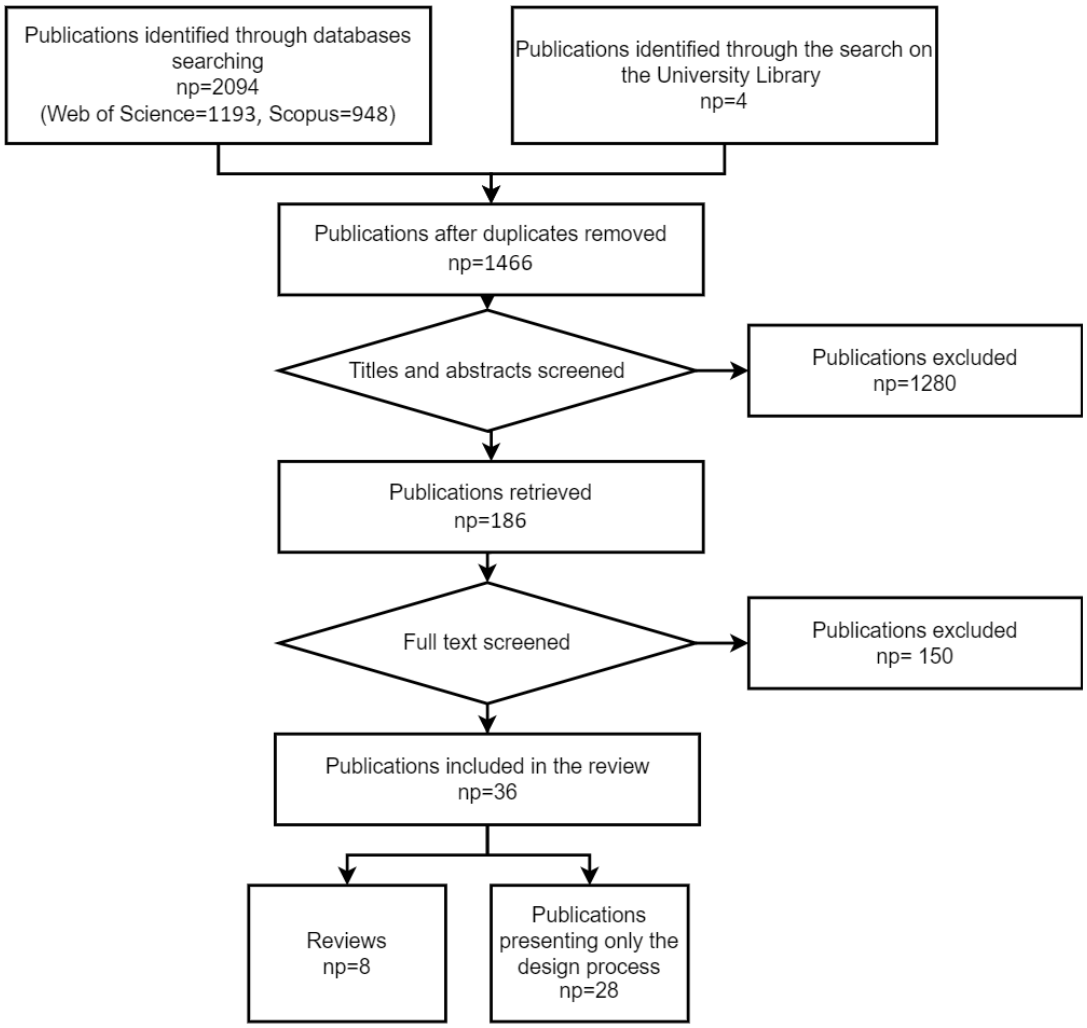

FIGURE 3.2 LITERATURE SEARCH FLOW DIAGRAM

Six of the eight reviews were focused on compliant actuators for rehabilitation systems and partially included AMSM as part of their scope. Peng et al. [42] focused on soft robots for rehabilitation and nursing care, but most of the analysis was centred on soft robots driven by electric motors and pneumatics. Shahid et al. [18] investigated the soft robotic devices designed for hand rehabilitation, where one device based on AMSM was included. Veale et al. [36] analysed the current technology on compliant actuators, addressing the potential of new smart materials to be used in wearable exoskeletons. Zhu et al. [45] look at the developments in soft wearable robots, covering the diverse application of AMSM where rehabilitation robots were included. Bardi et al. [281] researched SWRR for upper limb, where a section of devices using SMA was included. Finally, Aliseichik et al. [282] went through different AMs technologies including sections related to SMA and EAPs. Two reviews focused on specific smart materials, namely the SMA (Nematollahi et al. [283]) or DEA and plasticized PVC gel (Dong et al. [284]) in rehabilitation robots. The difference between the previous review papers and this work

is that the earlier papers only partially covered the SWRR based on AMSM, as their scope was more related to soft actuators in general without a focused analysis of AMSM.

Within the twenty-eight focused articles, four different types of AMSM technologies were found. Moreover, seventeen SWRR were noticed, eleven systems were designed for the upper limb, especially for treating the wrist and fingers, five for the lower limb and one for the face.

3.6 Discussion

This section is divided into five parts. The first part (3.6.1) discusses the different biomechanical requirements used in the design of the SWRR. The second part (3.6.2) presents the different AMSMs and the SWRR that use each technology. The next part (3.6.3) focuses on the challenges that the SWRR faces. Followed by a part that (3.6.4) is concerned with how the robot's design can enhance the AMSM properties. Finally (3.6.5), future developments are discussed.

3.6.1 Biomechanical Considerations

During the last decade, wearable exoskeletons have gained popularity [274] in different fields, like military, industrial and rehabilitation [276]. Each of these fields has different applications and purposes, sometimes with partial overlap. Military exoskeletons are intended to enhance the physical capabilities and increase the mobility of soldiers during load carriage [285]. Industrial exoskeletons focus on augmentation and reinforcing a worker's performance to increase productivity and lower the risk of injury [276]. In contrast, the rehabilitation exoskeleton's purpose is to restore the functionality and mobility of people with a physical disability and whose functional performance is often severely affected [19].

Moreover, another difference between military and industrial robots compared to rehabilitation robots is the range of populations they cover. For instance, military and industrial systems are mainly focused on healthy adults as the beneficiary. Concerning rehabilitation robots, there is a vast spectrum within the target population requiring different amounts of assistance, from children to the elderly [105, 115], different levels of disability [202], and different types of disease [239].

This variability in the target population has led to a different specification for each group as SWRR based on AMSM are in a developmental stage and still present limitations compared to traditional robots [36, 42]. Because of this, it is essential to appreciate the biomechanical requirements to develop a helpful SWRR. Furthermore, it will be valuable to understand the advantages and limitations of each AMSM.

Different biomechanical parameters can severely restrict the range of SWRR that could be utilized in rehabilitation. These parameters are the DOFs (number of planes of motion e.g. flexion, extension supination, pronation at the elbow joint), ROM, frequency (the maximum frequency that the actuator can be excited continuously), angular velocity (maximum during functional activity), the torque produced, device/system weight and control scheme [286]. These parameters change depending on the joint, as each of them moves limbs with different mass and lengths, often with different moments of inertia and is used to perform different activities. In tables 3.1-3.7, the biomechanical parameters of the biological joints and the SWRRs are presented to allow easy comparison between them.

Degrees of Freedom (DOF)

In respect of planes of motion, most robot DOFs vary from one to three, depending on the joint. Only three devices have covered all the DOFs observed in human joints. Of note, more DOFs are apparent in robots for the upper limb. This could be explained by the upper limb ADLs often requiring greater ranges of motion in multiple planes to perform different tasks like grasping and reaching [287]. In contrast, during many gait activities, the requirement for a larger range of motion is predominantly in the sagittal plane [73].

Range of Motion (ROM)

For ROM, two different values could be considered, the overall ROM and the ROM required to meet the demands of most tasks. The overall ROM is the maximum value that a joint can reach in a plane. In contrast, the activity ROM is the range of motion needed to perform a specific activity, which can be much less than the whole ROM of the joint (Table 3.1-3.7).

Therefore, in SWRR development, it is essential to know the ROM requirements for the tasks to be assisted [73, 287]. As the AMSM is starting the developmental phase, it is reasonable to focus on specific and uncomplicated tasks [288]. With this in mind, it may be easier to develop simple robots that can achieve the practical demands of the patient [289]. For example, consider the hip joint in the sagittal plane during flexion-extension movement, the full ROM is from ~120° flexion to ~20° extension. Yet, during walking, the required range would be approximately 40° flexion to 11° extension.

Joint Forces and Torques

For AMSM to generate the ROMs sufficient to undertake tasks often performed in daily living, it must be able to generate sufficient forces/torques. These forces need to overcome those associated with gravity and the inertia of the limb being moved. In most research in this area, the reported value was torque. However, for the hand, some devices have been developed to replicate/ generate the force required for grasping and pinch activities. In the case of facial expressions, as with the finger joint, it is not measured on torque but the force that muscles generate in a direction to generate facial expressions.

Regarding torques, as with ROM, two different values are most often considered by developers. Firstly, torque levels occurring during ADLs and the minimum torque that would move the limb against gravity. Interestingly, the ADLs torques are similar or less for many activities in the upper limbs than the passive torques. For example, considering the wrist in ADLs, the necessary torques were less than 1 Nm in all directions, but in the case of torque required to move it against gravity, they were in the order of 1.5N m [262, 290, 291]. In contrast, in the lower limb, some muscles need to activate to a sufficient level to carry the person's body weight in the stance phase of gait activities and, at the same time, generate appropriate torque to produce the joint motion required for the gait activity being performed. For instance, the bigger discrepancy occurs during ankle plantarflexion, where a peak torque above 100 Nm is required, while for passive movement, the required torque is around 5 Nm [78, 176].

Frequency and Angular Velocity

Human movements are dynamic tasks, and therefore these are characterized by temporal parameters like angular velocity and frequency of the movements. Even if these are related to each other, these are different concepts, and ideally, both should be reported. Angular velocity is the rate of flexion and extension of a joint, while frequency is related to the maximum trackable sinusoidal frequency of the amplitude of the movement. It is possible to approximate the angular velocity from the frequency with the next formula:

$$\omega = \lambda * 2 * F \tag{3.1}$$

Where ω is the angular velocity in °/s, λ is the amplitude of the sinusoidal wave in degrees and F is the frequency in Hz. In the case of the velocities is possible to notice that it varies depending the on the extremity from around 120 °/s in the case of the ankle to more than 400 °/s for the elbow (Tables 3.1 and 3.7). However, in the case of the

frequencies, they remain similar, around 1.5 Hz [61]. This could be related to the fact that speeds are not constant during the movement, while the frequencies are related to the median speed of a movement limited in a specific ROM. In the case of the SWRR, when the frequency is provided is essential to look at the amplitude to estimate how fast a device is.

Control strategies

The control strategy is a crucial element during the design process of SWRR. The control strategy's objective is to track the device's trajectory [138] and/or forces [292] to plan the desired action to apply a stimulus to the actuator later to generate a movement. This process is similar to the motor control of the human body, where the central nervous system plans the movement base on the sensory information and sends the command to drive the muscles [293]. From the founded devices is possible to identify mainly three different control strategies, pulses, state machine and PID controllers.

The pulse strategy is an open-loop control strategy as the system's output depends on the input, but the input is independent of the output. This scheme consists of applying a pulse or steps to generate a certain level of force or displacement from the AMSM. However, there is no feedback. Thus, it is impossible to compensate for the influence of external stimuli [60, 263].

In the case of the state machine, the device can change between different states in response to an event. The simple state machine is an on-off switch that changes based on an external stimulus, such as the change between the gait swing and stance phases [294].

PID is a closed-loop control mechanism employing feedback from the system output. The controller is continuously calculating an error value between the reference signal and the output and then applies a correction. PIDs are used to reject disturbances and to implement setpoint changes [262].

Weight

The weight of the AM and overall device is critical to establishing its usability by patients. Excessive weight can negatively affect the motion of the limbs as significant weight generates inertial forces that increase energy consumption and could make it uncomfortable and unsafe for patients to use [82]. For instance, the threshold for an acceptable weight on the hand and forearm is around 400 g to 500 g [295]. Furthermore, in the case of the lower limbs, a weight of 4 kg on foot doesn't seem to affect the gait kinematics. However, the net metabolic rate increased by 36 % [296].

3.6.2 Soft wearable rehabilitation robots

While biomechanical considerations are the main factors to consider in the design of SWRR, the system's capabilities depend more on the functional properties of the AMSM that are inherited from the material used to fabricate them. In this section, the different systems are presented and arranged by the material used to manufacture them to understand the advantages and disadvantages of each AMSM technology applied to SWRR.

Tables 3.1-3.8 presents the material utilized, the system's weight, the control strategy, the ROM at the joint involved, frequency of motion, typical joint angular velocities, and the associated torques. These parameters are presented within subsections related to body parts upon which systems were designed.

Table 3.1 Shoulder Soft Wearable Robots Biomechanical Properties

Research group	Material	DOF	ROM [°]	Torque/ Force	Frequency	Angular velocity [°/s]	Control strategy	Weight [Kg]
Human Body [231, 291, 297, 298]	Skeletal muscle	3	Typical values -60 to 180 Extension/ Flexion 0 to 180 Adduction/ Abduction	Minimum to lift the patient's limb against gravity 79.9 Nm Flexion 74.9 Nm Extension 73 Abduction 76.4 Adduction	Typical values < 20 Hz	Typical values > 50	N/A	N/A
			ADLs -18.3 to 62.3 Extension/ Flexion -14 to 133.6 Adduction/ Abduction	ADLs 9.6 Extension/ Flexion 10.05 Adduction/ Abduction	ADLs ≈ 1.1 Hz	ADLs 100 Extension/ Flexion 171.5 Adduction/ Abduction		
KAIST [59]	SMA (Spring)	1	90 Abduction	10.1 Nm	N/A	18	N/A	0.675 Wearable assembly

Table 3.2 Elbow Soft Wearable Robots Biomechanical Properties

Research group	Material	DOF	ROM [°]	Torque/ Force	Frequency	Angular velocity [°/s]	Control strategy	Weight [Kg]
Human Body [231, 262, 287, 290, 291, 299]	Skeletal muscle	3	Typical values 0 to 150 Flexion/ Extension -120 to 120 Pronation/ Supination	Minimum to lift the patient's limb against gravity ≈ 3.5 Nm Flexion/ Extension ≈ 1.85 Nm Pronation/ Supination	Typical values < 20 Hz	Typical values > 50	N/A	N/A
			ADLs > 81 Flexion/ Extension -13 to 53 Pronation/ Supination	ADLs ≈ 3.7 Nm Flexion/ Extension ≈ 0.04 Nm Pronation/ Supination	ADLs ≈ 1.25 Hz	ADLs < 135 Flexion/ Extension < 486 Pronation/ Supination		
University of Delaware[a)] [263]	DEA	1	19.5	1 N (applied) weight applied to the arm	N/A	16.2	Pulse train	N/A
Carlos III University of Madrid [262]	SMA	2	0 to 120 Flexion/ Extension -50 to 50 Pronation/ Supination	3.5 Nm Flexion/ Extension 1 Nm Pronation/ Supination	100° at 0.2 rad/s (0.0318 Hz)	N/A	BPID	< 1 (2.9 with power supply)
KAIST [300]	SMA (spring)	2	60 to 150 Flexion -27.6 to 27.6 Pronation/ Supination	3.2 Nm Flexion/ Extension 0.5 Nm Pronation/ Supination	N/A	Full movement in 10 s	Step signal	1.55 Wearable assembly

Table 3.2 Elbow Soft Wearable Robots Biomechanical Properties (continued)									
Korea Institute of Machinery and Materials[301]	SMA (spring)	1	Strain of 26.1 % (47 mm contraction)	80 N		N/A	Full movement in ≈ 5 s (With cooling system and an agonist-antagonist configuration)	Step signal	0.57 Total

[a)] Biomechanical Properties based on children 2 years old

Table 3.3 Wrist Soft Wearable Robots Biomechanical Properties

Research group	Material	DOF	ROM [°]	Torque/ Force	Frequency	Angular velocity [°/s]	Control strategy	Weight [Kg]
Human Body[231, 287, 290, 291, 302]	Skeletal muscle	2	Typical values -38 to 40 Flexion/ Extension -38 to 28 Ulnar deviation/ Radial deviation	Minimum to lift the patient's limb against gravity 1.43 Nm Flexion/ Extension 1.43 Nm Ulnar deviation/ Radial deviation	Typical values < 20 Hz	Typical values > 50	N/A	N/A
			ADLs -38 to 40 Flexion/ Extension -38 to 28 Ulnar deviation/ Radial deviation	ADLs ≈ 0.2 Nm Flexion/ Extension ≈ 0.3 Nm Ulnar deviation/ Radial deviation	ADLs 1-5 Hz	ADLs < 232 Flexion/ Extension < 203 Ulnar deviation/ Radial deviation		
MENRVA[63]	TCP	1	N/A	0.3 Nm	≈13 N at 0.1 Hz	N/A	PID	N/A
Carlos III University of Madrid [303]	SMA	2	80 Flexion/ Extension -45 to 45 Ulnar deviation/ Radial deviation	0.5 Nm in both directions	50° at < 0.04 Hz Extension 40° at ≈ 0.04 Hz Ulnar deviation/ Radial deviation	N/A	BPID	0.960 Total

Table 3.3 Wrist Soft Wearable Robots Biomechanical Properties (continued)

KAIST [304]	SMA (Spring)	2	-33.8 to 30.4 Flexion/ Extension 21.4 to 15.4 Ulnar deviation/ Radial deviation	1.32 Nm Extension 0.61 Nm Flexion 0.90 Nm Radial deviation 0.62 Nm Ulnar deviation	80° at 0.5 Hz	N/A	Step signal	0.151 Wearable assembly (Whole device ≈ 1)

Table 3.4 Hand (Fingers) Soft Wearable Robots Biomechanical Properties

Research group	Material	DOF	ROM [°]	Torque/ Force	Frequency	Angular velocity [°/s]	Control strategy	Weight [Kg]
Human Body [231, 305, 306]	Skeletal muscle	3 DOF Each finger	Typical values Index finger DIP = 70 PIP = 100 MCP = 90	Pinch of 1.4N to 31.4 N	Typical values < 20 Hz	Typical values > 50	N/A	N/A
					ADLs > 1 Hz			
University of Pisa [307]	DEA	1	N/A	1 N	N/A	N/A	Step signal	N/A
Bio-robotics and Smart Systems Laboratory [60]	TCP	3 DOF Each finger	Index finger DIP = 11 PIP = 21 MCP = 41	2 N	N/A	Full movement in 25 s (Pulsed 2s)	Step signal/ Pulsed actuation	≈ 0.1 Wearable assembly
Universidad Iberoamericana [62]	TCP	1	N/A	3 N	N/A	N/A	Step signal	N/A

Table 3.5 Hip Soft Wearable Robots Biomechanical Properties

Research group	Material	DOF	ROM [°]	Torque/ Force	Frequency	Angular velocity [°/s]	Control strategy	Weight [Kg]
Human Body [231, 308-311]	Skeletal muscle	3	Typical values -122 to 22 Flexion/ Extension -44 to 26 Abduction/ Adduction -33 to 34 Median rotation/ Lateral rotation	Minimum torque to lift the patient's limb against gravity 80 Nm (120° flexion) ≈ 10 Nm (40° Flexion)	Typical values < 20 Hz	Typical values > 50	N/A	N/A
			ADLs -37.8 to 10.5 Flexion/ Extension -9.7 to 6.9 Adduction/ Abduction -1.0 to 11.2 Median rotation/ Lateral rotation	Walking 80 Nm Flexion 65 Nm Extension 111 Nm Abduction 68 Nm Adduction 13 Nm Internal rotation 18.35 Nm External rotation	ADLs > 1.05 Hz	Walking < 115 Extension < 195 Flexion		
Zhejiang University of Technology [294]	PVC	1	N/A	≈ 70 Nm Flexion	N/A	N/A	State machine	0.6 Wearable assembly and 0.8 for the controller and the battery

Table 3.6 Knee Soft Wearable Robots Biomechanical Properties

Research group	Material	DOF	ROM [°]	Torque/ Force	Frequency	Angular velocity [°/s]	Control strategy	Weight [Kg]
Human Body [61, 309, 311, 312]	Skeletal muscle	1	Typical values -134 to 1 Flexion/ Extension	Passive Torque ≈ 50 Nm (≈ 50°)	Typical values < 20 Hz	Typical values > 50	N/A	N/A
			Walking -64.6 to 0 Flexion/ Extension	Walking 45.15 Nm	ADLs ≈ 1.15 Hz	Walking ≈ 360 Extension ≈ 300 Flexion		
Wyss Institute[a)] [313]	SMA (spring)	1	-34 to 0 Flexion	N/A	N/A	2.56	Step signal	N/A

[a)] Biomechanical Properties based on children 4 years old

Table 3.7 Ankle Soft Wearable Robots Biomechanical Properties

Research group	Material	DOF	ROM [°]	Torque/ Force	Frequency	Angular velocity [°/s]	Control strategy	Weight [Kg]
Human Body [61, 73, 78, 176, 311]	Skeletal muscle	3	Typical values -55 to 20 Plantarflexion/ Dorsiflexion -23 to 12 Inversion/ Eversion	Passive Torque ≈ 5 Nm (10°) Dorsiflexion ≈ 5 Nm (30°) Plantarflexion	Typical values < 20 Hz	Typical values > 50	N/A	N/A
			Walking -20 to 10 Plantarflexion/ Dorsiflexion	Walking Plantarflexion ≈ 110 Nm	ADLs ≈ 1.75 Hz	Walking ≈ 310 Plantarflexion ≈ 190 Dorsiflexion		
CNR Institute for Energetics and Interphases at Lecco [314, 315]	SMA	1	-5 to 20 Plantarflexion/ Dorsiflexion	15 N with a lever arm of 10 cm (Torque = 1.5 Nm)	N/A	N/A	Square pulse	N/A
State Key Laboratory of Mechanism System and Vibration [316]	SMA	1	-16 to 16 Plantarflexion/ Dorsiflexion	10.9 Nm	16° at 1 Hz	N/A	SBH Feedforward + PID	N/A
Ajou University [317, 318]	SMA	1	20 Plantarflexion	1 Nm	N/A	100 contraction	Step signal	0.428 g Without power supply

Table 3.8 Facial Soft Wearable Robots Biomechanical Properties

Research group	Material	DOF	Displacement	Torque/ Force	Frequency	Angular velocity [°/s]	Control strategy	Weight [Kg]
Human Body [319]	Skeletal muscle	N/A	N/A	1.1-3.5 N	N/A	N/A	N/A	N/A
Artificial Intelligence Laboratory [320]	SMA	N/A	20 mm	N/A	N/A	N/A	Feedback controller	N/A

Dielectric elastomer actuators

EAPs are polymers that can be stimulated to change their shape using electrical energy. One of the most common types of EAPs is DEAs [321]. They consist of a compliant capacitor composed of a thin elastic dielectric film coated on both surfaces by compliant electrodes. When DC voltage is applied to the electrodes, both attract each other, increasing the pressure over the dielectric film (Maxwell pressure) due to the electrostatic force while reducing thickness and area expansion (Figure 3.3) [284, 322]. Maxwell pressure is related to the permittivity of the material and the strength of the applied electric field. The relation can be expressed as:

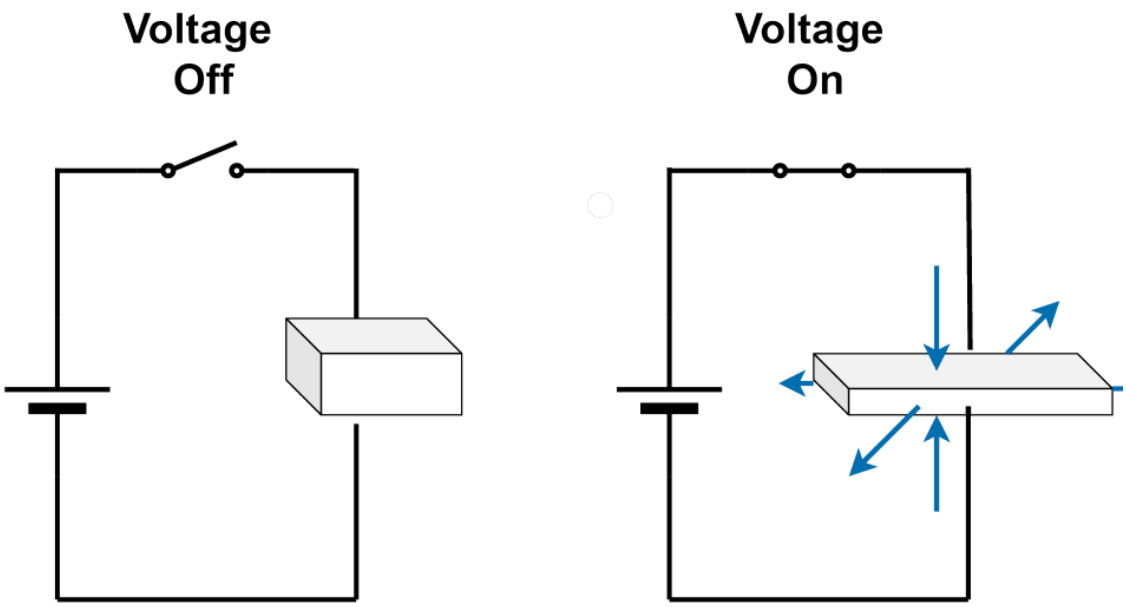

FIGURE 3.3 WORKING PRINCIPLE OF THE DEAS, WHEN A VOLTAGE IS APPLIED A MAXWELL PRESSURE IS GENERATED BETWEEN THE ELECTRODES

$$P = \varepsilon_0 \varepsilon_m E^2 = \varepsilon_0 \varepsilon_m (\frac{V}{d})^2 \quad (3.2)$$

Where P is the Maxwell pressure, ε_0 is the vacuum permittivity, ε_m is the material permittivity, E is the electric field strength that depends on the applied voltage V and the thickness of the film d.

DEAS IN WEARABLES DEVICES

DEA actuators are one of the most studied AMSMs due to their properties that, in most cases, surpass those of the muscle, with strain approaching 200 %, a high bandwidth up to the range of kilohertz, and high efficiency [14, 50, 231], which are all desirable properties for SWRR. However, they have limitations when placed in robotic applications that interact with people. DEAs need high voltage, in the order of hundreds of volts,

requires bulky and expensive electronics and are considered unsafe. Nevertheless, DEAs are challenging to produce in a compact size to generate appropriate amounts of power and force [36, 322].

Two different research groups developed SWRR with this AMSM. Carpi et al. [307] developed a hand rehabilitation device based on folded DEAs to generate flexion and extension movements at the finger joints actively. The structure of the hand-split consists of a plastic-made wrist guard with support for the actuator in combination with an aluminium rod. Three folded DEAs actuators were connected to a miniature DC to High Voltage DC converter to provide the required high voltage. The converters were able to supply voltage in the range of 0-10Kv. With this configuration, the device could generate forces in a range of 1N and a contraction of 7 % to the original length using an input voltage ranging from 0 to 6Kv.

Behboodi et al. [263] designed a platform for paediatric rehabilitation to generate flexion and extension movements of the elbow joint (Figure 3.4). The device used a bundle of stacked DEAs [322], with three parallel fibres consisting of 5 stacked DEAs in series. The bundle of actuators was mounted on a mannequin resembling the elbow joint of a 2-year-old child, and it was able to flex the elbow 19.5° with an angular velocity of 16.2 °/s. These results were obtained by applying a square signal with 1230 V amplitude.

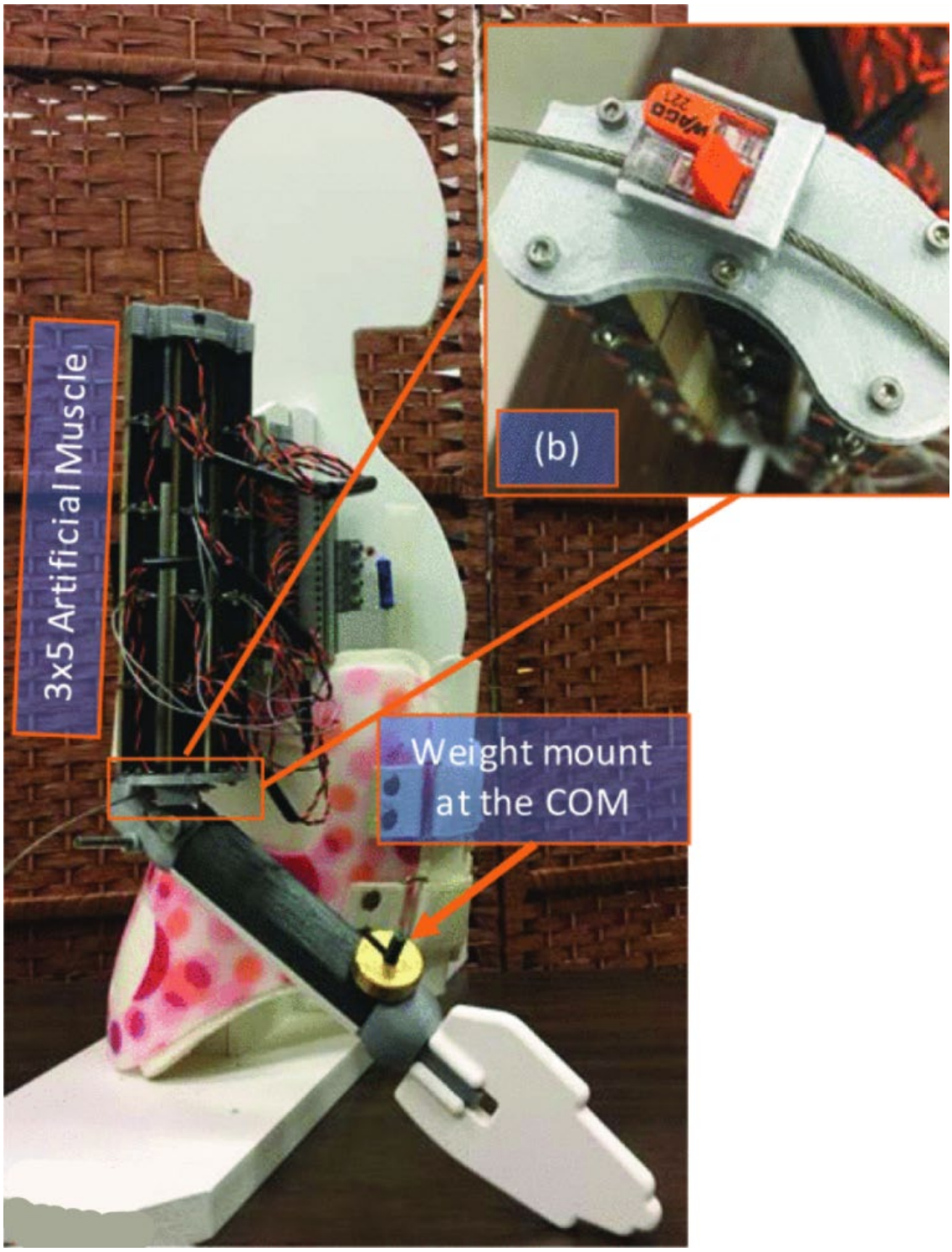

FIGURE 3.4 EXAMPLE OF AN SWRR BASED ON DEAS. REPRODUCED UNDER THE TERMS OF THE CC BY LICENSE. [263] COPYRIGHT 2020.

Plasticized Polyvinyl Chloride gel actuators

Plasticized PVC gel actuators are EAPs similar to DEAs. PVC gels are produced by thermally or chemically melting PVC resins with liquid plasticizers. When PVC gel is placed between electrodes and an electric field is applied, a creeping deformation on the anode can be observed, and when the electric field is discharged, the PVC gel returns

to its original shape [323, 324] (Figure 3.5). The creep deformation can generate different types of deformation like bending, crawling and linear contractions [53].

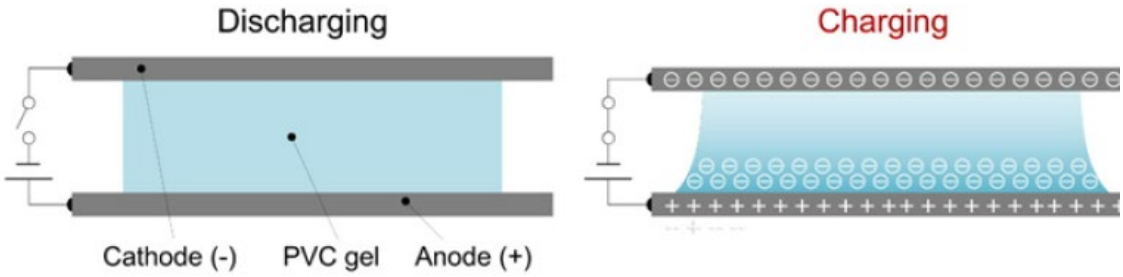

FIGURE 3.5 DEFORMATION MECHANISM OF PVC GEL WHEN AN ELECTRIC STIMULUS IS APPLIED. REPRODUCED UNDER THE TERMS OF THE CC BY LICENSE. [324] COPYRIGHT 2015.

Hashimoto et al. [325] developed an AMSM from PVC gel able to generate contractions. The PVC gel was sandwiched between a stainless mesh that acted as an anode, while a stainless foil served as a cathode. The cathode was located under the PVC gel, and the anode was above the gel. When the electric field is applied, the PVC gel creeps up the anode and moves into the mesh. The PVC electro-mechanical dynamics can be modelled as:

$$\frac{\alpha}{T_\alpha s + 1} * \frac{1}{R_1 R_2 C s + R_1 + R_2} E(s) = \beta X(s) + F_{ext}(s) \tag{3.3}$$

where $X(s)$ and $F_{ext}(s)$ are the contraction strain and output stress, respectively. $E(s)$ is the applied electric field. The terms R_1, R_2 and C are the resistances and capacitance from an equivalent electric circuit. T_α is the time constant of the system. α and β are gains that can be determined from the experimental results.

PVC GELS IN WEARABLE DEVICES

PVC gel actuators are a promising technology to be used as AMSM for SWRR, with their main advantages being relatively high actuation frequency (about 9 Hz), high strain (75 %), low power consumption (2.9 $\mu W/mm^2$) and a very long-life span (> 5 million cycles). However, they require high voltages to work (~3600 v), have low stress (0.6 MPa) and additionally, the electro-mechanical deformation mechanism is not fully understood, making it challenging to generate controlled joint movement [53, 294].

Only one SWRR has used this technology (Figure 3.6). Yi Li and Minoru Hashimoto are pioneers in using PVC gel actuators for wearable devices. In 2015, they presented their first prototype of a wearable system to assist in hip joint motion while walking [326]. Their latest development has been to upgrade the system with a new actuation unit [294]. The

actuation unit had a length of 200 mm, and to ensure appropriate fitting to the human body, it had a curved shape to mold more accurately to the body part. The whole device (for two legs) weighed 2 Kg (0.6 per actuation unit + 0.8 Kg for the control unit, including the battery). When the whole system was tested using a voltage of 400 V, the displacement of the assistive device was approximately 16 mm (8 %), the maximum output force was around 94 N, the response time was approximately 56 ms, and the power consumption was around 1.6W. The device was activated through a state machine controller strategy, switching the assistance on and off during the swinging and stance phase, respectively.

FIGURE 3.6 EXAMPLE OF AN SWRR BASED ON PVC GEL ACTUATOR. REPRODUCED WITH PERMISSION. [327] COPYRIGHT 2016, IEEE.

Twisted and Coiled Polymer Actuators

TCP actuators have emerged as a promising AMSM technology for SWRR. TCP actuators are constructed by continuously twisting polymer fibres or filaments (e.g. nylon fishing lines and sewing threads) until they form coils. The actuator works by converting a temperature change into strain or stress. In general, TCP actuators are driven by Joule heating (Figure 3.7a), adding a layer of a conductive material (e.g. silver) over the precursor fibre [328, 329] or by embedding a resistance wire within the actuator [330,

331] (Figure 3.7b). Consequently, the actuator can be modelled as an electro-thermal-mechanical system. The electro-thermal dynamics can be represented as a first-order linear system represented as [332, 333]:

$$C_{th}\frac{dT}{dt} = P(t) - \lambda(T - T_0) \tag{3.4}$$

where C_{th} and λ are the actuator's thermal mass and absolute thermal conductivity, respectively. T is the actuator's temperature, T_0 is the ambient temperature, and P(t) is the electrical input applied at a specific time t. To quantify the speed of the dynamics, the time constant, $\tau = \frac{C_{th}}{\lambda}$ can be adopted. τ can be obtained by examining the actuators' rise and fall response and is equal to the average time the actuator takes to reach the 63 % of a steady-state value given a step input under a steady-state condition.

In the case of the thermo-mechanical properties, this can be described as a spring-damper system with an added temperature-dependent term, which is expressed as:

$$F = k(x - x_0) + b\dot{x} + c(T - T_0) \tag{3.5}$$

Where x and x_0 are the loaded lengths and resting length of the actuator, respectively. K represents the stiffness, b is a damping term, and c denotes the thermal constant. Under steady conditions where $\dot{x}$=0, the overall model can be obtained by combining (3.4) and (3.5):

$$F = k(x - x_0) + \frac{c}{\lambda}P \tag{3.6}$$

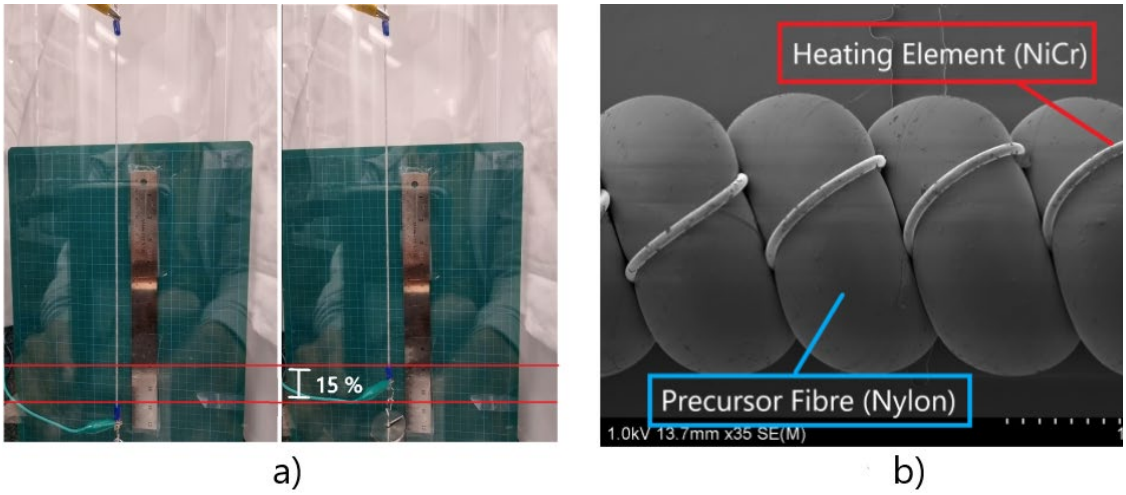

FIGURE 3.7. A) TCP ACTUATOR LIFTING A 1 KG LOAD BY 15 % STRAIN AFTER HEAT IS APPLIED. B) SCANNING ELECTRON MICROSCOPE IMAGE OF A NYLON TCP ACTUATOR WITH A NICR EMBEDDED WIRE AS THE HEATING ELEMENT.

TCPS IN WEARABLES DEVICES

TCPs are a recent discovery [334]. They have gained significant attention in the field of SWRR, with advantages such as high-power density (27 W/g) and stress (10 MPa), linear behaviour, and a high strain (21 %). In contrast, their main disadvantages are low efficiency (~1 %) [50, 56, 231] and the low frequencies (<3 Hz) at which they operate. Three promising examples of wearable devices based on TCPs were founded:

The assistive wrist orthosis developed by Sutton et al. [63] used an arrangement of 16 TCPs wires made of silver-coated Nylon 6.6 sewing thread (Figure 3.8a). The splint prototype consisted of 3D printed parts to mount the device on the arm and attachments for the nylon actuators. The device was designed to have one DOF and provide a torque of 0.3 Nm on the wrist joint in the flexion direction. The final prototype was able to produce torques around 0.32 Nm in 3.9s. Using a PID controller, the system could track a 0.1Hz with an amplitude of 10 N during actuation very closely, but during the relaxation time, the error increased due to the slow response time during the cooling down phase.

The group of Saharan et al. [60] designed iGrab, an ergonomic orthotic device powered by TCPs, to assist flexion and extension movement of the fingers. The prototype comprised 3D printed parts and sewn parts with artificial tendons routed from the fingers to the wrist using polytetrafluoroethylene (PTFE) pipes. The tendons were connected with a metallic ring to the TCPs mounted on a forearm bracelet. The TCP muscles were wrapped around frictionless pulleys to utilize long actuators. Furthermore, to improve the energy consumption, the extension motion was facilitated with the help of rubber strips. When a 0.6 A step signal was applied to the TCPs, the fingers were able to reach their maximum displacement after 25 s (i.e. the index finger was able to move 40° for the MCP joint, 21° for the PIP joint and 11° in the case of the DIP joint). The results were improved when a pulsed signal was used, reducing the actuation time from 25 s to less than 5 s.

Patiño et al. [62] also developed a wearable orthosis for hand rehabilitation movements, with a TCP actuator on each finger (Figure 3.8b). The exoskeleton is composed of two main parts fitted to the dorsum of the hand and the fingers. The dorsum of the hand was composed of five 3D printed plates, of which four are aligned with the fingers and one more adjustable plate that serves to fit the device to the user's hand. In the case of the fingers, each of them is composed of a silicone tube containing a TCP and a filament strain sensor. The TCP inside the finger structure could produce forces of around 3 N when a step input of 0.3 A was applied.

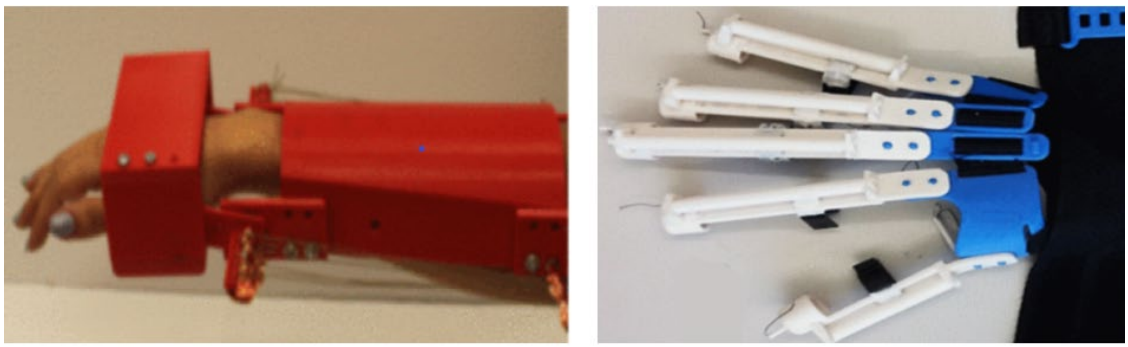

a) b)

FIGURE 3.8 EXAMPLES OF SWRR BASED ON TCP, A) MENRVA GROUP SWRR FOR WRIST. REPRODUCED WITH PERMISSION. [63] COPYRIGHT 2016, IEEE). B) UNIVERSIDAD IBEROAMERICANA SWRR FOR HAND. REPRODUCED WITH PERMISSION. [62] COPYRIGHT 2018, IEEE).

Shape Memory Alloys

SMAs are metallic materials that use the memory effect property to generate motion. The shape memory property is defined as the material's property to recover a previously described shape when an external stimulus is applied. Nickel-Titanium alloys are the most popular SMAs, and they recover their original "memorized" shape after being deformed when heated above their transformation temperature [283, 335] . SMA can be used as single fibres (Figure 3.9a) or as springs (Figure 3.9b) to generate linear displacement. SMA elements are generally heated through the Joule effect, where an electric current is applied to the SMA actuator. However they present a high thermal hysteresis between the transition that occurs from martensite (low temperatures) to austenite (high temperatures) and the one occurring from austenite to martensite [336] (Figure 3.9c). When using a model is essential to take into consideration the nonlinear hysteresis properties of the material as the system's behaviour in both phases is different. [316, 337].

Zhang et al. [316] propose a sigmoid-based hysteresis model for single SMA fibre where he introduce two different sigmoidal curves representing the major hysteresis properties:

$$y = \frac{k\,(\sigma, f)}{1 + e^{-a_+(\sigma,f)[u - r_+(\sigma,f)]}}\ For\ \dot{u} \geq 0 \tag{3.7}$$

$$y = \frac{k\,(\sigma, f)}{1 + e^{-a_-(\sigma,f)[u - r_-(\sigma,f)]}}\ For\ \dot{u} < 0 \tag{3.8}$$

Where u is the input voltage, y is the output displacement. k, represent maximum displacement. σ, signifies the prestress applied to the fibre. f, denotes the driving frequency. $a_{+/-}$ and $r_{+/-}$ represent curve slopes and voltage values at peak

transformation of martensite to austenite and austenite to martensite. Besides, the hysteresis gap can be represented by $\Delta r(\sigma, f)$, which is defined as follow:

$$\Delta r(\sigma, f) = r_{+}(\sigma, f) - r_{-}(\sigma, f) \tag{3.9}$$

In order to compensate for the minor hysteresis properties two suitable scaling factors $\beta_{+/-}$ (where $\beta_{+/-} \in [0,1]$) are introduced. Hence Equations 3.7 and 3.8 can be rewrote as:

$$y = \beta_{+} \frac{k\,(\sigma, f)}{1 + e^{-a_{+}(\sigma,f)[u - r_{+}(\sigma,f)]}}\ For\ \dot{u} \geq 0 \tag{3.10}$$

$$y = \beta_{-} \frac{k\,(\sigma, f)}{1 + e^{-a_{-}(\sigma,f)[u - r_{-}(\sigma,f)]}} + (1 - \beta_{-})k\,(\sigma, f)\ For\ \dot{u} < 0 \tag{3.11}$$

For SMA springs, Koh [337] introduced a model derived by combining the conventional coil spring equation and a large deformation term for the austenite (3.12) and martensite (3.13) phases, respectively:

$$F_A = \frac{G_A d^4}{8D^3 n}\left(\frac{cos^3\alpha_i}{cos^2\alpha_{AF}(cos^2\alpha_{AF} + sin^2\alpha_{AF}/(1+v))}\right)\delta_A \tag{3.12}$$

$$F_M = \frac{G_A d^4}{8D^3 n}\left(\frac{cos^3\alpha_i}{cos^2\alpha_{MF}(cos^2\alpha_{MF} + sin^2\alpha_{MF}/(1+v))}\right)\delta_M - \frac{\pi d^3}{8D} G_M \gamma_L \xi_{S\gamma} \tag{3.13}$$

Where the material properties are: G, the shear modulus, v, the Poisson´s ratio and γ_L, the residual strain. Then the design parameters determined by the user are: d, wire diameter, D, the coil diameter, α_i, initial pitch angle and n, the number of the coils. Lastly the variables are F, the force, $\xi_{S\gamma}$, the detwinned martensite volume fraction, that changes with temperature and stress, δ, the displacement and αf, the final pitch angle. Subscripts A and M denote the austenite and the martensite, respectively.

The deformation of the coil can be represented with δ, αf, γ. Although this variable are dependent variables, combining them complicates the equations. The pitch angle αf is the term that describes the large deformation of the spring, the δ is the original spring force-displacement and γ is the shear strain for the detwinning term. Equations, to describes the relationship of these three variables are provided so that they can be converted as needed. αf can be converted to δ with Equation (3.14). Also, the final pitch angle can be converted to γ with Equation (3.15):

$$\delta = \frac{\pi n D}{cos\alpha_i}\left(sin\alpha_f - sin\alpha_i\right) \tag{3.14}$$

$$\gamma = \frac{d}{D}\frac{cos^2\alpha_i(\sin\ \alpha_f + sin\ \alpha_i)}{cos^2\alpha_f\left(cos^2\alpha_f + \frac{sin^2\ \alpha_f}{1+v}\right)} \tag{3.15}$$

Furthermore the F can be converted to τ with Equation (3.16):

$$\tau = \frac{8DF}{\pi d^3} \tag{3.16}$$

The detwinned martensite volume fraction ($\xi_{S\gamma}$) is commonly a function of τ and temperature. However, to simplify the model $\xi_{S\gamma}$ is modified to be a function of γ as follows:

$$\xi_{S\gamma} = \frac{1}{2}\cos\left(\frac{\pi}{\gamma_s^{cr} - \gamma_f^{cr}}\left(\gamma - \gamma_f^{cr}\right)\right) \tag{3.17}$$

Where γ^{cr} is critical strain for detwinning start (γ_s^{cr}) and finish γ_f^{cr}, which a property the SMA. Summarizing, Equations (3.12) and (3.14) are used to plot the force-displacement relationship for the fully austenite phase and Equations (3.13) to (3.15) and (3.17) are used to plot the force-displacement relationship for the fully martensite phase. Equations (3.14) to (3.16) are used to convert the force-displacement relationship to a shear stress, shear strain relationship.

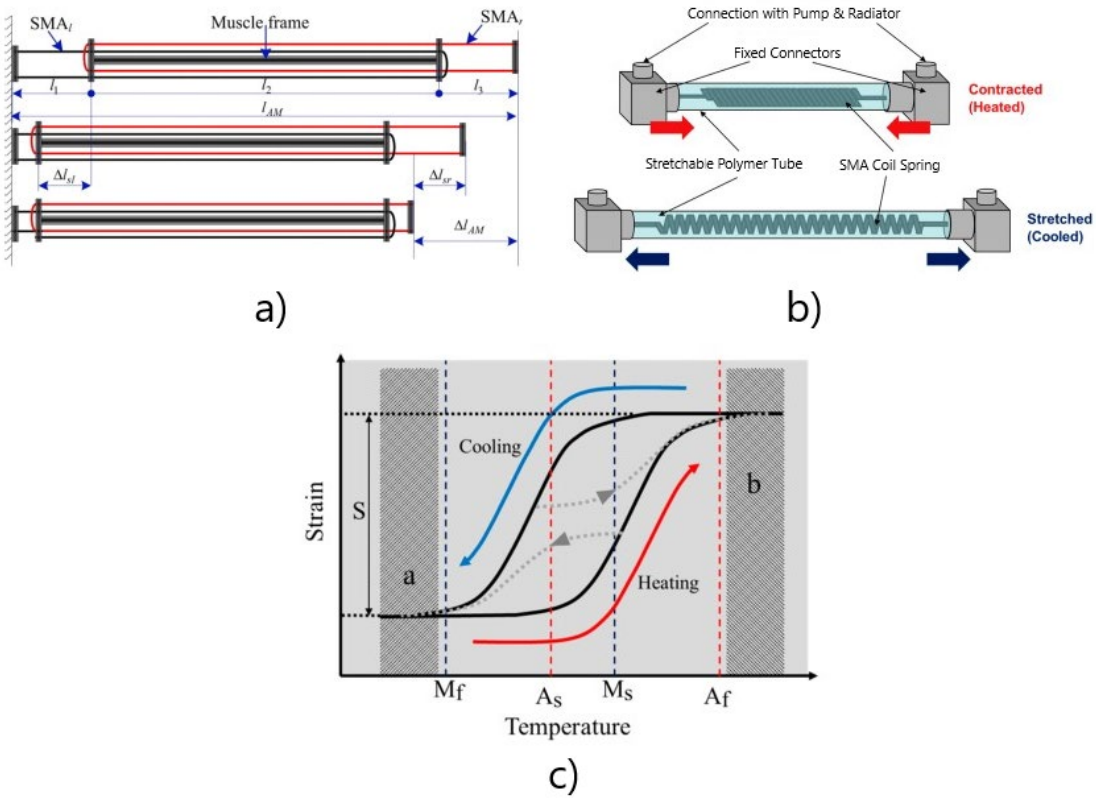

FIGURE 3.9 SMA ACTUATORS FUNCTIONING AFTER AND BEFORE APPLYING JOULE HEATING. AS A) WIRES OR B) SPRINGS. A) REPRODUCED WITH PERMISSION. [316] COPYRIGHT 2013, ELSEVIER. B) REPRODUCED UNDER THE TERMS OF THE CC BY LICENSE. [304] COPYRIGHT 2019. C) TEMPERATURE STRAIN RELATIONSHIP OF SMA ACTUATORS (AS = AUSTENITE START, AF = AUSTENITE FINISH, MS = MARTENSITE START, MF = MARTENSITE FINISH). REPRODUCED UNDER THE TERMS OF THE CC BY LICENSE. [337] COPYRIGHT 2018.

SMAS IN WEARABLES DEVICES

SMAs are superior to mammals' muscles and other AMSM in terms of power density and stress, these being as high as 50 W/g and 200 MPa, respectively. Consequently, SMA actuators have been successfully used in automotive, aerospace, and biomedical fields [338]. However, they have limitations in respect of robotic rehabilitation, and these are low efficiency, a small strain range (up to 8 %) and high thermal hysteresis making them difficult to control [36, 50, 231]. Nevertheless, SMA is the most used AMSM for rehabilitation robots, and it has been used within nine different devices.

Jayatilake et al. [320] investigated the ability of a device based on spring SMAs to help people with facial paralysis recover the ability to make facial expressions (Figure 3.10a). The device consisted of a wearable robotic external mask. The mask included six SMAs per side, and these were arranged in a specific position to replace or reproduce the face muscles' activity. The authors reported that it was possible to generate some facial expressions with a contraction of 20 mm, using a feedback controller. However, to create complex facial expressions, several SMAs are required.

Pittaccio et al. [314, 339] developed SHADE, an ankle orthosis capable of providing active and passive exercise for the dorsiflexion movement. The system used an SMA wire mounted on an insulated aluminium cartridge with dimensions of 150x20x15 mm. Inside the cartridge, the wire was led back-and-forth between two arrays of ten mini-pulleys, making it possible to store a long wire within a limited space. The prototype consisted of two cartridges and two thermoplastic shells hinged at the ankle joint. Later, three adult patients tested the prototype. During these trials, the prototype provided passive dorsiflexion movements in the range of 0°-23° to all the patients with speeds similar to the movement's natural speed. The control signal used during the experiments was a square signal with a current injection of 0.7 A for 7 s and a coiling phase of 30 s.

Zhang et al. [316] proposed using SMAs on an SWRR to assist the ankle dorsiflexion movement. To power the SWRR, an actuation unit composed of 2x250 mm SMA wires were developed. The system consisted of two parallel units and a bias spring mounted in two light-weight thermoplastic shells with articulated joints. To compensate for the hysteresis of the SMA, the prototype employed a Sigmoid-Based Hysteresis (SBH) feedforward controller with a PID controller. With this control configuration, the system was tested by following a sinusoidal signal with a peak-to-peak value of 30° at 0.2 Hz and 16° at 1 HZ. The system tracked the signal with a maximum tracking error lower than 16 % and the root-mean-square tracking error lower than 7.3 % in both cases.

Regarding plantarflexion at the ankle joint, Koo et al. [317, 318] produced a lower extremity SWRR using SMA wire. The system was light, silent and flexible. A prototype was built using a multi-layered structure consisting of functional fabrics, seam sealing tape, Velcro straps, Teflon tubes, and an SMA cable. The SMA was wrapped around the lower limb with both ends of the SMA anchored at the waist, and the middle part of the cable was attached to the ankle. The feasibility of the prototype was evaluated using an adult-like PVC mannequin. Joule heating was employed to activate the system, and when a 1A current was applied, an angular displacement of around 20° (plantar flexion) within 0.2 s was achieved.

For the knee joint, Stirling et al. [313] investigated the use of spring SMA on an Active Soft Orthotic (ASO) device. The ASO comprised four sets of actuators on the dorsal surface of the knee (to assist flexion) and one set on the frontal surface (to help extension). Each group of actuators consisted of four SMA springs with a length of 17.5 cm. The system was tested on a robotic leg resembling the size and mass of that of a four years old child. With the four sets of actuators activated through joule heating, the ASO flexed the knee by 34° in approximately 25s. The results were obtained after applying a step signal of 0.4 A to each set of actuators.

The Carlos III University of Madrid group has published a number of papers concerning SWRR actuated by SMA [262, 303, 335, 340, 341]. Recently, a wrist rehabilitation robot [303] was designed to assist flexion, extension, ulnar deviation, and radial deviation movement (Figure 3.10b). The rehabilitation robot consisted of a 3D printed mechanical structure sewed onto a glove. The device used three SMA wires, one for the extension movement and a pair to generate the ulnar/ radial deviation movements. A sinusoidal signal with a frequency of 0.04 Hz and a ROM of -10° to 40° was used to test the flexion-extension and the radial-ulnar deviation movements. The SWRR was able to track the extension movement, but it could not follow the signal input during flexion due to the slow cooling process of SMA. In ulnar/ radial deviation movement, it tracked the whole movement as it presented an agonist-antagonist structure, improving the performance compared to a single wire.

Another paper from this research group concerned an elbow SWRR [262] (Figure 3.10d) that had two DOFs (flexion/extension and pronation/supination). Each DOF had a pair of antagonists SMA actuation units. The units utilized a set of SMA wires encapsulated inside a PTFE tube. The number of SMA wires inside the actuation unit differed according to the direction of the movement. In the case of the flexion-extension, the actuation units were configured with a bundle of three SMA wires 1.5m in length for flexion and two for the extension. For the pronation-supination movement, each direction was actuated by a single SMA wire with a length of 2 m. To test the device, a sinusoidal signal with an amplitude of 100° and a frequency of 0.2 rad/sec was applied while performing a flexion-extension movement. The device could follow the pattern with an error of less than 4 degrees. In both devices, to control the contraction of the SMA wires, they used a four-term Bilinear PID (BPID). The BPID controller is a combination of a standard linear PID controller cascaded with a bilinear compensator to counteract the hysteresis behaviour of the SMA.

A group from the Korea Advanced Institute of Science and Technology (KAIST) [300, 304, 342] has designed SWRRs to assist patients who have difficulty moving the upper limb using SMA springs. The first SWRR they developed was a device to assist wrist movements [304, 342] (Figure 3.10e). They chose to use single SMA springs to generate a high contraction strain. The SWRR consisted of a wearable fingerless glove worn on the hand and a wearable strap placed on the forearm. Five actuators were used to provide the required movements, three over the forearm and two under the forearm. A cooling system pumping mineral oil was employed to improve the speed of the SMA springs. The device could provide torques of 1.32, 0.61, and 0.90, and a 0.62 Nm for extension, flexion, radial deviation, and ulnar deviation movements. Regarding the ROM while the SWRR was worn, it was 33.8°, 30.4°, 21.4°, and 15.4° for flexion, extension,

radial deviation, and ulnar deviation, respectively. To achieve a cycling performance of 0.5 HZ, a step signal of 4 A was applied to the SMA springs during the heating phase, while a step signal of 2.7 W was used for the pump during the cooling phase.

After the wrist device, the KAIST group developed a two DOFs SWRR to assist during the elbow's flexion and pronation/supination movements [300]. The device used AM units composed of a bundle of four SMA springs inside of a coolant-based vessel containing mineral oil. The robot presents three different AM units attached to soft braces to mimic the motions of human muscles. One unit is used by itself to assist elbow flexion, while the other two are arranged in an agonist/antagonist structure to help with the forearm pronation/supination. The device was able to provide torques up to 3.2 Nm with a ROM in the range of 60° to 150° for the flexion movement. Meanwhile, for the pronation/supination, the ROM was from -26.7° to 26.7° with a torque up to 0.5 Nm. The result from the forearm was obtained by applying a current of 1.5 A for 10 s in ambient temperature.

Finally, KAIST developed a four-bar linkage-based SWRR to assist with shoulder abduction [59]. An actuator was designed to generate the required forces using a bundle of 14 SMA springs. Each actuator produced an output force of 270 N when the actuator was stretched by up to 150 %. The system consisted of a four-bar linkage-based supported hinge and an actuator unit. Where the four links are constructed by the arm, the torso and two extra 100 mm and 200 mm connected linkages. Furthermore, the actuator was placed in the middle of the 200 mm link and the upper arm. With this configuration, the mechanism could produce assistive torque up to 10.1 Nm and a ROM of 90° during shoulder abduction. An electrical current of 1.5 A was supplied to each spring to activate the device. The effect of assistance was evaluated by measuring and analysing the difference in the EMG activity between assisted and unassisted activity. However, there were no significant differences between the two conditions.

At the Korea Institute of Machinery and Materials, Park et al. [301, 343] presented a SWRR made of fabric muscle with a cooling acceleration structure for elbow extension assistance (Figure 3.10c). The device is actuated by fabric muscle that consists of SMA spring bundles, conductive fabrics, cover fabrics, and electrical wiring. Furthermore, to improve the cooling rate of the fabric, two small fans are attached to each piece of fabric. The final exosuit consists of a shoulder anchor, forearm anchor, two overlapped biceps fabric muscles, one triceps fabric muscle, battery, and controller (with a total weight of 0.57 kg). The biceps fabric muscles were set on an agonists-antagonist configuration to improve the system's speed. Furthermore, when the fans were used, the system could contract 47 mm (26 % strain) and generate a force of 80 N while flexing the elbow in 5

s. This was achieved by applying 10 A to the bicep's fabric for 3 s and fan cooling and activating the triceps fabric (10 A) for 3 s.

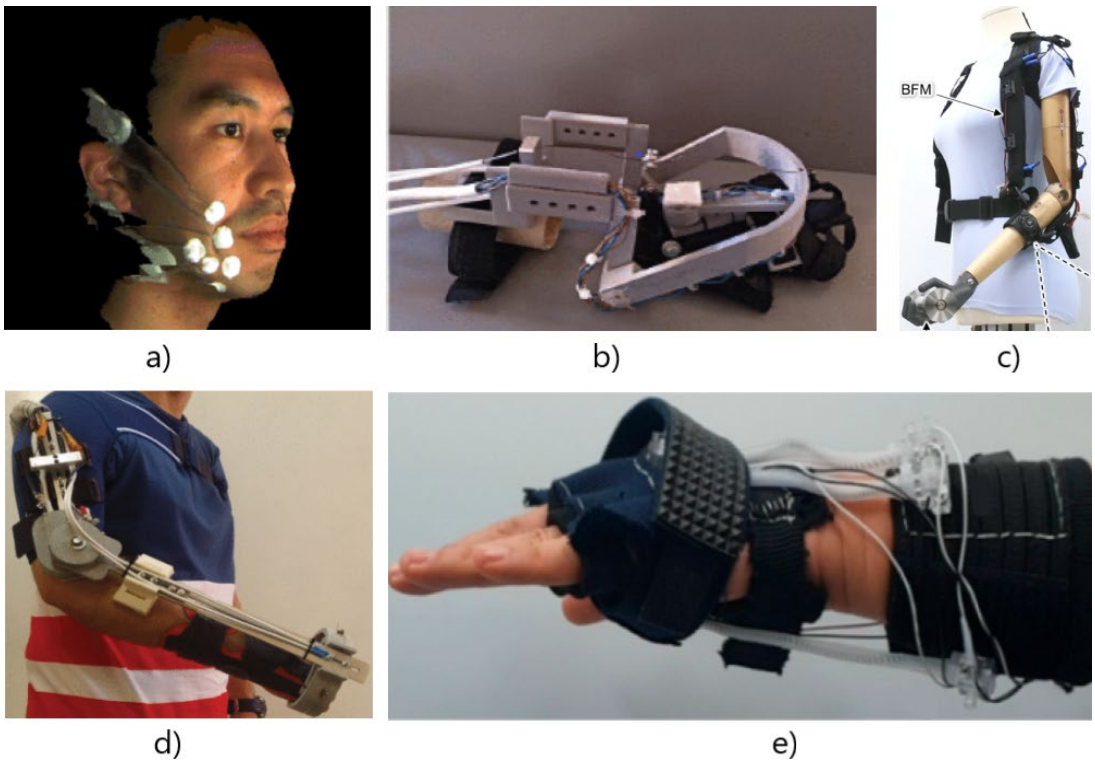

FIGURE 3.10 EXAMPLES OF SMA BASED SWRR. A) ARTIFICIAL INTELLIGENCE LABORATORY SMILE RECOVERY DEVICE. REPRODUCED WITH PERMISSION. [320] COPYRIGHT 2008, IEEE. B) CARLOS III UNIVERSITY OF MADRID WRIST DEVICE. REPRODUCED WITH PERMISSION. [303] COPYRIGHT 2018, IEEE. C) KOREA INSTITUTE OF MACHINERY AND MATERIALS ELBOW ROBOT. REPRODUCED UNDER THE TERMS OF THE CC BY LICENSE. [301] COPYRIGHT 2022. D) CARLOS III UNIVERSITY OF MADRID ELBOW SWRR. REPRODUCED UNDER THE TERMS OF THE CC BY LICENSE. [262] COPYRIGHT 2019. E) KAIST WRIST SWRR. REPRODUCED UNDER THE TERMS OF THE CC BY LICENSE. [304] COPYRIGHT 2019.

Other Smart Materials

While those materials presented above have been utilized for SWRR, there are other materials that had been highlighted as possible option in previous papers [282, 344], like IPMC [345], Hydraulically Amplified Self-healing Electrostatic (HASEL) [344] and SMP [346] that presents attractive properties as they have been use in similar applications (grippers, robotic hands, or as compliance mechanism inside a rehabilitation robot). However, their current limitations prevent their use on SWRR.

IPMCs are EAPs made by coating a thin sheet of ionic polymer with metal electrodes. When an external electric field is applied, ions of the same charge begin to move from the anode to the cathode. As a result, the system undergoes a fast-bending deformation, followed by a slow relaxation [347, 348] (Figure 3.11a). They have compelling advantages, such as efficiency, low working voltage (1-5 V), high working frequency up to 100 HZ, and considerable strain up to 40 %. Nevertheless, they present some

problems, such as relaxation under direct current (DC) voltage, low power density (0.02 W/g) and solvent evaporation that complicate their use in not watery environments [50, 349, 350]. He et al. [351] developed a microgripper using an air-operating IPMC actuator with consecutive channels. However, under this environment the actuator by itself was only able to produce a strain of 0.44 % and a force of 12.06 mN at 1 Hz using 5v input which is lower than what skeletal muscles can generate. Nevertheless, the actuator proved its functionality operating on air, as it was used on a microgripper (0.14 g) that was able to pick up and transfer a nut (0.656 g) 4.69 times its own weight (Figure 3.11b).

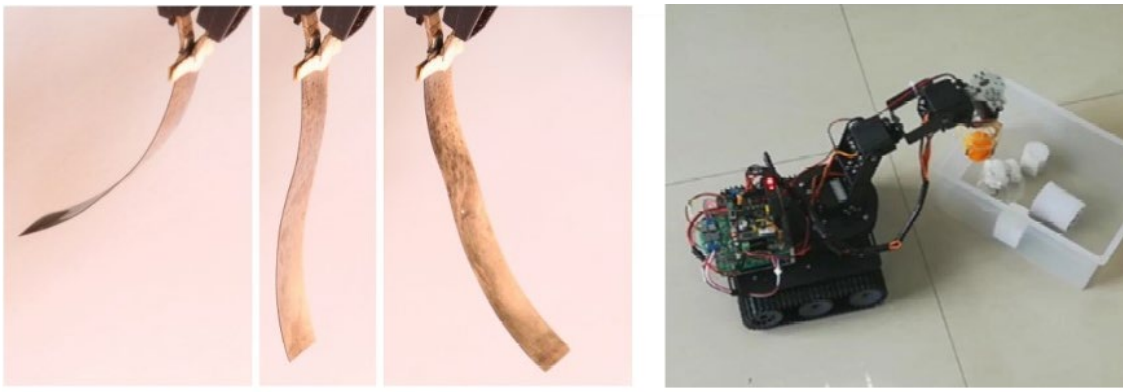

FIGURE 3.11 A) IPMC ACTUATOR BENDING IN RESPONSE TO AN ELECTRICAL INPUT WITH OPPOSITE POLARITIES (LEFT AND RIGHT) AND AT REST (MIDDLE). REPRODUCED UNDER THE TERMS OF THE CC BY LICENSE. [348] COPYRIGHT 2019. B) AIR-OPERATING IPMC SOFT GRIPPER ASSEMBLED WITH A MOBILE MECHANICAL ARM. REPRODUCED WITH PERMISSION. [351] COPYRIGHT 2020, IOP.

Recently introduced, HASEL actuators are fabricated from dielectric liquids filling pouches made of polymer films and partially covered by electrodes [352] (Figure 3.12a). HASEL actuators behave similarly to DEAs. They generate a Maxwell pressure when high voltage is applied, increasing the volume of the pouches and decreasing the length of the actuator [353]. Their main advantages for rehabilitation devices are their high linear strain (over 24 %) and high bandwidth (126 Hz). Nevertheless, as with the DEAs, their main limitation are low stress (<1 MPa) and the high voltage (in the range of KV) required to drive them [354]. To understand the advantages and disadvantages of the HASEL actuator in rehabilitation robots, Yoder et al. [355] compared the HASEL actuator with DC motors, activating the Bebionic v2 Prosthetic hand (Figure 3.12b). In this comparison, the HASEL actuator surpassed the speed (HASEL= 1,587 °/s, Motor = 150 °/s) and the energy consumption (HASEL= 0.94 mW, Motor =9,200 mW) of the motor. The ROM attained was similar in both cases (HASEL=77.17°, DC Motor = 85°). However, the force provided by the HASEL actuator was lower than the generated by the motor (HASEL=0.91 N, DC Motor = 13 N), and below that required to perform ADLs (Table 3.4).

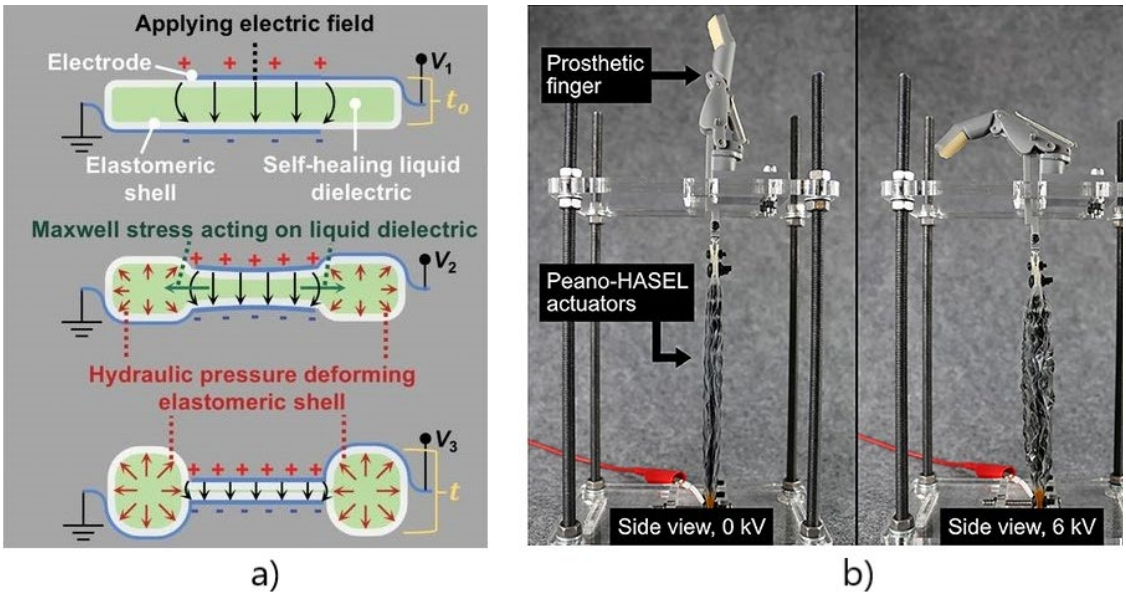

FIGURE 3.12 A) HASEL ACTUATOR SCHEMATIC SHOWN AT THREE DIFFERENT APPLIED VOLTAGES (WHERE V1<V2<V3). REPRODUCED WITH PERMISSION. [352] COPYRIGHT 2018, THE AMERICAN ASSOCIATION FOR THE ADVANCEMENT OF SCIENCE. B) AN ARRAY OF PEANO-HASEL ACTUATORS, DRIVING A CUSTOM PROSTHETIC FINGER. REPRODUCED UNDER THE TERMS OF THE CC BY LICENSE. [355] COPYRIGHT 2020.

Like SMA, SMP can recover a predetermined shape after certain stimuli are applied, such as light, moisture, electricity and heat [356, 357] (Figure 3.13a). Due to their versatility of activation to different stimuli and the possibility of being produced from biodegradable materials, SMPs have been used in different biomedical applications such as drug delivery, self-tightening sutures, stents and cellular surgery [358]. However, in the field of rehabilitation robotics, even though they have a high strain, which is a desirable feature (>10 %), they are still not used because they present the problem of low stress (1-3 MPa) and slow recovery response (<1Hz) [50]. An example of incorporation of this technology into rehabilitation set up is the soft facial rehabilitation robot developed by Firouzeh et al. [346]. They incorporate SMPs into a soft robot actuated by a cable driven system to improve the compliance of the system. The prototype had five points of actuation which each of them incorporate an SMP to control the stiffness (Figure 3.13b). The multiple DOFs presented by the robot allowed for initial reconfiguration and activation of different movement patterns depending on the needs of each patient and training. Nevertheless, the switch between different training position was time consuming (≈ 10 s) due to the slow transition of the SMP.

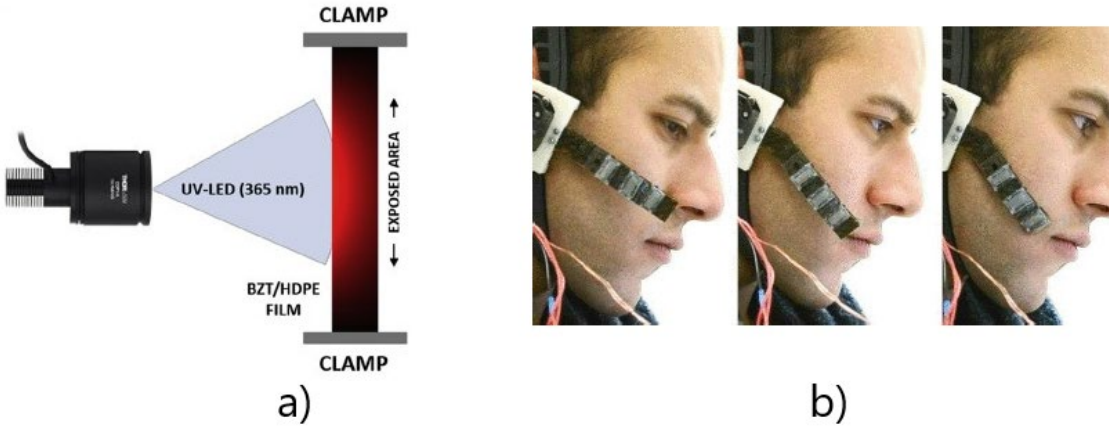

FIGURE 3.13 A) PHOTO-THERMAL EFFECT ORIGINATES FROM THE THERMAL ENERGY PRODUCED BY A BZT/HDPE FILM AFTER EXPOSURE TO A UV LIGHT. REPRODUCED WITH PERMISSION. [357] COPYRIGHT 2020, ELSEVIER. B) EXPERIMENTS USING A SINGLE ROBOT FINGER FOR PERFORMING THE INITIAL RECONFIGURATION UTILIZING A SMP. REPRODUCED WITH PERMISSION. [346] COPYRIGHT 2017, IEEE.

3.6.3 SWRR based on AMSM Limitations

AMSMs have outstanding flexibility and are light-weight, making them a promising choice to power the next generation of compliant rehabilitation robots. However, the use of these materials is still at the early stage of development, and the devices employing them have fundamental limitations that prevent their successful application.

Most of the robots utilizing AMSM were unable to generate the ROM to perform ADLs. For instance, this problem is related to the limited strain that most AMSM can produce, which is under the skeletal muscle's typical strain (20 %). Another requirement that is influenced by the actuator's strain is torque. As the displacement generated by the actuators is linear, and the robots require angular displacements, making the necessary structures to transform linear to angular displacements can lead to a loss of force in the transition. Nevertheless, the main factor in producing the desired torque is the force generated by the AMSM. Concerning the required torque, most of the devices could produce the necessary torque to move the limb against gravity, except for the elbow developed by Behboodi et al. [263]. Therefore, most of the evaluated AMSM can generate enough force to be used on wearable robots, except for DEAs that can not deliver high forces with small actuators.

The biggest obstacle for devices based on AMSM seems to be the actuation speed, as most of the reported frequencies and angular velocities were far from the required for ADLs (Tables 3.1-3.7). However, a possible option would be to use them for rehabilitation therapies where the required speeds to perform the exercises are slower, usually under 100 °/s and frequencies below 0.2 HZ [234, 359-361]. This limitation could also be related to the mathematical models that explain the actuation principles of the AMSM. As the

different technologies suffer from different problems like non-linearity, hysteresis, and electro-mechanical instability that are difficult to model. The mathematical models are necessary to develop robust control strategies required for high-performance applications [53, 336, 362]. Hence, most of the evaluated devices used open-loop control schemes toggling between two different predefined levels to alter the length of the AMSM.

Generally, it is possible to categorize the current AMSM for SWRR into two categories EAPs (DEAs and PVC gels) and thermally activated actuators (SMAs and TCPs). These two groups of actuators translate their limitation into the SWRR. The EAPs present a high actuation speed but low forces (high angular velocity/frequency but low torques). Contrary to the thermally activated actuator that shows low speeds but high forces (low angular velocities/frequency but high torques). Furthermore, the strain seems to be a general limitation (restrict ROM). Nevertheless, these constraints could be lessened with a proper design of the SWRR, as will be explored in the next section.

3.6.4 Artificial Muscles enhancements technics

Although some SWRRs has initially demonstrated their potential as an assistant rehabilitation tool, all of them have been used in experimental setups in the laboratory environment only. New materials vary in their ability to meet the biomechanical requirements to be useful in the clinical setting. However, SWRRs made of AMSM show great potential for rehabilitation, thanks to their inherent compliance and light-weight. Currently, an AMSM covering all the essential characteristics to behave like the skeletal muscles does not exist (Table 3.9). However, some of the deficiencies in smart materials can be remedied through the SWRR design.

The required torque depends on two different aspects, the generated force and the lever arm. In the case of force, SMA is the best material to generate forces, unlike DEAs that struggle to generate high forces. To overcome this limitation, the most used strategy is to employ bundles of actuators that generate the required force [59, 63, 262, 307]. An alternative to increase the torque is to use a larger lever arm. Nevertheless, this strategy presents the drawback that the lever arm length negatively influences the ROM generated by the AMSMs linear displacement [294, 316]. The relation of torque and linear displacement with relation to the lever arm could be expressed:

$$\begin{cases} \Delta l = a \ \sin \Delta\theta \\ T = Fa \end{cases} \tag{3.18}$$

Where Δl, is the required linear displacement of the AMSM, a the lever arm, $\Delta\theta$ angular displacement of the joint, T torque and F is the force.

The linear displacement is related to the strain of the AM. This is another aspect that limits the use of AMSM, as they usually have decreased strain compared to skeletal muscles (< 20 %). However, thanks to their flexibility and softness, it is possible to place long actuators in small spaces, allowing the device to attain the required displacement without impacting the actuator's performance [60, 314]. For SMA, another option to increase the strain is to fabricate springs made of single wires, similar to TCP, when coiled around a mandrel, with the disadvantage of reducing the generated force [313, 363].

In the case of the speed of the motion, it is mainly related to the frequency of the AMSM. DEAs and PVC gel actuators surpassed the frequencies observed in skeletal muscles. In contrast, TCP and SMA actuators experience frequency as the main limitation. The lower frequency of this technology is related to the slow cooling time of the actuators. To improve the speed of the system, actuators with small diameters with lower thermal mass could be utilized as they cool faster [318, 334]. Alternatively, one could use external cooling systems [342, 364], but they introduce two issues: increases in weight and power consumption of the device.

In general, to improve the performance of the actuators is necessary to implement closed-loop control strategies that allow the system to provide faster, accurate and efficient responses [60, 262, 332]. Applying these closed-loop control strategies usually requires different sensors to read external variables like position and force. Nevertheless, one of the advantages of AMSM is that they present self-sensing properties, allowing for more compact designs as they can be used as sensors and actuators simultaneously [365-367].

Table 3.9 Comparison of Artificial Muscles properties

Device	Actuator technology	Strain [%]	Force [N]	Stress [MPa]	Frequency [Hz]	Size (Length and area or diameter)
Human Body [231]	Skeletal Muscles	20	N/A	0.1	20 Maximum	N/A
Korea Institute of Machinery and Materials [301] (2022)	SMA (spring)	50	0.2	N/A	23.4 s	L: 26 mm DSMA:0.08 mm DSpring:0.44 mm
KAIST [59] (2022)	SMA (spring)	N/A	19.28	N/A	N/A	L: N/A DSMA:0.5 mm DSpring:2 mm
University of Delaware [322] [263] (2020)	DEA	5	10	0.0346	< 100	L: 39 mm A: 17 x 17 mm
University of Pisa [307] (2008)	DEA	N/A	0.33	0.000982	N/A	L: 85 mm A: 16 × 21 mm
Zhejiang University of Technology [294] (2017)	PVC	10	80	0.080	9	L: 200 mm A: 0.001m2
Universidad Iberoamericana [62](2018)	TCP	10	5.4	1.1	≈ 0.02	L: N/A D:2.5 mm
Bio-robotics and Smart Systems Laboratory [60] (2017)	TCP	16	3	2	≈ 0.04	L:380 mm D:1.35 mm
MENRVA Group [63] (2016)	TCP	15.	0.9	N/A	0.1	N/A
KAIST [300] (2022)	SMA (spring)	90 mm contraction	11.67	N/A	N/A	L:120 mm (unstreched) DSMA:0.5 mm DSpring:2 mm
Ajou University [318](2020)	SMA	5	10.5	594	≈ 1	L:800 mm D:0.15 mm

Table 3.9 Comparison of Artificial Muscles properties (continued)						
Carlos III University of Madrid [262] (2019)	SMA	4	35.6	181.3	≈ 0.046 rad/sec (0.007)	L:1.5m flexion/extension L:2m pronation/Supination D:0.5 mm
KAIST [304] (2019)	SMA (spring)	33	10	2	0.5 (cooling system with mineral oil)	L:150 mm DSMA:0.5 mm DSpring:2.5 mm
Carlos III University of Madrid [303] (2018)	SMA	5	35.6	181.3	≈ 0.04	L: 2.2m flexion L:1.7m Ulnar radial deviation D:0.5 mm
State Key Laboratory of Mechanism System and Vibration [316] (2013)	SMA	10	13.72	280	> 0.1 (free convection) 5 (cooling system with water)	L: 220 mm D:0.25 mm
Wyss Institute [313] (2011)	SMA (spring)	≈ 66	5	11	≈ 0.02	L:175 mm DSMA:0.25 mm DInnerSpring:0.51 mm
CNR Institute for Energetics and Interphases at Lecco [314] (2009)	SMA	≈ 3	10	203	≈ 0.025	L:2.5 m D:0.25 mm
Artificial Intelligence Laboratory [320] (2008)	SMA	20 mm contraction	N/A	N/A	N/A	N/A

3.6.5 Summary and future developments

The majority of exoskeletons are heavy and bulky, which may cause earlier fatigue or damage to the weak muscles of people with physical disabilities [29, 112]. AMSMs have emerged as a solution for this problem thanks to their properties of compliance and light-weight. Nevertheless, they require high voltages and present high-power consumption, making necessary the use of cumbersome equipment such as batteries and High-Voltage amplifiers, which are the main contributors to the final weight of the device. Furthermore, the power consumption and the high-voltages are problematic from other perspectives. They can limit the device's use time as well as its autonomy. In some instances, tethering to a power supply may be required [60], and in the case of the voltages, it may pose a safety risk to the users. However, energy storage and energy transmission are continually being developed, with improvements in the energy density [368, 369] and miniaturization of batteries [370-372], as well as downsized electronic systems [355], which will ultimately lead to the implementation of SWWR based on AMSM being feasible in the early future.

A specific problem for the thermal base AMSM (SMA and TCP) is the temperatures that they can reach. To generate the maximum force/displacement, they generate temperatures over the pain threshold of humans (44 °C at the dermal/epidermal interface of the skin) [60, 373]. For this reason, is still necessary to research into design and materials that help to incorporate the AMs seamlessly into the SWRR that can insulate the actuator from the users allowing for comfortable use [317, 374].

AMSM actuators have some properties exceeding those of the skeletal muscles (e.g. SMA generates higher output stress, and DEAs can work at higher frequencies than skeletal muscle). However, currently, there is no AMSM that can integrate all the properties needed to achieve the body's musculoskeletal movement (e.g. AMSM still have a lower strain). Furthermore, there is still a lack of mathematical models that can represent all the physical transformations that the actuators present [53, 336, 362]. Hence, research on new theoretical models and manufacturing processes that permit or use different compounds to improve the performance of AMSM is still needed.

Based on the data concerning biomechanical requirements related to human movement and the current capability of existing devices (Tables 3.1-3.7), it is still challenging to use AMSM in SWRR. Nevertheless, using them could be feasible if a proper control strategy is implemented and the assistive task is specific and simple [60, 316]. An example is

assisting ankle dorsiflexion through the swing phase of gait to help people with "foot drop" [72]. This task is in only one plane of motion, does not require fast movement nor high forces given the mass of the foot, and the ROM required is relatively small. Another possibility to start exploring the use of AMSM is to integrate them into hybrid devices with two or more actuation technologies. For instance, it is possible to find devices where the primary actuator generates the forces, and the movements are electric motors, with a smart material to add compliance to the device [346].

3.7 Conclusion

It can be concluded that AMSMs are promising actuators to be used in SWRR. However, a better understanding of the minimum biomechanical requirements is necessary to design solutions that can provide a reasonable level of assistance to specific tasks. It seems logical to address relatively simple tasks first before moving toward more complex multi-faceted movements that may require high forces, high angular velocities of joint motion with rapid acceleration and decelerations. There is applicability waiting to improve the quality of life of the elderly as well as younger individuals with diseases and injuries that have left them notably disabled due to muscle weakness.

3.8 Limitations

The sources analysed in regard to AMSM are limited to their relationship with SWRR. Therefore, it is not representative of the whole cohort of AMSM currently available for other applications.

On the other hand, as this work mainly focuses on the functionality and the gap in the technology of SWRR based on AMSM, AMs for rehabilitation with better performance could exist.

3.9 Chapter Summary

This chapter presents an exhaustive examination of AMSM technologies were conducted for their potential integration into SWRR. Through this evaluation, TCPs emerged as the preferred choice, attributed to their noteworthy force generation and linear behaviour. The selection of TCPs as the preferred AMSM option partially addresses research question two in this study. However, specific properties of TCPs, namely strain and temperature, necessitate careful consideration for the optimal functionality of the device. These properties are further explored in Chapter 4.

Chapter 4 : Artificial Muscles Performance based on TCP-NiCr Actuators.

4.1 Preface

The content of this Chapter is based on the conference article *"Artificial Muscles Performance based on TCP-NiCr actuators"*, published in the proceedings of the 2021 43rd Annual International Conference of the IEEE Engineering in Medicine and Biology Society (EMBC) [375]. All the sections of the article were expanded to provide a more extensive content and discussion on the effects of NiCr wire on TCP actuators.

Given the TCPs inherent requirement for a heat source for activation, a prevalent technique involves incorporating a controllable thermoelectric element. This technique is executed through two methods: one involves applying a layer of silver paint, while the other entails wrapping a resistance wire around the TCP. Notably, the silver paint in the first method exhibited a tendency to peel over time, leading to changes in electrical properties. In contrast, the metallic wire did not exhibit this issue.

However, an absence of studies on how the metallic wire affects TCP performance prompted further investigation. A comprehensive literature review revealed that implementing an embedded wire influences strain. The subsequent Chapter explores the impact on strain and thermoelectric response following the embedding of a NiCr wire with varying diameters using the same precursor fibre. This investigation aims to contribute valuable insights for informed decision-making concerning the size of the embedded NiCr wire.

4.2 Abstract

Exoskeleton technology has advanced significantly during the last years, providing a new variety of solutions to assist or rehabilitate people with physical disabilities. However, the current devices rely on the use of rigid robotic. The lack of wearability and portability, makes difficult to use them outside of clinical settings. This challenge has driven researchers to investigate compliant mechanisms, including soft actuators and AMs. TCP is becoming a viable solution to improve exoskeleton technology due to their high power to weight ratio, linear behaviour, and considerable strain. A recent introduced method to activate the TCP is to use an embedded metallic wire. This work presents an experimental setup to study the performance of TCP actuators with different NiCr wire

diameters and analyses the strain and the response time under a constant weight and applied power. The results could be used as a guideline to design TCP based AMs.

4.3 Introduction

In the last decade, exoskeletons have gain interest in the field of healthcare [274]. The technology is expected to improve the outcomes from rehabilitation therapies as they allow for massed practice and help people during ADLs [33]. However, most of the current exoskeleton's reliance on rigid, bulky, and heavy elements (e.g., DC motor) makes it difficult to overcome problems related to adaptability, comfort, safety, and efficiency that make easy their integration into wearable devices. Consequently, researchers started to pay attention to more complaints elements such as soft actuators [36].

AMs are soft actuators composed primarily of material with low young modulus similar to soft biological tissues (10^4 – 10^9 Pa) [41]. AMs encompasses soft actuators such as SMAs, DEAs, and Pneumatic ones. They offer many advantages over conventional rigid actuators (e.g., electric motors) like, high power-to-weight ratio, inherent compliance, and noiseless operation. Unfortunately, the use of AMs in rehabilitation robots are still at the early stage of development. Some drawback specific to each type of AM need to be tackled to become widespread [50].

Pneumatic, SMA and DEAs are promising solutions. However, they suffer from limitation to be used on exoskeletons for rehabilitation. Pneumatic AMs suffer from low portability as they need to use compressors or fluid tanks to generate pressure. In the case of DEAs, they are limited by the required high voltage power and manufacturing processes that are currently unable to produce a reliable actuator of a size that can provide valuable amounts of power and force. Finally, SMAs, present the problems of low efficiency, high thermal hysteresis that makes them hard to control, and a small strain range [50].

In 2014, TCP actuators were presented by Haines et al. [56]. TCP actuators are fabricated by inserting a twist in precursor fibre while attaching a dead weight at the end until it forms a coil structure, followed by heat treatment. TCPs are thermally driven actuators with high power to weight ratio like SMA. Nevertheless, in contrast to SMA, TCPs present a considerable strain, low hysteresis and low cost [56].

TCP can be fabricated by two different methods, auto-coiling and mandrel coiling. Auto-coiling is the process by which a filament is twisted to the point where it begins to coil onto itself. Conversely, mandrel coiling is the practice of wrapping a twisted fibre around a shaft or spindle for coiling. Mandrel coiling brings the advantage of larger stroke and

the possibility of fabricating TCP able to expand. However, mandrel coiled TCPs generate less force [56].

Table 4.1 Fabrication parameters used by different investigators

Author	Heating Method	Precursor fibre material	Precursor fibre diameter (μm)	Strain (%)
Wu et al.[57]	Nichrome wire	Nylon 6 fishing line	860	40
Liu et al. [376]	Copper wire	Nylon fibre	500	9.4
Chossat et al. [377]	Nichrome wire	UHMWPE braided fibres	200	5.5
Tang et al. [378]	Nickel wire	Nylon fibre	500	11.4
Wu et al. [379]	Silver Coated	2-ply Nylon 6,6 conductive sewing thread	850	8-14

In the case of auto-coiling, there are several factors to take into account during the manufacturing process, like the material of the precursor fibre, the diameter of the fibre, the load applied during the manufacturing process [56], the velocity of the motor during the twisting and coiling process and the heating method [380]. Regardless of the heating method, most authors active the TCP muscles through Joule heating using silver-coated sewing thread [381]. Another option that recently is gaining attention is to use metallic embedded wires into the TCP actuators, especially NiCr wire, as it is low-cost and accessible [62, 382-384], and therefore a viable solution for AMs in assistive and rehabilitations devices. However, this method can affect the actuators' performance, changing the actuator's strain in a wide range (from 5.5% to 40% [377, 385, 386]). For the understanding of the muscle behaviour, the fabrication parameters from various research groups (Table 4.1) is provided.

Although the TCP wire embedded manufacturing procedures are well described there is a lack of characterization of TCPs performance. Related guidelines for design AMs based on TCPs wire embedded has not been described. The main goal of this study is to evaluate the strain and the response time of TCPs in relation with the embedded metallic wire as the Joule heating element.

4.4 Muscle fabrication process

The fabrication process follows the one described by Chossat et al. [377]. Nylon fishing line was used as the precursor fibre (Mono fishing line 20lb, BURNSCO Ltd., New Zealand) with a diameter of 440 μm. The nylon fibres were twisted and coiled along with a NiCr wire. For the experiments, different diameters of NiCr wires were used (42-34 AWG, WIREOPTIM, USA). One side of the nylon fibre was fixed at the end of the output shaft of a NEMA17 motor. The other end is set on a slider, with a weight of 250 g (≈20

MPa). The NiCr wire was also suspended from the motor shaft but only straightened using a small weight (≈1.2 MPa) and were left free to untwist. The fibres were twisted and coiled at a slow speed of 250 rpm [380]. The actuator was annealed through joule heating using the embedded NiCr wires, using the same weight during the twisting and coiling process. The actuator was annealed in five consecutive five-minute-long periods, with an annealing power of 0.16 W/cm each period. Between every period, a cooling phase of 1 minute was applied. For each NiCr wire diameter. A total of 5 TCP samples and an extra double-wire one (*TCP* $_{2xAWG42}$, in Table 4.2), were fabricated. Table 4.2 provides the properties of each one.

4.5 Muscle performance testing

All the samples fabricated for the study were tested using a custom made experimental test bench, see Figure 4.1 The experimental setup consists of a displacement sensor (0d80 15p850, Sick Optex, Ltd. Japan) connected to a current sensor (INA169 Analog DC current sensor), an Arduino NANO connected to the computer, and an electrical circuit to control the voltage coming from the power supply. The actuator was hanging above the sensor, with a weight of 250 g. A square signal of 90 seconds on and 90 seconds off was applied. The power applied for all the test was equal to 1.5 W for all the different TCPs actuators. Furthermore, the temperature for the 1.5 W was measured for each sample using a thermal camera (i7, FLIR, USA).

Table 4.2 TCP Muscle fabrication parameters used during this study

Property	**TCP$_{AW}$ G42**	**TCP$_{AW}$ G40**	**TCP$_{AW}$ G38**	**TCP$_{AW}$ G36**	**TCP AWG34**	**TCP $_{2xAWG42}$**
Precursor fibre diameter (μm)	440	440	440	440	440	440
Precursor fibre length (mm)	300	300	300	300	300	300
Coiled length before annealing (mm)	90.1	89.8	89.2	88.4	88.16	91.0
Coiled length after annealing (mm)	106.64	117.92	111.3	100.1	97.56	108.6
Total No. of twists	350	346	341	332	329	346
Annealing current (mA)	100	140	180	220	280	150
Wire diameter (μm)	63	80	100	127	160	2 * 63
Resistance (Ω)	148.8	83.56	52.1	30.96	21.26	65.86
Mass on the wire (g)	0.4	0.7	1.05	1.6	2.5	2 * 0.4

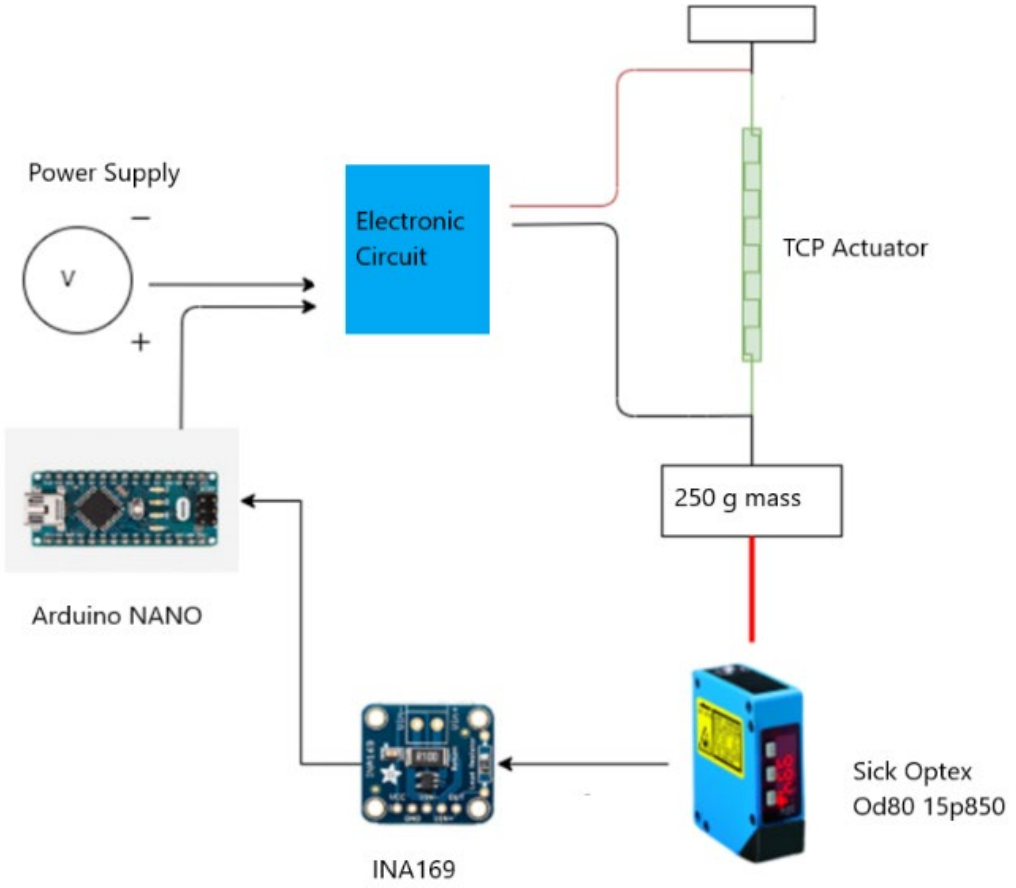

FIGURE 4.1 STRAIN TEST TESTBENCH DIAGRAM.

4.6 Results

Several performance tests were carried out on all the samples of equal lengths and under the same applied power of 1.5 W and load of 250 g. In Figure 4.2, it can be seen the contraction of the TCP actuator belonging to each group of different NiCr wire diameter after the square signal of 1.5 W were applied. It can be noticed how the contraction is reduced with the increment in the wire diameter. The maximum obtained contraction was around 14 mm with the NiCr wire diameter of 0.06 mm, and it is reduced gradually with the increase of the diameter.

Strain is obtained as the relation of the measured displacement *Disp*, and the fully extended TCP under loading *Flen*, Equation 4.1. The relationship between strain and the NiCr wire diameter for the five different samples is plotted in Figure 4.3. The figure shows how the strain decrease as the wire increase on the dimeter. However, it is interesting to notice how this relation is not linear, and there is a valley between 0.08 mm and 0.10 mm.

$$Strain\ (\%) = \frac{Disp}{Flen} * 100 \tag{4.1}$$

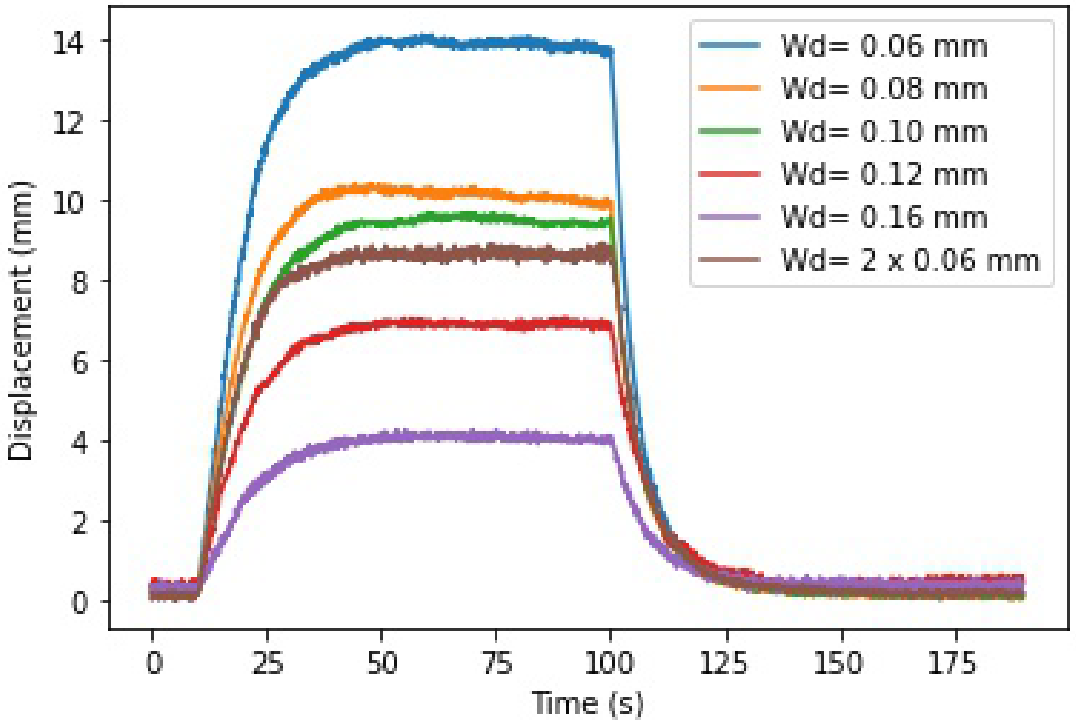

FIGURE 4.2 THE DISPLACEMENT OF DIFFERENT MUSCLE WHEN A SQUARE SIGNAL OF 1.5 W IS APPLIED

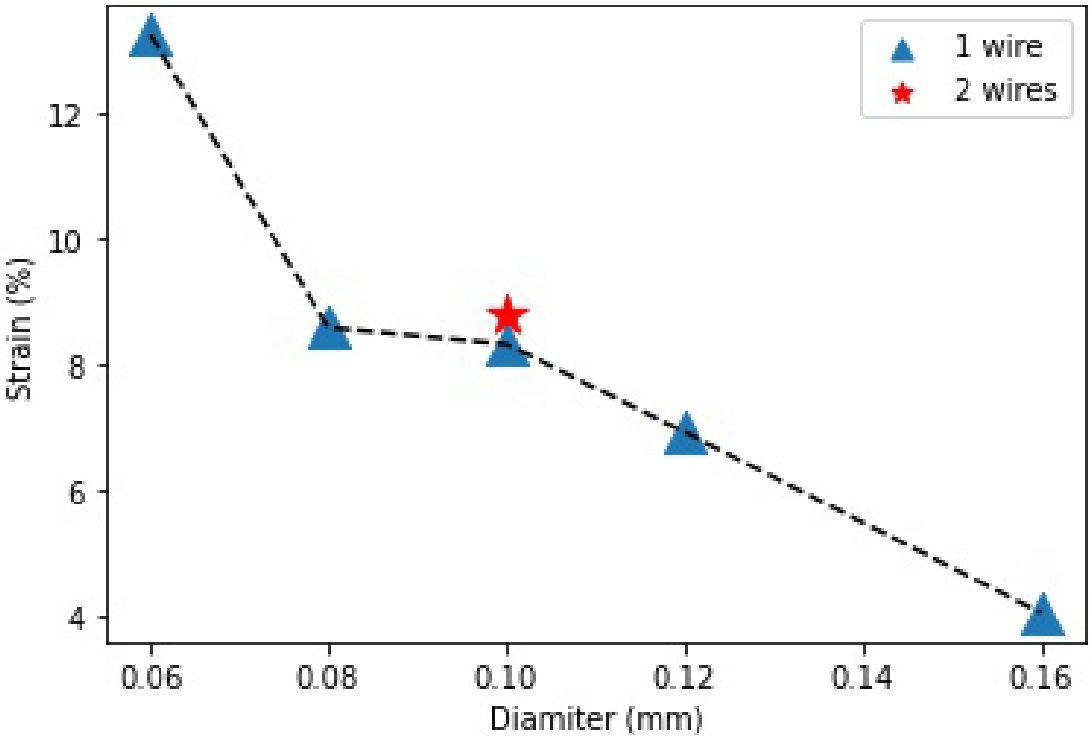

FIGURE 4.3 STRAIN OF THE TCP MUSCLES THAT FABRICATED WITH DIFFERENT NICR WIRE DIAMETERS.

Additionally, to the strain analysis of the TCP, the response time of the actuators was measured. In Figure 4.4, it notices how the response time is reduced from 0.06 mm to 0.08 mm, but after this slight reduction in the response time, it starts to increase as the wire diameter increases. The temperature was the same for all the different samples (around 60 °C) when they reached a stable state after few seconds.

In order to compare the performance of one single wire against a double wire embedded configuration, an extra two wires 42 American Wire Gauge (AWG) TCP set of actuators were analysed. The test showed identical properties for each one (***TCP*** $_{2xAWG42}$ properties described in Table 4.2). From Figure 4.3 and Figure 4.4, it can be seen how the performance also declines both in contraction and response time. The behaviour was similar to the TCP with the 36 AWG (d=0.1 mm). After applying 1.5 W power, the reached temperature was the same as previous experiments (Figure 4.5).

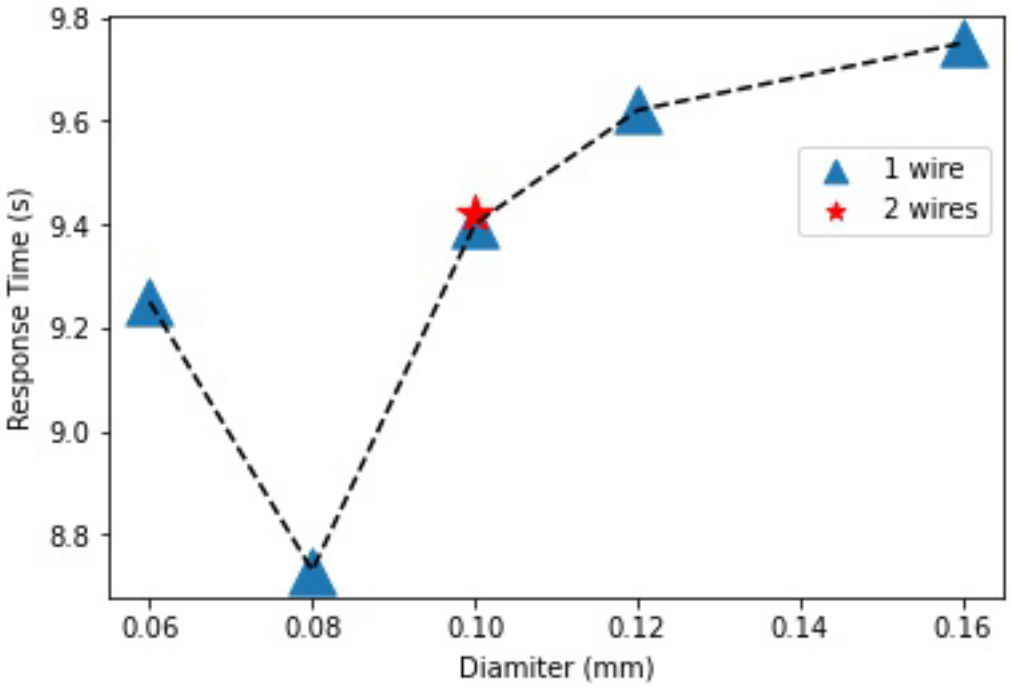

FIGURE 4.4 RESPONSE TIME OF THE TCP MUSCLES FABRICATED WITH DIFFERENT NICR WIRE DIAMETERS

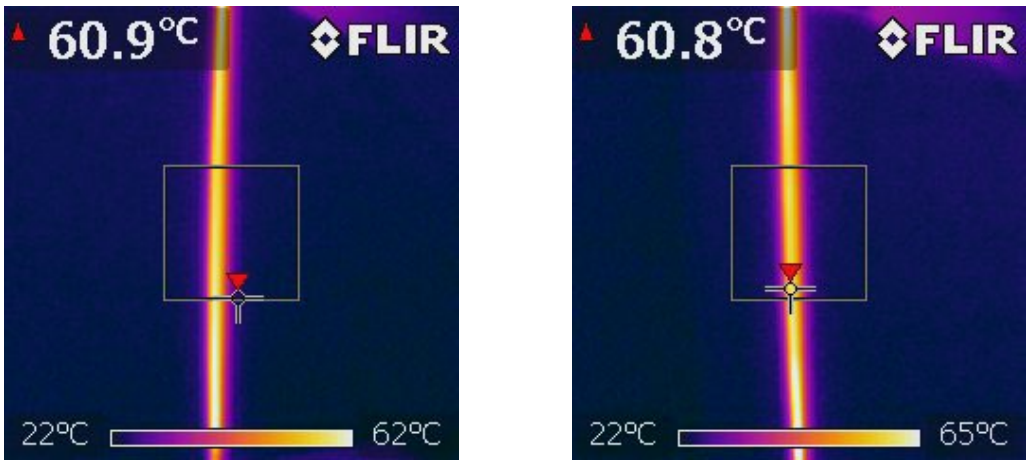

a) b)

FIGURE 4.5 THERMAL IMAGE TAKEN 50 SECONDS AFTER POWER ACTIVATION OF A TCP USING A) ONE 42 AWG NICR WIRE AND B) TWO 42 AWG NICR WIRE.

4.7 Discussion and conclusion

This study provides a pilot guidance for manufacturing reproducible joule heating TCPs with metallic embedded wires. The TCPs elaborated with this technique were able to reach strains (14 %) comparable with previous joule heating techniques like the use of silver coating treads (Tables 4.1 and 4.2). The method followed will allow to fabricate in a simple manner TCP actuator made of fishing line and NiCr that are both also accessible and inexpensive materials.

The study shows how the metallic wire negatively affects the TCP performance, both in response time and strain, as the wire diameter increases. It suggests one single thin wire configuration could be the option for the design of AMs.

The strain reduces proportionally to the increment of wire diameter, what could be related with the increase of the TCP stiffness. To confirm it, further investigation with a larger sample range will be required.

The relations strain, and response-time, against wire diameter, does not seem to be linear. In both cases strain (Figure 4.3) and response-time (Figure 4.4), the discontinuity occurs at 0.08 mm. Without the 0.08 mm, the system could be approximated with a linear equation:

$$Strain\ (\%) = -0.0924\ d_{wire} + 18.56 \tag{4.2}$$

$$\tau = 0.0054\ d_{wire} + 8.8978 \tag{4.3}$$

Equation 4.2 for strain and Equation 4.3 for response-time respectively.

As mentioned, the behaviour with two embedded wires was explored as well. It is interesting to notice how the two wires 42 AWG TCP behave similarly to the TCP with only one 38 AWG. This performance can be explained as the 38 AWG have a cross-sectional area (0.0079 mm^2) similar to the sum of two 42 AWG cross-sectional area (0. 0.003147 mm^2 * 2 = 0.006294 mm^2). Furthermore, the resultant resistance of the TCP was also similar, around 65 Ω for the two 42 AWG TCP, and around 50 Ω for the TCP with the 38 AWG wire. Consequently, the use of two embedded wires could be seen as using a single wire with a double-cross section area.

According to:

$$P = \frac{V^2}{R} \tag{4.4}$$

The use of a high resistance value could make the necessary voltage to power the system higher than the standards of batteries (from 1.5 V to 24 V). This constrain indicates that it could be necessary either to implement an extra electric circuit, to increase the nominal voltage value, or to optimize the diameter in the design process of AMs for specific applications (for instance, portable and/or untether rehabilitation robotic devices).

Although this study has it owns limitations and only one diameter of precursor fibre was used, it provides a pilot guideline for the design of AMs with TCPs for rehabilitation robotic devices. To better understand the relationship between the metallic wire and the performance of TCPs, the use of different precursor fibres of different sizes will be required. The size of the precursor fibre is an important characteristic to consider as it is tied to the force and response time that the final TCP actuator can reach [334]. Further research is needed to obtain a relation between the size of the precursor fibre, the metallic wire diameter, and how these variables affect the strain and response-time of the TCPs AMs.

4.8 Chapter Summary

The outcomes presented in this chapter indicated that a reduction in the thickness of the embedded NiCr wire, compared to the precursor fibre, resulted in an observable enhancement in strain. However, it is essential to note that while strain is indicative, it does not directly correlate with angular displacement, as angular displacement depends on linear contraction (contingent upon the actuator length and strain) and design parameters of the SWRR, as seen in Chapter 3. By synthesizing the insights gained from previous Chapters 3 and 4, it becomes feasible to address research question two. The exploration in Chapter 5 will commence by addressing research question three.

Chapter 5 : Improved Performance in Temperature and Speed of TCP Artificial Muscles for Soft Wearables Robots by Length Modification

5.1 Preface

The content of this Chapter is a copy of the article “Improved Performance in Temperature and Speed of TCP Artificial Muscles for Soft Wearables Robots by Length Modification”, published in the journal Smart Materials and Structures [387].

In Chapter 5, enhancements are introduced to augment the operational speed and temperature management of TCPs by leveraging two distinct properties:

(a) the first entails the enlargement of the TCP fibre,
(b) while the second involves the integration of a PID controller.

Despite extensive exploration of various fibre characteristics in the existing literature, such as the force generated by a thicker actuator, the influence of polymer material on response time, and the impact of tension in the manufacturing process on strain, the role of actuator length has remained largely unaddressed. Drawing on insights from research on other AMSMs, wherein length has been employed to enhance displacement in cases where strain is constrained, this Chapter delves into exploring the impact of actuator length on TCP actuators. Moreover, the extension of actuator length opens avenues for employing displacement offset to enhance speed. However, it is imperative to implement a control strategy for accurate tracking of the required displacement at the utilized speeds. Consequently, the following article focuses on implementing an offset technique with a PID controller and evaluates the role of actuator length in this context.

5.2 Abstract

AMs provide a unique solution for Wearable Rehabilitation Robots (WRRs) because they are compliant, compact, and lightweight. TCPs are AMs from thermally activated polymer fibres. They present high power density, linearity, stress and strain compared to other AMs. Nevertheless, as TCPs require heat to start, their main barrier for widespread use in WRRs are their slow reaction times and the high temperatures they reach. Previous studies have analysed different parameters, like fibre material, fibre diameter, and various cooling systems, to improve TCP frequency response and working temperature.

Nevertheless, the length of the actuator has not been explored as a possible parameter to enhance the actuation performance in this regard.

This work focuses on studying the behaviour of TCPs with different lengths and how the performance in frequency response and temperature can be improved using the length as a primary parameter, as they are critical for wearable robots. First, a characterisation of the TCPs was performed. Then, a method to improve frequency response, based on offsets on long actuators was implemented and validated using a chirp signal. The experimental results show that the mechanical characteristics are similar regardless of the actuator's length. They reached a strain of 10 % with a power of 0.16 W/cm. However, the electrothermal properties changed as the power needed to increase temperature was higher when the actuator was enlarged. Therefore, an improvement in the required temperature was found, able to reduce the temperature with the same frequency response. Regarding the technique to enhance the speed of the actuator, it was possible to increase the frequency by 0.0006 Hz for each mm applied as an offset. Hence, the frequency response for the same displacement was increased linearly as the actuator was elongated.

5.3 Introduction

People with a physical disability caused by conditions like CP, Stroke, Muscular Dystrophy, or ageing; face reduced quality of life due to limited mobility and independence [262]. The standard rehabilitation therapies used to manage the musculoskeletal system's deterioration and improve or maintain physical ability, include physiotherapy [37]. These therapies often involve intensive stretching and strengthening exercises facilitated by the physiotherapist to improve motor skills [8]. These interventions are often highly labour-intensive and challenging to perform [13].

During the last decade, WRRs have gained popularity in rehabilitation [274]. WRRs are expected to improve the outcomes of rehabilitation therapies as they allow for mass practice with reduced intervention of the physiotherapists and help people during ADLs [33]. However, most current WRRs use electric motors and rigid links to actuate them and often have heavy and bulky designs that are difficult to wear outside clinical facilities safely [29]. Consequently, researchers started to develop SWRR through the use of more compliant elements such as AMs [36] like SMAs [262], DEAs [263], pneumatic [233], and TCPs.

TCPs are AMs fabricated by inserting a twist in precursor polymer fibre while attaching a dead weight at the end until it forms a coil structure, followed by heat treatment [56].

To activate the TCPs is necessary to use an external source of heat as they are made of plastic thread. One option is to utilise joule heating by applying an electric current through a conductive heating element embedded into a TCP, such as metallic wires (e.g., Nichrome wires). This method presents the advantage of making the actuators electrically controllable [57, 58]. In comparison to other AMs, TCPs stand out due to their high power density (27 W/g), high stress (10 MPa), large strain (21%), and linear behaviour with low hysteresis [50]. Nevertheless, they suffer from low frequencies (< 1 Hz) and high temperatures (> 65 °C), all critical aspects for SWRR [50, 59, 60].

For SWRR applications, there are biomechanical considerations that need to be fulfilled, like torque/force, ROM/displacement, and velocity/frequency [273, 286]. Due to their advantages, TCPs have gained attention in the SWRR area, as they present high forces and strains. However, they still require improvements in their overall performance as it is still not optimum for the SWRR applications. The main drawbacks are the frequency response and the working temperature.

To overcome these drawbacks, researchers have investigated how different TCPs parameters and techniques impact the actuators' frequency response and working temperature to be used on SWRRs. Hiraoka et al. [388] used hard linear low-density polyethene (LLDPE) fibres to improve the operating temperature. Haines et al. [334] demonstrated that the response time depends on the fibre diameter. Yip et al. [332] used a closed-loop control strategy to improve the speed of the fibres during the heating phase. Edmonds et al. [389] showed how an active cooling system can increase the maximum frequency where the TCPs can work.

Even if length is one of the primary parameters to consider when designing an application, there is no literature exploring the use of length to improve the response time and temperature of the TCPs. Therefore, this article explores how different lengths impact the actuator's temperature and response time behaviour. Furthermore, a new methodology is presented to improve the TCP frequency response based on the actuator's length without using external cooling systems.

This work is divided into four parts: the first one, Section 5.4, aims to investigate the length impact on the TCPs behaviour by using TCPs of three different lengths (75, 180 and 295 mm) in isotonic contraction (i.e., the muscle contract generating a displacement). The second part, Section 5.5, implements a methodology to improve the frequency response and manage the operational temperature base on the length of the actuator and a PID displacement control. Then, Section 5.6 discusses the advantages of longer fibres in SWRR. Finally, a conclusion is presented in section 5.7.

5.4 Actuator Characterisation

An isotonic contraction test was applied to the TCPs to characterise the actuators and understand their properties in force, strain, response time and temperature, as they are the main requirements for SWRR.

5.4.1 Materials and Methods

The TCP actuators to be analysed were fabricated similarly to the process described by Chossat et al. [377]. 1.25 m Nylon fishing line was used as the precursor fibre (Trilene Big Game fishing line 50 lb) with a diameter of 700 μm. The nylon fibres were twisted and coiled along with a 36 AWG (127 μm) NiCr 80 wire (Fogslord). One side of the nylon fibre was fixed at the end of the output shaft of a NEMA17 (T-Trees Technology) motor. The other end is on a slider weighing 800 g (≈20 MPa). The NiCr wire was also suspended from the motor shaft but only straightened using a small weight of 1.6 g (≈1.2 MPa) and was left free to untwist. The fibres were twisted and coiled at a slow speed of 250 rpm [380]. The embedded NiCr wire generated joule heating for the annealing phase. The annealing process involves applying five consecutive five-minute-long periods with an annealing current of 240 mA each. Between every period, a cooling phase of 1 minute was used.

After this process, TCPs with an average length of 330 mm were obtained (Figure 5.1a). They were manually trimmed into three sizes of approximately one-quarter, two-quarters, and three-quarters of the initial measurement. They resulted in actuators with a length of 75 mm, 165 mm, and 250 mm. Then the outcoming actuators were clamped with insulated male spade electric terminals, reducing the functional area by 10 mm as each electrical terminal required 5 mm to be crimped (Figure 5.1b). The final active lengths of the TCPs were 65 mm, 155 mm and 240 mm with resistance values of 25 Ω, 59 Ω and 92 Ω respectively, meaning that all of them present a resistivity ρ ≈ 0.38 Ω/mm. The relation between length and resistance can be described with a linear approximation:

$$R = 0.38281 \times L - 0.0305 \tag{5.1}$$

where R is the resistance (in ohms), and L is the actuator's length (in mm).

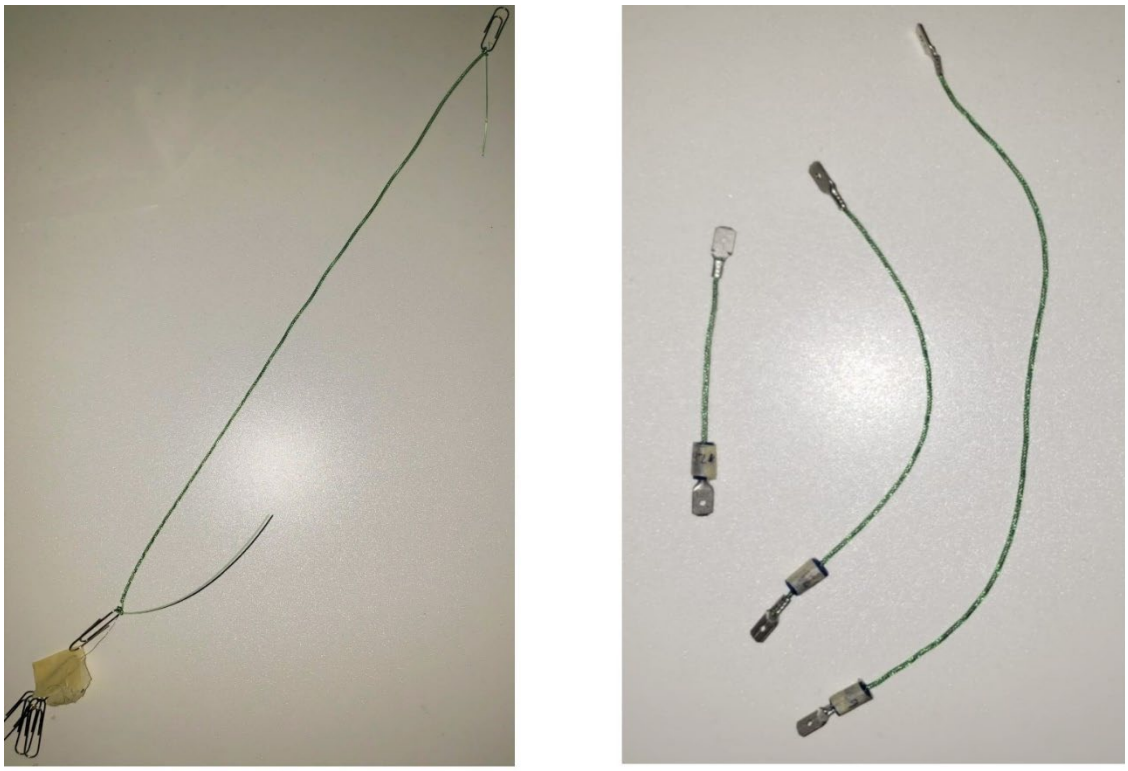

FIGURE 5.1 TCP ACTUATORS, A) INITIAL ACTUATOR, B) ACTUATORS OF DIFFERENT SIZES WITH SPADE ELECTRIC TERMINALS.

Three TCP actuators of each size were manufactured, following the mentioned method. All the samples fabricated for the study were tested using a custom-made experimental test bench. The experimental setup consists of a displacement sensor (Sick Optex 0d80 15p850) connected to a current sensor (Texas Instruments INA269), an Arduino NANO connected to the computer, and a transistor (Vishay Siliconix IRF540) to control the voltage coming from the power supply. The actuator was hanging above the sensor, weighing 700 g. Furthermore, the temperature and the power to activate the TCP were measured using an NTC thermistor (5K3A1, TE Connectivity) and an extra current sensor (Texas Instruments INA269).

A square signal of 150 s on and 150 s off was applied to obtain the strain and power relation. The 150 s was chosen to give enough time to the system to reach a stable condition. The experiment was repeated for different current levels ranging from 160 mA to 220 mA with increments of 20 mA. After applying the load (700 g), the actuator's length was 75 mm, 180 mm and 295 mm. The loaded lengths were the ones used in the results section. Throughout the trial, the TCA temperatures, power consumed, and the weight distance from the sensor were logged into a computer using an Arduino NANO with a sampling time of 50 ms. This test was performed for every actuator of different sizes.

5.4.2 Results

After performing all of the trials for each different size, the resulting power, displacement, and temperature values were obtained (Figure 5.2). The power consumption was derived from the applied current and the resistance values of the different actuators. When full power was applied to the actuators (1.2 W, 2.8 W and 4.5 W, respectively), the maximum achieved displacements were 7.12 mm, 17.1 mm, and 28.9 mm for the 75 mm, 180 mm, and 295 mm, respectively. The maximum strain of all the TCP of different sizes was ≈ 10 % of the initial length. Regarding the temperature (Figure 5.2g-5.2i), the maximum average temperatures obtained were 81.26 °C, 80.36 °C, and 76.83 °C for the 75 mm, 180 mm, and 295 mm TCP actuators, respectively.

Other interesting information that can be obtained from the data is the rise (τ_r) and fall (τ_f) response times of the actuators. This is the average time the actuator takes to reach 63% of a steady-state value given a step input. For the 75 mm actuators, $\tau_r = 17.98\ s$ and $\tau_f = 14.51\ s$. In the case of the 180 mm actuators, the τ_r and τ_f were 22.59 s and 16.10 s, respectively. Finally, for the 295 mm actuators, the τ_r and τ_f were 23.58 s and 16.49 s.

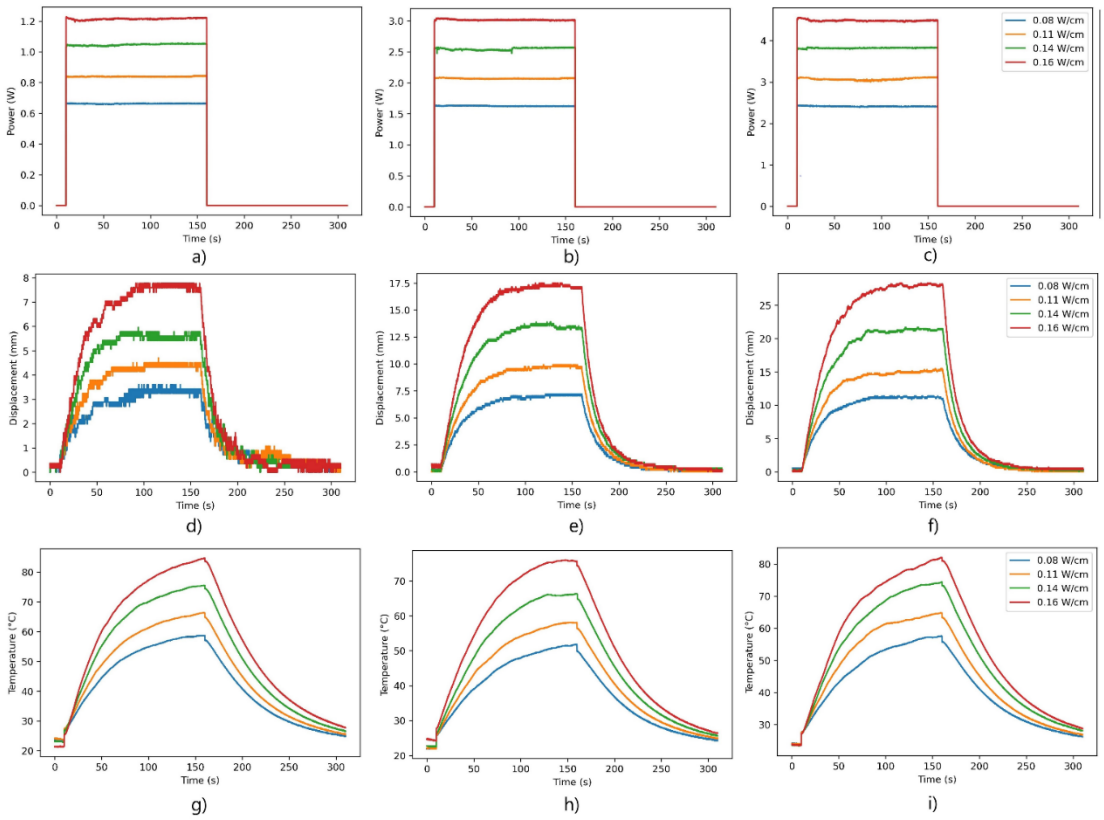

FIGURE 5.2 POWER CONSUMED BY THE ACTUATORS DURING THE ISOTONIC CONTRACTION TESTS A) 75 MM, B) 180 MM, C) 295 MM. RESULTANT CONTRACTION FROM THE ACTUATOR DURING THE ISOTONIC CONTRACTION TEST D) 75 MM, E) 180 MM, F) 295 MM. REACHED TEMPERATURES FROM THE ACTUATOR DURING THE ISOTONIC CONTRACTION TEST G) 75 MM, H) 180 MM, I) 295 MM.

The stroke and power levels were calculated for each set of actuators. Then, a linear regression was applied to the mean values of each set of actuators to determine a linear model. In Figure 5.3a, the linear relation between the applied power in W and the generated stroke can be seen. From this relation, it is possible to observe that, independently of the length of the actuator, the applied power will generate the same amount of stroke. This relation can be represented as (R^2 =0.9708):

$$D = 6.1033 \times P - 1.6426 \tag{5.2}$$

where D is the generated stroke in mm, and P is the required power in watts.

Furthermore, the idea remains that the relationship between the stroke and the applied power is independent of the actuator length. The TCP length normalised the stroke and the power during the experiments (Figure 5.3b), and the following linear relation was obtained (R^2 = 0.9821):

$$S = 75.2979 \times NP - 2.6920 \tag{5.3}$$

In this case, S is the strain of the actuator, and NP is the normalised power (W/cm). The strain of the system is the relation between the initial length (L) of the actuator and the generated stroke (ΔL) when activated, expressed in % as follows:

$$S = \frac{\Delta L}{L} \times 100 \tag{5.4}$$

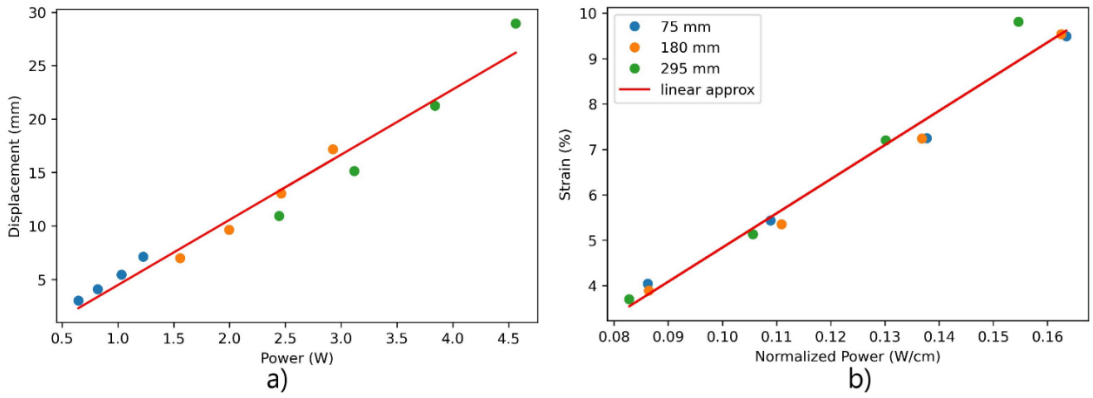

FIGURE 5.3 MAXIMUM DISPLACEMENT RELATION WITH RESPECT TO POWER, WITH OVERLAID LINEAR REGRESSION, B) NORMALISED TO TCP LENGTH RELATION.

Regarding the temperature, a linear trend was found between the temperature and the applied normalised power (R^2 = 0.9624):

$$T = 326.9759 \times NP + 27.0464 \tag{5.5}$$

Where T is the temperature in °C and NP is the normalised power. Finally, a linear relation was found between temperature and strain (R^2 = 0.9296):

$$S = 0.2204 \times T - 8.2573 \tag{5.6}$$

With the observed relation (Equation 5.3), it is possible to witness that independently of any unit of length, the strain stay the same due to the asymmetric thermal expansion of polymer monofilaments [56]. Nevertheless, when it comes to the thermal properties, they will change with the length of the actuator [390]. The central values on the electrothermal relation (Equation 5.7) are dependent on the length (thermal resistance (R_{th}) and thermal capacitance (C_{th})) (Figure 5.4a). The dependency on length could be seen in Equation 5.8 and Equation 5.9 as it forms part of the surface area and volume; respectively.

$$C_{th}\frac{dT(t)}{dt} = P(t) - \frac{\left(T_{tcp}(t) - T_{\infty}\right)}{R_{th}} \tag{5.7}$$

Where C_{th} is the thermal capacitance, P is the applied power, R_{th} is the thermal resistance, T_{tcp} is the surface temperature of the TCP and T_{∞} the ambient temperature.

$$R_{th} = \frac{1}{A_{tcp}\, x\, (h + \varepsilon_{tcp} \times \sigma \times \left(T_{tcp} + T_{\infty}\right) \times (T_{tcp}^2 + T_{\infty}^2))} \tag{5.8}$$

R_{th} can be calculated using the surface area A_{tca}, the thermal convection coefficient h, the emissivity ε_{tcp}, the Stefan Boltzmann's constant σ, and the temperatures generated by the TCP T_{tcp} and the environmental temperature T_{∞}. Moreover A_{tca} can be calculated with:

$$A_{tcp} = 2\pi rL + 2\pi r^2 \tag{5.9}$$

Being the r the radius of the TCP cross sectional area and the actuator length L .

$$C_{th} = \rho\, x\, c\, xv \tag{5.10}$$

Finally, C_{th} is obtained multiplying the ρ density, the specific heat capacity c and the volume of the sample v.

It is possible to see the advantages of implementing long actuators into WRR. It is feasible to obtain the same stroke using the same amount of power from a more extended actuator rather than a small actuator's full stroke range and reduce the generated temperature from the TCP actuator (Figure 5.4b-5.4d) without increasing the time. The main disadvantage of the actuator's increases in length, is the R_{th} decrease

as the surface area increase (Equation 5.8). The change in R_{th} will cause an increase in power consumption to generate the same temperature (Equation 5.7). Nevertheless, the response time will remain similar:

$$\tau = C_{th}\, x\, R_{th} \tag{5.11}$$

where is possible to notice from Equation 5.8 and Equation 5.9 that the increased and decreased values of C_{th} and R_{th} will change in the same linear manner with the length of the actuator.

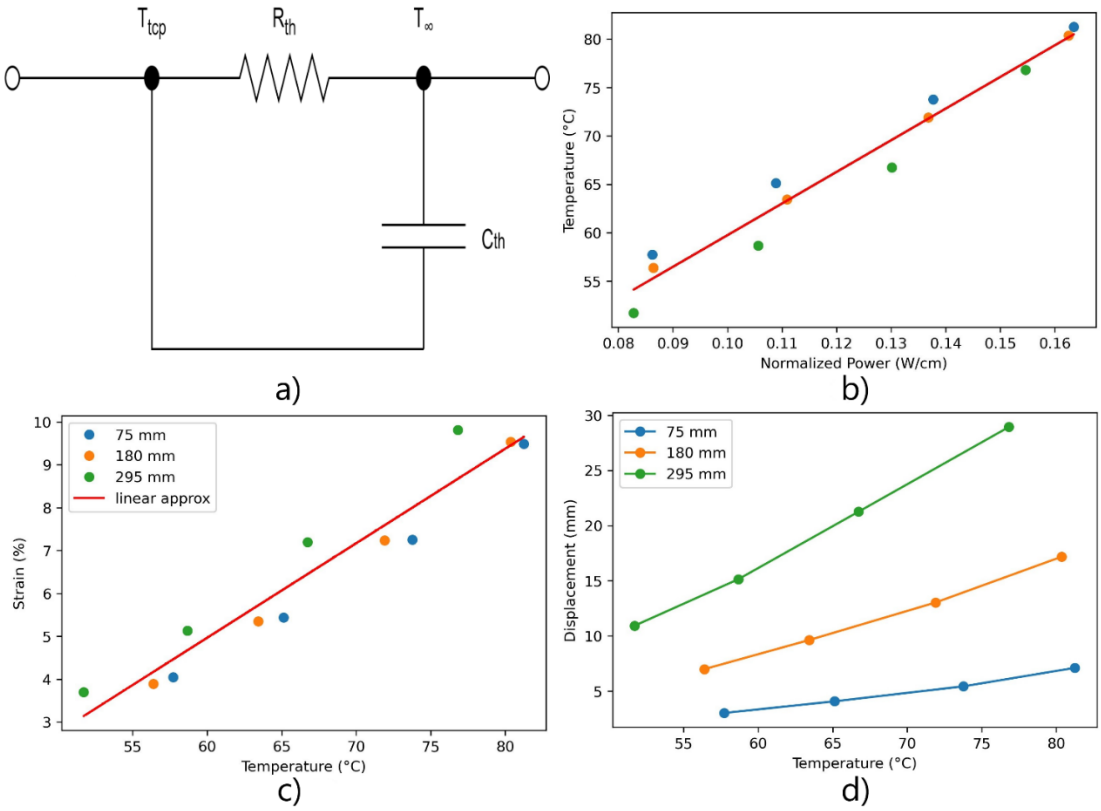

FIGURE 5.4 A) SIMPLIFIED THERMAL MODEL OF THE TCP, CONSISTING OF THE THERMAL CAPACITANCE C_{th}, THE THERMAL RESISTANCE R_{th}, THE TCP SURFACE TEMPERATURE T_{tcp} AND THE AMBIENT TEMPERATURE T_{∞}. TEMPERATURE RELATIONS DURING THE ISOTONIC CONTRACTION TEST. B) TEMPERATURE AGAINST THE NORMALISED POWER, AND C) STRAIN VERSUS TEMPERATURE. D) GENERATED DISPLACEMENT WITH THE THREE DIFFERENT LENGTHS AGAINST THE TEMPERATURE.

5.5 Displacement Control Implementation

In the previous section, the characterisation of the TCP actuators was performed. Furthermore, the advantage of a reduction in temperature using longer actuators was found. However, one of the main disadvantages of TCPs is the low frequencies at which

they can work (<1 Hz). A strategy to increase the response time could be to briefly apply a pulsed signal with high power peaks [48, 57]. However, the continuation of a high-power pulse will produce an overheating of the actuator, causing it to break or burn out [62]. Hence, a control strategy should be applied to avoid overheating the actuator and work under safety actuation ranges. However, this strategy can only be used during the rising time but not during the falling time, as TCPs are unidirectionally actuated. A popular approach to reducing the response time during the falling time is to implement a cooling system, decreasing the overall response time, with the constraint of requiring external equipment like pumps or fans [332, 389].

This section investigates a method to improve the actuation speed but using long actuators. From the isotonic test in the previous section, it could be seen that length impacts the actuation temperature, as it is possible to obtain a more significant displacement with a lower temperature. Furthermore, Cho et al. [391] show that the falling time in the temperature of the TCPs depends on how different the final temperature is from the starting temperature. Moreover, Tang et al. [378] proposed to constrain the range of the activation to improve the speed of a crawling robot. Considering the previous concepts, a method combining both approaches is presented and analysed on how the actuator length could benefit from them and increase the frequency without needing an external cooling system. The technique consists of actuating a specific displacement using different distance-offsets on the actuators. As the actuator lengthens is possible to add more offsets, which will change the actuation range in temperatures, and therefore increasing the actuation speed as the cooling time is reduced.

5.5.1 Materials and Methods

After characterising, in section 5.4, the strain production of the actuator in an open-loop system, a closed-loop control scheme to operate the displacement output of the actuator is provided. Two different experiments were performed to test the response of the controlled system. First, a step signal was used to analyse the response time while heating, and later a chirp signal was used to analyse the system's frequency response on the proposed control method based on the actuator length.

The test bench was the same as in the characterisation experiments (section 5.4), with two differences. The sensor reading the current across the TCP was removed due to the higher power values needed to activate the actuator when the PID controller is on. Instead of using the MOSFET as a digital on-off switch, a power Pulse Width Modulation (PWM) strategy was implemented (100 ms cycle time). It allows the usage of high-power

signals controlled by the microcontroller. The power was constrained to 0.86 W/cm, equal to 6.5 W, 16.4 W, and 25.5 W for the 75 mm, 190 mm and 295 mm, respectively. The maximum applied power was chosen due to limitations with the power supply at full power.

5.5.2 System Identification

The controller was constructed based on the stroke characterisation experiment results, which generated a time-domain relationship between stroke output and the input power. The input signal was the maximum applied power for each actuator size, and the output signal was the generated displacement. Later, the curves' pairs were input into the System Identification Toolbox in MATLAB, which derived the power–displacement transfer functions G_{PD} (s) for each actuator length (Table 5.1). The proposed model by Yip et al. [332] was used as the initial guess to find the order of the transfer function. In this work, the model was divided into a temperature-force relation, a power-force relation, and a force-movement relation.

First, a temperature-force relation was modelled as a spring and damper model with the addition of a linear temperature-dependent term:

$$f(t) = k(x - x_0) + b\dot{x} + c(T(t) - T_0) \tag{5.12}$$

Where f is the force of the system, k is the spring constant, b is the damping coefficient, c is the thermal constant, x is the position, x_0 is the initial position and $\dot{x}$ is the speed.

When the wires are held in isometric tension, the force can be modelled by:

$$f(t) = c(T(t) - T_0) \tag{5.13}$$

To obtain the power-force relation, Equation 5.13 is combined with the thermoelectric model of the actuators (Equation 5.7):

$$\frac{F(s)}{P(s)} = \frac{c}{C_{th}s + \frac{1}{R_{th}}} \tag{5.14}$$

Then to obtain the force-displacement relation can be modelled as a second-order mass-spring-damper system:

$$f = m\frac{d^2x}{dt^2} + b\frac{dx}{dt} + k(x - x_0) \tag{5.15}$$

That will result in the following transfer function:

$$\frac{X(s)}{F(s)} = \frac{1}{ms^2 + bs + k} \tag{5.16}$$

Finally, combining Equation 5.14 and Equation 5.16, a third-order system of the following form is obtained:

$$\frac{X(s)}{P(s)} = \frac{A}{Bs^3 + Cs^2 + Ds + E} \tag{5.17}$$

A, B, C, D, and E are values derived from the model constants.

The initial estimation of the system was a third-order transfer function with no zeros. However, it was noticed that adding a zero increased the system's accuracy (Table 5.1). Hence the used models were those with one zero.

Table 5.1 Frequency domain transfer functions for the power–stroke relationships $G_{PD}(s)$ with one or non-zero for each actuator size

Actuator size (mm)	G_{PD} (no zero)	Accuracy	G_{PD} (1 zero)	Accuracy
75	$\frac{0.2815}{s^3 + 4.295\,s^2 + 1.232\,s + 0.4748}$	94.8%	$\frac{5.947\,s + 3.119}{s^3 + 55.48\,s^2 + 13.73\,s + 0.5228}$	96.47%
180	$\frac{0.0003572}{s^3 + 0.162\,s^2 + 0.0061\,s + 5.77e^{-5}}$	93.82%	$\frac{1.326\,s + 0.1758}{s^3 + 7.25\,s^2 + 0.8503\,s + 0.02774}$	98.98%
295	$\frac{0.0003575}{s^3 + 0.1514\,s^2 + 0.00643\,s + 5.55e^{-5}}$	97.85%	$\frac{14.53\,s + 2.132}{s^3 + 89.27\,s^2 + 11.24\,s + 0.3366}$	98.93%

5.5.3 Control strategy

When using the transfer functions, a PID controller was tuned using the Control system toolbox in MATLAB. Then the closed loop with the PID controller system was simulated in MATLAB/Simulink. In particular, special care was taken to minimise the overshoot, settling error of the controller, and the necessary power to activate the system, as errors of that nature would result in an incorrect application of force to the user, which could cause harm.

Applying the maximum power, the speed to achieve the highest contraction (10 % of the initial length) was 7.5 s. However, the values for a reaction time of 1 s equivalent to a frequency of 1 Hz were also investigated and applied in the chirp test. As most ADLs frequencies are around 1 Hz [61, 302]. According to Table 5.2, the PID values are similar for all the different lengths. The values obtained for the 295 mm model were used, as this model was the best of the 3 cases obtaining accuracies over 83% when fitting to the data.

Table 5.2 PID controller values

Actuator length (mm)	Speed (s)	KP	KI	KD
75	7.5	1.394	0.08267	0
180	7.5	1.309	0.07955	0
295	7.5	1.484	0.08365	0
295	1	12.05	4.408	0

After the closed-loop controller was tuned, it was implemented on an Arduino NANO microcontroller. Two different tests were performed. First, a step input test was applied to determine their performance in controlling the actuator, and then a chirp test was used to test the bandwidth of the actuator.

5.5.4 Results

Step Response

The step response was applied to the full stroke (a strain of 10 %). Figure 5.5a shows the position reference and the output when a step signal was applied for the different actuator sizes. It can be observed that the output follows the reference, but the system presents an underdamped response. The time from 0 to 10 % of the initial length was less than 10 seconds. Contraction time can be minimised by changing the controller

gains, but an aggressive control signal will increase the peak power required to produce the change.

Nevertheless, the falling time was the same as the open-loop system and depended on the convective air to cool down the system. From Figure 5.5c, it is possible to notice the difference between the required power to make a fast movement and the power to maintain a steady state. In the case of the steady-state power, once the actuator reaches a steady-state, the consumed power is similar to the power required on the open-loop system (approx. 1.2 W, 2.13 W and 3.1 W for the 75 mm, 180 mm and 295 mm, respectively). The consumed power was calculated as a function of the percentage of the duty cycle on the PWM. Figure 5.5d shows the percentage of the PWM duty cycle, and it can be noticed that the PWM values are similar for all the sizes. Finally, Figure 5.5b shows the reached temperatures during the experiments. They were comparable to those obtained during the open-loop experiments, with the difference of a faster temperature increase at the beginning due to the higher applied energy. Interestingly, in any case, the temperature surpassed 70°C-80°C, which were the maximum temperatures before the actuator failed.

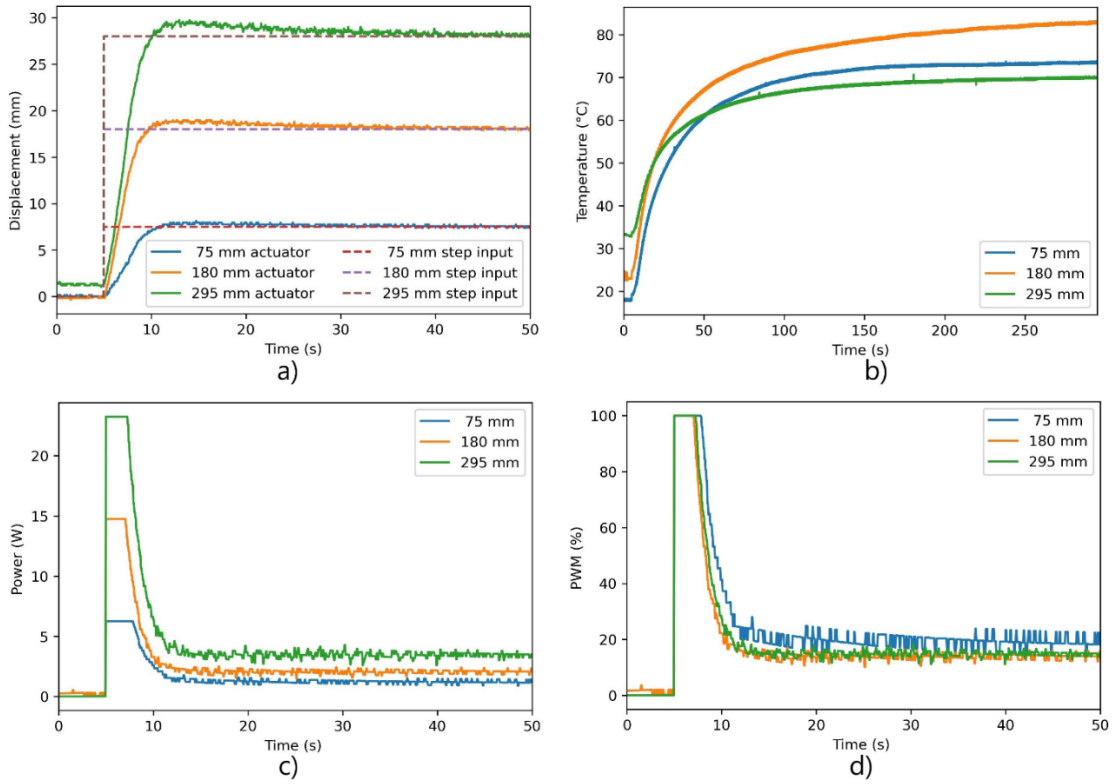

FIGURE 5.5 A) STEP RESPONSE AND B) TEMPERATURE FROM DIFFERENT SIZES OF TCPS WHEN THE PID CONTROLLER STRATEGY IS APPLIED. PWM CONTROL SIGNAL EXPRESSED C) IN CONSUMED POWER AND D) IN % OF THE PWM.

Chirp response

The benchmarking for the actuator speed using the proposed variable length method was performed by applying a linear chirp signal [292]. It consists of a sinusoidal sweep signal that varies its frequency over time, which can be expressed as follow:

$$chirp(t) = \mathrm{A}\sin\left[2\pi\left(\frac{c}{2}t^2 + f_0 t\right)\right] \tag{5.18}$$

Were f_0 is the final frequency, A is the amplitude of the sinewave, and c is the chirp rate, described by:

$$c = \frac{f_e - f_0}{T} \tag{5.19}$$

where f_e is the final frequency, and T is the time it takes to sweep from f_0 to f_e.

The sinewave amplitude was 6 mm for testing, making the base displacement 1 mm - 7 mm. This was chosen to use the whole stroke of the 75 mm actuator. From here, offsets of 60 mm were applied to the longer actuators. Hence, in the case of the 180 mm, experiments with a maximum displacement of 7, 13 and 19 mm were performed. Moreover, with the 290 mm, a maximum displacement of 25 mm was added.

The initial chirp frequency was 0.01 Hz. This frequency was chosen as it is lower than 0.05 Hz, which is the inverse of the response time of the actuator (τ_f = 23.58 s). Furthermore, the final frequency is equal to 0.1 Hz, near the maximum frequency of the controller speed of 7.5 seconds (0.133 Hz). In the case of the final frequency, it was chosen to be lower than the inverse of the maximum rate with the controller, as the controller only works in the contraction direction, making it slow when cooling down. The maximum working frequency for each TCP was established when the actuator lost -3dB in amplitude (when the active actuator range was reduced by half) in the frequency analysis of the output signal.

As with the previous experiments, the behaviour of the lower range in the 180 mm and 290 mm actuators was similar to using a 75 mm (except the maximum temperature), and the same applies to the 180 mm to with the 290 mm, meaning that the linear behaviour of different lengths is still valid. Due to these similarities, Figure 5.6 presents only the result of the 290 mm TCP at various levels.

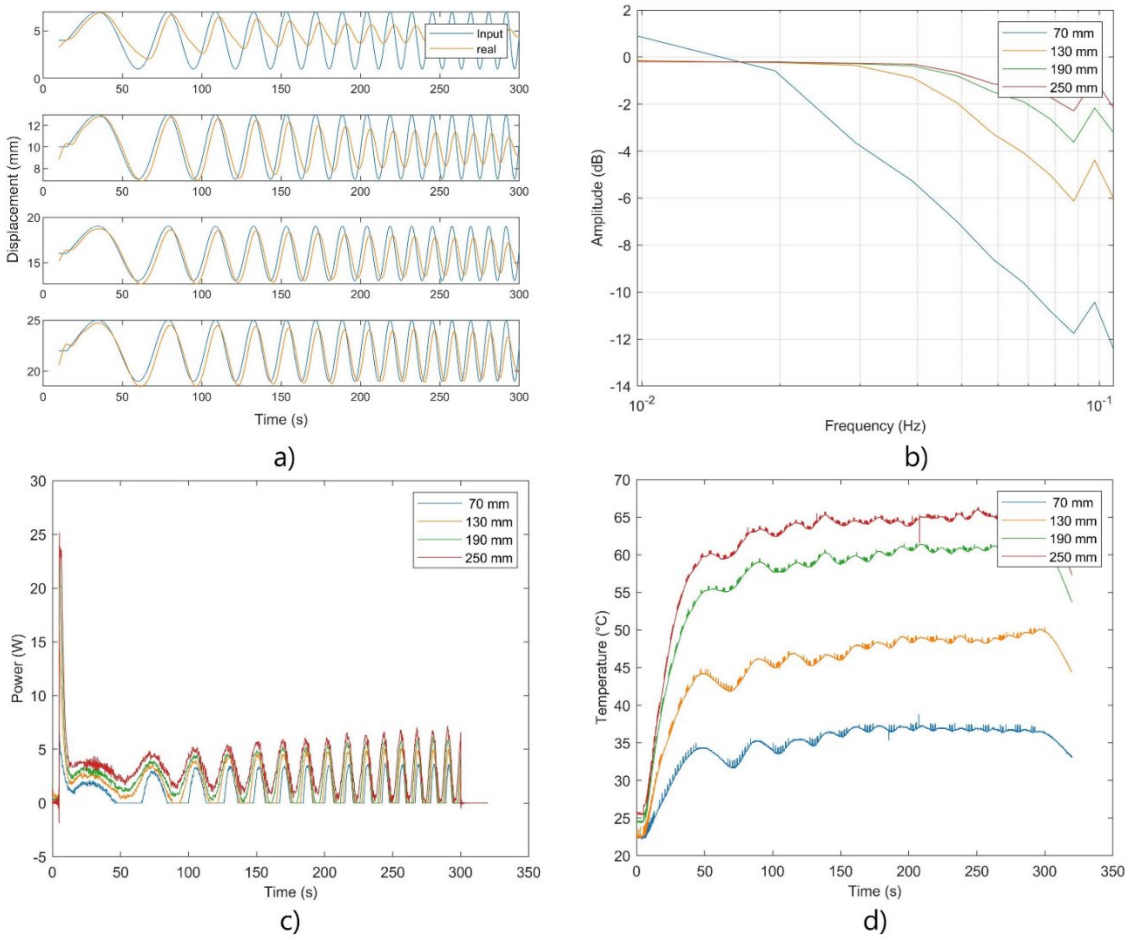

FIGURE 5.6 A) POSITION RESPONSE WITH CHIRP SIGNAL REFERENCE (0.01-0.1 HZ) TO DIFFERENT OFFSETS ON THE 295 MM TCP WITH A 7.5 S RESPONSE TIME PID CONTROLLER. B) MAGNITUDE BODE PLOT FOR THE 295 MM WITH DIFFERENT OFFSETS. C) POWER CONSUMPTION CORRESPONDS TO THE CHIRP TEST RESPONSE (0.01-0.1 HZ). D) REACHED TEMPERATURES DURING THE CHIRP TEST.

After analysing the data of the 190 mm TCP, there was a slight difference between the 120 and 180 mm offset, and neither reached the -3 dB in amplitude (Figure 5.6a-5.6b). Furthermore, during the test, the maximum power was only applied at the beginning of the test to reach the offset. After that, the used power was less than half of the maximum power (Figure 5.6c). Hence, a new chirp was used, but this time with a maximum frequency of 1 Hz, PID values were changed to those that allowed the actuator for 1 s reaction times (Table 5.2). In the case of the temperature, as the speed increases, it reaches temperatures as if a step signal were applied. This is because the system can not respond to those frequencies and starts behaving like a DC voltage signal (Figure 5.6d).

Table 5.3 shows the maximum temperature reached during the test, the frequency at -3dB, and the peak power consumption at this frequency for each actuator and offset.

Table 5.3 Maximum values of the 1 Hz Chirp Test

Actuator (offset)	Maximum temperature (°C)	Frequency at -3dB (Hz)	Power at -3dB (W)
75 mm	72.74	0.051	4.0
180 mm	45.5	0.046	4.16
180 mm (60 mm)	60.35	0.09	7.63
180 mm (120 mm)	71.4	0.127	10.15
295 mm	40.03	0.043	4.27
295 mm (60 mm)	52.17	0.082	7.78
295 mm (120 mm)	63.23	0.11	10.19
295 mm (180 mm)	71.07	0.15	13.64

After increasing the chirp frequency and the PID controller, the difference between 120 and 180 mm offset increases. Both reach the mark of -3dB in amplitude at different frequencies, 0.11 and 0.15 Hz, respectively (Figure 5.7a-5.7b). It is possible to appreciate how the response time of the actuator change as the offset is increased in both time (Figure 5.7a) and frequency domains (Figure 5.7b). In this case, as the speed increases, the maximum power starts to be used during the activation time to achieve the actuation at the high frequencies (1 Hz). Nevertheless, during relaxation times, the cooling process is slow. This slow cooling process is what sets the frequency. The temperature was not pictured for the 1 s PID as the temperature tends to be a constant similar to that achieved during the step test.

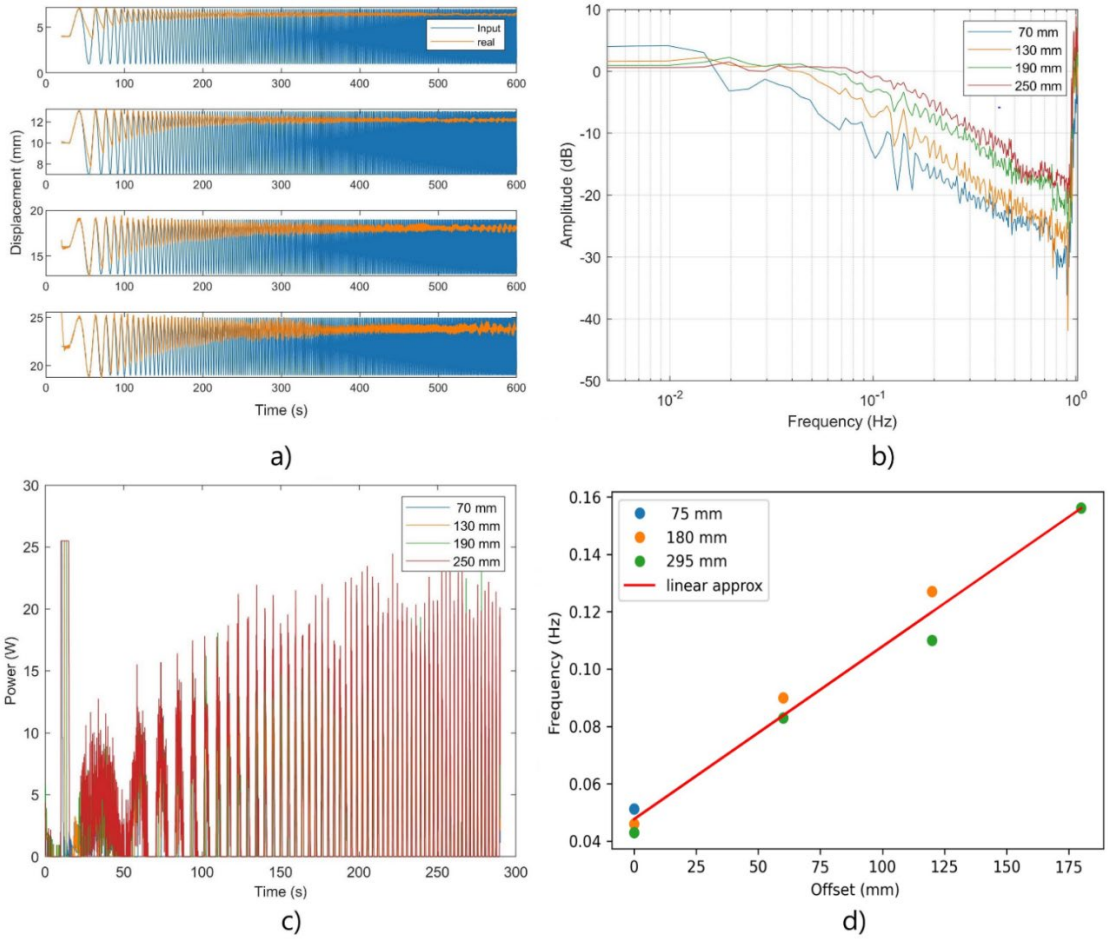

FIGURE 5.7 A) POSITION RESPONSE WITH CHIRP SIGNAL REFERENCE (0.01-1 HZ) TO DIFFERENT OFFSETS ON THE 295 MM TCP WITH A 1 S RESPONSE TIME PID CONTROLLER. B) MAGNITUDE BODE PLOT FOR THE 295 MM WITH DIFFERENT OFFSETS. C) POWER CONSUMPTION FOR THE 295 MM WITH DIFFERENT OFFSETS (0.01-0.5 HZ). D) LINEAR RELATIONSHIP BETWEEN OFFSET INCREMENT AND FREQUENCY INCREMENT.

When they reached frequencies (F) are compared to the given offset a linear relation was found (R^2 = 0.9809):

$$F = 0.0006 \times Offset + 0.0477 \quad (5.20)$$

For every mm increased as an offset a gain of 0.0006 Hz is obtained. In the proposed example, the initial frequency of the 6 mm displacement was 0.051 Hz, and it improved to 0.15 Hz with the 295 mm actuator (approximately three times faster). The change in the frequency is due to the displacement range used. The relation is independently of the length of the actuator, it can be seen the trend of the 180 mm and 295 mm actuator are similar for the first two offsets. Furthermore, the maximum temperature was almost the same for the faster test on the 295 mm than in the case of the 75 mm, providing an advantage as it is possible to reduce the temperature with the same or better performance in speed. However, the consumed power will increase (Figure 5.7c) as higher frequencies require more significant offsets.

5.6 Discussion

This work presents the properties of long TCP actuators to increase the bandwidth and reduce the working temperature to explore their use on WRR.

From the result of the characterisation test, the length does not affect the maximum stroke that an actuator can generate, as all the different sizes presented a strain of ≈ 10% of the initial length. Furthermore, the mechanical properties are maintained, and a linear relationship was found between the applied power and the achieved stroke.

Another advantage is the temperature reduction to generate a particular stroke as the actuator length increases. This advantage is a crucial design feature for SWRR using thermally activated actuators, as the temperature for the pain threshold of humans is 44 °C at the dermal/epidermal interface of the skin [60]. Meanwhile, if the actuator is activated at its full range, it can reach a temperature above 70° C (Figure 5.4b).

For example, in the case of a wrist SWRR, which requires a ROM of 40° extension and 38° flexion during ADLs, a stroke of ≈ 23 mm is needed [389]. From the used actuators, the most similar to get this length with the maximum stroke will be 180 mm; at its maximum stroke ≈ 18 mm, the temperature is ≈ 82°. In contrast, if the 295 mm actuator is used to obtain the same displacement, the temperature will be ≈ 62°. And it can be reduced more if a longer actuator were to be used. Furthermore, space should not be a constraint. Like SMA [314], TCP actuators could be wrapped around pulleys [60, 392] to utilise longer muscle lengths allowing larger strokes.

Regarding the speed of the actuators, during open-loop activation, there is no difference between the different lengths of actuators as the time response is similar, independently of the length. In the case of the fabricated actuators, it was around 20 s. Nevertheless, reaching high contraction speeds independently of the length is possible with a correct closed-loop control strategy and high-power values. Furthermore, as the electromechanical model is similar for all the lengths, using the same PID controller is possible.

As noticed from previous research [332, 389], the problem with the TCP actuators is the cooling time to recover the initial length, which is found during the isotonic contraction tests. The typical method to improve the speed is to reduce the TCP diameter with the disadvantage of reducing the force or using a cooling system that will increase the system's complexity. In this work, a different strategy is proposed for single TCP actuators. The proposed approach uses actuators to produce more significant

contractions than the required ones. It is possible to provide offsets and use different activation regions to improve the closed-loop bandwidth for the whole movement and not only the contraction [58]. Using offsets equal to the required contraction, it was found that the base bandwidth increases linearly by 0.0006 Hz. In the case of the used actuators, the bandwidth improves from 0.051 Hz to 0.15 Hz without requiring any external cooling system and keeping the output force. However, if speed is the main objective, it could use thinner TCP actuators. For instance, if an offset of 1 m is use, the final frequency will be 0.6477 Hz. This frequency is useful for physical rehabilitation therapy and low frequency ADLs, as the minimum frequency for these activities is 0.5 Hz [48, 342].

Considering that contraction speeds depend on the controller and the applied power, another option to improve the system's speed is using agonist and antagonist fibres that allow the system to actuate in two different directions. Their main disadvantage is that they accumulate heat, preventing the actuators' recovery and making them unable to finish the whole pattern after three cycles [262]. The use of long actuators could also benefit this structure. It will be possible to obtain the same displacement as with a smaller actuator but with the advantage of reducing the temperature. It will be harder to saturate the actuators, and it will be possible to go for higher frequencies. Moreover, as noticed from both the isotonic and the closed-loop controllers' experiments, the consumed power is related to the produced stroke rather than the length of the actuator, so in theory, the power consumption will not increase if the activation frequencies are the same. Nevertheless, research on the variable stiffness actuator and stiffness control algorithm is missing to implement a system of this characteristic.

5.7 Conclusion

The work in this paper presents the study on the usage of longer TCP actuators to improve the frequency and temperature characteristics of the TCP actuators, where it was found that the strain is independent of the length. However, electrothermal properties change with the length. As a result, the activation temperature to obtain displacement can be reduced with longer actuators. Furthermore, a new strategy to increase TCP actuators' speed without external cooling systems is presented. The model takes into consideration the advantages of long actuator fibres. This was done by estimating an electromechanical system model through an isotonic contraction test. The model was invariant on the length, meaning that the actuators behave similarly independently of the size. Then a PID controller was implemented to control the displacement of the actuator, in the case of the contraction is dependent on the applied power. However, it was found that the cooling time can also be improved by varying the

activation section of the used actuator, so having long actuators can improve linear movement by increasing its length. Furthermore, the temperature generated by the TCP fibres is reduced by increasing length.

5.8 Chapter Summary

The findings presented in this chapter highlight that the length of the actuator does not significantly impact its mechanical characteristics, as evidenced by similar outcomes (reaching 10% strain) under the same load conditions. Notably, the power required to achieve equivalent displacement in actuators of varying lengths remains consistent. Additionally, the time needed for contraction and relaxation of the actuator remains unchanged, irrespective of its length. Building upon these findings - a novel approach incorporating displacement offsets and a PID control strategy was employed to enhance the overall speed of the actuators. This discovery offers a valuable foundation for addressing research question three, as rapid and controlled contractions are imperative for generating precise movements in the ankle.

Chapter 6 : Paediatric Ankle Rehabilitation System based on Twisted and Coiled Polymer Actuators.

6.1 Preface

The content of this Chapter is a copy of the article *"Paediatric Ankle Rehabilitation System Based on Twisted and Coiled Polymer Actuators"*, published and peer-reviewed in journal Smart Materials and Structures [393].

Chapter 6 synthesises the knowledge derived from the antecedent Chapters, with the principal research objective centred on evaluating the feasibility of integrating SWRR tailored for children with physical disabilities. Chapter 2 delineates the paediatric requisites for SWRR, pinpointing weight, safety, and operability as pivotal attributes. Subsequent exploration of AMSM in Chapter 3 underscores their potential to meet these requirements due to their lightweight, compliant, and deformable characteristics. This exploration culminates in selecting TCPs as the technology capability of generating higher forces than skeletal muscles, notwithstanding challenges such as the need for elevated temperatures, lower strain compared to skeletal muscles, and low working frequencies, explained in Chapters 4 and 5.

With a comprehensive understanding of TCP advantages and limitations, the subsequent phase entails the development of the prototype of a paediatric ankle SWRR based on TCPs. The mechanical design intricately aligns with TCP characteristics related to force and strain, meticulously tailored to fulfil biomechanical specifications detailed in Chapter 3. The TCPs and the associated control strategy are then formulated based on the insights learned in previous Chapters 4 and 5. Furthermore, to cover all the main parts of a SWRR, a surface electromyography HCI was implemented. The outcomes of subsequent tests yield promising results, pushing further technological advancement. However, the realisation of TCP technology in a practical SWRR setting, potentially enhancing the quality of life for children with physical disabilities, necessitates ongoing and future work.

6.2 Abstract

Rehabilitation is crucial for children with physical disabilities arising from various conditions. Traditional exoskeletons, reliant on electric motors and rigid components, making them cumbersome, heavy, and unsuitable for use outside clinical facilities. To overcome these, researchers are turning to SWRRs with artificial muscles based on

smart materials like TCPs. TCPs offer enhanced compliance, adaptability, comfort, safety, and reduced weight—critical for paediatric use. Despite facing challenges like low operating frequencies and high temperatures, TCPs are explored as potential artificial muscles for SWRRs, due to their advantages on the force they can generate, the strain and a linear behaviour. This study details a proof of concept for a paediatric rehabilitation system for ankles based on TCPs, including the actuator characterization, mechanical design, control strategy, and HCI. The resulting device achieved a 1.4 Nm torque, a 10° range of motion in dorsiflexion within 5 seconds, and integrated electromyographic HCI. This research marks a promising step towards innovative, soft wearable rehabilitation solutions for children with physical disabilities.

6.3 Introduction

Ongoing paediatric physical disabilities can result from various causes, including neurological conditions like Cerebral Palsy [394], strokes [395], acquired brain injuries [396], neuromuscular diseases such as Duchenne Muscular Dystrophy [397] and Spinal Muscular Atrophy [398], as well as traumatic injuries. Children with physical disabilities often face limitations in performing daily activities independently, which can impede their typical development. Mobility and exploration are crucial aspects of a child's development, contributing to cognitive, physical, social, and emotional growth[64].

Rehabilitation plays a vital role in assisting these children in recovering or maintaining functionality, enabling them to interact with their environment, and ultimately improving their quality of life and autonomy [3]. Rehabilitation exoskeletons have gained significant attention for their potential to address mobility challenges in individuals with physical disabilities. They offer advantages such as enabling extensive practice for children with substantial disabilities, reducing the effort required from therapists during exercises, and providing a quantitative assessment of the patient's motor function[25].

However, most existing rehabilitation exoskeletons rely on electric motors and rigid components for their functionality. Unfortunately, these designs are often cumbersome, heavy, and unsuitable for use outside clinical facilities [128]. To overcome these limitations, researchers are now focusing on developing SWRRs that incorporate AMSMs. AMSM provides increased compliance, adaptability, comfort, safety, and reduced weight [273].

Due to this advantages they are interesting to be used in paediatric devices as the main characteristics that differentiate them from the adults version are safety, operability, weight and motivation [82]. Safety can be improved thanks to the compliance of the

materials [13]. And the weight can be reduce drastically preventing abnormal movements pattern and increase energy consumption[129, 399]. Due to this advantages they are interesting to be used in paediatric devices as the main characteristics that differentiate them from the adults version are safety, operability, weight and motivation [82]. Safety can be improved thanks to the compliance of the materials [13]. And the weight can be reduce drastically preventing abnormal movements pattern and increase energy consumption[129, 399].

AMSMs are soft actuators composed primarily of material with a low Young's modulus like that of soft biological materials (10^4–10^9 Pa) that can sense and directly convert physical stimulus (e.g., light, electrical, heat) into physical displacement[41, 43, 44].

SMAs [283] and DEAs [284] are indeed promising AMSM solutions for SWRR. However, they each have limitations that hinder their widespread use in this context.

DEAS present desirable characteristics with strain reaching 200 %, a high bandwidth up to the range of kHz and high efficiency [14, 50, 231]. However, DEAs need high voltage, in the order of hundreds of volts, requires bulky and expensive electronics. Moreover, DEAs are challenging to produce in a compact size to generate appropriate amounts of power and force [36, 322].

SMAs present the advantages of power density and stress, these being as high as 50 W/g and 200 MPa, respectively. [50, 338]. These advantages have made them the most popular option on SWRR prototypes [273]. However, they have limitations to be used on SWRR, as they have low efficiency, a small strain range (up to 8 %) and high thermal hysteresis making them difficult to control [36, 50, 231]. SMAs present the advantages of power density and stress, these being as high as 50 W/g and 200 MPa, respectively. [50, 338]. These advantages have made them the most popular option on SWRR prototypes [273]. However, they have limitations to be used on SWRR, as they have low efficiency, a small strain range (up to 8 %) and high thermal hysteresis making them difficult to control [36, 50, 231].

Another noteworthy type of AMSM is the TCPs. TCPs are created by twisting precursor polymer fibres and applying heat treatment [56]. To activate TCPs, an external heat source, such as metallic wires, is employed to induce joule heating, thereby enabling precise electrical control. TCPs offer several advantages, including high power density (27 W/g), stress (10 MPa), strain capacity (21 %), and linear behaviour with minimal hysteresis. However, they do face certain limitations, such as low operating frequencies (<1 Hz), low power efficiency (< 1.32 %) and high operating temperatures (> 80 °C) [50,

60, 231]. Due to their advantages three promising examples of wearable devices based on TCPs were founded:

Sutton et al. [63] developed an assistive wrist orthosis with a single degree of freedom. This device employed 16 TCP) actuators made of silver-coated Nylon 6.6 sewing thread. It generated a torque of 0.3 Nm to the wrist joint in the flexion direction within 3.9 seconds. They implemented a PID controller to accurately follow a 0.1 Hz sinusoidal signal with a 10 N amplitude. The prototype was able to track the movement during activation but encountered challenges with slow response times during the relaxation phase.

IGrab [60], an ergonomic orthotic device to assist in finger flexion and extension movements, was designed by Saharan et al. The device featured a combination of 3D-printed components and sewn parts, including artificial tendons routed from the fingers to the wrist. The finger tendons were linked to TCP actuators, which were mounted on a forearm bracelet. Frictionless pulleys optimised TCP actuation, and rubber strips enhanced energy efficiency. When applying a 0.6 A step signal, the fingers reached their maximum displacements within 25 seconds (i.e., the index finger was able to move 40° for the metacarpophalangeal joint, 21° for the proximal interphalangeal joint, and 11° in the case of the distal interphalangeal joint), with further improvements observed when using pulsed signals, reducing actuation time to under 5 seconds.

Patiño et al. [62] developed a wearable orthotic device for hand rehabilitation featuring individual TCP actuators for each finger. The orthosis consisted of two main components: one fitted to the dorsum of the hand and another for the fingers. Each finger incorporated a silicone tube housing a TCP and a filament strain sensor. The TCP actuators within the finger structure could generate forces of approximately 3 N when a 0.3 A step input was applied.

The orthotic devices mentioned demonstrate the application of TCPs in hand and wrist rehabilitation. However, there is a notable absence of studies exploring the feasibility of TCP utilization in the lower limb or paediatric systems. Moreover, previous literature has extensively investigated TCP as an actuation type and its mechanical design (inherent to the explored joint). Nevertheless, other critical components remain insufficiently explored in these works. These unexplored parameters may include considerations related to control strategy and HCI, which are crucial for successfully developing and implementing paediatric SWRR systems[82, 400] (Figure 6.1).

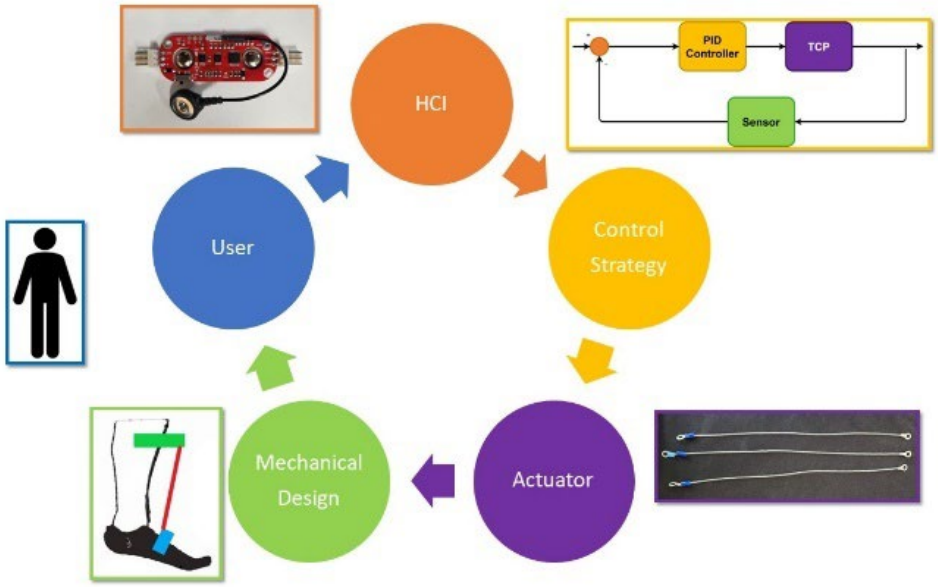

FIGURE 6.1 SWRR COMPONENTS

This paper explores the feasibility of TCPs as artificial muscles to drive SWRRs for children with physical disabilities. It highlights the advantages and the current limitations of TCPs on SWRR. The paper presents the design process of a prototype for paediatric ankle SWRRs based on TCPs covering the main parameters of SWRRs being the actuator characterization, the mechanical design based on the biomechanical requirements for paediatric ankle dorsiflexion, the implementation of a control strategy that is merged with an HCI, with this covering the essential parameters that require a paediatric SWRR.

6.4 Design of the Device and Methods

This section presents a description of the TCP manufacturing process and its behaviour. Then, the biomechanical structure of the ankle and a dummy based on it are given as they are required to design and test the SWRR. Later, the design process of the SWRR is presented. Finally, the behaviour of the prototype and a mathematical model are shown.

6.4.1 TCPs manufacturing

The TCP actuators were fabricated using the process similar to Chossat et al. [377]. A 1.5 m Nylon fishing line as the precursor fibre (EDGE Mono trace 80 LB) with a diameter of 840 µm. The nylon fibres were twisted and coiled alongside a 36 AWG (127 µm) NiCr 80 wire (Fogslord). One end of the nylon fibre was firmly attached to the output shaft of

a NEMA17 motor, while the other end was connected to a slider carrying a 1000 g weight (17.68 MPa, value according with: Force (1Kg*9.8m/s2)/ Fibre Cross Sectional Area (π*(420x10-4 m)2)). The NiCr wire was also suspended from the motor shaft but was only weighted with 1.6 g (1.2 MPa) to maintain it in a straightened state. The nylon fibres were twisted and coiled at a slow rotation speed of 250 RPM. The twisting and coiling process was stopped manually once the precursor fibre was fully coiled.

For the annealing process, the embedded NiCr wire was employed to produce Joule heating. This annealing process consisted of five consecutive five-minute periods, each applying an annealing current of 240 mA. A 1-minute cooling phase was inserted between each annealing period. After this treatment, TCPs with an average length of 44 cm and a diameter of 1.97 ± 0.04 mm were produced, the measurement were taken with a digital calliper (Duratool). The resulting actuators were trimmed to 39.5 cm and clamped with insulated male spade electric terminals. Each electrical terminal required 5 mm for crimping, which led to a 10 mm reduction in the functional area. Table 6.1 depict the main manufacturing parameters of the fabricated TCPs.

Table 6.1 TCP Manufacturing Parameters

Parameter	**Value**
Precursor fibre material	Nylon
Precursor fibre diameter (mm)	0.84
Precursor fibre length (mm)	1500
Precursor fibre tension (g/ MPa)	1000/17.68
Resistance wire material	Nichrome 80
Resistance wire diameter (AWG/ µm)	36/127
Resistance wire length (mm)	1670
Resistance wire tension (g/MPa)	1.6/1.2
RPM	250
Motor turns	726 ± 6
TCP after coiling length (mm)	375± 5
TCP after annealing length (mm)	440 ± 5
Annealing current (mA)	240
TCP resistance (Ω)	137.1 ±7.8
TCP diameter (mm)	1.97 ± 0.04

To test the fabricated samples, a custom-made experimental test bench was utilised to measure force and displacement (Figure 6.2a). In both cases, an Arduino NANO served as the data acquisition system. A transistor (Vishay Siliconix IRF540) regulated the voltage from the power supply, while an NTC thermistor (TE Connectivity, 5K3A1) was employed to monitor the temperature of the TCP.

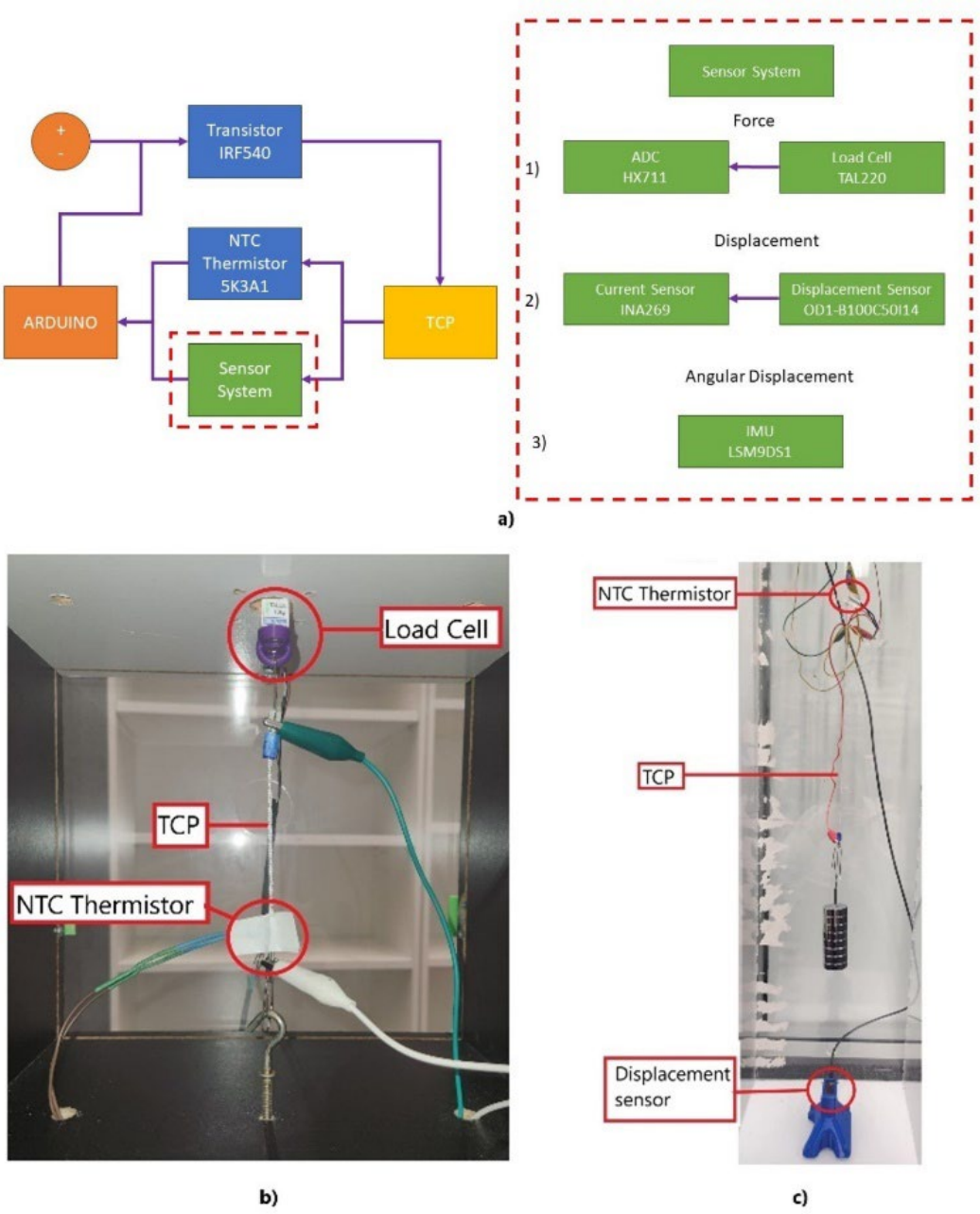

FIGURE 6.2 A) TEST BENCH BLOCK DIAGRAM FOR 1) FORCE, 2) DISPLACEMENT AND 3) ANGULAR DISPLACEMENT TEST. B) FORCE TEST BENCH. C) DISPLACEMENT TEST BENCH.

In the force test (Figure 6.2b), one end of the actuator was fastened to a fixed hook, and the other end was connected to a 10 Kg load cell (TAL220). This load cell was interfaced with the Arduino through an analog-to-digital converter (Avia semiconductor, HX711). For the displacement test (Figure 6.2c), the actuator was suspended with a weight above a laser displacement sensor (Sick OD mini OD1-B100C50I14), which was connected to a current sensor (Texas Instruments INA269) interfacing with the Arduino. The calibration process for the sensor can be found in the supplementary information (Calibration Procedures, Appendix B).

Both force and displacement tests applied a square signal of 2400 seconds on and 240 seconds off to observe the strain and power relationship. The 240-second duration was chosen to allow the system to reach a stable condition. Experiments were repeated at different power levels ranging from 160 mA to 240 mA with the applied current incrementing by 20 mA.

Throughout the experiments, data on TCA temperatures, power consumption, and the weight distance from the sensor were continuously recorded using an Arduino NANO with a sampling time of 50 ms. In the case of the displacement test, various weight values ranging from 600 g to 1000 g were employed to assess the actuator's performance. Each test (force and strain) was performed using 5 different actuators, each one used 4 times, for 20 trials per test.

6.4.2 TCP Behavior

Characterising the performance of the manufactured actuators is essential to determine their suitability for the SWRR requirements. In these tests using TCPs as linear actuators, two primary parameters of interest are force and strain, which will later be converted into torque and ROM. The mean of the last 50 samples before turning off the applied power was averaged to calculate the maximum in both tests. This average represents the system's steady state after the step signal was applied. Then, from the 20 maximum values, the mean and standard deviation of the maximum force, temperature, displacement, and strain were obtained.

Figure 6.3 displays the results obtained from the force test. The TCP actuator's maximum force output is 7.9 ± 0.5 N (807.9 ± 57.6 grams) when a current of 240 mA is applied. However, it's important to note that when considering the prestress of the fibre (0.7 ± 0.2 N or 76.8 ± 21.2 g), the maximum change in force is 7.1 ± 0.4 N (730.0 ± 46.3 grams) (Figure 6.3a). To assess the response times for heating (τ_h) and cooling (τ_c), the analysis focused on the average time required for the actuator to reach 63% of a steady-state value after a step input. The analysis results indicate that the average τ_h is 31.42 ± 1.02 seconds, and τ_c is 28.2 ± 0.4 seconds. At the highest applied power level, the generated temperature reached 78.35 ± 2.07 °C (Figure 6.3b).

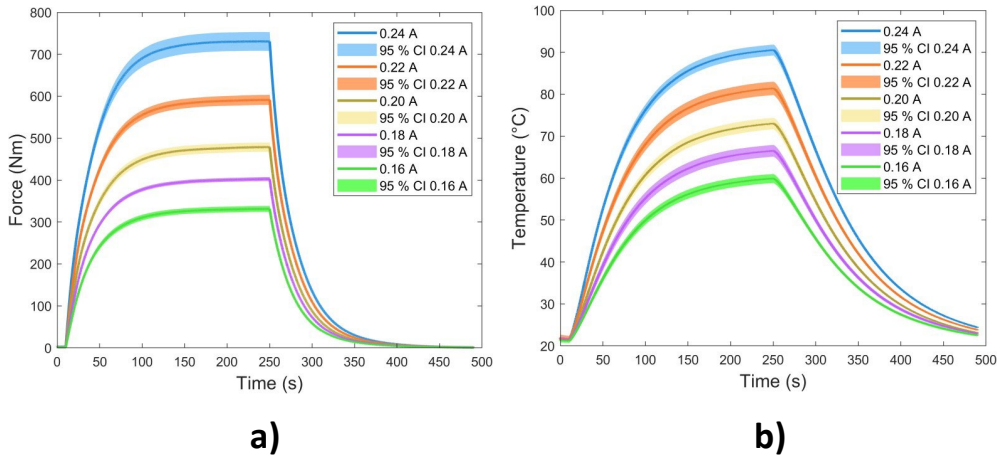

FIGURE 6.3 FORCE POWER RELATIONSHIP A) AND TEMPERATURE POWER RELATIONSHIP DURING THE ISOTONIC FORCE TEST. CONFIDENT INTERVALS (CI) INCLUDED.

In contrast, the results from the displacement test highlight the noticeable impact of pre-strain (generated by the weights) on the actuator's length, causing it to contract from 386.0 ± 3.7 mm to 380.2 ± 3.7, 373.88 ± 4.08, 365.3 ± 4.8, 357.9 ± 5.3 mm. This pre-strain has a direct effect on the actuator's contraction. When a current of 240 mA was applied with different loads, the maximum displacements were as follows 38.7 ± 1.9, 39.8 ± 0.8, 40.4 ± 2.1, 43.5 ± 2.4, 44.5 ± 1.1 mm for weights of 1000 g, 900 g, 800 g, 700 g, and 600 g, respectively (Figure 6.4a). Nevertheless, when the final elongation is considered, the strain can be obtained using the following formula:

$$S = \frac{\Delta L}{L} X\ 100 \tag{6.1}$$

Here, strain (S) represents the relationship between the initial length (L) of the actuator and the resulting stroke (ΔL) when activated, expressed as a percentage. Analysing the strain data, the results were as follows: 10.02 ± 0.45, 10.4 ± 0.1, 10.9 ± 0.6, 11.7 ± 0.7, 12.3 ± 0.3 % for weights of 1000 g, 900 g, 800 g, 700 g, and 600 g, respectively (Figure 6.4b). It's noteworthy that these strain values align with the findings from the maximum force analysis, where the maximum generated force was observed at 7.1 N (730.0 ± 46.3 grams). After this point is possible to see a fall in the displacement and strain. The average response times (τ_h) and (τ_c) are measured at 39.2 ± 1.3 s and 20.6 ± 0.5 s, respectively.

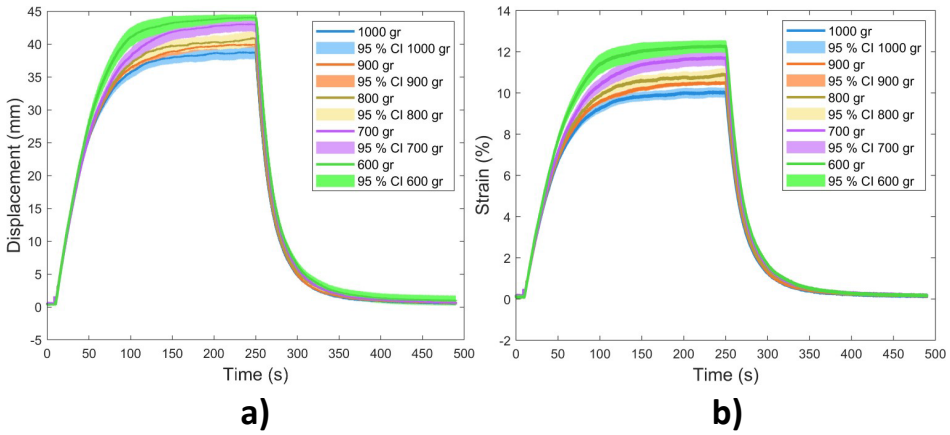

FIGURE 6.4 A) DISPLACEMENT-WEIGHT RELATIONSHIP AND B) STRAIN-WEIGHT RELATIONSHIP. CONFIDENT INTERVALS (CI) INCLUDED.

6.4.3 Ankle Biomechanics

The ankle, characterised by its intricate anatomy, comprises the tibiotalar joint and the transverse tarsal joint, collectively affording a broad spectrum of multidirectional motion. Critical motions within the ankle joint complex encompass plantar- and dorsiflexion, occurring predominantly in the sagittal plane, as well as ab-/adduction in the transverse plane and inversion-eversion in the frontal plane. Combinations of rotations across the subtalar and tibiotalar joints generate three-dimensional motions called supination and pronation[27, 73].

However, it's worth mentioning that the majority of ankle movement primarily occurs within the sagittal plane, with plantar and dorsiflexion being predominantly governed by the tibiotalar joint. The total ankle ROM in the sagittal plane typically spans from 65° to 75°, encompassing 25° to 30° of dorsiflexion and 40° to 45° of plantarflexion. Nevertheless, during activities like walking, the required ROM in the sagittal plane is considerably reduced to approximately 25°. In this context, adult ankles generally move from 20° of plantar flexion to 10° of dorsiflexion, while children exhibit a range of 5° dorsiflexion. Regarding ankle stiffness, which pertains to the mechanical resistance to passive movement, achieving 10° of dorsiflexion necessitates 6.21 Nm of torque for adults, whereas children require 1.5 Nm [79, 401].

The plantar-dorsiflexion movement within a 66° range is commonly observed during daily activities such as walking, climbing stairs, etc. These activities typically occur at a frequency of around 1.75 Hz. However, it's important to note that during rehabilitation sessions, these movements are often executed at much lower frequencies, usually falling below 0.2 Hz [273, 314, 359].

6.4.4 Dummy testing platform

For conducting trials on the paediatric ankle SWRR, a mannequin designed to replicate the lower limb proportions of an average 10-year-old child was employed. Accurate measurements for the leg were derived from the WHO child growth standards [402] and the anthropometric data provided by Winters [403]. These references guided the determination of limb dimensions, resulting in a crus length (knee to ankle) of 40 cm, foot length and width of 22 cm and 7cm respectively. Thet total foot weight 300 g. The used dummy is shown in Figure 6.5.

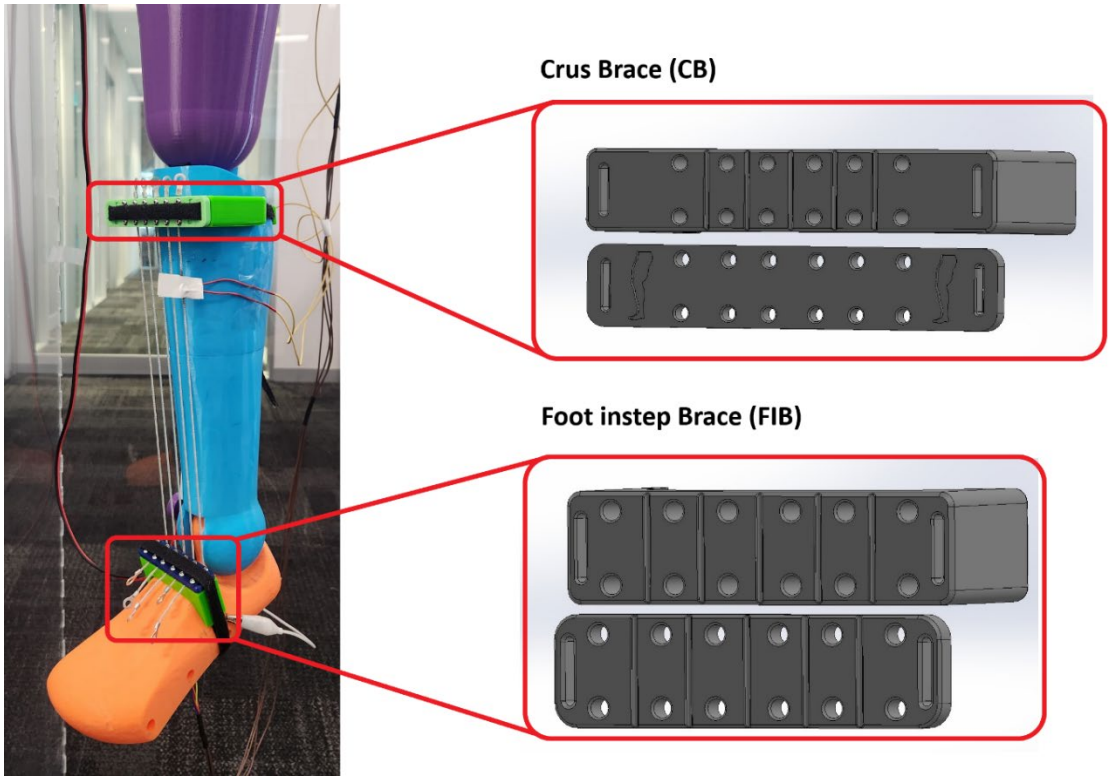

FIGURE 6.5 PAEDIATRIC LEG DUMMY AND CAD DESIGN OF THE SWRR BRACES

To assess the exoskeleton's response to various torques, diverse weights were added to the foot, situated 10 cm from the ankle's centre of rotation. The weights ranged from 500 g to 3000 g, incremented in 500 g intervals. This weight variation corresponded to a torque spectrum from 3 Nm to 0.5 Nm.

6.4.5 Paediatric Ankle SWRR Design

The SWRR consisted of two 3D-printed braces that wrapped around the top part of the crus brace (CB) and the second one on top of the foot instep brace (FIB), Figure 6.5.

The FIB was positioned 5 cm away from the centre of rotation of the ankle. Both braces use Velcro to maintain the position over the mannequin. Furthermore, the braces are divided into two different parts: the brace and the lid. This design allowed the connection of the TCPs in series using copper tape between both parts as the electrical connection. The computer-aided design (CAD) model of both braces is displayed in Figure 6.5. The entire device weight was 300 grams (without a power supply or battery), making each brace weight 150 grams.

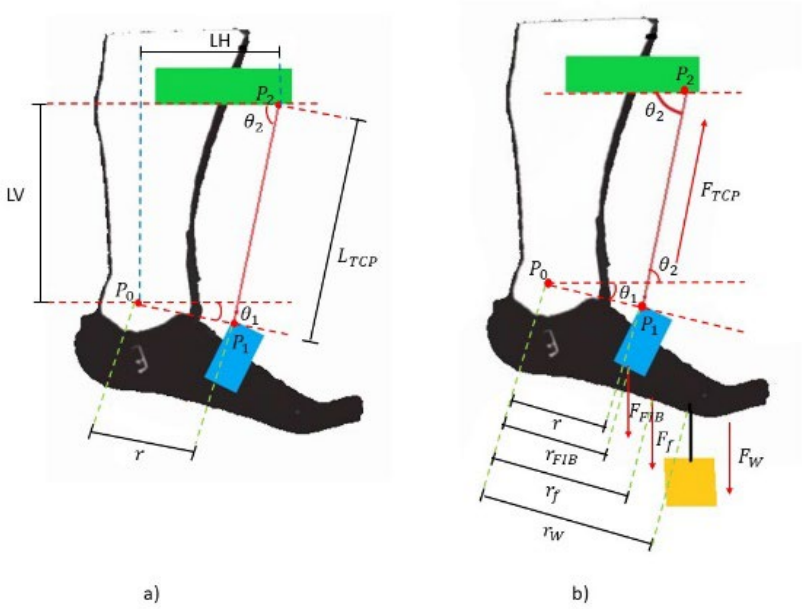

FIGURE 6.6 FREE BODY DIAGRAM FOR A) DISPLACEMENT AND B) FORCES ACTING ON THE DUMMY

On Figure 6.6 an ankle model is showed. P1 is the point at where the TCPs are connected to FIB, P2 is the point where the TCP is connected to CB and P0 the point at the centre of rotation with coordinate (0,0). The coordinate of P1(X_{p1}, Y_{p1}) is:

$$X_{p1} = r\cos\theta_1 \, , Y_{p1} = r\sin\theta_1 \tag{6.2}$$

Then L_{Tcp} can be written as:

$$L_{Tcp} = \sqrt{\left(L_H - X_{p1}\right)^2 + \left(L_V + Y_{p1}\right)^2} \tag{6.3}$$

And θ_2:

$$\theta_2 = \tan^{-1}\left(\frac{L_V + Y_{p1}}{L_H - X_{p1}}\right) \tag{6.4}$$

Where r is the radius between the centre of rotation and P1, θ_1 is the angle of the foot during dorsiflexion, θ_2 is the angle between the TCPs and the braces, L_V is the distance between P1 and p2 when $\theta_1 = 0$, L_H is the distance between the centre of rotation and the connection of the TCP on CB (x axis). Finally, L_{Tcp} is the length of the TCPs.

In the case of the generated Torque (T), the system can be evaluated as follows:

$$T = F_{TCP}\ x \sin\theta_2\ x\ r\ x\ \cos\theta_1 - F_w\ x\ r_w\ x \cos\theta_1 - F_f\ x\ r_f\ x\ \cos\theta_1 - F_{FIB}\ x\ r_{FIB}\ x\ \cos\theta_1 \quad (6.5)$$

Where F_W is the force generated by the weight used on the experiments, r_W the distance of the weight to the centre of rotation, F_f is the force generated by the weight of the foot and r_f is the foot centre of gravity, F_{FIB} is the force generated by the weight of the FIB and r_{FIB} the distance of the weight to the centre of rotation, F_{TCP} is the force generated by the TCPs.

With the mechanical model of the SWRR, the behaviour of the TCP and the requirements given in Section 6.4.3. Then The SWRR was designed to provide dorsiflexion movement of children with the following characteristics: i) Being able to provide an angular displacement of 10° in the plantarflexion direction, ii) providing a torque of 1.5 Nm. Hence, five TCPs of 30 cm, when unloaded, were used for this. The number of fibres was constrained to five as the biggest challenge for TCPs is the speed. Keeping in mind that the width of the leg was 7 cm, a gap of 12 mm was left to prevent heat crosstalk and improve the cooling time [334]. Furthermore, this study is centred on reaching frequencies that can be used in a rehabilitation set-up of 0.2 Hz. Hence, a PID controller was developed to achieve the desired angular displacement in 5 seconds (Section 6.5).

6.4.6 SWRR Test

The performance assessment of the paediatric ankle SWRR was carried out using the testing setup described in section 6.4.4. The electronic components used were nearly identical to those employed in the force and displacement tests for the unit TCP. These components included an Arduino, a MOSFET, and a thermistor. However, a key distinction lies in the sensor utilised to record angular displacement (Figure 6.2). To fulfil this purpose, a 9-degree-of-freedom Inertial Measurement Unit (IMU), was employed (LSM9DS1, STMicroelectronics).

Both testing procedures followed the application of a square signal, consisting of 180 seconds on and 180 seconds off, to establish the strain-power relationship. The selection of the 180-second duration allowed sufficient time for the system to reach a stable equilibrium. The experiments were conducted across various current levels, spanning from 160 mA to 240 mA (incrementally adjusted by increasing the current in 20 mA steps), encompassing all the different TCP actuators. Throughout the test, data about TCA (Thermally Activated Contractile) temperatures, power consumption, and the angular displacement of the foot were recorded and stored on a computer, with the data acquisition performed using an Arduino NANO at a sampling rate of 50 ms. The testing protocol encompassed a range of torque conditions, spanning from 0.5 Nm to 3.0 Nm in 0.5 Nm increments. In addition to the torque generated by the load, it's essential to account for the total negative torque produced by the combined weight of the foot and the FIB (300 grams from the dummy and 150 grams from FIB), which amounts to approximately 0.4 Nm.

Each test was conducted four times utilizing the identical set of actuators. The mean of the last 50 samples before deactivating the applied power was computed to determine the maximum in both tests. This average reflects the system's steady state following the application of the step signal. Subsequently, from the 4 maximum values obtained, the mean and standard deviation of the maximum angular displacement, and temperature were calculated.

The results depicted in Figure 6.7a sows the effect of the load on the TCPs fibres, stretching the fibres decreasing the initial starting point to -15, -27°, -33°, -37.5°, -40° and -42.5° respectively to the applied torque of 0.5 Nm, 1 Nm, 1.5 Nm, 2 Nm, 2.5 Nm, and 3 Nm. After removing this offset figure 6.7b illustrate that the maximum ROM was attained under a 1.0 Nm load. These findings align with the design objectives, as they are closest to the specified 1.5 Nm torque requirement, registering at around 1.4 Nm. The resulting angular displacement was of 25.1 ± 0.3°. The observed behaviour resembled that of the linear displacement of the TCP; as the load increased, displacement decreased, and elongation increased (indicated by a shift to a higher negative angle in the starting position). Conversely, when the load was too low (e.g., 0.5 Nm), the device experienced saturation. The relation between the input power and displacement can be seen as a linear relation. For example, the linear equation for the 1.0 Nm load will be equal to:

$$\alpha = 0.1916\ (mA) - 20.397 \tag{6.6}$$

Where α is the angular displacement in degrees, furthermore the R^2 if the linear equation is 0.9896 and a RMSE of 0.556.

The values for τ_h and τ_c ranged between 19 and 30 seconds (Figure 6.7c). Additionally, the relationship between input power and temperature resembled that of the single fibre configuration, having its maximum temperature at 83.7 ± 0.2 °C when the 240 mA was applied (Figure 6.7d).

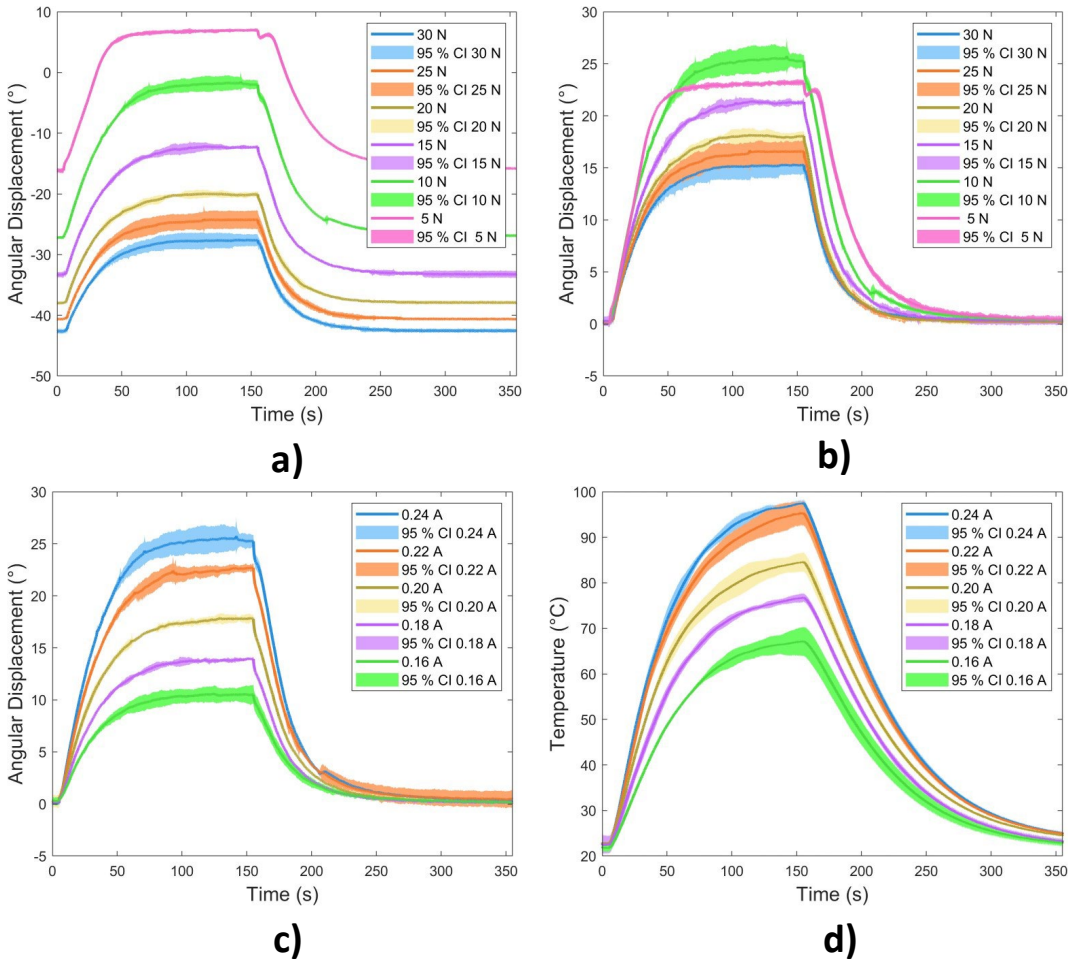

FIGURE 6.7 TCPS RELATIONS DUMMY TEST CHARACTERISTICS. A) ANGULAR DISPLACEMENT-TORQUE RELATION WHEN THE MAXIMUM CURRENT OF 240 MA IS APPLIED. B) ANGULAR DISPLACEMENT-POWER RELATION AND C) TEMPERATURE-POWER RELATION WHEN A TORQUE OF 1 NM IS APPLIED. CONFIDENT INTERVALS (CI) INCLUDED.

6.4.7 SWRR Model.

After acquiring experimental data from the SWRR prototype, a computer model was developed by establishing a connection between ROM and input power. For this purpose, the 1.0 Nm load scenario was selected, as it closely approximated to the required torque of 1.5 Nm when the weight of the foot is taken into account and offered

the most significant ROM (25°, sufficient for full dorsiflexion). The input signal comprised the applied power, while the output signal represented the resulting angular displacement. This dataset was then processed using the System Identification Toolbox in MATLAB. The Toolbox produced a power-angular displacement transfer function denoted as TFPD(s). The best model was as follows:

$$TFPD(s) = \frac{0.01406\,s + 0.000249}{s^4 + 0.6203\,s^3 + 0.0327\,s^2 + 0.0003954} \quad (6.7)$$

The model provides an accuracy of 92.83 %.

6.5 Control strategy and results

Utilising the transfer function $TFDP(s)$, a PID controller was tuned with the aid of the Control System Toolbox in MATLAB. Subsequently, a closed-loop system with the PID controller was simulated in MATLAB/Simulink. The simulation was focused on minimising potential issues such as overshoot, controller settling error, and power requirements, as any such errors could lead to the incorrect application of force to the user, potentially causing harm. To attain the desired maximum ROM of 10°, it took 5 seconds, corresponding to an inverse of 0.2 Hz. The proportional, integral, and derivative components of the controller were configured as follows: Kp = 17.14, Ki = 1.489, Kd = 33.84.

After the closed-loop controller was tuned, it was implemented on an Arduino NANO microcontroller. A maximum power limit of 148 W was imposed, as determined by the capacity of the available power supply (60 V, 2.46 A). A PWM strategy was employed to apply the requisite power. Three distinct tests were conducted: a step input test to evaluate the controller's performance, followed by a chirp test to assess the actuator's bandwidth. Lastly, an HRI was established using an EMG sensor MyoWare 1.0 (MyoWare) to capture muscle signals from the calf, demonstrating its potential as a control mechanism for the SWRR. Ag/AgCl electrodes were used, with bipolar electrodes situated on the belly of the tibialis anterior muscle and a reference electrode placed on the tibia. The EMG signal acquisition was performed with a 33-year-old male subject, using the same test bench employed for SWRR characterisation, now including the EMG sensor for the HCI test (as show in Video S1, https://content.cld.iop.org/journals/0964-1726/33/7/075009/revision2/smsad50b0supp2.mp4?Expires=1719200057&Signature=RmaPWfq15urT4z6PAiUkES7HZoH~EQqHwkHPY3aA3Wl5W0TZf7HG3Yk~G7cBzh8mMskcoSEFlif9Ll71-

jNjHEMhaUu3EINARq33j2SrVUAvqc9V0r~Hv9s45oGmhpCrNHLB0iIgczcyRcgXwCgf5lTz7izJXtebStWD08IfWk9t0r3Rq5JyvALpcxIn7GfbvA-z-8Yt1FIiO1kUiKzywMNVFiDsxp0nNqMI8ZAMvS1iMDfYQtyooK25XoYbuAU3nWshj89~khuDArNLRGe9LpemKb7gNJDP9ns8vStTjj5KX7OA4~j8vfnWVO7nmppjCSuLmAXMrRIkDsKSibg5ZA__&Key-Pair-Id=KL1D8TIY3N7T8).

6.5.1 Step signal

The reference signal for the step response was set at 10°, representing the ROM commonly observed during walking activities. In Figure 6.8a, the plot illustrates the position reference and the system's output when subjected to a step signal in the SWRR. The output closely tracks the reference signal; however, the system exhibits an overshoot response. It takes approximately 5 seconds to move from 0° to 10°. The power graph reveals that the controller initially requires the maximum available power of 148 W, which decreases to an average of 17 W (Figure 6.8b).

Concerning temperature, it experiences a rapid rise initially but stabilises at 60°C (Figure 6.8a). Notably, the power and temperature values in the steady state closely resemble those observed during the open-loop test (with a step input of 180 mA).

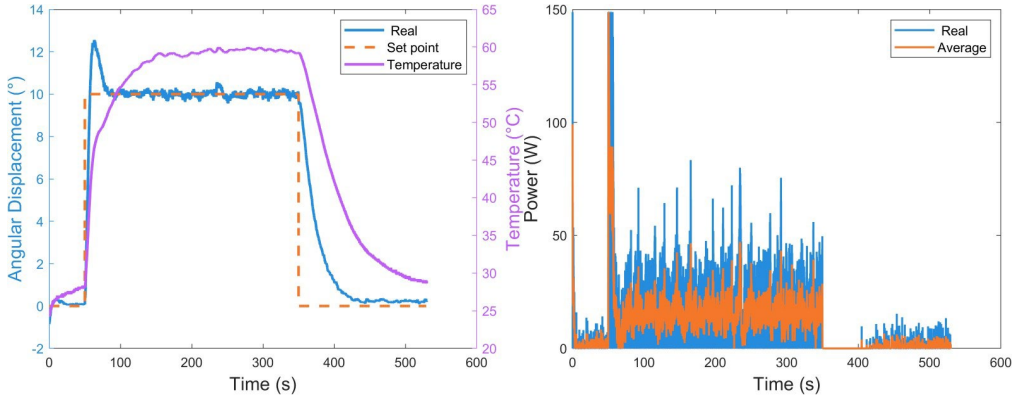

FIGURE 6.8 A) ANGULAR DISPLACEMENT AND TEMPERATURE OF THE SWRR AFTER APPLYING A STEP SIGNAL OF 10° USING A PID CONTROLLER. B) POWER WAS APPLIED TO GENERATE THE 10° DISPLACEMENT.

6.5.2 Chirp signal

A chirp test was used to benchmark the working frequency of the whole system to understand its capabilities. A chirp signal consists of a sinusoidal sweep signal that varies its frequency over time, which can be expressed as follows:

$$chirp(t) = A\sin\left[2\pi\left(\frac{c}{2}t^2 + f_0 t\right)\right] \tag{6.8}$$

Here f_0 is the final frequency, A is the amplitude of the sinewave, t is the time, and c is the chirp rate, described by:

$$c = \frac{f_e - f_0}{T_s} \tag{6.9}$$

where f_e is the final frequency, and T_s is the time it takes to sweep from f_0 to f_e.

The sinewave had an amplitude of 10°, aligning with the required displacement, covering from a baseline of 0° to 10°. The frequency range was from 0.001 Hz to 0.1 Hz (Figure 6.9a). The cutoff frequency was identified when the magnitude decreased to -3 dB. During the test, the actuator reached the -3 dB threshold at a frequency of 0.025 Hz (Figure 6.9b). Regarding temperature, the actuator maintained an average temperature of 53°C, indicating that the TCP struggled to track the chirp signal precisely (Figure 6.9c). The power response was distinct, as the system attempted to operate at that frequency by oscillating between maximum power and zero (Figure 6.9d). To enhance response time without requiring an external cooling system, an offset of 10° was introduced on the ROM, operating within the 10° to 20° range. With this adjustment, the working frequency improved to 0.034 Hz, which was 1.36 times faster. Nevertheless, it still fell short of the target of 0.2 Hz.

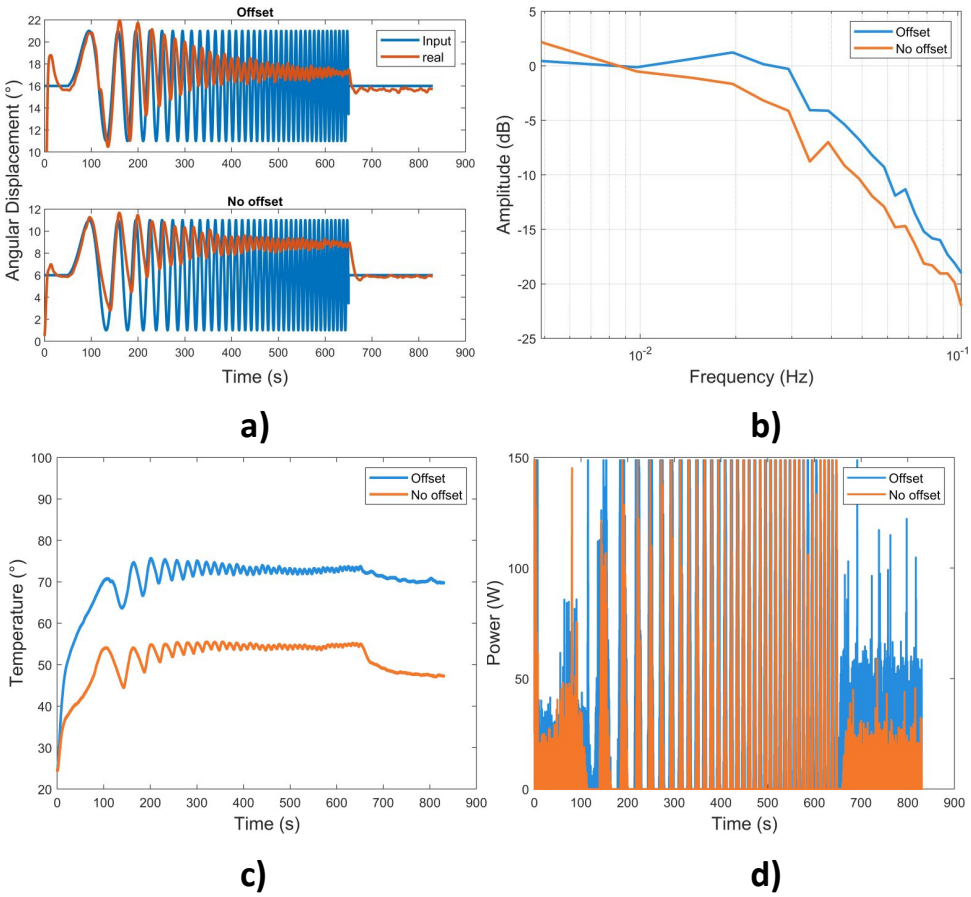

FIGURE 6.9 CHIRP TEST RESULTS. A) ANGULAR DISPLACEMENT OF THE SWRR FOLLOWING THE CHIRP SIGNAL. B) TCP TEMPERATURE. C) MANITUDE DECAY IN DB THROUGH FREQUENCY. D) POWER USED BY THE SWRR.

6.5.3 EMG HCI

The EMG signal was sampled at a frequency of 20 Hz, corresponding to the speed of the serial communication. Using the MyoWare 1.0 sensor, two types of signals were obtained: the EMG raw signal and the EMG envelope (EMGe) signal. The latter serves as an amplitude-modulated representation of the raw signal. To identify muscle activation, a threshold of 150 mV was set for the EMGe signal, preventing errors coming from movement artefacts. The activation pattern remained active for 8 seconds to achieve the 10° movement, followed by 90 seconds to allow the system to cool down and return to the starting position, following a similar approach to Pittaccio et al [314].

From the graphical representations, it is evident that the system is triggered when the EMG envelope surpasses the 150-mV threshold (Figures 6.10a and 6.10c). This activation prompts the utilisation of the entire power output, which relaxes over 90 seconds (Figure 6.10b). These observations confirm that the SWRR device responds effectively to the EMG signal.

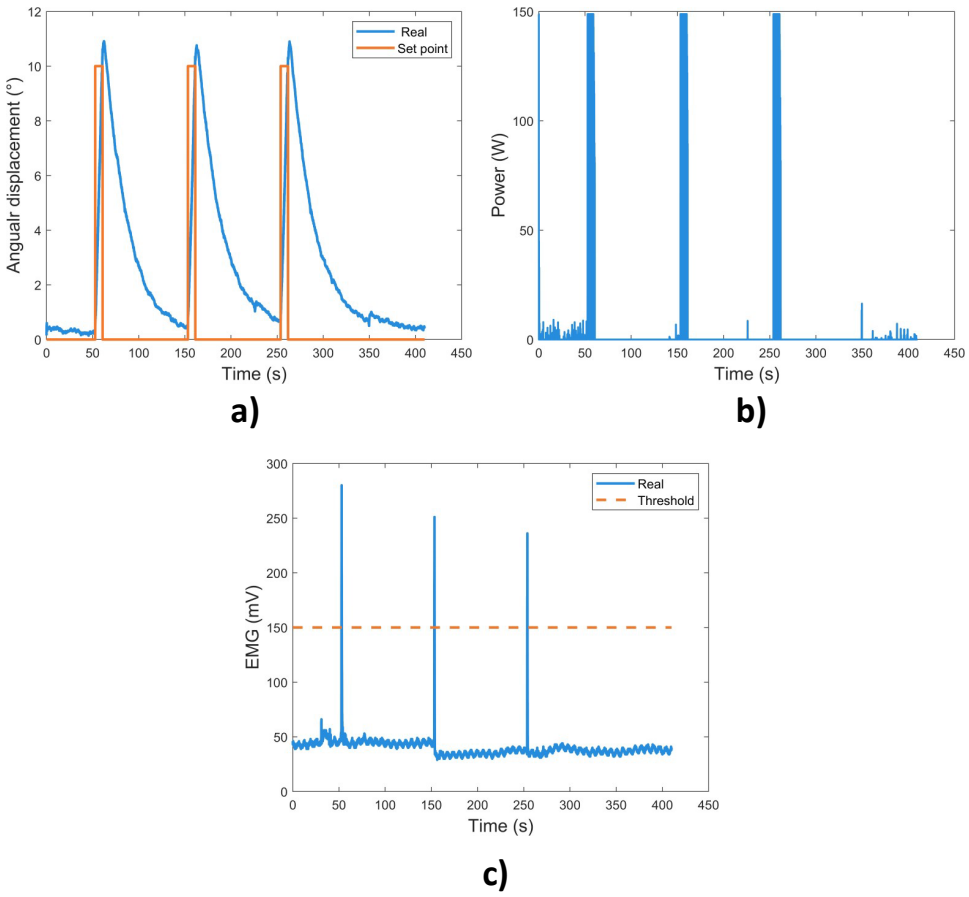

FIGURE 6.10 A) ANGULAR DISPLACEMENT GENERATED AFTER THE EMG THRESHOLD WAS SURPASSED. B) POWER CONSUMPTION OF THE SWRR DURING THE EMG ACTIVATION. C) AN EMG SIGNAL IS USED TO TRIGGER THE SWRR.

6.6 Discussion and conclusion

This study explored the proof of concept for a SWRR system using TCP AMSM. The research included an actuator characterisation and the design process to meet biomechanical requirements. The resulting device is lightweight, flexible, and compact, meeting the minimum biomechanical needs of children with physical disabilities. This includes achieving a 10° ROM within 5 seconds, a torque of 1.5 Nm and an HRI. However, several improvements are needed before this technology can be applied in rehabilitation settings.

The study's results indicate that the behaviour of single fibres is similar to the multifibre approach integrated in the SWRR. With differences in displacement and force as they translate into angular displacement and Torque. These differences are due to the mechanical design, and there's a trade-off between torque and displacement, as they are inversely proportional.

Despite the challenges, the technology appears highly adaptable, and many approaches can be taken to improve the performance. To enhance torque, incorporating additional fibres, as seen in previous TCP studies, is a viable direction [48, 334]. In this study, that approach was followed to get the required torque, as a single fibre would be insufficient to generate the necessary force.

Using longer actuators can significantly improve ROM, as this study shows. While the initial design requirement was a 10° ROM, the longer actuators enabled an impressive 25.18 ° ROM, effectively covering the full dorsiflexion range. This approach offers an additional advantage, as previously emphasised by Gonzalez et al. [387] , which is the reduction in temperature. This temperature control is vital for ensuring the device's safety during use. It's worth noting that the pain threshold for human skin at the dermal/epidermal layer is approximately 44°C [60]. In this context, when considering the 10° ROM, the temperature was 65°C lower compared to the temperatures reached when the actuator operated at its maximum stroke, which often exceeded 90°C. Nonetheless, if the device is intended for use with children, the incorporation of an insulation layer, such as Polytetrafluoroethylene, is advisable to ensure optimal comfort and safety [262].

Nevertheless, coming from equations 2 and 5, the variation of r affect the linear displacement need to generate an angular displacement and the toque in an inverse manner. Is possible to improve this factor by tunning these distances, in the case of the study the r was chosen to be as small as possible because is the technology is envisioned to be used as a fabric that will be incorporated in clothes like socks.

The primary challenge associated with this technology pertains to its reaction time. However, this initial disadvantage could be solved by dividing this problem into two distinct aspects due to the actuator's unidirectional nature, where applying power triggers contraction but cannot control elongation.

On one side, accelerating the contraction time necessitates increased applied power, leading to higher temperatures more quickly. The critical constraint lies in the need to carefully regulate this applied power to prevent heat-induced damage to the actuator. The research demonstrated that implementing the suggested control strategy allowed faster speeds without harming the actuator, preventing the fibre from overheating and burning [62]. Nevertheless, this approach demands substantial power levels to achieve rapid responses, often exceeding 100 Watts. This power requirement poses a challenge given the limitations of current battery technology. Nonetheless, advancements in energy storage and transmission are ongoing, promising improvements in energy density and battery miniaturisation [368, 372, 404].

On the other hand, addressing the relaxation phase poses a more complex challenge. This research sought to optimise the device's cooling process without external systems, relying on convective airflow. These optimisations involved creating sufficient spacing between each actuator to prevent heat transfer between individual fibres [334]. Regrettably, this consideration is counterproductive in the design as it limits the number of fibres used in the SWRR to produce higher torques.

Additionally, it was experimented with operating within an optimal temperature range, introducing an offset from the initial working point (from 0° to 10°) to achieve a faster movement previously investigated by Gonzalez et al. [387]. This approach increased the frequency by 1.36 times. However, it did not significantly improve due to the actuator's considerably slower natural frequency than the required frequencies (0.02 Hz in TCP versus 1 Hz in walking activity).

Two potential alternatives come to light to address this issue. The first is incorporating a cooling system, as seen in numerous TCP research studies [332, 364]. The second option involves adopting agonist-antagonist muscle systems [262, 301]. However, it's important to note that these approaches entail increased system complexity, requiring additional components that expand the system's size and weight. Furthermore, it necessitates more sophisticated control strategies to activate each component as needed.

Finally, another crucial facet of SWRR technology is the HCI. To demonstrate the device's feasibility, a straightforward EMG HCI was implemented, showcasing the technology's capabilities. This approach allowed system activation to be controlled based on the user's intent through muscle activation, a pivotal component of rehabilitation therapy that enhances user engagement. Looking ahead, it would be compelling to explore the incorporation of various wearable sensor technologies in conjunction with TCP technology to create SWRR devices that can seamlessly integrate into the daily lives of children. This advancement holds the promise of substantially improving their overall quality of life.

This study presents innovative components to design paediatric ankle SWRRs. These elements provide solutions to specific issues of traditional exoskeletons (weight and compliance) and can be translated to develop SWRR for different purposes. Nevertheless, as discussed, the technology still needs to be improved for its widespread adoption in rehabilitation settings. Additionally, it is essential to collaborate closely with human users to understand better and address any technology shortcomings.

6.7 Limitations

The current device was not tested on paediatric patients due to ethical limitations. Hence, the performance shown in the study could change when applied to paediatric patients.

In the case of the used metric from the biomechanical requirements, all the analysed metrics were the minimum requirements for all the attributes. However, it recognised the need for additional refinement before clinical use. This research is proof of concept of the technology aimed to explore its strengths and limitations, emphasising the ongoing work required for its potential widespread clinical implementation.

6.8 Chapter Summary

This chapter successfully realized a proof-of-concept for a paediatric SWRR targeting the ankle, achieving a torque of 1.5 Nm, a ROM of 10° in dorsiflexion within 5 seconds, and an EMG HCI. This accomplishment underscores the feasibility of employing TCP technology in paediatric SWRR, as it meets the minimum biomechanical requirements for ankle rehabilitation in the paediatric population. Research questions three and four can be addressed with these results. However, it is acknowledged that further comprehensive exploration and refinement are imperative to develop a paediatric prototype ready for practical use.

Chapter 7 : Discussion and Conclusion

SWRR will be the next revolution in assistive devices for children, as technology is integrating more into people's daily lives. It is now possible to find wearable devices that sense most biological signals and predict many diseases. The next step on wearables is to transition from smart sensors to smart actuators to actively help children with their activities.

It's possible to see that efforts into paediatric wearable robots are being taken as researchers and companies with the knowledge acquired on SWRR for adults are starting to develop paediatric versions not just by downsizing but by getting specific requirements from them. It will still take time as working with children is more complex than working with adults as they are not fully mentally and physically developed. Furthermore, it is necessary to think about the requirements of portable robots that can be worn outside of clinical facilities. In the first step into SWRR, the main goal in the short term is to provide physiotherapy through repetitive movements without the need for a physiotherapist all the time. This will boost the children's activity, reducing or keeping the deterioration of their muscles, resulting in a better quality of life. After physical therapy is achieved, the next obvious step will be to use SWRR during daily life, becoming a natural part of the children’s garments.

The objective of this study was to carry out a thorough investigation into understanding the feasibility of using SWRR for children with physical disabilities based on AMSM. Over the course of this thesis, we have sought to answer four research questions spread across five sequential peer-reviewed publications serving as individual Chapters that delved into paediatric rehabilitation robots, AMSM, TCPs characterisation, TCPs control and enhancement and the potential to use TCPs in a paediatric SWRR to generate ankle dorsiflexion movements. The research questions were:

1. Why is different to develop paediatric SWRR than normal SWRR?
2. To what extent does the developed proposed TCPs AMSMs produce forces and displacement that can be used to generate the ROM and torques in the sagittal plane that are similar to those needed to move a child's ankle during passive dorsiflexion movement?
3. How a control strategy developed for SWRR performs in generating dorsiflexion movements?
4. Can a feasibility study identify the critical attributes for SWRR that could assist ankle dorsiflexion movement in children's sagittal plane?

The progression of these peer-reviewed publications began with Chapter 2, which specifically addresses the first question on the difference between adult and paediatric rehabilitation robots. Chapters 3 and 4 collectively delve into the mechanical characteristics of TCPs that are required for the paediatric SWRR for ankle, answering question 2. Chapter 5 is the starting point for solving question 3 as it analyses the control properties of a single fibre that later is extrapolated to the SWRR system developed on Chapter 6 to properly solve the question. Finally, Chapter 6 addresses research question 4 by synthesizing the knowledge of single-fibre behaviour acquired from Chapters 4 and 5. This synthesis is applied to a bundle of fibres powering a paediatric SWRR for the ankle. The developed prototype provides valuable insights into the feasibility of implementing TCPs in SWRR, elucidating their advantages and limitations when integrated into paediatric exoskeletons.

In Chapter 2 was found that children have often been overlooked in the realm of rehabilitation robots, as they present unique challenges in their development while growing. Limited resources delve into the crucial characteristics to consider when creating devices for paediatric use. This study employs a literature review encompassing 206 publications, identifying 58 robotic devices utilized by children with physical disabilities. The analysis underscores key attributes crucial in developing rehabilitation robots for children, emphasizing weight, safety, operability, and motivation.

In addition, the study reveals a prevalence of neurological diseases, particularly CP, among users. The predominant training strategy involves assistive methods. In terms of technology, the admittance/impedance HCI proves most popular, with electric motors as the commonly used actuators. Moreover, current research in paediatric rehabilitation robotics is trending towards the development of exoskeletons designed for use outside clinical facilities.

On Chapter 3 the analysis delves into the biomechanical requirements, evaluating the strengths and weaknesses of SWRR based on AMSM. AMSM emerges as a trend due to its compliance, lightweight nature, and independence from external components. A scrutiny of 36 research papers reveals 17 SWRR robots employing four different technologies: DEAs, PVC gels, SMA, and TCP. DEAs and PVC excel in high frequencies but exhibit lower forces compared to skeletal muscles, while SMAs and TCPs offer higher forces at the expense of lower frequencies. Despite all technologies demonstrating lower strain than human muscles, SMAs and TCPs are preferred in SWRR for their force-generating capabilities, and their lower speeds remain suitable for therapeutic setups requiring slow movements under 0.25 Hz.

TCPs emerged as the preferred AMSM due to their advantageous attributes, including high-power density, substantial stress, considerable strain, linear behaviours with low hysteresis, and electrical controllability through joule heating. However, the challenges of low frequencies and high temperatures in the context of SWRR prompted researchers to explore various TCP parameters and techniques affecting frequency response and working temperature, such as polymer types, fibre diameter, closed-loop control, and active cooling. Notably, the effects of embedded wire and actuator length on TCP performance were critical aspects not extensively studied in TCP characterizations.

Chapter 4 of this thesis delves into the effects of embedding NiCr wire into TCPs, utilizing a nylon fibre with varying NiCr wire diameters. Findings reveal a negative impact on TCP performance as wire diameter increases, leading to reduced strain proportional to the wire diameter increment. This reduction, potentially linked to increased TCP stiffness, results in a strain decrease by a factor of 0.0924 and an increase in response time by 0.0054 for each wire diameter increment. Additionally, the study highlights considerations related to voltage values, indicating potential challenges for long actuators requiring high voltages, exceeding standard battery values of 24 V.

Upon comprehending the impact of NiCr on TCPs, an investigation into how actuator length influences temperature management and frequency was executed in Chapter 5. Employing a 0.71 mm diameter fishing line with a 36 AWG NiCr (0.127 mm) wire, characterized by a 12% strain, the study utilized three distinct actuator sizes. The larger actuator was three times the size of the smaller one, and the middle-sized actuator was twice the size of the smaller one. Regardless of the length, the study revealed a consistent relationship between strain and temperature. This consistency implies the possibility of achieving equivalent displacement with lower temperatures, a critical consideration for SWRR given the human tolerance limit of 65°C.

Following the assessment of length's impact on actuators, a novel strategy to reduce response time through displacement offset was introduced. By increasing actuator length, it becomes feasible to adjust the temperature range in which TCPs operate to produce displacement. The expanded temperature range facilitates more effective cooling. Using a PID controller and applying various displacement offsets to the actuator, the study demonstrated an enhancement in frequency by 0.0006 Hz for every millimetre applied as an offset. This means that is possible to reach frequencies that can be used on rehabilitation if a long offset is provided (e.g. an offset of 1000 mm will result in a frequency of 0.6 Hz). Furthermore, the technique can be improve using thinner fibres as their thermal capacitance is lower loosing heat faster [334].

Finally on Chapter 6, the paediatric SWRR for ankle based on TCPs was tested on a dummy model resembling a ten-year-old child to assess the developed paediatric ankle SWRR based on TCPs as obtaining approval for clinical trials involving children presents challenges, and the technology needs additional improvement before being tested with children. The established minimal requirements for ankle rehabilitation included achieving a 10° dorsiflexion, 1.5 Nm torque, and completing movements within 5 seconds. Various techniques devised in this study to enhance force, displacement, and working frequency were implemented successfully in the proposed device using 5 TCPs. Additionally, the working temperature remained below 65 °C.

With Chapter 6 serving as the concluding chapter and addressing the ultimate question, TCPs emerge as a feasible technology for paediatric SWRR, effectively addressing the primary needs of paediatric users. Their lightweight nature, notably demonstrated by the present device weighing 300 grams, stands as a significant advantage over traditional motors. The softness of TCPs enhances compliance with the desired movements of children, thereby minimizing the risk of harm and promoting safety. In terms of operability, the flexibility of TCPs facilitates easy adaptation to different SWRR shapes and sizes. This adaptability extends to shaping the device, presenting an additional motivational advantage as future iterations of SWRR are envisioned to function as clothing, contributing to a reduction in awareness of the disability. Crucially, this work attains minimal biomechanical requirements for ankle dorsiflexion, promising further improvement as inherent limitations are systematically addressed.

Through this work limitations were identified, such as the device being active in only one direction, the absence of external cooling aid, and a prolonged relaxation phase taking over 20 seconds to return to the initial position. An additional consideration for devices employing resistance wires is the wire resistance, influencing the PID controller speed limited by the voltage supplied to the device. Despite these constraints, the results of this test exhibit promising advancements in utilizing soft actuators for paediatric rehabilitation robots, paving the way for further research to address challenges associated with TCPs.

7.1 Study Limitations and Future Research Directions

The new revolution of actuators comes in a soft package. These new technologies resemble how the human body works. The human body is deformable but strong, so soft actuators are one of the best options to integrate into SWRR. It will be possible to mimic how our skeletal muscle system works, making adopting the exoskeletons easy. Nevertheless, soft robotic technology is still in the early stages of development and is a

change in the robotics paradigm. The expectation for soft robotics is significant as they can solve problems that traditionally rigid robotics can not.

Nevertheless, no soft robotic technology can compare to traditional robotics at this moment, but this is expected to change. There is plenty of research on soft robotics, from understanding the physics and how they behave to analysing how they interact with the environment. In this regard, some technologies can work better than others, depending on the application. For example, IPMC, due to its wet nature, could be used in underwater activities, DEAs could be used in agriculture to pick fruits and vegetables that require a delicate, precise touch, and SMA is extensible researched in SWRR.

In this work, TCPs were analysed as they present behaviour similar to SMAs but with the advantages of higher strains and linear behaviour that have been the main challenges of SMAs. But there remain the challenges of requiring high temperatures about those that humans can withstand and the main disadvantage of requiring extended periods of time to recover their original form as they can only be activated in one direction.

Nevertheless, the approaches presented in this work provides good insight in paediatric SWRR using TCPs as the actuators. If this technology is mean to be used on a paediatric cohort advance in different areas are required.

The subsequent phase involves extrapolating the insights garnered from this study to diverse body parts, each with distinct requirements. A key differentiator among joints is the varying torque demands. This challenge could be addressed by bundling fibres into a larger unit or employing thicker fibres. Using long actuators is suggested to generate a broad ROM. The space restriction in exoskeletons can be solved by implementing a pulley system that uses long actuators [60]. Lastly, exploring the application of TCPs in prosthetic components becomes intriguing, considering their lightweight nature, which is an advantage over traditional motors.

A primary area for future research involves the integration of HCI into the device. The thesis utilizes a basic sEMG interface for actuator triggering, posing a limitation in terms of potential false positives in the activation pattern. Future developments should explore sophisticated HCI integration, potentially leveraging various wearable sensor technologies in tandem with TCP technology. This integration aims to create SWRR devices that seamlessly blend into children's daily lives, significantly enhancing their overall quality of life.

Exciting technologies for integration include Electrical Impedance, capable of recording muscle activation with a more in-depth view of activated muscle fibres compared to sEMG [405]. Additionally, considering the challenges posed by weak muscles in children,

EEG signals from the brain present an alternative, overcoming limitations associated with myographic signals. For enhanced pattern identification robustness, the fusion of different HCI technologies emerges as another compelling avenue for exploration.

The primary challenge associated with TCP technology revolves around its reaction time, and it is essential to dissect this issue into two distinct facets due to the actuator's unidirectional nature. The application of power triggers contraction but lacks control over elongation. On one side, accelerating the contraction time requires increased applied power, resulting in quicker temperature elevation. The critical constraint is the need for precise regulation of applied power to prevent heat-induced damage, posing a potential safety risk. Incorporating a temperature controller into the control strategy becomes imperative to allow for higher frequencies while mitigating the risk of actuator damage. However, achieving faster reactions often demands higher power, exceeding 100 Watts, necessitating efficient DC-DC converters or larger batteries for untethered use, considering the current limitations in battery technologies (commonly in the range of 24 V). Nevertheless, ongoing advancements in energy storage and transmission promise significant improvements in energy density and battery miniaturization. These developments pave the way for the feasibility of employing SWRR outside of clinical facilities.

On the other hand, addressing the relaxation phase presents a more intricate challenge. This research aimed to optimize the cooling process without external systems, relying on convective airflow. Strategies involved creating sufficient spacing between actuators to prevent heat transfer, yet this consideration proved counterproductive as it limited the number of fibres, consequently restricting torque production. Despite efforts, improvements were marginal due to the actuator's considerably slower natural frequency compared to required frequencies for activities like walking (0.02Hz in TCP versus 1 Hz in walking activity).

Drawing insights from TCP research studies, two potential alternatives for improvement involve incorporating a cooling system or adopting agonist-antagonist muscle systems. In the case of the cooling system, various options exist, including fans, fluid-based systems, and Peltier cells. Opting for a cooling system based on fluids requires carefully considering the fluid type, such as air, water, or mineral oils. Each fluid type will impact the system's performance differently, necessitating thorough analysis. Additionally, the encapsulation of the cooling system must be evaluated to ensure compatibility and effectiveness.

For the agonist-antagonist muscle system, understanding the effect of heat on the fibres is crucial. The increased energy to compensate for the opposing force from the

antagonistic fibre will generate additional heat, which is dangerous for the fibres and the user. One potential solution is to use longer actuators with a displacement range larger than necessary to account for the increased heat buildup.

However, it's crucial to acknowledge that these approaches introduce increased system complexity, requiring additional components that contribute to a larger size and weight. Consequently, more sophisticated control strategies become necessary to activate each element selectively.

An additional consideration stemming from the actuators' temperature generation pertains to interfacing with human skin while keeping the external temperature of the device below 65°C. The use of different materials in TCP insulation, such as Teflon or Kevlar, is anticipated. Therefore, further work is essential to understand how the shape and materials of the insulation component impact temperature changes in TCPs.

Another interesting area to cover and main limitation of this study is to perform test with children. Nevertheless, despite the work focuses on paediatric device, it has not progressed to a phase of testing with actual patients. Ethical considerations and challenges associated with working directly with children with physical disabilities contribute to this limitation. The use of a dummy model, while informative, does not fully capture the diversity in movement that a child might present, restricting the evaluation to the sagittal plane.

The work presented in this thesis demonstrates the potential of TCPs to function effectively as actuators for paediatric ankle SWRR, as well as for SWRR systems in broader applications. TCPs have shown the capability to effectively meet the minimum biomechanical requirements for paediatric ankle rehabilitation. Furthermore, this research aims to inspire future studies that could evaluate the effects of a rehabilitation system based on SWRR TCP activities in clinical trials for children.

By showcasing the feasibility and efficacy of TCPs in addressing ankle rehabilitation needs, this thesis lays the foundation for broader applications of TCP-based SWRR systems in clinical settings. The hope is that future research will build upon these findings, leading to innovative rehabilitation solutions that can positively impact the lives of children with ankle-related challenges.

References

[1] S. McIntyre *et al.*, "Global prevalence of cerebral palsy: A systematic analysis," *Developmental Medicine & Child Neurology,* vol. 64, no. 12, pp. 1494-1506, 2022.

[2] P. B. Sporns *et al.*, "Childhood stroke," *Nature Reviews Disease Primers,* vol. 8, no. 1, p. 12, 2022.

[3] C. Gmelig Meyling, O. Verschuren, I. R. Rentinck, R. H. Engelbert, and J. W. Gorter, "Physical rehabilitation interventions in children with acquired brain injury: a scoping review," *Developmental Medicine & Child Neurology,* vol. 64, no. 1, pp. 40-48, 2022.

[4] D. C. Petian-Alonso, A. C. de Castro, G. Barroso de Queiroz Davoli, E. Z. Martinez, and A. C. Mattiello-Sverzut, "Defining ambulation status in patients with Duchenne muscular dystrophy using the 10-metre walk test and the motor function measure scale," *Disability and Rehabilitation,* vol. 45, no. 18, pp. 2984-2988, 2023.

[5] C. Cumplido-Trasmonte *et al.*, "Effects of ATLAS 2030 gait exoskeleton on strength and range of motion in children with spinal muscular atrophy II: a case series," *Journal of NeuroEngineering and Rehabilitation,* vol. 19, no. 1, pp. 1-10, 2022.

[6] M. Greenham *et al.*, "Predictors of participation and quality of life following major traumatic injuries in childhood: A systematic review," *Disability and rehabilitation,* vol. 44, no. 12, pp. 2591-2607, 2022.

[7] P. Mary, L. Servais, and R. Vialle, "Neuromuscular diseases: Diagnosis and management," *Orthop Traumatol Surg Res,* vol. 104, no. 1S, pp. S89-S95, Feb 2018, doi: 10.1016/j.otsr.2017.04.019.

[8] H. K. Graham *et al.*, "Cerebral palsy," *Nature Reviews Disease Primers,* vol. 2, p. 15082, Jan 7 2016, doi: 10.1038/nrdp.2015.82.

[9] D. J. Birnkrant *et al.*, "Diagnosis and management of Duchenne muscular dystrophy, part 1: diagnosis, and neuromuscular, rehabilitation, endocrine, and gastrointestinal and nutritional management," *The Lancet Neurology,* vol. 17, no. 3, pp. 251-267, 2018, doi: 10.1016/s1474-4422(18)30024-3.

[10] B. O. Olusanya *et al.*, "Cerebral palsy and developmental intellectual disability in children younger than 5 years: Findings from the GBD-WHO Rehabilitation Database 2019," *Frontiers in public health,* vol. 10, p. 894546, 2022.

[11] C. Bayón, M. v. Hoorn, A. Barrientos, E. Rocon, J. P. Trost, and E. H. v. Asseldonk, "Perspectives on ankle-foot technology for improving gait performance of children with Cerebral Palsy in daily-life: requirements, needs and wishes," *Journal of neuroengineering and rehabilitation,* vol. 20, no. 1, p. 44, 2023.

[12] C. M. McDonald *et al.*, "The 6-minute walk test as a new outcome measure in Duchenne muscular dystrophy," *Muscle Nerve,* vol. 41, no. 4, pp. 500-10, Apr 2010, doi: 10.1002/mus.21544.

[13] F. Patane, S. Rossi, F. Del Sette, J. Taborri, and P. Cappa, "WAKE-Up Exoskeleton to Assist Children With Cerebral Palsy: Design and Preliminary Evaluation in Level Walking," *IEEE Transactions on Neural Systems and Rehabilitation Engineering,* vol. 25, no. 7, pp. 906-916, Jul 2017, doi: 10.1109/TNSRE.2017.2651404.

[14] B. Shi *et al.*, "Wearable Ankle Robots in Post-stroke Rehabilitation of Gait: A Systematic Review," *Frontiers in Neurorobotics,* vol. 13, p. 63, 2019, doi: 10.3389/fnbot.2019.00063.

[15] K. Low, "Robot-assisted gait rehabilitation: From exoskeletons to gait systems," in *2011 Defense Science Research Conference and Expo (DSR)*, 2011: IEEE, pp. 1-10.

[16] G. Orekhov, Y. Fang, J. Luque, and Z. F. Lerner, "Ankle exoskeleton assistance can improve over-ground walking economy in individuals with cerebral palsy," *IEEE*

Transactions on Neural Systems and Rehabilitation Engineering, vol. 28, no. 2, pp. 461-467, 2020.

[17] R. Pérez-San Lázaro, I. Salgado, and I. Chairez, "Adaptive sliding-mode controller of a lower limb mobile exoskeleton for active rehabilitation," *ISA transactions,* 2020.

[18] T. Shahid, D. Gouwanda, S. G. Nurzaman, and A. A. Gopalai, "Moving toward Soft Robotics: A Decade Review of the Design of Hand Exoskeletons," *Biomimetics,* vol. 3, no. 3, Jul 18 2018, doi: 10.3390/biomimetics3030017.

[19] P. Maciejasz, J. Eschweiler, K. Gerlach-Hahn, A. Jansen-Troy, and S. Leonhardt, "A survey on robotic devices for upper limb rehabilitation," *Journal of Neuroengineering and Rehabilitation,* vol. 11, no. 1, p. 3, 2014.

[20] M. Jansen, N. van Alfen, A. C. Geurts, and I. J. de Groot, "Assisted bicycle training delays functional deterioration in boys with Duchenne muscular dystrophy: the randomized controlled trial “no use is disuse”," *Neurorehabilitation and Neural Repair,* vol. 27, no. 9, pp. 816-827, 2013.

[21] A. Cook, P. Encarnação, and K. Adams, "Robots: Assistive technologies for play, learning and cognitive development," *Technology and Disability,* vol. 22, no. 3, pp. 127-145, 2010, doi: 10.3233/tad-2010-0297.

[22] F. Kuo, H. Lee, H. Hsiao, and J. Lin, "Robotic-assisted hand therapy for improvement of hand function in children with cerebral palsy: a case series study," *European Journal of Physical and Rehabilitation Medicine,* 2020.

[23] X. Zhang, Z. Yue, and J. Wang, "Robotics in Lower-Limb Rehabilitation after Stroke," *Behavioural Neurology,* vol. 2017, p. 3731802, 2017, doi: 10.1155/2017/3731802.

[24] S. E. Fasoli, B. Ladenheim, J. Mast, and H. I. Krebs, "New horizons for robot-assisted therapy in pediatrics," *American Journal of Physical Medicine & Rehabilitation,* vol. 91, no. 11 Suppl 3, pp. S280-9, Nov 2012, doi: 10.1097/PHM.0b013e31826bcff4.

[25] R. L. Hawe, A. M. Kuczynski, A. Kirton, and S. P. Dukelow, "Assessment of bilateral motor skills and visuospatial attention in children with perinatal stroke using a robotic object hitting task," *Journal of NeuroEngineering and Rehabilitation,* vol. 17, no. 1, pp. 1-12, 2020.

[26] E. D. Ona, R. Cano-de la Cuerda, P. Sanchez-Herrera, C. Balaguer, and A. Jardon, "A Review of Robotics in Neurorehabilitation: Towards an Automated Process for Upper Limb," *Journal of Healthcare Engineering,* vol. 2018, p. 9758939, 2018, doi: 10.1155/2018/9758939.

[27] M. G. Alvarez-Perez, M. A. Garcia-Murillo, and J. J. Cervantes-Sanchez, "Robot-assisted ankle rehabilitation: a review," *Disability and Rehabilitation: Assistive Technology,* pp. 1-15, Mar 11 2019, doi: 10.1080/17483107.2019.1578424.

[28] A. J. McDaid, "Design, Analysis, and Multicriteria Optimization of an Overground Pediatric Robotic Gait Trainer," *IEEE/ASME Transactions on Mechatronics,* vol. 22, no. 4, pp. 1674-1684, 2017, doi: 10.1109/tmech.2017.2696498.

[29] Y. He, D. Eguren, T. P. Luu, and J. L. Contreras-Vidal, "Risk management and regulations for lower limb medical exoskeletons: a review," *Medical Devices: Evidence and Research,* vol. 10, pp. 89-107, 2017, doi: 10.2147/MDER.S107134.

[30] C. Y. Chu and R. M. Patterson, "Soft robotic devices for hand rehabilitation and assistance: a narrative review," *Journal of NeuroEngineering and Rehabilitation,* vol. 15, no. 1, p. 9, Feb 17 2018, doi: 10.1186/s12984-018-0350-6.

[31] R. A. R. C. Gopura, D. S. V. Bandara, K. Kiguchi, and G. K. I. Mann, "Developments in hardware systems of active upper-limb exoskeleton robots: A review," *Robotics and Autonomous Systems,* vol. 75, pp. 203-220, 2016, doi: 10.1016/j.robot.2015.10.001.

[32] U. Keller, H. J. A. van Hedel, V. Klamroth-Marganska, and R. Riener, "ChARMin: The First Actuated Exoskeleton Robot for Pediatric Arm Rehabilitation," *IEEE/ASME Transactions on Mechatronics,* vol. 21, no. 5, pp. 2201-2213, 2016, doi: 10.1109/tmech.2016.2559799.

[33] T. Bützer *et al.*, "PEXO-A Pediatric Whole Hand Exoskeleton for Grasping Assistance in Task-Oriented Training," in *2019 IEEE 16th International Conference on Rehabilitation Robotics (ICORR)*, 2019: IEEE, pp. 108-114.
[34] E. Fosch-Villaronga, A. Čartolovni, and R. L. Pierce, "Promoting inclusiveness in exoskeleton robotics: Addressing challenges for pediatric access," *Paladyn, Journal of Behavioral Robotics,* vol. 11, no. 1, pp. 327-339, 2020.
[35] M. d. Onis, A. W. Onyango, E. Borghi, A. Siyam, C. Nishida, and J. Siekmann, "Development of a WHO growth reference for school-aged children and adolescents," *Bulletin of the World health Organization,* vol. 85, pp. 660-667, 2007.
[36] A. J. Veale and S. Q. Xie, "Towards compliant and wearable robotic orthoses: A review of current and emerging actuator technologies," *Medical Engineering and Physics,* vol. 38, no. 4, pp. 317-25, Apr 2016, doi: 10.1016/j.medengphy.2016.01.010.
[37] Z. F. Lerner, T. A. Harvey, and J. L. Lawson, "A Battery-Powered Ankle Exoskeleton Improves Gait Mechanics in a Feasibility Study of Individuals with Cerebral Palsy," *Annals of Biomedical Engineering,* vol. 47, no. 6, pp. 1345-1356, Jun 2019, doi: 10.1007/s10439-019-02237-w.
[38] R. A. Bos, K. Nizamis, B. F. Koopman, J. L. Herder, M. Sartori, and D. H. Plettenburg, "A case study with SymbiHand: an sEMG-controlled electrohydraulic hand orthosis for individuals with Duchenne muscular dystrophy," *IEEE Transactions on Neural Systems and Rehabilitation Engineering,* vol. 28, no. 1, pp. 258-266, 2019.
[39] A. Borboni, M. Mor, and R. Faglia, "Gloreha—hand robotic rehabilitation: Design, mechanical model, and experiments," *Journal of Dynamic Systems, Measurement, and Control,* vol. 138, no. 11, 2016, doi: 10.1115/1.4033831.
[40] B. W. Ang and C.-H. Yeow, "Design and modeling of a high force soft actuator for assisted elbow flexion," *IEEE Robotics and Automation Letters,* vol. 5, no. 2, pp. 3731-3736, 2020.
[41] D. Rus and M. T. Tolley, "Design, fabrication and control of soft robots," *Nature,* vol. 521, no. 7553, pp. 467-75, May 28 2015, doi: 10.1038/nature14543.
[42] Z. Peng and J. Huang, "Soft rehabilitation and nursing-care robots: A review and future outlook," *Applied Sciences,* vol. 9, no. 15, p. 3102, 2019.
[43] M. Bengisu and M. Ferrara, *Materials that move: smart materials, intelligent design*. Springer, 2018.
[44] S. Bahl, H. Nagar, I. Singh, and S. Sehgal, "Smart materials types, properties and applications: A review," *Materials Today: Proceedings,* vol. 28, pp. 1302-1306, 2020.
[45] M. Zhu, S. Biswas, S. I. Dinulescu, N. Kastor, E. W. Hawkes, and Y. Visell, "Soft, Wearable Robotics and Haptics: Technologies, Trends, and Emerging Applications," *Proceedings of the IEEE,* vol. 110, pp. 246-272, 2022.
[46] W.-S. Chu *et al.*, "Review of biomimetic underwater robots using smart actuators," *International Journal of Precision Engineering and Manufacturing,* vol. 13, no. 7, pp. 1281-1292, 2012, doi: 10.1007/s12541-012-0171-7.
[47] R. Granberry, J. Barry, B. Holschuh, and J. Abel, "Kinetically Tunable, Active Auxetic, and Variable Recruitment Active Textiles from Hierarchical Assemblies," *Advanced Materials Technologies,* vol. 6, no. 3, p. 2000825, 2021.
[48] V. Murphy, B. P. Edmonds, and A. L. Trejos, "Characterisation and Control of a Woven Biomimetic Actuator for Wearable Neurorehabilitative Devices," *Actuators,* vol. 10, no. 2, p. 37, 2021.
[49] J. Guo, C. Xiang, T. Helps, M. Taghavi, and J. Rossiter, "Electroactive textile actuators for wearable and soft robots," in *2018 IEEE International Conference on Soft Robotics (RoboSoft)*, 2018: IEEE, pp. 339-343.
[50] J. Zhang *et al.*, "Robotic Artificial Muscles: Current Progress and Future Perspectives," *IEEE Transactions on Robotics,* 2019.

[51] U. Gupta, L. Qin, Y. Wang, H. Godaba, and J. Zhu, "Soft robots based on dielectric elastomer actuators: a review," *Smart Materials and Structures,* vol. 28, no. 10, p. 103002, 2019, doi: 10.1088/1361-665X/ab3a77.

[52] W. Peng, Y. Zhang, J. Gao, Y. Wang, Y. Chen, and Y. Zhou, "Fabrication and performance of ionic polymer-metal composites for biomimetic applications," *Sensors and Actuators A: Physical,* vol. 299, p. 111613, 2019, doi: 10.1016/j.sna.2019.111613.

[53] Y. Li, M. Guo, and Y. Li, "Recent advances in plasticized PVC gels for soft actuators and devices: a review," *Journal of Materials Chemistry C,* vol. 7, no. 42, pp. 12991-13009, 2019.

[54] H. Jin, E. Dong, M. Xu, C. Liu, G. Alici, and Y. Jie, "Soft and smart modular structures actuated by shape memory alloy (SMA) wires as tentacles of soft robots," *Smart Materials and Structures,* vol. 25, no. 8, p. 085026, 2016, doi: 10.1088/0964-1726/25/8/085026.

[55] Y. Zhang *et al.*, "4D printing of a digital shape memory polymer with tunable high performance," *ACS applied materials & interfaces,* vol. 11, no. 35, pp. 32408-32413, 2019.

[56] C. S. Haines *et al.*, "Artificial muscles from fishing line and sewing thread," *science,* vol. 343, no. 6173, pp. 868-872, 2014.

[57] L. Wu, I. Chauhan, and Y. Tadesse, "A Novel Soft Actuator for the Musculoskeletal System," (in English), *Advanced Materials Technologies,* vol. 3, no. 5, May 2018, doi: 10.1002/admt.201700359.

[58] X. Tang, K. Li, Y. Liu, D. Zhou, and J. Zhao, "A soft crawling robot driven by single twisted and coiled actuator," *Sensors and Actuators A: Physical,* vol. 291, pp. 80-86, 2019, doi: 10.1016/j.sna.2019.03.049.

[59] K. Hyeon, J. Jeong, C. Chung, M. Cho, S. Hussain, and K.-U. Kyung, "Design of a Wearable Mechanism with Shape Memory Alloy (SMA)-based Artificial Muscle for Assisting with Shoulder Abduction," *IEEE Robotics and Automation Letters,* vol. 7, no. 4, pp. 10635-10642, 2022.

[60] L. Saharan, M. J. de Andrade, W. Saleem, R. H. Baughman, and Y. Tadesse, "iGrab: hand orthosis powered by twisted and coiled polymer muscles," *Smart Materials and Structures,* vol. 26, no. 10, p. 105048, 2017.

[61] A. Proto, M. Penhaker, D. Bibbo, D. Vala, S. Conforto, and M. Schmid, "Measurements of generated energy/electrical quantities from locomotion activities using piezoelectric wearable sensors for body motion energy harvesting," *Sensors,* vol. 16, no. 4, p. 524, 2016.

[62] A. G. Patiño, A. Ferrone, C. G. D. Gastélum, and C. Menon, "A novel biomedical technology based on the use of artificial muscles to assist with hand functions," in *2018 IEEE 9th Annual Information Technology, Electronics and Mobile Communication Conference (IEMCON)*, 2018: IEEE, pp. 620-625.

[63] L. Sutton, H. Moein, A. Rafiee, J. D. Madden, and C. Menon, "Design of an assistive wrist orthosis using conductive nylon actuators," in *2016 6th IEEE International Conference on Biomedical Robotics and Biomechatronics (BioRob)*, 2016: IEEE, pp. 1074-1079.

[64] M. L. Hall and M. A. Lobo, "Design and development of the first exoskeletal garment to enhance arm mobility for children with movement impairments," *Assistive Technology,* vol. 30, no. 5, pp. 251-258, 2018, doi: 10.1080/10400435.2017.1320690.

[65] S. Messina and G. L. Vita, "Clinical management of Duchenne muscular dystrophy: the state of the art," *Neurological Sciences,* vol. 39, no. 11, pp. 1837-1845, 2018.

[66] A. Behboodi, A. Sansare, N. Zahradka, and S. C. Lee, "Case report: The gait deviation index may predict neurotherapeutic effects of FES-assisted gait training in children with cerebral palsy," *Frontiers in Rehabilitation Sciences,* vol. 4, p. 1002222, 2023.

[67] M. A. de Souza, M. M. Figueiredo, C. R. de Baptista, R. D. Aldaves, and A. C. Mattiello-Sverzut, "Beneficial effects of ankle-foot orthosis daytime use on the gait of Duchenne

muscular dystrophy patients," *Clin Biomech (Bristol, Avon),* vol. 35, pp. 102-10, Jun 2016, doi: 10.1016/j.clinbiomech.2016.04.005.
[68] J. Rodda and H. Graham, "Classification of gait patterns in spastic hemiplegia and spastic diplegia: a basis for a management algorithm," *European journal of neurology,* vol. 8, pp. 98-108, 2001.
[69] R. Don *et al.*, "Foot drop and plantar flexion failure determine different gait strategies in Charcot-Marie-Tooth patients," *Clin Biomech (Bristol, Avon),* vol. 22, no. 8, pp. 905-16, Oct 2007, doi: 10.1016/j.clinbiomech.2007.06.002.
[70] K. K. Karunakaran, R. Pilkar, N. Ehrenberg, K. S. Bentley, J. Cheng, and K. J. Nolan, "Kinematic and Functional Gait Changes After the Utilization of a Foot Drop Stimulator in Pediatrics," *Front Neurosci,* vol. 13, p. 732, 2019, doi: 10.3389/fnins.2019.00732.
[71] J. Gil-Castillo, F. Alnajjar, A. Koutsou, D. Torricelli, and J. C. Moreno, "Advances in neuroprosthetic management of foot drop: a review," *Journal of neuroengineering and rehabilitation,* vol. 17, pp. 1-19, 2020.
[72] F. Alnajjar, R. Zaier, S. Khalid, and M. Gochoo, "Trends and Technologies in Rehabilitation of Foot Drop: A Systematic Review," *Expert review of medical devices,* pp. 1-16, 2020.
[73] C. L. Brockett and G. J. Chapman, "Biomechanics of the ankle," *Orthopaedics and trauma,* vol. 30, no. 3, pp. 232-238, 2016.
[74] S. Siegler, J. Chen, and C. Schneck, "The three-dimensional kinematics and flexibility characteristics of the human ankle and subtalar joints—Part I: Kinematics," 1988.
[75] V. L. Chester, M. Tingley, and E. N. Biden, "A comparison of kinetic gait parameters for 3–13 year olds," *Clinical Biomechanics,* vol. 21, no. 7, pp. 726-732, 2006.
[76] P. Weiss, R. Kearney, and I. Hunter, "Position dependence of ankle joint dynamics—I. Passive mechanics," *Journal of biomechanics,* vol. 19, no. 9, pp. 727-735, 1986.
[77] S. K. Grimston, B. M. Nigg, D. A. Hanley, and J. R. Engsberg, "Differences in ankle joint complex range of motion as a function of age," *Foot & ankle,* vol. 14, no. 4, pp. 215-222, 1993.
[78] K. J. Ganley and C. M. Powers, "Gait kinematics and kinetics of 7-year-old children: a comparison to adults using age-specific anthropometric data," *Gait & posture,* vol. 21, no. 2, pp. 141-145, 2005.
[79] S. G. Chung, E. Van Rey, Z. Bai, E. J. Roth, and L.-Q. Zhang, "Biomechanic changes in passive properties of hemiplegic ankles with spastic hypertonia," *Archives of physical medicine and rehabilitation,* vol. 85, no. 10, pp. 1638-1646, 2004.
[80] J. R. Engsberg, S. A. Ross, K. S. Olree, and T. S. Park, "Ankle spasticity and strength in children with spastic diplegic cerebral palsy," *Developmental Medicine & Child Neurology,* vol. 42, no. 1, pp. 42-47, 2000.
[81] R. T. Abresch, J. J. Han, and G. T. Carter, "Rehabilitation management of neuromuscular disease: the role of exercise training," *Journal of clinical neuromuscular disease,* vol. 11, no. 1, pp. 7-21, 2009.
[82] A. Gonzalez, L. Garcia, J. Kilby, and P. McNair, "Robotic devices for paediatric rehabilitation: a review of design features," *BioMedical Engineering OnLine,* vol. 20, no. 1, pp. 1-33, 2021.
[83] D. S. Tsze and J. H. Valente, "Pediatric stroke: a review," *Emergency Medicine International,* vol. 2011, p. 734506, 2011, doi: 10.1155/2011/734506.
[84] E. Beretta, A. Cesareo, E. Biffi, C. Schafer, S. Galbiati, and S. Strazzer, "Rehabilitation of Upper Limb in Children with Acquired Brain Injury: A Preliminary Comparative Study," *Journal of Healthcare Engineering,* vol. 2018, p. 4208492, 2018, doi: 10.1155/2018/4208492.
[85] S. Ryder *et al.*, "The burden, epidemiology, costs and treatment for Duchenne muscular dystrophy: an evidence review," *Orphanet Journal of Rare Diseases,* vol. 12, no. 1, p. 79, Apr 26 2017, doi: 10.1186/s13023-017-0631-3.

[86] M. T. Robinson and D. Estupinan, "Neuromuscular Diseases," in *Neuropalliative Care*: Springer, 2019, pp. 101-115.
[87] D. J. Thurman, "The epidemiology of traumatic brain injury in children and youths: a review of research since 1990," *Journal of Child Neurology,* vol. 31, no. 1, pp. 20-27, 2016.
[88] N. Umraw, Y. Chan, M. Gomez, R. C. Cartotto, and J. S. Fish, "Effective hand function assessment after burn injuries," *Journal of Burn Care & Research,* vol. 25, no. 1, pp. 134-9; discussion 128, Jan-Feb 2004, doi: 10.1097/01.BCR.0000105050.53263.30.
[89] L. E. Case *et al.*, "Rehabilitation management of the patient with Duchenne muscular dystrophy," *Pediatrics,* vol. 142, no. Supplement 2, pp. S17-S33, 2018.
[90] V. Falzarano, F. Marini, P. Morasso, and J. Zenzeri, "Devices and Protocols for Upper Limb Robot-Assisted Rehabilitation of Children with Neuromotor Disorders," *Applied Sciences,* vol. 9, no. 13, p. 2689, 2019.
[91] E. Beretta *et al.*, "Effect of Robot-Assisted Gait Training in a Large Population of Children With Motor Impairment Due to Cerebral Palsy or Acquired Brain Injury," *Archives of Physical Medicine and Rehabilitation,* vol. 101, no. 1, pp. 106-112, Jan 2020, doi: 10.1016/j.apmr.2019.08.479.
[92] G. Roberts, K. Howard, A. J. Spittle, N. C. Brown, P. J. Anderson, and L. W. Doyle, "Rates of early intervention services in very preterm children with developmental disabilities at age 2 years," *Journal of Paediatrics and Child Health,* vol. 44, no. 5, pp. 276-80, May 2008, doi: 10.1111/j.1440-1754.2007.01251.x.
[93] C. O. P. E. MEDICINE, "Management of pediatric trauma," *Pediatrics,* vol. 138, no. 2, p. e20161569, 2016.
[94] C. M. McDonald and E. Mercuri, "Evidence-based care in Duchenne muscular dystrophy," *The Lancet Neurology,* vol. 17, no. 5, pp. 389-391, 2018, doi: 10.1016/s1474-4422(18)30115-7.
[95] M. Shishehgar, D. Kerr, and J. Blake, "A systematic review of research into how robotic technology can help older people," *Smart Health,* vol. 7, pp. 1-18, 2018.
[96] A. Khan and Y. Anwar, "Robots in healthcare: A survey," in *Science and Information Conference*, 2019: Springer, pp. 280-292.
[97] E. Martinez-Martin, A. Costa, and M. Cazorla, "PHAROS 2.0—A PHysical assistant RObot system improved," *Sensors,* vol. 19, no. 20, p. 4531, 2019.
[98] S. Lippross *et al.*, "Robot assisted spinal surgery-A technical report on the use of DaVinci in orthopaedics," *Journal of orthopaedics,* vol. 19, pp. 50-53, 2020.
[99] E. R. SPARC, "Robotics 2020 Multi-Annual Roadmap for Robotics in Europe, Call 2 ICT24–Horizon 2020," *Initial Release B,* vol. 15, no. 01, p. 2014, 2015.
[100] M. del Carmen Sanchez-Villamañan, J. Gonzalez-Vargas, D. Torricelli, J. C. Moreno, and J. L. Pons, "Compliant lower limb exoskeletons: a comprehensive review on mechanical design principles," *Journal of Neuroengineering and Rehabilitation,* vol. 16, no. 1, p. 55, 2019.
[101] J. Narayan, B. Kalita, and S. K. Dwivedy, "Development of Robot-Based Upper Limb Devices for Rehabilitation Purposes: a Systematic Review," *Augmented Human Research,* vol. 6, no. 1, pp. 1-33, 2021.
[102] I. Carvalho, S. M. Pinto, D. das Virgens Chagas, J. L. P. dos Santos, T. de Sousa Oliveira, and L. A. Batista, "Robotic gait training for individuals with cerebral palsy: a systematic review and meta-analysis," *Archives of physical medicine and rehabilitation,* vol. 98, no. 11, pp. 2332-2344, 2017.
[103] J. Mehrholz, S. Thomas, C. Werner, J. Kugler, M. Pohl, and B. Elsner, "Electromechanical-assisted training for walking after stroke," *Cochrane Database Systematic Reviews,* vol. 5, p. CD006185, May 10 2017, doi: 10.1002/14651858.CD006185.pub4.

[104] F. Martelli *et al.*, "Estimation of multivariable dynamic ankle impedance after botulinum toxin injection in children with cerebral palsy," in *2016 IEEE International Symposium on Medical Measurements and Applications (MeMeA)*, 2016: IEEE, pp. 1-6.
[105] A. Kapsalyamov, S. Hussain, and P. K. Jamwal, "State-of-the-art assistive powered upper limb exoskeletons for elderly," *IEEE Access,* vol. 8, pp. 178991-179001, 2020.
[106] T. Yan, M. Cempini, C. M. Oddo, and N. Vitiello, "Review of assistive strategies in powered lower-limb orthoses and exoskeletons," *Robotics and Autonomous Systems,* vol. 64, pp. 120-136, 2015.
[107] B. Maalej, H. Medhaffar, A. Chemori, and N. Derbel, "A Fuzzy Sliding Mode Controller for Reducing Torques Applied to a Rehabilitation Robot," in *2020 17th International Multi-Conference on Systems, Signals & Devices (SSD)*, 2020: IEEE, pp. 740-746.
[108] R. Jribi, B. Maalej, and N. Derbel, "Exoskeletons Control via Computed Torque for Lower Limb Rehabilitation," in *New Trends in Robot Control*: Springer, 2020, pp. 131-151.
[109] J. Chen, D. L. Damiano, Z. F. Lerner, and T. C. Bulea, "Validating Model-Based Prediction Of Biological Knee Moment During Walking With An Exoskeleton in Crouch Gait: Potential Application for Exoskeleton Control," in *2019 IEEE 16th International Conference on Rehabilitation Robotics (ICORR)*, 2019: IEEE, pp. 778-783.
[110] J. Narayan and S. K. Dwivedy, "Towards Neuro-Fuzzy Compensated PID Control of Lower Extremity Exoskeleton System for Passive Gait Rehabilitation," *IETE Journal of Research,* pp. 1-18, 2020, doi: 10.1080/03772063.2020.1838346.
[111] X. Zeng, G. Zhu, M. Zhang, and S. Q. Xie, "Reviewing Clinical Effectiveness of Active Training Strategies of Platform-Based Ankle Rehabilitation Robots," *Journal of Healthcare Engineering,* vol. 2018, p. 2858294, 2018, doi: 10.1155/2018/2858294.
[112] A. Plaza, M. Hernandez, G. Puyuelo, E. Garces, and E. Garcia, "Lower-limb medical and rehabilitation exoskeletons: A review of the current designs," *IEEE Reviews in Biomedical Engineering,* 2021.
[113] U. Keller, V. Klamroth, H. J. van Hedel, and R. Riener, "ChARMin: A robot for pediatric arm rehabilitation," in *2013 IEEE International Conference on Robotics and Automation*, 2013: IEEE, pp. 3908-3913.
[114] J. Borenstein, A. R. Wagner, and A. Howard, "Overtrust of pediatric health-care robots: A preliminary survey of parent perspectives," *IEEE Robotics & Automation Magazine,* vol. 25, no. 1, pp. 46-54, 2018.
[115] M. A. Lobo, M. L. Hall, B. Greenspan, P. Rohloff, L. A. Prosser, and B. A. Smith, "Wearables for Pediatric Rehabilitation: How to Optimally Design and Use Products to Meet the Needs of Users," *Physical Therapy,* vol. 99, no. 6, pp. 647-657, 2019.
[116] R. Wessels, B. Dijcks, M. Soede, G. Gelderblom, and L. De Witte, "Non-use of provided assistive technology devices, a literature overview," *Technology and Disability,* vol. 15, no. 4, pp. 231-238, 2003.
[117] A. Liberati *et al.*, "The PRISMA statement for reporting systematic reviews and meta-analyses of studies that evaluate health care interventions: explanation and elaboration," *Journal of Clinical Epidemiology,* vol. 62, no. 10, pp. e1-e34, 2009.
[118] A. Meyer-Heim and H. J. van Hedel, "Robot-assisted and computer-enhanced therapies for children with cerebral palsy: current state and clinical implementation," in *Seminars in Pediatric Neurology*, 2013, vol. 20, no. 2: Elsevier, pp. 139-145.
[119] C. Bayon and R. Raya, "Robotic Therapies for Children with Cerebral Palsy: A Systematic Review," *Translational Biomedicine,* vol. 7, no. 1, 2016, doi: 10.21767/2172-0479.100044.
[120] J. A. Vova and E. M. Eggebrecht, "Utilizing Functional Electrical Stimulation and Exoskeletons in Pediatrics: a Closer Look at Their Roles in Gait and Functional Changes in Cerebral Palsy," *Current Physical Medicine and Rehabilitation Reports,* vol. 7, no. 2, pp. 57-66, 2019.

[121] J. G. Zwicker and T. A. Mayson, "Effectiveness of treadmill training in children with motor impairments: an overview of systematic reviews," *Pediatric Physical Therapy,* vol. 22, no. 4, pp. 361-77, Winter 2010, doi: 10.1097/PEP.0b013e3181f92e54.
[122] Y.-P. Chen and A. M. Howard, "Effects of robotic therapy on upper-extremity function in children with cerebral palsy: a systematic review," *Developmental neurorehabilitation,* vol. 19, no. 1, pp. 64-71, 2016.
[123] F. Mahamud and A. Anuar, "Usage of robotic rehabilitation technology for lower limbs therapy of children with cerebral palsy-a review," in *2014 IEEE International Symposium on Robotics and Manufacturing Automation (ROMA)*, 2014: IEEE, pp. 126-130.
[124] J. G. Donenberg, L. Fetters, and R. Johnson, "The effects of locomotor training in children with spinal cord injury: a systematic review," *Developmental neurorehabilitation,* vol. 22, no. 4, pp. 272-287, 2019.
[125] I. Andrew, J. Batavia, and S. H. Guy, "Toward the development of consumer-based criteria for the evaluation of assistive devices," *Journal of Rehabilitation Research and Development,* vol. 27, no. 4, p. 425, 1990.
[126] A. P. H. Weightman, N. Preston, R. Holt, M. Allsop, M. Levesley, and B. Bhakta, "Engaging children in healthcare technology design: developing rehabilitation technology for children with cerebral palsy," *Journal of Engineering Design,* vol. 21, no. 5, pp. 579-600, 2009, doi: 10.1080/09544820802441092.
[127] W. H. Organization, *International Classification of Functioning, Disability, and Health: Children & Youth Version: ICF-CY*. World Health Organization, 2007.
[128] D. Eguren, M. Cestari, T. P. Luu, A. Kilicarslan, A. Steele, and J. L. Contreras-Vidal, "Design of a customizable, modular pediatric exoskeleton for rehabilitation and mobility," in *2019 IEEE International Conference on Systems, Man and Cybernetics (SMC)*, 2019: IEEE, pp. 2411-2416.
[129] S. Rossi, A. Colazza, M. Petrarca, E. Castelli, P. Cappa, and H. I. Krebs, "Feasibility study of a wearable exoskeleton for children: is the gait altered by adding masses on lower limbs?," *PloS one,* vol. 8, no. 9, 2013.
[130] Z. F. Lerner *et al.*, "An Untethered Ankle Exoskeleton Improves Walking Economy in a Pilot Study of Individuals With Cerebral Palsy," *IEEE Transactions on Neural Systems and Rehabilitation Engineering,* vol. 26, no. 10, pp. 1985-1993, Oct 2018, doi: 10.1109/TNSRE.2018.2870756.
[131] T. Yamada, H. Kadone, Y. Shimizu, and K. Suzuki, "An Exoskeleton Brake Unit for Children with Crouch Gait Supporting the Knee Joint During Stance," in *2018 International Symposium on Micro-NanoMechatronics and Human Science (MHS)*, 2018: IEEE, pp. 1-7.
[132] K. P. Michmizos and H. I. Krebs, "Pediatric robotic rehabilitation: Current knowledge and future trends in treating children with sensorimotor impairments," *NeuroRehabilitation,* vol. 41, no. 1, pp. 69-76, 2017, doi: 10.3233/NRE-171458.
[133] M. L. Hall and B. T. Orzada, "Expressive prostheses: meaning and significance," *Fashion Practice,* vol. 5, no. 1, pp. 9-32, 2013.
[134] T. Schuler, K. Brütsch, R. Müller, H. J. van Hedel, and A. Meyer-Heim, "Virtual realities as motivational tools for robotic assisted gait training in children: A surface electromyography study," *NeuroRehabilitation,* vol. 28, no. 4, pp. 401-411, 2011.
[135] T. C. Bulea, Z. F. Lerner, A. J. Gravunder, and D. L. Damiano, "Exergaming with a pediatric exoskeleton: facilitating rehabilitation and research in children with cerebral palsy," in *2017 International Conference on Rehabilitation Robotics (ICORR)*, 2017: IEEE, pp. 1087-1093.
[136] U. Keller and R. Riener, "Design of the pediatric arm rehabilitation robot ChARMin," in *5th IEEE RAS/EMBS International Conference on Biomedical Robotics and Biomechatronics*, 2014: IEEE, pp. 530-535.
[137] P. M. Aubin, H. Sallum, C. Walsh, L. Stirling, and A. Correia, "A pediatric robotic thumb exoskeleton for at-home rehabilitation: the Isolated Orthosis for Thumb Actuation

(IOTA)," in *2013 IEEE 13th International Conference on Rehabilitation Robotics (ICORR)*, 2013: IEEE, pp. 1-6.
[138] C. A. Laubscher and J. T. Sawicki, "Gait Guidance Control for Damping of Unnatural Motion in a Powered Pediatric Lower-Limb Orthosis," in *2019 IEEE 16th International Conference on Rehabilitation Robotics (ICORR)*, 2019: IEEE, pp. 676-681.
[139] J. Sancho-Perez, M. Perez, E. Garcia, D. Sanz-Merodio, A. Plaza, and M. Cestari, "Mechanical Description of ATLAS 2020, A 10-DOF Paediatric Exoskeleton," in *Advances in Cooperative Robotics*: World Scientific, 2017, pp. 814-822.
[140] M. Volpini, V. Bartenbach, M. Pinotti, and R. Riener, "Clinical evaluation of a low-cost robot for use in physiotherapy and gait training," *Journal of rehabilitation and assistive technologies engineering,* vol. 4, p. 2055668316688410, 2017.
[141] K. Cleary *et al.*, "Pedbothome: Robotically-Assisted Ankle Rehabilitation System For Children With Cerebral Palsy," in *2019 IEEE 16th International Conference on Rehabilitation Robotics (ICORR)*, 2019: IEEE, pp. 13-20.
[142] F. Frascarelli, L. Masia, G. Di Rosa, M. Petrarca, P. Cappa, and E. Castelli, "Robot-mediated and clinical scales evaluation after upper limb botulinum toxin type A injection in children with hemiplegia," *Journal of Rehabilitation Medicine,* vol. 41, no. 12, pp. 988-94, Nov 2009, doi: 10.2340/16501977-0412.
[143] F. Marini, V. Squeri, P. Morasso, C. Campus, J. Konczak, and L. Masia, "Robot-aided developmental assessment of wrist proprioception in children," *Journal of NeuroEngineering and Rehabilitation,* vol. 14, no. 1, p. 3, 2017.
[144] S. Dehem *et al.*, "Assessment of upper limb spasticity in stroke patients using the robotic device REAplan," *Journal of Rehabilitation Medicine,* vol. 49, no. 7, pp. 565-571, Jul 7 2017, doi: 10.2340/16501977-2248.
[145] H. I. Krebs, N. Hogan, M. L. Aisen, and B. T. Volpe, "Robot-aided neurorehabilitation," *IEEE Transactions on Rehabilitation Engineering,* vol. 6, no. 1, pp. 75-87, 1998.
[146] B. Ladenheim *et al.*, "The effect of random or sequential presentation of targets during robot-assisted therapy on children," *NeuroRehabilitation,* vol. 33, no. 1, pp. 25-31, 2013.
[147] L. Masia, M. Casadio, P. Giannoni, G. Sandini, and P. Morasso, "Performance adaptive training control strategy for recovering wrist movements in stroke patients: a preliminary, feasibility study," *Journal of NeuroEngineering and Rehabilitation,* vol. 6, p. 44, Dec 7 2009, doi: 10.1186/1743-0003-6-44.
[148] F. Marini *et al.*, "Robotic wrist training after stroke: Adaptive modulation of assistance in pediatric rehabilitation," *Robotics and Autonomous Systems,* vol. 91, pp. 169-178, 2017, doi: 10.1016/j.robot.2017.01.006.
[149] G. G. Fluet *et al.*, "Robot-assisted virtual rehabilitation (NJIT-RAVR) system for children with upper extremity hemiplegia," in *2009 Virtual Rehabilitation International Conference*, 2009: IEEE, pp. 189-192.
[150] Q. Qiu *et al.*, "The New Jersey Institute of Technology Robot-Assisted Virtual Rehabilitation (NJIT-RAVR) system for children with cerebral palsy: a feasibility study," *Journal of NeuroEngineering and Rehabilitation,* vol. 6, p. 40, Nov 16 2009, doi: 10.1186/1743-0003-6-40.
[151] B. Koo *et al.*, "Design and evaluation of a hybrid passive and active gravity neutral orthosis (GNO)," in *2009 Annual International Conference of the IEEE Engineering in Medicine and Biology Society*, 2009: IEEE, pp. 1573-1576.
[152] P. Sale, V. Lombardi, and M. Franceschini, "Hand robotics rehabilitation: feasibility and preliminary results of a robotic treatment in patients with hemiparesis," *Stroke Research and Treatment,* vol. 2012, p. 820931, 2012, doi: 10.1155/2012/820931.
[153] A. F. Samhan, N. M. Abdelhalim, and R. K. Elnaggar, "Effects of interactive robot-enhanced hand rehabilitation in treatment of paediatric hand-burns: A randomized, controlled trial with 3-months follow-up," *Burns,* vol. 46, no. 6, pp. 1347-1355, Sep 2020, doi: 10.1016/j.burns.2020.01.015.

[154] M. Gilliaux, T. Lejeune, C. Detrembleur, J. Sapin, B. Dehez, and G. Stoquart, "A robotic device as a sensitive quantitative tool to assess upper limb impairments in stroke patients: a preliminary prospective cohort study," *Journal of Rehabilitation Medicine,* vol. 44, no. 3, pp. 210-217, 2012.

[155] A. Koenig, U. Keller, K. Pfluger, A. Meyer-Heim, and R. Riener, "PASCAL: Pediatric arm support robot for combined arm and leg training," in *2012 4th IEEE RAS & EMBS International Conference on Biomedical Robotics and Biomechatronics (BioRob)*, 2012: IEEE, pp. 1862-1868.

[156] U. Keller, G. Rauter, and R. Riener, "Assist-as-needed path control for the PASCAL rehabilitation robot," in *2013 IEEE 13th International Conference on Rehabilitation Robotics (ICORR)*, 2013: IEEE, pp. 1-7.

[157] T. L. Zhu, J. Klein, S. A. Dual, T. C. Leong, and E. Burdet, "reachMAN2: A compact rehabilitation robot to train reaching and manipulation," in *2014 IEEE/RSJ International Conference on Intelligent Robots and Systems*, 2014: IEEE, pp. 2107-2113.

[158] L. Z. Tong *et al.*, "Pediatric rehabilitation with the reachMAN's modular handle," in *2015 37th Annual International Conference of the IEEE Engineering in Medicine and Biology Society (EMBC)*, 2015: IEEE, pp. 3933-3936.

[159] J. Gallagher, N. Preston, R. Holt, M. Mon-Williams, M. Levesley, and A. Weightman, "Assessment of upper limb movement with an autonomous robotic device in a school environment for children with Cerebral Palsy," in *2015 IEEE International Conference on Rehabilitation Robotics (ICORR)*, 2015: IEEE, pp. 770-774.

[160] A. M. Kuczynski, A. Kirton, J. A. Semrau, and S. P. Dukelow, "Bilateral reaching deficits after unilateral perinatal ischemic stroke: a population-based case-control study," *Journal of NeuroEngineering and Rehabilitation,* vol. 15, no. 1, p. 77, Aug 17 2018, doi: 10.1186/s12984-018-0420-9.

[161] V. Varalta, A. Picelli, C. Fonte, G. Montemezzi, E. La Marchina, and N. Smania, "Effects of contralesional robot-assisted hand training in patients with unilateral spatial neglect following stroke: a case series study," *Journal of Neuroengineering and Rehabilitation,* vol. 11, no. 1, p. 160, 2014.

[162] Y. Shimizu *et al.*, "Voluntary Elbow Extension-Flexion Using Single Joint Hybrid Assistive Limb (HAL) for Patients of Spastic Cerebral Palsy: Two Cases Report," *Frontiers in Neurology,* vol. 10, p. 2, 2019, doi: 10.3389/fneur.2019.00002.

[163] K. O. Thielbar *et al.*, "Training finger individuation with a mechatronic-virtual reality system leads to improved fine motor control post-stroke," *Journal of NeuroEngineering and Rehabilitation,* vol. 11, no. 1, p. 171, Dec 26 2014, doi: 10.1186/1743-0003-11-171.

[164] S. H. Scott, "Apparatus for measuring and perturbing shoulder and elbow joint positions and torques during reaching," *Journal of Neuroscience Methods,* vol. 89, no. 2, pp. 119-127, 1999.

[165] N. M. Lopez, N. de Diego, R. Hernandez, E. Perez, G. Ensinck, and M. E. Valentinuzzi, "Customized device for pediatric upper limb rehabilitation in obstetric brachial palsy," *American Journal of Physical Medicine & Rehabilitation,* vol. 93, no. 3, pp. 263-6, Mar 2014, doi: 10.1097/PHM.0b013e3182a51c95.

[166] D. Holley, M. Johnson, G. Harris, and S. Beardsley, "A modular low-clearance wrist orthosis for improving wrist motion in children with cerebral palsy," in *2014 36th Annual International Conference of the IEEE Engineering in Medicine and Biology Society*, 2014: IEEE, pp. 3069-3072.

[167] J. V. McCall, M. C. Ludovice, J. A. Blaylock, and D. G. Kamper, "A Platform for Rehabilitation of Finger Individuation in Children with Hemiplegic Cerebral Palsy," in *2019 IEEE 16th International Conference on Rehabilitation Robotics (ICORR)*, 2019: IEEE, pp. 343-348.

[168] P. Bobrov *et al.*, "REHABILITATION OF PATIENTS WITH CEREBRAL PALSY USING HAND EXOSKELETON CONTROLLED BY BRAIN-COMPUTER INTERFACE," *Bulletin of Russian State Medical University,* no. 4, 2020.

[169] A. B. Tornberg and K. Lauruschkus, "Non-ambulatory children with cerebral palsy: effects of four months of static and dynamic standing exercise on passive range of motion and spasticity in the hip," *PeerJ,* vol. 8, p. e8561, 2020, doi: 10.7717/peerj.8561.

[170] M. Wu, J. Kim, P. Arora, D. J. Gaebler-Spira, and Y. Zhang, "Kinematic and EMG Responses to Pelvis and Leg Assistance Force during Treadmill Walking in Children with Cerebral Palsy," *Neural Plasticity,* vol. 2016, p. 5020348, 2016, doi: 10.1155/2016/5020348.

[171] F. Chrif, T. Nef, M. Lungarella, R. Dravid, and K. J. Hunt, "Control design for a lower-limb paediatric therapy device using linear motor technology," *Biomedical Signal Processing and Control,* vol. 38, pp. 119-127, 2017, doi: 10.1016/j.bspc.2017.05.011.

[172] S. Hesse and D. Uhlenbrock, "A mechanized gait trainer for restoration of gait," *Journal of Rehabilitation Research and Development,* vol. 37, no. 6, pp. 701-708, 2000.

[173] N. Smania *et al.*, "Improved gait after repetitive locomotor training in children with cerebral palsy," *American Journal of Physical Medicine & Rehabilitation,* vol. 90, no. 2, pp. 137-49, Feb 2011, doi: 10.1097/PHM.0b013e318201741e.

[174] S. Muraki, Y. Ehara, and M. Yamasaki, "Cardiovascular responses at the onset of passive leg cycle exercise in paraplegics with spinal cord injury," *European Journal of Applied Physiology,* vol. 81, no. 4, pp. 271-274, 2000.

[175] D. L. Damiano, C. J. Stanley, L. Ohlrich, and K. E. Alter, "Task-Specific and Functional Effects of Speed-Focused Elliptical or Motor-Assisted Cycle Training in Children With Bilateral Cerebral Palsy: Randomized Clinical Trial," *Neurorehabil Neural Repair,* vol. 31, no. 8, pp. 736-745, Aug 2017, doi: 10.1177/1545968317718631.

[176] L. Q. Zhang *et al.*, "Intelligent stretching of ankle joints with contracture/spasticity," *IEEE Transactions on Neural Systems and Rehabilitation Engineering,* vol. 10, no. 3, pp. 149-57, Sep 2002, doi: 10.1109/TNSRE.2002.802857.

[177] K. Chen *et al.*, "Home-Based Versus Laboratory-Based Robotic Ankle Training for Children With Cerebral Palsy: A Pilot Randomized Comparative Trial," *Archives of Physical Medicine and Rehabilitation,* vol. 97, no. 8, pp. 1237-43, Aug 2016, doi: 10.1016/j.apmr.2016.01.029.

[178] C. Schmidt-Lucke *et al.*, "Effect of assisted walking-movement in patients with genetic and acquired neuromuscular disorders with the motorised Innowalk device: an international case study meta-analysis," *PeerJ,* vol. 7, p. e7098, 2019, doi: 10.7717/peerj.7098.

[179] M. Yazici, A. Livanelioglu, K. Gucuyener, L. Tekin, E. Sumer, and Y. Yakut, "Effects of robotic rehabilitation on walking and balance in pediatric patients with hemiparetic cerebral palsy," *Gait Posture,* vol. 70, pp. 397-402, May 2019, doi: 10.1016/j.gaitpost.2019.03.017.

[180] F.-C. Wang, C.-H. Yu, and T.-Y. Chou, "Design and implementation of robust controllers for a gait trainer," *Proceedings of the Institution of Mechanical Engineers, Part H: Journal of Engineering in Medicine,* vol. 223, no. 6, pp. 687-696, 2009.

[181] M. Wu, T. G. Hornby, J. M. Landry, H. Roth, and B. D. Schmit, "A cable-driven locomotor training system for restoration of gait in human SCI," *Gait Posture,* vol. 33, no. 2, pp. 256-60, Feb 2011, doi: 10.1016/j.gaitpost.2010.11.016.

[182] M. Wu, J. Kim, P. Arora, D. J. Gaebler-Spira, and Y. Zhang, "Effects of the Integration of Dynamic Weight Shifting Training Into Treadmill Training on Walking Function of Children with Cerebral Palsy: A Randomized Controlled Study," *American Journal of Physical Medicine & Rehabilitation,* vol. 96, no. 11, pp. 765-772, Nov 2017, doi: 10.1097/PHM.0000000000000776.

[183] C. A. Nelson, J. M. Burnfield, Y. Shu, T. W. Buster, A. P. Taylor, and A. Graham, "Modified Elliptical Machine Motor-Drive Design for Assistive Gait Rehabilitation," *Journal of Medical Devices,* vol. 5, no. 2, 2011, doi: 10.1115/1.4003693.

[184] J. M. Burnfield, T. W. Buster, C. M. Pfeifer, S. L. Irons, G. M. Cesar, and C. A. Nelson, "Adapted motor-assisted elliptical for rehabilitation of children with physical disabilities," *Journal of Medical Devices,* vol. 13, no. 1, 2019.

[185] D. Cioi, A. Kale, G. Burdea, J. Engsberg, W. Janes, and S. Ross, "Ankle control and strength training for children with cerebral palsy using the Rutgers Ankle CP," in *2011 IEEE international conference on rehabilitation robotics*, 2011: IEEE, pp. 1-6.

[186] M. Girone, G. Burdea, and M. Bouzit, "The Rutgers ankle orthopedic rehabilitation interface," in *Proceedings of the ASME Haptics Symposium*, 1999, vol. 67: DSC, pp. 305-312.

[187] Y. Ren, S. J. Lee, H. S. Park, and L. Q. Zhang, "A pivoting elliptical training system for improving pivoting neuromuscular control and rehabilitating musculoskeletal injuries," *IEEE Transactions on Neural Systems and Rehabilitation Engineering,* vol. 21, no. 5, pp. 860-8, Sep 2013, doi: 10.1109/TNSRE.2013.2273874.

[188] S. J. Lee, D. Jin, S. H. Kang, D. Gaebler-Spira, and L. Q. Zhang, "Combined Ankle/Knee Stretching and Pivoting Stepping Training for Children With Cerebral Palsy," *IEEE Transactions on Neural Systems and Rehabilitation Engineering,* vol. 27, no. 9, pp. 1743-1752, Sep 2019, doi: 10.1109/TNSRE.2019.2934139.

[189] V. Vashista, X. Jin, and S. K. Agrawal, "Active tethered pelvic assist device (a-tpad) to study force adaptation in human walking," in *2014 IEEE International Conference on Robotics and Automation (ICRA)*, 2014: IEEE, pp. 718-723.

[190] J. Kang, D. Martelli, V. Vashista, I. Martinez-Hernandez, H. Kim, and S. K. Agrawal, "Robot-driven downward pelvic pull to improve crouch gait in children with cerebral palsy," *Science Robotics,* vol. 2, no. 8, p. eaan2634, 2017.

[191] R. Monfaredi *et al.*, "Robotically assisted ankle rehabilitation for pediatrics," in *2016 6th IEEE International Conference on Biomedical Robotics and Biomechatronics (BioRob)*, 2016: IEEE, pp. 612-616.

[192] E. J. Park *et al.*, "Design and preliminary evaluation of a multi-robotic system with pelvic and hip assistance for pediatric gait rehabilitation," in *2017 International Conference on Rehabilitation Robotics (ICORR)*, 2017: IEEE, pp. 332-339.

[193] S. Ricklin, A. Meyer-Heim, and H. J. A. van Hedel, "Dual-task training of children with neuromotor disorders during robot-assisted gait therapy: prerequisites of patients and influence on leg muscle activity," *Journal of NeuroEngineering and Rehabilitation,* vol. 15, no. 1, p. 82, Sep 17 2018, doi: 10.1186/s12984-018-0426-3.

[194] L. F. Aycardi *et al.*, "Evaluation of biomechanical gait parameters of patients with Cerebral Palsy at three different levels of gait assistance using the CPWalker," *Journal of NeuroEngineering and Rehabilitation,* vol. 16, no. 1, p. 15, Jan 28 2019, doi: 10.1186/s12984-019-0485-0.

[195] M. Germanotta *et al.*, "Spasticity measurement based on tonic stretch reflex threshold in children with cerebral palsy using the PediAnklebot," *Frontiers in Human Neuroscience,* vol. 11, p. 277, 2017.

[196] K. Chen *et al.*, "Ankle passive and active movement training in children with acute brain injury using a wearable robot," *Journal of Rehabilitation Medicine,* vol. 50, no. 1, pp. 30-36, Jan 10 2018, doi: 10.2340/16501977-2285.

[197] Z. F. Lerner, D. L. Damiano, and T. C. Bulea, "The effects of exoskeleton assisted knee extension on lower-extremity gait kinematics, kinetics, and muscle activity in children with cerebral palsy," *Scientific Reports,* vol. 7, no. 1, pp. 1-12, 2017.

[198] B. Maalej, R. Jribi, N. Ayadi, F. Abdelhedi, and N. Derbel, "On a Robotic Application for Rehabilitation Systems Dedicated to Kids Affected by Cerebral Palsy," *2018 15th International Multi-Conference on Systems, Signals & Devices (SSD),* pp. 414-419, 2018.

[199] A. Meyer-Heim *et al.*, "Feasibility of robotic-assisted locomotor training in children with central gait impairment," *Developmental Medicine & Child Neurology,* vol. 49, no. 12, pp. 900-906, 2007.

[200] K. Suzuki, G. Mito, H. Kawamoto, Y. Hasegawa, and Y. Sankai, "Intention-based walking support for paraplegia patients with Robot Suit HAL," *Advanced Robotics,* vol. 21, no. 12, pp. 1441-1469, 2007.
[201] S. Nakagawa *et al.*, "Newly developed hybrid assistive limb for pediatric patients with cerebral palsy: a case report," *Journal of Physical Therapy Science,* vol. 31, no. 8, pp. 702-707, 2019.
[202] S. Kawasaki, K. Ohata, T. Yoshida, A. Yokoyama, and S. Yamada, "Gait improvements by assisting hip movements with the robot in children with cerebral palsy: a pilot randomized controlled trial," *Journal of NeuroEngineering and Rehabilitation,* vol. 17, no. 1, pp. 1-8, 2020.
[203] N. Tanaka *et al.*, "Effect of stride management assist gait training for poststroke hemiplegia: a single center, open-label, randomized controlled trial," *Journal of Stroke and Cerebrovascular Diseases,* vol. 28, no. 2, pp. 477-486, 2019.
[204] N. Smania *et al.*, "Applicability of a new robotic walking aid in a patient with cerebral palsy," *European Journal of Physical and Rehabilitation Medicine,* vol. 147, no. 2, pp. 135-40, 2011.
[205] F. Molteni *et al.*, "Wearable robotic exoskeleton for overground gait training in sub-acute and chronic hemiparetic stroke patients: preliminary results," *European Journal of Physical and Rehabilitation Medicine,* vol. 53, no. 5, pp. 676-684, 2017.
[206] K. K. Karunakaran, N. Ehrenberg, J. Cheng, and K. J. Nolan, "Effects of Robotic Exoskeleton Gait Training on an Adolescent with Brain Injury," in *2019 41st Annual International Conference of the IEEE Engineering in Medicine and Biology Society (EMBC)*, 2019: IEEE, pp. 4445-4448.
[207] K. P. Michmizos, S. Rossi, E. Castelli, P. Cappa, and H. I. Krebs, "Robot-Aided Neurorehabilitation: A Pediatric Robot for Ankle Rehabilitation," *IEEE Transactions on Neural Systems and Rehabilitation Engineering,* vol. 23, no. 6, pp. 1056-67, Nov 2015, doi: 10.1109/TNSRE.2015.2410773.
[208] D. R. Lee, Y. K. Shin, J.-H. Park, and J. H. You, "Concurrent Validity and Test-Retest Reliability of the Walkbot-K System for Robotic Gait Training," *Journal of Mechanics in Medicine and Biology,* vol. 16, no. 08, p. 1640029, 2016, doi: 10.1142/s0219519416400297.
[209] L. H. Jin, S.-s. Yang, J. Y. Choi, and M. K. Sohn, "The Effect of Robot-Assisted Gait Training on Locomotor Function and Functional Capability for Daily Activities in Children with Cerebral Palsy: A Single-Blinded, Randomized Cross-Over Trial," *Brain Sciences,* vol. 10, no. 11, p. 801, 2020.
[210] D. Erbil *et al.*, "Effects of robot-assisted gait training in chronic stroke patients treated by botulinum toxin-a: A pivotal study," *Physiotherapy Research International,* vol. 23, no. 3, p. e1718, 2018.
[211] H. Sucuoglu, "Effects of robot-assisted gait training alongside conventional therapy on the development of walking in children with cerebral palsy," *Journal of Pediatric Rehabilitation Medicine,* vol. 13, no. 2, pp. 127-135, 2020, doi: 10.3233/PRM-180541.
[212] I. Mileti, J. Taborri, S. Rossi, M. Petrarca, F. Patanè, and P. Cappa, "Evaluation of the effects on stride-to-stride variability and gait asymmetry in children with Cerebral Palsy wearing the WAKE-up ankle module," in *2016 IEEE International Symposium on Medical Measurements and Applications (MeMeA)*, 2016: IEEE, pp. 1-6.
[213] J. L. Cornejo, J. F. Santana, and S. A. Salinas, "Exoskeleton for gait rehabilitation of children: Conceptual design," in *2017 International Conference on Rehabilitation Robotics (ICORR)*, 2017: IEEE, pp. 452-454.
[214] C. Bayón *et al.*, "Development and evaluation of a novel robotic platform for gait rehabilitation in patients with Cerebral Palsy: CPWalker," *Robotics and Autonomous Systems,* vol. 91, pp. 101-114, 2017, doi: 10.1016/j.robot.2016.12.015.
[215] Y. Ren, Y. N. Wu, C. Y. Yang, T. Xu, R. L. Harvey, and L. Q. Zhang, "Developing a Wearable Ankle Rehabilitation Robotic Device for in-Bed Acute Stroke Rehabilitation," *IEEE*

Transactions on Neural Systems and Rehabilitation Engineering, vol. 25, no. 6, pp. 589-596, Jun 2017, doi: 10.1109/TNSRE.2016.2584003.

[216] D. SANZ-MERODIO, J. SANCHO, M. PÉREZ, and E. GARCÍA, "Control architecture of the ATLAS 2020 lower-limb active orthosis," in *Advances in Cooperative Robotics*: World Scientific, 2017, pp. 860-868.

[217] D. SANZ-MERODIO, M. PEREZ, M. PRIETO, J. SANCHO, and E. GARCIA, "RESULT OF CLINICAL TRIALS WITH CHILDREN WITH SPINAL MUSCULAR ATROPHY USING THE ATLAS 2020 LOWER-LIMB ACTIVE ORTHOSIS," 2017: World Scientific, 2017.

[218] D. Sanz-Merodio, G. Puyuelo, A. Ganguly, E. Garces, A. Goñi, and E. Garcia, "EXOtrainer Project Clinical Evaluation of Gait Training with Exoskeleton in Children with Spinal Muscular Atrophy," in *Advances in Robotics Research: From Lab to Market*: Springer, 2020, pp. 211-227.

[219] Z. F. Lerner, D. L. Damiano, H. S. Park, A. J. Gravunder, and T. C. Bulea, "A Robotic Exoskeleton for Treatment of Crouch Gait in Children With Cerebral Palsy: Design and Initial Application," *IEEE Transactions on Neural Systems and Rehabilitation Engineering,* vol. 25, no. 6, pp. 650-659, Jun 2017, doi: 10.1109/TNSRE.2016.2595501.

[220] M. Medina-De-La-Cruz, A. Mujaico-Mariano, and G. Tirado-Mendoza, "Implementation of a mechanical-electronic system for children from 7 to 11 years old with Duchenne muscular dystrophy," in *2018 IEEE XXV International Conference on Electronics, Electrical Engineering and Computing (INTERCON)*, 2018: IEEE, pp. 1-4.

[221] M. A. H. M. Adib *et al.*, "Restoration of Kids Leg Function Using Exoskeleton Robotic Leg (ExRoLEG) Device," in *Proceedings of the 10th National Technical Seminar on Underwater System Technology 2018*, 2019: Springer, pp. 335-342.

[222] C. A. Laubscher, R. J. Farris, and J. T. Sawicki, "Design and preliminary evaluation of a powered pediatric lower limb orthosis," in *ASME 2017 International Design Engineering Technical Conferences and Computers and Information in Engineering Conference*, 2017: American Society of Mechanical Engineers Digital Collection.

[223] R. M. Andrade, S. Sapienza, and P. Bonato, "Development of a “transparent operation mode” for a lower-limb exoskeleton designed for children with cerebral palsy," in *2019 IEEE 16th International Conference on Rehabilitation Robotics (ICORR)*, 2019: IEEE, pp. 512-517.

[224] M. Jansen, I. J. de Groot, N. van Alfen, and A. C. Geurts, "Physical training in boys with Duchenne Muscular Dystrophy: the protocol of the No Use is Disuse study," *BMC Pediatrics,* vol. 10, no. 1, p. 55, 2010.

[225] M. Wu and J. M. Landry, "Toward Flexible Assistance for Locomotor Training: Design and Clinical Testing of a Cable-Driven Robot for Stroke, Spinal Cord Injury, and Cerebral Palsy," in *Neurorehabilitation Technology*: Springer, 2016, pp. 435-459.

[226] H. I. Krebs, K. P. Michmizos, L. Monterosso, and J. Mast, "Pediatric anklebot: pilot clinical trial," in *2016 6th IEEE International Conference on Biomedical Robotics and Biomechatronics (BioRob)*, 2016: IEEE, pp. 662-666.

[227] G. M. Gasparri, M. O. Bair, R. P. Libby, and Z. F. Lerner, "Verification of a robotic ankle exoskeleton control scheme for gait assistance in individuals with cerebral palsy," in *2018 IEEE/RSJ International Conference on Intelligent Robots and Systems (IROS)*, 2018: IEEE, pp. 4673-4678.

[228] H. Xiong and X. Diao, "A review of cable-driven rehabilitation devices," *Disability and Rehabilitation: Assistive Technology,* vol. 15, no. 8, pp. 885-897, Nov 2020, doi: 10.1080/17483107.2019.1629110.

[229] M. Cestari, D. Sanz-Merodio, and E. Garcia, "A New and Versatile Adjustable Rigidity Actuator with Add-on Locking Mechanism (ARES-XL)," *Actuators,* vol. 7, no. 1, p. 1, 2018, doi: 10.3390/act7010001.

[230] D. Sanz-Merodio, M. Cestari, J. C. Arevalo, and E. Garcia, "A lower-limb exoskeleton for gait assistance in quadriplegia," in *2012 IEEE International Conference on Robotics and Biomimetics (ROBIO)*, 2012, pp. 122-127, doi: 10.1109/robio.2012.6490954.

[231] S. M. Mirvakili and I. W. Hunter, "Artificial Muscles: Mechanisms, Applications, and Challenges," *Advance Materials,* vol. 30, no. 6, p. 1704407, Feb 2018, doi: https://doi.org/10.1002/adma.201704407.
[232] J. Wirekoh, L. Valle, N. Pol, and Y. L. Park, "Sensorized, Flat, Pneumatic Artificial Muscle Embedded with Biomimetic Microfluidic Sensors for Proprioceptive Feedback," *Soft Robot,* vol. 6, no. 6, pp. 768-777, Dec 2019, doi: 10.1089/soro.2018.0110.
[233] B. Ugurlu, P. Forni, C. Doppmann, E. Sariyildiz, and J. Morimoto, "Stable Control of Force, Position, and Stiffness for Robot Joints Powered via Pneumatic Muscles," *IEEE Transactions on Industrial Informatics,* vol. 15, no. 12, pp. 6270-6279, 2019, doi: 10.1109/tii.2019.2916228.
[234] Y. N. Wu, M. Hwang, Y. Ren, D. Gaebler-Spira, and L. Q. Zhang, "Combined passive stretching and active movement rehabilitation of lower-limb impairments in children with cerebral palsy using a portable robot," *Neurorehabilitation and Neural Repair,* vol. 25, no. 4, pp. 378-85, May 2011, doi: 10.1177/1545968310388666.
[235] A. M. Kuczynski *et al.*, "Sensory tractography and robot-quantified proprioception in hemiparetic children with perinatal stroke," *Human Brain Mapping,* vol. 38, no. 5, pp. 2424-2440, May 2017, doi: 10.1002/hbm.23530.
[236] Y. Cherni, G. Girardin-Vignola, L. Ballaz, and M. Begon, "Reliability of maximum isometric hip and knee torque measurements in children with cerebral palsy using a paediatric exoskeleton–Lokomat," *Neurophysiologie Clinique,* vol. 49, no. 4, pp. 335-342, 2019.
[237] B. C. Conner, J. Luque, and Z. F. Lerner, "Adaptive Ankle Resistance from a Wearable Robotic Device to Improve Muscle Recruitment in Cerebral Palsy," *Annals of Biomedical Engineering,* vol. 48, no. 4, pp. 1309-1321, Jan 16 2020, doi: 10.1007/s10439-020-02454-8.
[238] Q. Qiu, S. Adamovich, S. Saleh, I. Lafond, A. S. Merians, and G. G. Fluet, "A comparison of motor adaptations to robotically facilitated upper extremity task practice demonstrated by children with cerebral palsy and adults with stroke," in *2011 IEEE International Conference on Rehabilitation Robotics*, 2011: IEEE, pp. 1-5.
[239] K. Nizamis *et al.*, "Transferrable Expertise From Bionic Arms to Robotic Exoskeletons: Perspectives for Stroke and Duchenne Muscular Dystrophy," *IEEE Transactions on Medical Robotics and Bionics,* vol. 1, no. 2, pp. 88-96, 2019, doi: 10.1109/tmrb.2019.2912453.
[240] M. Chandrasiri, R. Ranaweera, and R. Gopura, "Development of a surface muscle pressure monitoring system for wearable robotic devices," in *2019 Moratuwa engineering research conference (MERCon)*, 2019: IEEE, pp. 544-549.
[241] J. Taborri, S. Rossi, E. Palermo, and P. Cappa, "A HMM distributed classifier to control robotic knee module of an active orthosis," in *2015 IEEE International Conference on Rehabilitation Robotics (ICORR)*, 2015: IEEE, pp. 277-282.
[242] T. C. Bulea, Z. F. Lerner, and D. L. Damiano, "Repeatability of EMG activity during exoskeleton assisted walking in children with cerebral palsy: implications for real time adaptable control," in *2018 40th Annual International Conference of the IEEE Engineering in Medicine and Biology Society (EMBC)*, 2018: IEEE, pp. 2801-2804.
[243] F. Digiacomo *et al.*, "Improvement of motor performance in children with cerebral palsy treated with exoskeleton robotic training: A retrospective explorative analysis," *Restorative Neurology and Neuroscience,* vol. 37, no. 3, pp. 239-244, 2019, doi: 10.3233/RNN-180897.
[244] C. Bayon *et al.*, "A robot-based gait training therapy for pediatric population with cerebral palsy: goal setting, proposal and preliminary clinical implementation," *Journal of NeuroEngineering and Rehabilitation,* vol. 15, no. 1, p. 69, Jul 27 2018, doi: 10.1186/s12984-018-0412-9.
[245] G. C. Burdea, D. Cioi, A. Kale, W. E. Janes, S. A. Ross, and J. R. Engsberg, "Robotics and gaming to improve ankle strength, motor control, and function in children with

cerebral palsy--a case study series," *IEEE Transactions on Neural Systems and Rehabilitation Engineering,* vol. 21, no. 2, pp. 165-73, Mar 2013, doi: 10.1109/TNSRE.2012.2206055.

[246] M. Druzbicki *et al.*, "Functional effects of robotic-assisted locomotor treadmill thearapy in children with cerebral palsy," *Journal of Rehabilitation Medicine,* vol. 45, no. 4, pp. 358-63, Apr 2013, doi: 10.2340/16501977-1114.

[247] M. Gilliaux *et al.*, "Upper limb robot-assisted therapy in cerebral palsy: a single-blind randomized controlled trial," *Neurorehabilitation and Neural Repair,* vol. 29, no. 2, pp. 183-92, Feb 2015, doi: 10.1177/1545968314541172.

[248] S. E. Fasoli, M. Fragala-Pinkham, R. Hughes, H. I. Krebs, N. Hogan, and J. Stein, "Robotic therapy and botulinum toxin type A: a novel intervention approach for cerebral palsy," *American journal of physical medicine & rehabilitation,* vol. 87, no. 12, pp. 1022-1026, 2008.

[249] E. Beretta, E. Molteni, E. Biffi, R. Morganti, P. Avantaggiato, and S. Strazzer, "Robotically-driven orthoses exert proximal-to-distal differential recovery on the lower limbs in children with hemiplegia, early after acquired brain injury," *European Journal of Paediatric Neurology,* vol. 22, no. 4, pp. 652-661, Jul 2018, doi: 10.1016/j.ejpn.2018.03.002.

[250] F. Marini *et al.*, "Adaptive wrist robot training in pediatric rehabilitation," in *2015 IEEE International Conference on Rehabilitation Robotics (ICORR)*, 2015: IEEE, pp. 175-180.

[251] E. Molteni, E. Beretta, D. Altomonte, F. Formica, and S. Strazzer, "Combined robotic-aided gait training and 3D gait analysis provide objective treatment and assessment of gait in children and adolescents with Acquired Hemiplegia," in *2015 37th Annual International Conference of the IEEE Engineering in Medicine and Biology Society (EMBC)*, 2015: IEEE, pp. 4566-4569.

[252] E. Beretta, M. Romei, E. Molteni, P. Avantaggiato, and S. Strazzer, "Combined robotic-aided gait training and physical therapy improve functional abilities and hip kinematics during gait in children and adolescents with acquired brain injury," *Brain Injury,* vol. 29, no. 7-8, pp. 955-62, 2015, doi: 10.3109/02699052.2015.1005130.

[253] A. Ganguly, D. Sanz-Merodio, G. Puyuelo, A. Goñi, E. Garces, and E. Garcia, "Wearable pediatric gait exoskeleton-a feasibility study," in *2018 IEEE/RSJ International Conference on Intelligent Robots and Systems (IROS)*, 2018: IEEE, pp. 4667-4672.

[254] E. Garcia, J. Sancho, D. Sanz-Merodio, and M. Prieto, "Atlas 2020: The pediatric gait exoskeleton project," in *Human-centric Robotics-Proceedings Of The 20th International Conference Clawar 2017*, 2017: World Scientific, p. 29.

[255] T. G. Hornby, D. H. Zemon, and D. Campbell, "Robotic-assisted, body-weight–supported treadmill training in individuals following motor incomplete spinal cord injury," *Physical Therapy,* vol. 85, no. 1, pp. 52-66, 2005.

[256] B. D. Chaparro-Rico, D. Cafolla, M. Ceccarelli, and E. Castillo-Castaneda, "NURSE-2 DoF Device for Arm Motion Guidance: Kinematic, Dynamic, and FEM Analysis," *Applied Sciences,* vol. 10, no. 6, p. 2139, 2020.

[257] A. Kapeller, M. H. Nagenborg, and K. Nizamis, "Wearable robotic exoskeletons: A socio-philosophical perspective on Duchenne muscular dystrophy research," *Paladyn, Journal of Behavioral Robotics,* vol. 11, no. 1, pp. 404-413, 2020.

[258] H. Zhu, J. Doan, C. Stence, G. Lv, T. Elery, and R. Gregg, "Design and validation of a torque dense, highly backdrivable powered knee-ankle orthosis," in *2017 IEEE International Conference on Robotics and Automation (ICRA)*, 2017: IEEE, pp. 504-510.

[259] C. Krishnan, R. Ranganathan, Y. Y. Dhaher, and W. Z. Rymer, "A pilot study on the feasibility of robot-aided leg motor training to facilitate active participation," *PloS one,* vol. 8, no. 10, p. e77370, 2013.

[260] H. L. Heung, Z. Q. Tang, X. Q. Shi, K. Y. Tong, and Z. Li, "Soft rehabilitation actuator with integrated post-stroke finger spasticity evaluation," *Frontiers in bioengineering and biotechnology,* vol. 8, p. 111, 2020.

[261] H. D. Yang, M. Cooper, T. Akbas, L. Schumm, D. Orzel, and C. J. Walsh, "A Soft Inflatable Wearable Robot for Hip Abductor Assistance: Design and Preliminary Assessment," in *2020 8th IEEE RAS/EMBS International Conference for Biomedical Robotics and Biomechatronics (BioRob)*: IEEE, pp. 692-699.

[262] D. Copaci, F. Martín, L. Moreno, and D. Blanco, "SMA based elbow exoskeleton for rehabilitation therapy and patient evaluation," *IEEE Access,* vol. 7, pp. 31473-31484, 2019.

[263] A. Behboodi, C. DeSantis, J. Lubsen, and S. Lee, "A Mechanized Pediatric Elbow Joint Powered by a De-Based Artificial Skeletal Muscle," in *2020 42nd Annual International Conference of the IEEE Engineering in Medicine & Biology Society (EMBC)*, 2020: IEEE, pp. 4930-4935.

[264] T. Aurich-Schuler, F. Grob, H. J. A. van Hedel, and R. Labruyere, "Can Lokomat therapy with children and adolescents be improved? An adaptive clinical pilot trial comparing Guidance force, Path control, and FreeD," *Journal of NeuroEngineering and Rehabilitation,* vol. 14, no. 1, p. 76, Jul 14 2017, doi: 10.1186/s12984-017-0287-1.

[265] T. Aurich-Schuler and R. Labruyère, "An Increase in Kinematic Freedom in the Lokomat Is Related to the Ability to Elicit a Physiological Muscle Activity Pattern: A Secondary Data Analysis Investigating Differences Between Guidance Force, Path Control, and FreeD," *Frontiers in Robotics and AI,* vol. 6, p. 109, 2019, doi: 10.3389/frobt.2019.00109.

[266] M. Wu, J. Kim, D. J. Gaebler-Spira, B. D. Schmit, and P. Arora, "Robotic resistance treadmill training improves locomotor function in children with cerebral palsy: a randomized controlled pilot study," *Archives of physical medicine and rehabilitation,* vol. 98, no. 11, pp. 2126-2133, 2017.

[267] A. Elias, A. Frizera, T. F. Bastos, and C. Valadão, "Robotic walkers from a clinical point of view: Feature-based classification and proposal of the UFES Walker," in *2012 ISSNIP Biosignals and Biorobotics Conference: Biosignals and Robotics for Better and Safer Living (BRC)*, 2012: IEEE, pp. 1-5.

[268] T. Aurich-Schuler *et al.*, "Practical Recommendations for Robot-Assisted Treadmill Therapy (Lokomat) in Children with Cerebral Palsy: Indications, Goal Setting, and Clinical Implementation within the WHO-ICF Framework," *Neuropediatrics,* vol. 46, no. 4, pp. 248-60, Aug 2015, doi: 10.1055/s-0035-1550150.

[269] M. Rinaldi *et al.*, "EMG-based Indicators of Muscular Co-Activation during Gait in Children with Duchenne Muscular Dystrophy," in *2019 41st Annual International Conference of the IEEE Engineering in Medicine and Biology Society (EMBC)*, 2019: IEEE, pp. 3845-3848.

[270] N. Larina, M. Nacharova, L. Korsunskaya, S. Vlasenko, and V. Pavlenko, "CHANGES IN EEG PATTERNS IN THE α-FREQUENCY BAND FOLLOWING BCI-BASED THERAPY IN CHILDREN WITH CEREBRAL PALSY," *Bulletin of Russian State Medical University,* no. 4, pp. 41-46, 2020, doi: 10.24075/brsmu.2020.043.

[271] L. N. A. Struijk, B. Bentsen, M. Gaihede, and E. R. Lontis, "Error-free text typing performance of an inductive intra-oral tongue computer interface for severely disabled individuals," *IEEE Transactions on Neural Systems and Rehabilitation Engineering,* vol. 25, no. 11, pp. 2094-2104, 2017.

[272] D. Johansen, D. B. Popovic, S. Dosen, and L. N. A. Struijk, "Hybrid Tongue-Myoelectric Control Improves Functional Use of a Robotic Hand Prosthesis," *IEEE Transactions on Biomedical Engineering,* vol. 68, no. 6, pp. 2011-2020, 2021, doi: 10.1109/TBME.2021.3052065.

[273] A. Gonzalez-Vazquez, L. Garcia, J. Kilby, and P. McNair, "Soft Wearable Rehabilitation Robots with Artificial Muscles based on Smart Materials: A Review," *Advanced Intelligent Systems,* p. 2200159, 2023.

[274] D. J. Reinkensmeyer, "JNER at 15 years: analysis of the state of neuroengineering and rehabilitation," *J Neuroeng Rehabil,* vol. 16, no. 1, p. 144, Oct 30 2019, doi: 10.1186/s12984-019-0610-0.
[275] A. Zoss, H. Kazerooni, and A. Chu, "On the mechanical design of the Berkeley Lower Extremity Exoskeleton (BLEEX)," in *2005 IEEE/RSJ international conference on intelligent robots and systems*, 2005: IEEE, pp. 3465-3472.
[276] J. Howard, V. V. Murashov, B. D. Lowe, and M. L. Lu, "Industrial exoskeletons: Need for intervention effectiveness research," *American journal of industrial medicine,* vol. 63, no. 3, pp. 201-208, 2020.
[277] M. Kuroda *et al.*, "Robot-assisted gait training using a very small-sized Hybrid Assistive Limb® for pediatric cerebral palsy: A case report," *Brain and Development,* 2020.
[278] R. Lee, "The demographic transition: three centuries of fundamental change," *Journal of economic perspectives,* vol. 17, no. 4, pp. 167-190, 2003.
[279] W. H. Organization, "The global burden of disease: 2004 update," 2008.
[280] R. S. Araujo, C. R. Silva, S. P. Netto, E. Morya, and F. L. Brasil, "Development of a Low-Cost EEG-Controlled Hand Exoskeleton 3D Printed on Textiles," *Frontiers in Neuroscience,* vol. 15, 2021.
[281] E. Bardi, M. Gandolla, F. Braghin, F. Resta, A. L. Pedrocchi, and E. Ambrosini, "Upper limb soft robotic wearable devices: a systematic review," *Journal of NeuroEngineering and Rehabilitation,* vol. 19, no. 1, pp. 1-17, 2022.
[282] A. Aliseichik *et al.*, "Artificial Muscles," *Journal of Computer and Systems Sciences International,* vol. 61, no. 2, pp. 270-293, 2022.
[283] M. Nematollahi, K. S. Baghbaderani, A. Amerinatanzi, H. Zamanian, and M. Elahinia, "Application of NiTi in Assistive and Rehabilitation Devices: A Review," *Bioengineering (Basel),* vol. 6, no. 2, Apr 29 2019, doi: 10.3390/bioengineering6020037.
[284] T.-y. Dong, X.-l. Zhang, and T. Liu, "Artificial muscles for wearable assistance and rehabilitation," *Frontiers of Information Technology & Electronic Engineering,* vol. 19, no. 11, pp. 1303-1315, 2018, doi: 10.1631/fitee.1800618.
[285] K. L. Mudie *et al.*, "Consensus paper on testing and evaluation of military exoskeletons for the dismounted combatant," *Journal of science and medicine in sport,* vol. 21, no. 11, pp. 1154-1161, 2018.
[286] M. Cenciarini and A. M. Dollar, "Biomechanical considerations in the design of lower limb exoskeletons," in *2011 IEEE International conference on rehabilitation robotics*, 2011: IEEE, pp. 1-6.
[287] D. H. Gates, L. S. Walters, J. Cowley, J. M. Wilken, and L. Resnik, "Range of motion requirements for upper-limb activities of daily living," *American Journal of Occupational Therapy,* vol. 70, no. 1, pp. 7001350010p1-7001350010p10, 2016.
[288] H. Tanaka, M. Yoshikawa, E. Oyama, Y. Wakita, and Y. Matsumoto, "Development of assistive robots using international classification of functioning, disability, and health: concept, applications, and issues," *Journal of Robotics,* vol. 2013, p. 12, 2013.
[289] H. S. Nam, H. G. Seo, J.-H. Leigh, Y. J. Kim, S. Kim, and M. S. Bang, "External Robotic Arm vs. Upper Limb Exoskeleton: What Do Potential Users Need?," *Applied Sciences,* vol. 9, no. 12, p. 2471, 2019.
[290] H. I. Krebs *et al.*, "Robot-aided neurorehabilitation: a robot for wrist rehabilitation," *IEEE transactions on neural systems and rehabilitation engineering,* vol. 15, no. 3, pp. 327-335, 2007.
[291] J. Rosen, J. C. Perry, N. Manning, S. Burns, and B. Hannaford, "The human arm kinematics and dynamics during daily activities-toward a 7 DOF upper limb powered exoskeleton," in *ICAR'05. Proceedings., 12th International Conference on Advanced Robotics, 2005.*, Seattle, WA, USA, 2005: IEEE, pp. 532-539.
[292] R. Vicario *et al.*, "Benchmarking Force Control Algorithms," in *The 14th PErvasive Technologies Related to Assistive Environments Conference*, Corfu, Greece, 2021, pp. 359-364.

[293] D. M. Wolpert, "Computational approaches to motor control," *Trends in cognitive sciences,* vol. 1, no. 6, pp. 209-216, 1997.
[294] Y. Li and M. Hashimoto, "PVC gel soft actuator-based wearable assist wear for hip joint support during walking," *Smart Materials and Structures,* vol. 26, no. 12, p. 125003, 2017.
[295] C. J. Nycz, T. Bützer, O. Lambercy, J. Arata, G. S. Fischer, and R. Gassert, "Design and characterization of a lightweight and fully portable remote actuation system for use with a hand exoskeleton," *IEEE Robotics and Automation Letters,* vol. 1, no. 2, pp. 976-983, 2016.
[296] R. C. Browning, J. R. Modica, R. Kram, and A. Goswami, "The effects of adding mass to the legs on the energetics and biomechanics of walking," *Medicine & Science in Sports & Exercise,* vol. 39, no. 3, pp. 515-525, 2007.
[297] P. Dehail, D. Gagnon, L. Noreau, and S. Nadeau, "Assessment of agonist–antagonist shoulder torque ratios in individuals with paraplegia: a new interpretative approach," *Spinal Cord,* vol. 46, no. 8, pp. 552-558, 2008.
[298] M. R. Gross, *Anatomical Kinesiology*. Jones & Bartlett Learning, 2020.
[299] H. Shaaban, C. Pereira, R. Williams, and V. Lees, "The effect of elbow position on the range of supination and pronation of the forearm," *Journal of Hand Surgery (European Volume),* vol. 33, no. 1, pp. 3-8, 2008.
[300] J. Jeong *et al.*, "Soft Wearable Robot With Shape Memory Alloy (SMA)-Based Artificial Muscle for Assisting With Elbow Flexion and Forearm Supination/Pronation," *IEEE Robotics and Automation Letters,* vol. 7, no. 3, pp. 6028-6035, 2022.
[301] S. J. Park, K. Choi, H. Rodrigue, and C. H. Park, "Fabric muscle with a cooling acceleration structure for upper limb assistance soft exosuits," *Scientific reports,* vol. 12, no. 1, pp. 1-13, 2022.
[302] K. A. Mann, F. W. Wernere, and A. K. Palmer, "Frequency spectrum analysis of wrist motion for activities of daily living," *Journal of Orthopaedic research,* vol. 7, no. 2, pp. 304-306, 1989.
[303] D. Serrano, D. S. Copaci, L. Moreno, and D. Blanco, "SMA based wrist exoskeleton for rehabilitation therapy," in *2018 IEEE/RSJ International Conference on Intelligent Robots and Systems (IROS)*, 2018: IEEE, pp. 2318-2323.
[304] J. Jeong, I. B. Yasir, J. Han, C. H. Park, S.-K. Bok, and K.-U. Kyung, "Design of Shape Memory Alloy-Based Soft Wearable Robot for Assisting Wrist Motion," *Applied Sciences,* vol. 9, no. 19, p. 4025, 2019.
[305] A. P. Tjahyono, K. C. Aw, H. Devaraj, W. Surendra, E. Haemmerle, and J. Travas-Sejdic, "A five-fingered hand exoskeleton driven by pneumatic artificial muscles with novel polypyrrole sensors," *Industrial Robot: An International Journal,* 2013.
[306] N. Smaby, M. E. Johanson, B. Baker, D. E. Kenney, W. M. Murray, and V. R. Hentz, "Identification of key pinch forces required to complete functional tasks," *Journal of Rehabilitation Research & Development,* vol. 41, no. 2, 2004.
[307] F. Carpi, A. Mannini, and D. De Rossi, *Elastomeric contractile actuators for hand rehabilitation splints* (SPIE Smart Structures and Materials + Nondestructive Evaluation and Health Monitoring). International Society for Optics and Photonics, 2008, p. 692705.
[308] L. E. Diamond, T. V. Wrigley, K. L. Bennell, R. S. Hinman, J. O'Donnell, and P. W. Hodges, "Hip joint biomechanics during gait in people with and without symptomatic femoroacetabular impingement," *Gait & posture,* vol. 43, pp. 198-203, 2016.
[309] N. B. Reese and W. D. Bandy, *Joint range of motion and muscle length testing-E-book*. Elsevier Health Sciences, 2016.
[310] T. B. Palmer, N. D. Jenkins, and J. T. Cramer, "Reliability of manual versus automated techniques for assessing passive stiffness of the posterior muscles of the hip and thigh," *Journal of sports sciences,* vol. 31, no. 8, pp. 867-877, 2013.

[311] B. F. Mentiplay, M. Banky, R. A. Clark, M. B. Kahn, and G. Williams, "Lower limb angular velocity during walking at various speeds," *Gait & posture,* vol. 65, pp. 190-196, 2018.
[312] S. R. Freitas, J. R. Vaz, P. M. Bruno, M. J. Valamatos, and P. Mil-Homens, "Comparison of different passive knee extension torque-angle assessments," *Physiological measurement,* vol. 34, no. 11, p. 1483, 2013.
[313] L. Stirling *et al.*, "Applicability of Shape Memory Alloy Wire for an Active, Soft Orthotic," *Journal of Materials Engineering and Performance,* vol. 20, no. 4-5, pp. 658-662, 2011, doi: 10.1007/s11665-011-9858-7.
[314] S. Pittaccio *et al.*, "SHADE: A Shape-Memory-Activated Device Promoting Ankle Dorsiflexion," *Journal of Materials Engineering and Performance,* vol. 18, no. 5-6, pp. 824-830, 2009, doi: 10.1007/s11665-009-9405-y.
[315] S. Pittaccio, S. Viscuso, E. Beretta, A. C. Turconi, and S. Strazzer, "Pilot studies suggesting new applications of NiTi in dynamic orthoses for the ankle joint," *Prosthet Orthot Int,* vol. 34, no. 3, pp. 305-18, Sep 2010, doi: 10.3109/03093641003702253.
[316] J. Zhang, Y. Yin, and J. Zhu, "Sigmoid-based hysteresis modeling and high-speed tracking control of SMA-artificial muscle," *Sensors and Actuators A: Physical,* vol. 201, pp. 264-273, 2013, doi: 10.1016/j.sna.2013.07.036.
[317] S. H. Koo, Y. B. Lee, C. Kim, G. Kim, G. Lee, and J. S. Koh, "Development of gait assistive clothing-typed soft wearable robot for elderly adults," (in English), *Int J Cloth Sci Tech,* Nov 24 2020, doi: 10.1108/Ijcst-04-2020-0052.
[318] C. Kim *et al.*, "Shape memory alloy actuator-embedded smart clothes for ankle assistance," *Smart Materials and Structures,* vol. 29, no. 5, p. 055003, 2020.
[319] J. G. Neely and R. G. Pomerantz, "Measurement of facial muscle strength in normal subjects," *The Laryngoscope,* vol. 112, no. 9, pp. 1562-1568, 2002.
[320] D. Jayatilake, A. Gruebler, and K. Suzuki, "An analysis of facial morphology for the robot assisted smile recovery," in *2008 4th International Conference on Information and Automation for Sustainability*, Colombo, Sri Lanka, 2008: IEEE, pp. 395-400.
[321] Y. Bar-Cohen and Y. Bar-Cohen, *Electroactive polymer (EAP) actuators as artificial muscles: reality, potential, and challenges*. SPIE press Bellingham, WA, 2004.
[322] A. Behboodi and S. Lee, "Benchmarking of a Commercially Available Stacked Dielectric Elastomer as an Alternative Actuator for Rehabilitation Robotic Exoskeletons," in *2019 IEEE 16th International Conference on Rehabilitation Robotics (ICORR)*, 2019: IEEE, pp. 499-505.
[323] Y. Li and M. Hashimoto, "PVC gel based artificial muscles: Characterizations and actuation modular constructions," *Sensors and Actuators A: Physical,* vol. 233, pp. 246-258, 2015.
[324] Y. Li, Y. Maeda, and M. Hashimoto, "Lightweight, soft variable stiffness gel spats for walking assistance," *International Journal of Advanced Robotic Systems,* vol. 12, no. 12, p. 175, 2015.
[325] M. Yamano, N. Ogawa, M. Hashimoto, M. Takasaki, and T. Hirai, "A contraction type soft actuator using poly vinyl chloride gel," in *2008 IEEE International Conference on Robotics and Biomimetics*, 2009: IEEE, pp. 745-750.
[326] Y. Li and M. Hashimoto, "A proposal of a light-weight walking assist wear using PVC gel artificial muscles," in *2015 IEEE International Conference on Robotics and Automation (ICRA)*, 2015: IEEE, pp. 2920-2925.
[327] Y. Li and M. Hashimoto, "Development of a lightweight walking assist wear using PVC gel artificial muscles," in *2016 6th IEEE International Conference on Biomedical Robotics and Biomechatronics (BioRob)*, 2016: IEEE, pp. 686-691.
[328] S. M. Mirvakili *et al.*, *Simple and strong: twisted silver painted nylon artificial muscle actuated by Joule heating* (SPIE Smart Structures and Materials + Nondestructive Evaluation and Health Monitoring). SPIE, 2014, p. 90560I.
[329] S. Y. Yang *et al.*, "Design and Control of Lightweight Bionic Arm Driven by Soft Twisted and Coiled Artificial Muscles," *Soft Robotics,* 2022.

[330] S. A. Horton and P. Dumond, "Consistent Manufacturing Device for Coiled Polymer Actuators," *IEEE/ASME Transactions on Mechatronics,* vol. 24, no. 5, pp. 2130-2138, 2019, doi: 10.1109/tmech.2019.2935181.
[331] Y. Almubarak, M. Schmutz, M. Perez, S. Shah, and Y. Tadesse, "Kraken: A wirelessly controlled octopus-like hybrid robot utilizing stepper motors and fishing line artificial muscle for grasping underwater," 2021.
[332] M. C. Yip and G. Niemeyer, "On the Control and Properties of Supercoiled Polymer Artificial Muscles," *IEEE Transactions on Robotics,* vol. 33, no. 3, pp. 689-699, 2017, doi: 10.1109/tro.2017.2664885.
[333] A. Simeonov *et al.*, "Bundled Super-Coiled Polymer Artificial Muscles: Design, Characterization, and Modeling," *IEEE Robotics and Automation Letters,* vol. 3, no. 3, pp. 1671-1678, 2018, doi: 10.1109/lra.2018.2801469.
[334] C. S. Haines and G. Niemeyer, "Closed-loop temperature control of nylon artificial muscles," in *2018 IEEE/RSJ International Conference on Intelligent Robots and Systems (IROS)*, 2018: IEEE, pp. 6980-6985.
[335] D. Copaci, E. Cano, L. Moreno, and D. Blanco, "New Design of a Soft Robotics Wearable Elbow Exoskeleton Based on Shape Memory Alloy Wire Actuators," *Appl Bionics Biomech,* vol. 2017, p. 1605101, 2017, doi: 10.1155/2017/1605101.
[336] Á. Villoslada *et al.*, "Position control of a shape memory alloy actuator using a four-term bilinear PID controller," *Sensors and Actuators A: Physical,* vol. 236, pp. 257-272, 2015.
[337] J.-s. Koh, "Design of shape memory alloy coil spring actuator for improving performance in cyclic actuation," *Materials,* vol. 11, no. 11, p. 2324, 2018.
[338] J. M. Jani, M. Leary, A. Subic, and M. A. Gibson, "A review of shape memory alloy research, applications and opportunities," *Materials & Design (1980-2015),* vol. 56, pp. 1078-1113, 2014.
[339] S. Pittaccio *et al.*, "Primary sensory and motor cortex activities during voluntary and passive ankle mobilization by the SHADE orthosis," *Human brain mapping,* vol. 32, no. 1, pp. 60-70, 2011.
[340] D. Copaci, D. Blanco, and L. Moreno, "Wearable elbow exoskeleton actuated with Shape Memory Alloy in antagonist movement," in *Proceedings of the Joint Workshop on Wearable Robotics and Assistive Devices, International Conference on Intelligent Robots and Systems (IROS 2016), Daejeon, Korea*, 2016, pp. 9-14.
[341] A. Villoslada, A. Flores, D. Copaci, D. Blanco, and L. Moreno, "High-displacement flexible shape memory alloy actuator for soft wearable robots," *Robotics and Autonomous Systems,* vol. 73, pp. 91-101, 2015.
[342] J. Jeong *et al.*, "Wrist Assisting Soft Wearable Robot with Stretchable Coolant Vessel integrated SMA Muscle," *IEEE/ASME Transactions on Mechatronics,* vol. 27, no. 2, pp. 1046-1058, 2021.
[343] S. J. Park and C. H. Park, "Suit-type wearable robot powered by shape-memory-alloy-based fabric muscle," *Scientific reports,* vol. 9, no. 1, pp. 1-8, 2019.
[344] A. Behboodi, J. F. Alesi, and S. C. Lee, "An artificial skeletal muscle for use in pediatric rehabilitation robotics," in *Soft Robotics in Rehabilitation*: Elsevier, 2021, pp. 241-258.
[345] A. Washington, J. Neubauer, and K. J. Kim, "Soft actuators and their potential applications in rehabilitative devices," in *Soft Robotics in Rehabilitation*: Elsevier, 2021, pp. 89-110.
[346] A. Firouzeh and J. Paik, "Soft actuation and sensing towards robot-assisted facial rehabilitation," in *2017 IEEE/RSJ International Conference on Intelligent Robots and Systems (IROS)*, 2017: IEEE, pp. 306-313.
[347] T. Mirfakhrai, J. D. W. Madden, and R. H. Baughman, "Polymer artificial muscles," *Materials Today,* vol. 10, no. 4, pp. 30-38, 2007, doi: 10.1016/s1369-7021(07)70048-2.

[348] W. MohdIsa, A. Hunt, and S. H. HosseinNia, "Sensing and Self-Sensing Actuation Methods for Ionic Polymer-Metal Composite (IPMC): A Review," *Sensors (Basel),* vol. 19, no. 18, Sep 14 2019, doi: 10.3390/s19183967.
[349] S. M. Mirvakili and I. W. Hunter, "Artificial Muscles: Mechanisms, Applications, and Challenges," *Adv Mater,* vol. 30, no. 6, Feb 2018, doi: 10.1002/adma.201704407.
[350] M. Hao, Y. Wang, Z. Zhu, Q. He, D. Zhu, and M. Luo, "A compact review of IPMC as soft actuator and sensor: current trends, challenges, and potential solutions from our recent work," *Frontiers in Robotics and AI,* vol. 6, p. 129, 2019.
[351] Q. He *et al.*, "The highly stable air-operating ionic polymer metal composite actuator with consecutive channels and its potential application in soft gripper," *Smart Materials and Structures,* vol. 29, no. 4, p. 045013, 2020.
[352] E. Acome *et al.*, "Hydraulically amplified self-healing electrostatic actuators with muscle-like performance," *Science,* vol. 359, no. 6371, pp. 61-65, 2018.
[353] S. K. Mitchell *et al.*, "An Easy-to-Implement Toolkit to Create Versatile and High-Performance HASEL Actuators for Untethered Soft Robots," *Advanced Science,* vol. 6, no. 14, p. 1900178, 2019.
[354] N. Kellaris *et al.*, "Spider-Inspired Electrohydraulic Actuators for Fast, Soft-Actuated Joints," *Advanced Science,* p. 2100916, 2021.
[355] Z. Yoder *et al.*, "Design of a High-Speed Prosthetic Finger Driven by Peano-HASEL Actuators," *Frontiers in Robotics and AI,* vol. 7, p. 181, 2020, doi: 10.3389/frobt.2020.586216.
[356] H. Meng and J. Hu, "A brief review of stimulus-active polymers responsive to thermal, light, magnetic, electric, and water/solvent stimuli," *Journal of Intelligent Material Systems and Structures,* vol. 21, no. 9, pp. 859-885, 2010.
[357] M. R. A. Bhatti, E. Bilotti, H. Zhang, C. W. Bastiaansen, and T. Peijs, "Photo-thermal actuation of ultra-drawn high-density polyethylene," *Polymer,* vol. 207, p. 122897, 2020.
[358] L. Sun *et al.*, "Stimulus-responsive shape memory materials: a review," *Materials & Design,* vol. 33, pp. 577-640, 2012.
[359] S.-H. Chen *et al.*, "Assistive control system for upper limb rehabilitation robot," *IEEE Transactions on Neural Systems and Rehabilitation Engineering,* vol. 24, no. 11, pp. 1199-1209, 2016.
[360] R. Michnik *et al.*, "Kinematic analysis of complex therapeutic movements of the upper limb," in *Information Technologies in Biomedicine*: Springer, 2008, pp. 551-558.
[361] S. J. Bae, S. H. Jang, J. P. Seo, and P. H. Chang, "The Optimal Speed for Cortical Activation of Passive Wrist Movements Performed by a Rehabilitation Robot: A Functional NIRS Study," (in English), *Frontiers in Human Neuroscience,* Original Research vol. 11, no. 194, 2017-April-20 2017, doi: 10.3389/fnhum.2017.00194.
[362] F. Karami, L. Wu, and Y. Tadesse, "Modeling of One-ply and Two-ply Twisted and Coiled Polymer (TCP) Artificial Muscles," *IEEE/ASME Transactions on Mechatronics,* vol. 26, no. 1, pp. 300-310, 2020.
[363] T. Tsabedze, C. Mullen, R. Coulter, S. Wade, and J. Zhang, "Helically wrapped supercoiled polymer (HW-SCP) artificial muscles: Design, characterization, and modeling," in *2020 IEEE International Conference on Robotics and Automation (ICRA)*, 2020: IEEE, pp. 5862-5868.
[364] B. P. Edmonds and A. L. Trejos, "Design of an Active Cooling System for Thermally Activated Soft Actuators," in *2019 IEEE 16th International Conference on Rehabilitation Robotics (ICORR)*, 2019: IEEE, pp. 368-373.
[365] K. Ly *et al.*, "Miniaturized circuitry for capacitive self-sensing and closed-loop control of soft electrostatic transducers," *Soft Robotics,* vol. 8, no. 6, pp. 637-686, 2020.
[366] D. Zhou, W. Zuo, X. Tang, J. Deng, and Y. Liu, "A multi-motion bionic soft hexapod robot driven by self-sensing controlled twisted artificial muscles," *Bioinspiration & Biomimetics,* vol. 16, no. 4, p. 045003, 2021.

[367] S. Wang, H. Huang, H. Huang, B. Li, and K. Huang, "A Lightweight Soft Gripper Driven by Self-Sensing Super-Coiled Polymer Actuator," *IEEE Robotics and Automation Letters,* vol. 6, no. 2, pp. 2775-2782, 2021.
[368] L. Ma *et al.*, "Achieving both high voltage and high capacity in aqueous zinc-ion battery for record high energy density," *Advanced Functional Materials,* vol. 29, no. 46, p. 1906142, 2019.
[369] B. Zhu, X. Wang, P. Yao, J. Li, and J. Zhu, "Towards high energy density lithium battery anodes: silicon and lithium," *Chemical science,* vol. 10, no. 30, pp. 7132-7148, 2019.
[370] M. Synodis, J. Pikul, S. A. B. Allen, and M. Allen, "Integrated Fabrication of Serially Connected High Voltage Microbatteries via Multilayer Electrodeposition," in *2019 20th International Conference on Solid-State Sensors, Actuators and Microsystems & Eurosensors XXXIII (TRANSDUCERS & EUROSENSORS XXXIII)*, Berlin, Germany, 2019: IEEE, pp. 789-792.
[371] B. He *et al.*, "High-performance flexible all-solid-state aqueous rechargeable Zn–MnO 2 microbatteries integrated with wearable pressure sensors," *Journal of Materials Chemistry A,* vol. 6, no. 30, pp. 14594-14601, 2018.
[372] Q. Liu *et al.*, "The First Flexible Dual-Ion Microbattery Demonstrates Superior Capacity and Ultrahigh Energy Density: Small and Powerful," *Advanced Functional Materials,* vol. 30, no. 38, p. 2002086, 2020.
[373] J. Lawrence and J. Bull, "Thermal conditions which cause skin burns," *Engineering in Medicine,* vol. 5, no. 3, pp. 61-63, 1976.
[374] J. Berzowska and M. Coelho, "Kukkia and vilkas: Kinetic electronic garments," in *Ninth IEEE International Symposium on Wearable Computers (ISWC'05)*, 2005: IEEE, pp. 82-85.
[375] A. Gonzalez, L. Garcia, J. Kilby, and H. Singh, "Artificial Muscles Performance Based on TCP-NiCr Actuators," in *2021 43rd Annual International Conference of the IEEE Engineering in Medicine & Biology Society (EMBC)*, 2021: IEEE, pp. 5156-5156.
[376] S. Liu, X. Tang, D. Zhou, and Y. Liu, "Fascicular module of nylon twisted actuators with large force and variable stiffness," (in English), *Sensors and Actuators A: Physical,* vol. 315, Nov 1 2020.
[377] J. B. Chossat, D. K. Y. Chen, Y. L. Park, and P. B. Shull, "Soft Wearable Skin-Stretch Device for Haptic Feedback using Twisted and Coiled Polymer Actuators," *IEEE Trans Haptics,* Sep 24 2019, doi: 10.1109/TOH.2019.2943154.
[378] X. Tang *et al.*, "Temperature self-sensing and closed-loop position control of twisted and coiled actuator," *Sensors and Actuators A: Physical,* vol. 285, pp. 319-328, 2019.
[379] L. Wu, M. Jung de Andrade, L. K. Saharan, R. S. Rome, R. H. Baughman, and Y. Tadesse, "Compact and low-cost humanoid hand powered by nylon artificial muscles," *Bioinspir Biomim,* vol. 12, no. 2, p. 026004, Feb 3 2017, doi: 10.1088/1748-3190/aa52f8.
[380] L. Saharan and Y. Tadesse, "Fabrication parameters and performance relationship of twisted and coiled polymer muscles," in *ASME 2016 International Mechanical Engineering Congress and Exposition*, 2016: American Society of Mechanical Engineers Digital Collection.
[381] L. Saharan and Y. Tadesse, "Novel twisted and coiled polymer artificial muscles for biomedical and robotics applications," pp. 45-75, 2019, doi: 10.1016/b978-0-12-816909-4.00003-8.
[382] A. Hamidi, Y. Almubarak, and Y. Tadesse, "Multidirectional 3D-printed functionally graded modular joint actuated by TCPFL muscles for soft robots," *Bio-Design and Manufacturing,* vol. 2, no. 4, pp. 256-268, 2019, doi: 10.1007/s42242-019-00055-6.
[383] X. Tang, K. Li, Y. Liu, D. Zhou, and J. Zhao, "A general soft robot module driven by twisted and coiled actuators," *Smart Materials and Structures,* vol. 28, no. 3, p. 035019, 2019.
[384] T. Arakawa, K. Takagi, K. Tahara, and K. Asaka, "Position control of fishing line artificial muscles (coiled polymer actuators) from nylon thread," in *Electroactive Polymer*

Actuators and Devices (EAPAD) 2016, 2016, vol. 9798: International Society for Optics and Photonics, p. 97982W.

[385] S. Liu, X. Tang, D. Zhou, and Y. Liu, "Fascicular module of nylon twisted actuators with large force and variable stiffness," *Sensors and Actuators A: Physical,* vol. 315, p. 112292, 2020.

[386] L. Wu, I. Chauhan, and Y. Tadesse, "A Novel Soft Actuator for the Musculoskeletal System," *Advanced Materials Technologies,* vol. 3, no. 5, p. 1700359, 2018, doi: 10.1002/admt.201700359.

[387] A. Gonzalez, L. Garcia, and J. Kilby, "Improved performance in temperature and speed of TCP artificial Muscles for Soft Wearables Robots by length modification," *Smart Materials and Structures,* 2023.

[388] M. Hiraoka *et al.*, "Power-efficient low-temperature woven coiled fibre actuator for wearable applications," *Sci Rep,* vol. 6, p. 36358, Nov 4 2016, doi: 10.1038/srep36358.

[389] B. P. Edmonds and A. L. Trejos, "Frequency Response Analysis of Actively Cooled Nylon Twisted Coiled Actuators for Use in Wrist Rehabilitation Devices," in *2020 8th IEEE RAS/EMBS International Conference for Biomedical Robotics and Biomechatronics (BioRob)*, 2020: IEEE, pp. 434-439.

[390] B. P. Edmonds, C. T. DeGroot, and A. L. Trejos, "Thermal modeling and characterization of twisted coiled actuators for upper limb wearable devices," *IEEE/ASME Transactions on Mechatronics,* vol. 26, no. 2, pp. 966-977, 2020.

[391] K. H. Cho *et al.*, "Fabrication and modeling of temperature-controllable artificial muscle actuator," in *2016 6th IEEE International Conference on Biomedical Robotics and Biomechatronics (BioRob)*, 2016: IEEE, pp. 94-98.

[392] J. Hope and A. McDaid, "Development of wearable wrist and forearm exoskeleton with shape memory alloy actuators," *Journal of Intelligent & Robotic Systems,* vol. 86, no. 3-4, p. 397, 2017.

[393] A. Gonzalez, L. Garcia, and J. Kilby, "Paediatric ankle rehabilitation system based on twisted and coiled polymer actuators," *Smart Materials and Structures,* 2024.

[394] D. Chen *et al.*, "Risk factors of cerebral palsy in children: a systematic review and meta-analysis," *Translational Pediatrics,* vol. 11, no. 4, p. 556, 2022.

[395] S. Abgottspon *et al.*, "Effect of age at pediatric stroke on long-term cognitive outcome," *Neurology,* vol. 98, no. 7, pp. e721-e729, 2022.

[396] J. L. Ryan *et al.*, "Gross motor change after inpatient rehabilitation for children with acquired brain injury: a 10-year retrospective review," *Developmental Medicine & Child Neurology,* vol. 65, no. 7, pp. 953-960, 2023.

[397] I. Vandekerckhove *et al.*, "Longitudinal Alterations in Gait Features in Growing Children With Duchenne Muscular Dystrophy," *Frontiers in Human Neuroscience,* vol. 16, p. 861136, 2022.

[398] F. E. Scheijmans *et al.*, "Population-based assessment of nusinersen efficacy in children with spinal muscular atrophy: a 3-year follow-up study," *Brain Communications,* vol. 4, no. 6, p. fcac269, 2022.

[399] Z. F. Lerner *et al.*, "An Untethered Ankle Exoskeleton Improves Walking Economy in a Pilot Study of Individuals With Cerebral Palsy," *IEEE Transactions on Neural Systems and Rehabilitation Engineering* vol. 26, no. 10, pp. 1985-1993, Oct 2018, doi: 10.1109/TNSRE.2018.2870756.

[400] M. Sarajchi, M. K. Al-Hares, and K. Sirlantzis, "Wearable lower-limb exoskeleton for children with cerebral palsy: A systematic review of mechanical design, actuation type, control strategy, and clinical evaluation," *IEEE Transactions on Neural Systems and Rehabilitation Engineering,* vol. 29, pp. 2695-2720, 2021.

[401] Q. Peng *et al.*, "Quantitative evaluations of ankle spasticity and stiffness in neurological disorders using manual spasticity evaluator," *Journal of rehabilitation research and development,* vol. 48, no. 4, p. 473, 2011.

[402] W. H. Organization. "Growth reference 5-19 years." https://www.who.int/growthref/en/ (accessed 2020).
[403] D. A. Winter, *Biomechanics and motor control of human movement*. John Wiley & Sons, 2009.
[404] K. Subasinghage, K. Gunawardane, N. Padmawansa, N. Kularatna, and M. Moradian, "Modern supercapacitors technologies and their applicability in mature electrical engineering applications," *Energies,* vol. 15, no. 20, p. 7752, 2022.
[405] C. Ngo *et al.*, "A Wearable, Multi-Frequency Device to Measure Muscle Activity Combining Simultaneous Electromyography and Electrical Impedance Myography," *Sensors,* vol. 22, no. 5, p. 1941, 2022.

Appendix A: Published Papers

Paper 1: A. Gonzalez, L. Garcia, J. Kilby, and P. McNair, "Robotic devices for paediatric rehabilitation: a review of design features," BioMedical Engineering OnLine, vol. 20, no. 1, pp. 1-33, 2021.

Paper 2: A. Gonzalez-Vazquez, L. Garcia, J. Kilby, and P. McNair, "Soft Wearable Rehabilitation Robots with Artificial Muscles based on Smart Materials: A Review," Advanced Intelligent Systems, p. 2200159, 2023.

Paper 3: A. Gonzalez, L. Garcia, J. Kilby, and H. Singh, "Artificial Muscles Performance Based on TCP-NiCr Actuators," in 2021 43rd Annual International Conference of the IEEE Engineering in Medicine & Biology Society (EMBC), 2021: IEEE, pp. 5156-5156.

Paper 4: A. Gonzalez, L. Garcia, and J. Kilby, "Improved performance in temperature and speed of TCP artificial Muscles for Soft Wearables Robots by length modification," Smart Materials and Structures, 2023.

Paper 5: A. Gonzalez, L. Garcia, and J. Kilby, "Paediatric ankle rehabilitation system based on twisted and coiled polymer actuators," Smart Materials and Structures, 2024.

Paper 1:

Gonzalez et al. BioMed Eng OnLine (2021) 20:89
https://doi.org/10.1186/s12938-021-00920-5

BioMedical Engineering OnLine

REVIEW Open Access

Robotic devices for paediatric rehabilitation: a review of design features

Alberto Gonzalez[1], Lorenzo Garcia[1*], Jeff Kilby[1] and Peter McNair[2]

*Correspondence: lorenzo.garcia@aut.ac.nz
[1] BioDesign Lab, School of Engineering, Computer and Mathematical Sciences, Auckland University of Technology, Auckland, New Zealand
Full list of author information is available at the end of the article

Abstract

Children with physical disabilities often have limited performance in daily activities, hindering their physical development, social development and mental health. Therefore, rehabilitation is essential to mitigate the adverse effects of the different causes of physical disabilities and improve independence and quality of life. In the last decade, robotic rehabilitation has shown the potential to augment traditional physical rehabilitation. However, to date, most robotic rehabilitation devices are designed for adult patients who differ in their needs compared to paediatric patients, limiting the devices' potential because the paediatric patients' needs are not adequately considered. With this in mind, the current work reviews the existing literature on robotic rehabilitation for children with physical disabilities, intending to summarise how the rehabilitation robots could fulfil children's needs and inspire researchers to develop new devices.
A literature search was conducted utilising the Web of Science, PubMed and Scopus databases. Based on the inclusion–exclusion criteria, 206 publications were included, and 58 robotic devices used by children with a physical disability were identified. Different design factors and the treated conditions using robotic technology were compared. Through the analyses, it was identified that weight, safety, operability and motivation were crucial factors to the successful design of devices for children. The majority of the current devices were used for lower limb rehabilitation. Neurological disorders, in particular cerebral palsy, were the most common conditions for which devices were designed. By far, the most common actuator was the electric motor. Usually, the devices present more than one training strategy being the assistive strategy the most used. The admittance/impedance method is the most popular to interface the robot with the children. Currently, there is a trend on developing exoskeletons, as they can assist children with daily life activities outside of the rehabilitation setting, propitiating a wider adoption of the technology. With this shift in focus, it appears likely that new technologies to actuate the system (e.g. serial elastic actuators) and to detect the intention (e.g. physiological signals) of children as they go about their daily activities will be required.

Keywords: Robotic, Exoskeletons, Rehabilitation, Assistance, Children, Physical disability

Introduction

Mobility and exploration are essential in children's development and contribute towards cognitive, physical, social and emotional development. However, children with physical disabilities present limitations when performing activities autonomously, which hinders their typical development [1]. Ongoing paediatric physical disability arose from many different causes, including neurological disorders like cerebral palsy (CP) [2], Stroke [3] and acquired brain injury (ABI) [4], neuromuscular diseases such as Duchenne muscular dystrophy (DMD) [5] and spinal muscular atrophy (SMA) [6], or traumatic injuries [7, 8] (Table 1).

Rehabilitation is essential to help the children recover or maintain functionality when interacting with their environment, improving the quality of life and autonomy [9, 10]. Furthermore, early access to rehabilitation is critical for children while they are in the stage of development. The gait pattern and motor abilities are still malleable [11], intending to reduce the probability of developing more severe levels of disability [12, 13].

The standard therapies to manage the musculoskeletal system's deterioration and improve and maintain physical ability include passive orthoses, surgery, and physiotherapy [15, 16]. Physiotherapists prescribe, monitor, and guide exercise, which can prevent an unnecessarily sedentary or immobile lifestyle. The most extensively investigated aspect of physiotherapy is the effect of direct interventions on upper or lower limbs. Such interventions often involve intensive stretching and strengthening exercises facilitated by the physiotherapist [2] to improve motor skills. These interventions are often highly labour intensive and can be challenging to perform [17]. Furthermore, the effectiveness of physiotherapy often depends on the experience of the physiotherapist. Thus, it is not easy to achieve optimal consistency and repeatability between rehabilitation sessions [18, 19].

There is a growing interest in robots that can support the patient, the family and the medical professional in a wide range of activities used for the care of people with physical disabilities, for example, companion robots [20, 21], monitoring robots [22] and surgery robots [23], all of them can be considered as healthcare robots.

Healthcare robots can be divided into three main categories, clinical robots, assistive robots and rehabilitation robots [24, 25]. Clinical robots are focus on supportive care and cure process (e.g. help in surgery and diagnosis) in clinical environments; assistive robots primary function is to provide assistive help either to carers or directly to patients either in a hospital or in a specialist care facility (e.g. patient lifting and to assist in routine services); rehabilitation robots are robots design towards restoring the functionality and mobility of people with physical disabilities, in that case, the recovery of

Table 1 Incidence or prevalence of conditions that cause physical disabilities in children

Condition	Incidence or prevalence
Cerebral palsy	Prevalence of 1 per 500 live births [2]
Stroke	Incidence of 1.2 to 13 per 100,000 children per year [3]
Traumatic brain injury	Incidence of 691 per 100,000 children [7]
Duchenne muscular dystrophy	Prevalence of 1 per 5000 live male births [14]
Spinal muscular atrophy	Prevalence of 7.8–10 per 100,000 live births [7]

mobility could be achieved by assisting the patient during ADLs (e.g. walking and grasping objects) [17, 26] or with physical training therapy [24, 27–30], and are the main focus of this study.

Rehabilitation therapy for the recovery of mobility based on robots has been proposed as a new procedure for children with physical disabilities [31]. This robot-assisted rehabilitation therapy consists of a mechatronic device that provides highly repetitive and task-specific guided movements autonomously [32, 33]. The use of robots in rehabilitation therapies bring advantages over traditional therapies, as they allow extensive practice in children with substantial disabilities, reduced effort required of therapists during the exercises, and provide a quantitative assessment of the patient's motor function (e.g. quantitative feedback of range of motion (ROM) and strength with each repetition) [34–38].

Rehabilitation robots are often classified by their mechanical structure and are generally divided into end-effectors and exoskeletons [28, 39]. End-effector devices work by applying forces to the distal segments of limbs, creating what is termed a "mechanical chain" that prompts movements of other parts of the limb generating a pattern of specific activity across different joints. If utilised on a single segment and joint, their simple structure makes it easier to adapt them to many patients and needs less complicated control algorithms. However, it is difficult to isolate specific joints since they produce complex movements that involve the whole limb [40].

Contrarily, robotic exoskeletons could be termed "wearable machines" that mirror the patient's skeletal structure; therefore, they only move the joint of the limb where the exoskeleton is worn. This approach allows for independent and concurrent control of specific segments of the limb. However, it is essential to adjust the length of sections of the robot to the lengths of the segments of the patient limb. Moreover, when the joint is in motion, the position of the centre of rotation can change, creating discomfort in the user. Thus, increasing the number of degrees of freedom of the robot increases the control algorithm's complexity, weight, mechanical complexity, and power requirements, making it unattainable for home use [18, 41].

Apart from mechanical structure, robots possess essential elements to ensure the systems' reliability and robustness [42]. Actuators, training strategy and the Human–computer interface (HCI) are among these essential elements. The actuators play a crucial role because they determine the torque and movement provided by the robot and influence the total weight and compliance of the system [29, 43]. The training strategy and the HCI are an integral part of the robot-assisted rehabilitation since it determines how the patient interacts with the robot and the type of assistance that the robot can provide. Many authors have analysed these last two characteristics as part of the robots control [28, 30, 44]. However, control also involves "low level" considerations that are more related to the internal communication of the components (sensors, structures, microcontrollers, actuators, etc.) at a hardware level rather than how the device interacts with the patient [45–49].

Although multiple devices for the robotic rehabilitation of upper and lower limbs have been developed, at least in a proof-of-concept phase [24, 39, 42, 44, 45, 50, 51], most presented robots were designed for adult users, impeding their use on the paediatric

population. For example, commercial exoskeletons are made for a subject 150 cm tall onwards [52], while the average height for a 5-year-old child will be around 110 cm [53].

However, to develop technology planned to be used on the paediatric population is not only a matter of reducing the size of the robots. But it should be tailored to their own capabilities and goals that differ from those of the adults. For instance, a simple downscaling of the robots is not enough as the normalised joint torques on adults are greater than those of a child [54, 55], making them potentially dangerous when used on small children. Additionally, in the case of children, as their cognitive abilities are still developing, it could be hard for them to fully understand how the technology works [52, 56]. Hence, it is hard to adapt a robot made for adults to be used by children since the robots do not fulfil the children's needs [26, 57].

Consequently, to address the children's needs adequately, it is essential to include them and other stakeholders (e.g. family members, clinicians, and health care providers) during the development process, providing feedback to identify possible issues of importance [1, 43]. Furthermore, it is essential to focus not only on addressing the impairment or limitation in users' functional abilities, but also on other fundamental needs, like accessibility and aesthetics [58], to avoid the user abandoning the rehabilitation device due to frustration [59].

Despite the progressive development of robotic rehabilitation devices, their application to the paediatric population is still scarce. Consequently, the key features to design an optimal robotic rehabilitation device that better enhance children's abilities with physical disabilities have not been well defined yet. Based on this framework, this review aims to address the following questions: (1) What are the design requirements for paediatric rehabilitation robots? (2) How does the current technology contribute to achieving the paediatric design requirements? And (3) How do the paediatric conditions impact the device design?

Methods

An in-depth literature search was performed to conduct the review, following the search strategy of the Preferred Reporting Items for Systematic Reviews and Meta-Analyses (PRISMA) guidelines [60].

A literature search was conducted to identify literature associated with the topic based on searches in PubMed, Scopus, and Web of Science, using the combination of the following keywords: (pediatric OR kid* OR child*) AND (aid OR assist* OR improve* OR augment* OR enhance* OR reinforce* OR therap* OR rehabilitation) AND (active ortho* OR exoskeleton* OR wearable robot* OR portable robot* OR robot* suit OR robot*) AND (movement OR motion OR walk* OR gait OR grasp* OR handl*). To make our search as complete as possible, a search through the university library databases was also conducted.

After the preliminary search, the following inclusion and exclusion criteria to narrow the literature search were used. The inclusion criteria were:

1) Studies involving robotic devices for robot-assisted rehabilitation therapy,
2) Studies involving robotic devices for assessment of patients with Physically disabilities,

3) Studies involving devices designed for children or utilised with a paediatric population (< 18 years old),
4) written in English,
5) full-text articles.

And the exclusion criteria were:

1) Studies that only present software solutions or simulations,
2) Studies involving passive devices (do not have actuators),
3) Studies involving postural change,
4) Studies involving only the adult population and
5) Studies involving robots that do not replace the movement itself (e.g. wheelchairs).

Findings

The outcome of this literature review is compiled in the following sections:

- An overview of the literature search,
- the paediatric robotic rehabilitation design requirements,
- an analysis of the type of robots used in paediatric robotic rehabilitation;
- the actuators to drive the robots;
- training strategy of the robots;
- the human–computer interface of the assistive systems, and
- the treated conditions in children with physical disabilities.

Literature search

Based on the keywords mentioned in the methods section, 1604 publications were found, with:

- 811 publications from Web of Science,
- 547 publications from PubMed,
- 241 from Scopus, and
- 5 from a search on the University library.

First, a check was made for duplicated publications. After this process, the abstracts of 1248 publications were screened, and 301 titles were selected for full-text reading. After carefully applying the inclusion–exclusion criteria to the full read papers, 206 publications were selected. Among the chosen publications, 10 were reviews, 42 only discussed a section of the design process of the rehabilitation robot, 138 presented a clinical application, and 16 included the design process plus a clinical application (Fig. 1 shows a flow diagram that illustrates the process of the selection of the papers).

The ten review articles examined a variety of rehabilitation robots for children with physical disabilities. They were focused on children with neurological problems (e.g. CP, ABI, and Stroke) or SCI and only investigated their use as part of physical therapy. In Fasoli et al. [35], Meyer et al. [61], and Bayon et al. [62], the robot

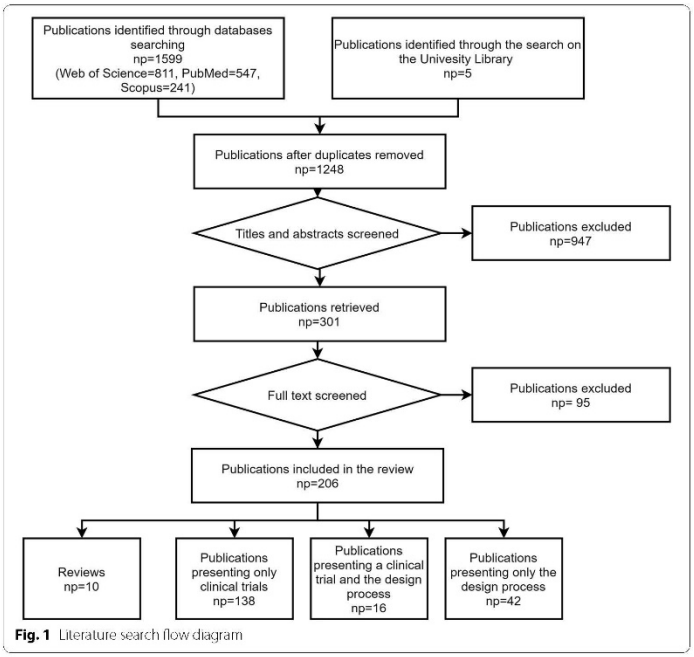

Fig. 1 Literature search flow diagram

assistive therapies for children with CP were examined. Vova et al. [63] reviewed the efficacy of functional electrical stimulation and exoskeletons in gait training to improve motor function and gait pattern in children with CP. Zwicker et al. [64] reviewed the efficiency of robot-assisted treadmill training compared to traditional treadmill training in children with CP. Chen et al. [65] examined the effectiveness of various devices for upper limb robotic therapy on children with CP. The effects of robotic gait training practices in individuals with CP were investigated in Carvalho et al. [31]. Falzarano et al. [10] and Mahamud et al. [66] investigated upper and lower limb rehabilitation devices for neurological diseases. Dannenberg et al. [67] compared different locomotor training, including robotic training, in children with SCI. Compared with the previous reviews, this work analyses a broader range of aspects of paediatric rehabilitation robots, focused on the design parameters to fulfil the paediatric needs and how the technology and different conditions affect the robot design.

Paediatric robotic rehabilitation design requirements

Fifteen different requirements were identified (Table 2). The requirements are based on those proposed by Batavia and Hammer for assistive devices [68] and expanded by proposed requirements for paediatric rehabilitation devices highlighted by Weightman et al.

Table 2 Paediatric rehabilitation robots' requirements and examples

Requirement	Definition	Example
Target group	Range of ages and problem of the users	ChARMin covered an age range from 5–18 years old [99]
Mechanical functionality	The device performance, including the controlling level of assistance, the functional workspace, smoothness of movement and robustness	McDaid designed a gait trainer that allows children to stretch their legs through the entire ROM and support body weight up to 80kg [40]
Weight	Total unsupported or unpowered mass of the device in relation to the user's body weight	Lerner developed a Bowden cable structure for an ankle exoskeleton with a weight of 1.85 kg and placed 65% of the total mass above the waist to minimise the metabolic cost of walking due to the device's weight [73]
Therapeutic benefit	The type of exercise that the rehabilitation system should promote and how this will improve the user quality of life	The paediatric Anklebot provided intensive task-specific sensorimotor therapy to the ankle of children with motor disabilities to promote motor learning [75]
Safety	The potential for the device to harm its user	IOTA device included a security stop button that immediately halts the servo motors [175]
Comfort	The user can use the device without physical pain or discomfort	The P-LEG robot used 3D printed braces based on 3D scans of the child's legs to improve the child's comfort [71]
Reliability	The consistency of the device operation in normal operating conditions	Laubscher designed a gait guidance controller to guide the motion of the patient's legs to follow healthy gait patterns to avoid unnatural gait patterns [176]
Operability	The device is easy to control and adaptable to changes in the user's ability and sizes	ATLAS exoskeleton used a slide and tubular regulation size system to adapt to the fast growth of the patients at all stages [177]
Product appeal	User satisfaction with the design, like fit, appearance, and sound of the device	One of the main requirements for PEXO was an appealing design, so the kidPexo version resembles a crocodile [26]
Quality of construction	Typical use and care should cause no damage, distortion, or hinder the expected useful lifetime of the device	PEXO device did not have electronics in the hand module, making the device water and dustproof [26]
Social acceptability	Matches user needs for discretion or attention to avoid stigmatisation	Weightman selected the handgrip of his robot through a questionnaire with different aspects like shape, style, feel, and colour [69]
Motivation	Encompass any aspect of the device considered to motivate the child	ChARMin used an Audio-visual interface with various game-based virtual reality scenarios to motivate the child for active participation [57]
Cost	The financial burden of the initial purchase and ongoing costs of the device	Volpini developed a low-cost robotic gait trainer to be used in developing countries [87]
Easy to maintain/repair	The ease of keeping the device fully operational, including when damaged	P-Legs' brace 3D print fabrication method made it easy to get new braces as the children grow [71]
Portability	The possibility of the device to be transported between locations	Cleary developed a smaller version of Pedbot that can be used at home [153]

[69], Bützer et al. [26] and Keller et al. [57]. In paediatric rehabilitation, it was apparent that the stakeholder's needs related to operability, weight, safety, and motivation factors were relevant.

In paediatric rehabilitation devices, operability is critical as children are in a continuous development phase during which their bodies, cognitive capabilities and physical abilities (e.g. skill levels) are changing, making them a "heterogeneous population" [52, 70]. Consequently, the device must adapt to different children's abilities and sizes [71].

An important consideration is that the robot's weight could obstruct the movement pattern of the limb and increase the child's energy consumption [72, 73]. Furthermore, due to their musculoskeletal system's immature development, their muscle strength and joint torque generation may not be adequate to assist in the movement being undertaken [74].

Concerning safety, children often cannot adequately assess the hazards of using complex technological devices [56]. Therefore, it is crucial to design safety mechanisms that minimise risky situations. These should be able to be activated remotely by adults with the child [57]. Furthermore, the use of compliant materials with shock-absorbing features (e.g. elastic elements like spring and Bowden cables) would be beneficial [17].

Finally, motivation is crucial because function recovery is not enough to engage children in the rehabilitation process [75]. Consequently, researchers have used strategies to engage children, like aesthetic designs attractive to the children [26, 76] or a virtual environment where they can interact with virtual objects [77, 78].

Type of robots used on paediatric robotic rehabilitation

Fifty-eight different devices were found that at least had a prototype in action. In Tables 3, 4, 5, 6, 7 (Figs. 2, 3, 4, 5, 6), the rehabilitation robots are presented chronologically and separated by their mechanical structure (end-effector or exoskeleton) and the anatomical part of the body where they are working (upper limb or lower limb). Furthermore, the tables summarise the characteristic features of the selected devices. This tabulated summary constitutes the reference for information provided in subsequent sections.

In respect of the developmental stage of the devices, the stages were classified into four categories: (1) commercial in the case the robots are available for its commercialisation; (2) clinical trial when the robot undergo a study where the participants were assigned to groups undergoing similar forms of therapy, but at different intensities, using various devices or undergoing various forms of therapy in a different order, aiming to determine the efficiency of therapy [28]; (3) feasibility study when the experiments conducted with a low number of people, often using the prototype of a device, to evaluate its safety and clinical feasibility without showing the potential benefits of the device [28]; (4) prototypes when the robots had not performed any test that involves people. It can be observed that 18 of them reached the commercialisation phase, but only 9 of them are certified by the US Food and Drug Administration (FDA). However, only 5 of the commercially available devices present a paediatric version of the rehabilitation system. In the case of clinical studies, 34 systems conduct at least one clinical trial, 9 presented a feasibility study, and 15 are in the prototyping phase.

From the 58 devices, it was apparent that the majority (67%) were designed or had been redesigned for children. When it comes to the type of robot, more than half were an exoskeleton type structure. In the past five years, there is a trend (Tables 3, 4, 5, 6, 7)

Table 3 Upper limb end-effectors rehabilitation robots

System (year)	Treated part of the body	DOFs	Actuator	Type of rehabilitation	Type of training	HCI input	Paediatric disease (design for or treated condition)	Paediatric design	Stage of the device
Inmotion2/ Mitmanus (BIONIK, Canada) (1998) [126, 178]	Shoulder/ elbow	2	DC motors	Physical therapy	Passive/ active/ assistive	Imped-ance	Neurological	No	Clinical trial/com-mercial (FDA)
Wrist-Robot (2009) [119, 179]	Forearm/ wrist	3	DC motors	Physical therapy	Passive/ active/ assistive	Imped-ance	Neurological	No	Clinical trial
NJIT-RAVR (2009) [124, 180]	Shoulder/ elbow/ forearm	6	DC motors	Physical therapy	Active/ assistive/ resistive	Admit-tance	Neurological	No	Clinical trial
GNO arm (2009) [149]	Elbow	1	DC motor/ Cable driven	Assistance	Assistive	Finger move-ment	DMD	Yes	Feasibility study
AMADEO (Tyromo-tion, Aus-tria) (2012) [150, 181]	Fingers	5	DC motors	Physical therapy	Passive/ active/ assistive	Imped-ance	Physical disabled children	No	Clinical trial/com-mercial (FDA)
REAplan (AXINESIS, France) (2012) [81, 182]	Shoulder/ elbow	2	DC motors	Physical therapy	Passive/ active/ assistive	Position	Neurological	No	Clinical trial/com-mercial
PASCAL (2013) [183, 184]	Shoulder/ elbow	3	Dc motors	Physical therapy	Passive/ active/ assistive	Velocity	Neurological	Yes	Clinical trial
ReHaptic (2014) [125, 185]	Forearm/ wrist	2	DC motors	Physical therapy	Passive/ active/ assistive/ resistive	Admit-tance	Neurological	Yes	Clinical trial
MyPam (2015) [166]	Shoulder/ elbow	2	Electric motors	Physical therapy	Active/ assistive	Position	CP	Yes	Feasibility study

for this structure to be more popular with designers than end-effectors for this structure robotic rehabilitation in paediatrics. Additionally, it can be noted that the majority of robots not explicitly designed for children are end-effector devices. In the case of the exoskeletons, the degrees of freedom (DOFs) are related to the number of joints and limbs that are powered. Therefore, it is possible to find exoskeletons with passive DOFs, which means that those joints are not actuated, but allow the free movement of the children´s joint. In contrast, for the end-effectors, the relation of DOFs of the robot and the actuated joints is not linear and depends on the robot's mechanical design.

Actuators

Rehabilitation robots are moved by devices called actuators. Actuators convert a source of energy (e.g. electrical, thermal, pneumatic) into mechanical motion. Commonly rehabilitation assisted robots are powered by electrical actuators. Among the compared systems in Tables 3, 4, 5, 6, 7, over 93% of the robots used electric motors as the actuator, and about 7% used pneumatic actuators.

Table 4 Upper limb exoskeleton rehabilitation robots

System (year)	Treated part of the body	DOFs	Actuator	Type of rehabilitation	Type of training	HCI input	Paediatric disease (design for or treated condition)	Paediatric design	Stage of the device
KINARM (KinArm, Canada) (1999) [82, 186]	Shoulder/elbow	2	DC motors	Physical therapy	Passive/active	–	Neurological	No	Clinical trial/commercial
IOTA (2013) [175]	Thumb	2	DC motors/cable driven	Physical therapy	Passive/active/assistive	Movement	Neurological	Yes	Prototype
ChARMin (2014) [57]	Shoulder/elbow/wrist	6	Electric motors	Physical therapy	Passive/active/assistive	Movement	Neurological	Yes	Feasibility study
Universidad Nacional de San Juan (2014) [130]	Elbow	1	DC Motor	Physical therapy	Passive/assistive	EMG	Injuries	Yes	Clinical trial
Milwaukee University (2014) [187]	Wrist	2 actuated + 2 passives	DC motors/cable driven	Physical therapy	Assistive	Position	CP	Yes	Prototype
GLOREHA (2016) (IDROGENET, Italy) [33, 107]	Hand	5	Pneumatic	Physical therapy	Passive/active/assistive	Movement	Neurological	No	Clinical trial/commercial (FDA)
HAL single joint (Cyberdyne, Japan) (2019) [84]	Elbow	1	DC motor	Physical therapy/assistance	Assistive	EMG	CP	No	Clinical trial/commercial
PEXO (2019) [26]	Hand	2 Actuated + 1 passive	DC motors/cable driven	Physical therapy/assistance	Passive/assistive	Push buttons or EMG	Neurological	Yes	Feasibility study
PneuGlove (2019) [113]	Hand	5	Pneumatic	Physical therapy	Active/assistive/resistive	Movement	CP	Yes	Feasibility study
Exohand-2 (Android Technics, Russia) (2020) [131]	Hand	2 Each hand	Electric motors	Physical therapy	Assistive	EEG	CP	No	Clinical trial/commercial

Motor actuator

In robotic-assisted rehabilitation, the most common actuators are electrical motors with a rigid power transmission element such as a harmonic drive, ball-screws, timing belts, and chains. Unfortunately, their need for transmission negatively affects the back-drivability, efficiency, safety, size, and mass [97]. Nevertheless, they were likely chosen since they are efficient and easy to control. Some examples of paediatric robotic rehabilitation devices using electrical motors and rigid transmission are the Pedianklebot that used two brushless dc motors and a Rohlix linear traction device [98], the electric motor with

Table 5 Lower limb end-effectors rehabilitation robots

System (year)	Treated part of the body	DOFs	Actuator	Type of rehabilitation	Type of training	HCI input	Paediatric disease (design for or treated condition)	Paediatric design	Stage of the device
GAIT trainer GT 1 (REHA-STIM MEDTEC, Switzerland) (2000) [188, 189]	Hip/knee	2	DC Motors	Physical therapy	Passive/assistive	Velocity	Neurological	No	Clinical trial/commercial
MOTOmed gracile (RECK, Germany) (2000) [190, 191]	Hip/knee	2	DC motors	Physical therapy	Passive / active/assistive/resistive	Velocity	Physical disabled	Yes	Clinical trial/commercial (FDA)
IntelliStretch (Rehabtek, USA) (2002) [192, 193]	Ankle	1	DC motor	Physical therapy	Passive/active/assistive/resistive	Velocity and torque	Neurological	No	Clinical trial/commercial (FDA)
Innowalk (Made for Movement, Norway) (2009) [114, 194]	Hip/knee	2	Electric motors	Physical therapy	Passive	–	Neuromuscular problems	Yes	Clinical trial/commercial
National Taiwan University (2009) [195]	Hip/knee	2	DC motors	Physical therapy	Passive	–	CP	Yes	Prototype
3DcaLT (2011) [134, 196]	Hip/knee	4	Electric motors/cable driven	Physical therapy	Active / assistive/resistive	Motion	CP	No	Clinical trial
Paediatric ICARE (2011) [197, 198]	Hip/knee	2	DC motors	Physical therapy	Active/assistive/resistive	Speed	Neurological	Yes	Feasibility study
Rutger ankle CP system (2011) [112, 199]	Ankle	6	Pneumatic	Physical therapy	Active/resistive	–	CP	Yes	Clinical trial
SS-POINT (2013) [135, 200]	Ankle	2	DC motors	Physical therapy	Passive/active/resistive	–	Neurological	No	Clinical trial
TPAD (2014) [102, 103]	Hip/knee	6	AC motors	Physical therapy	Assistive/resistive	Motion	CP	No	Clinical trial
Pedbot(2016) [153, 201]	Ankle	3	DC motors	Physical therapy	Active/assistive/resistive	Position	CP	Yes	Clinical trial
Wyss Institute (2017) [202]	Hip/knee	8	DC motors/cable driven	Physical therapy	Assistive	Gait segmentation/motion/force	CP	Yes	Prototype
Pro-Gait (2017) [40]	Hip/knee	2	DC motors	Physical therapy	Passive		CP	Yes	Prototype
UFMG (2017) [87]	Hip/knee	2	Electric motors	Physical therapy	Passive	–	CP	Yes	Prototype
Leg Press (2017) [89]	Knee	2	Linear electrical motors	Physical therapy	Assistive/resistive	Impedance	Neurological	Yes	Prototype

timing belt used in ChARMin [99], or the motor with chain transmission used in P.REX [100].

Some researchers [64] used a cable-driven transmission to replace the rigid transmission for an elastic cable to improve the power to weight ratio and lower the inertia over the treated body segment. Examples include the ankle exoskeleton designed by The University of Arizona [101] or TPAD [102], an end-effector robot for gait rehabilitation that used Bowden cables attached to the hip to generate assistive forces. This change in the transmission brings other advantages like modularity, simple architecture and is convenient for reconfiguration, even though they present some disadvantages being unidirectional and difficult to model and control [97, 103, 104].

Following the concept of adding a flexible element in series with the actuator to improve the electric motors' compliance, serial elastic actuators (SEAs) incorporate an elastic part in series with the electric actuator. This elastic element helps to decrease the actuator's impedance and inertia and increases the back-drivability allowing better force control, even though they are limited by a large volume, heavy mass and complicated structure [17, 105]. An example of the use of this technology is the ATLAS exoskeleton [106].

Pneumatic actuators

Some authors considered that the mechanical linkage of the electric actuators is too heavy and can generate resistance at the joints, making them inadequate for rehabilitation applications [74, 107]. Instead of electrical motors, they used pneumatic actuators, consisting of a simple air pressurisation mechanism in an expandable chamber, converting the energy from the compressed air to mechanical motion [18, 108, 109]. Their main advantage is improved back-drivability, and they are often lightweight at the site of actuation, have high power density, and can generate fast movements. They are not without limitations; firstly, poor portability because they need external compressors or fluid tanks as the power source. Secondly, it is challenging to create a good model and control strategy due to their nonlinear response to input pressure [109–111]. Among the devices analysed that used pneumatic actuators were the Rutgers ankle platform [112] for CP children and two gloves for hand rehabilitation PneuGlove [113] and Gloreha [33].

Training strategy

Devices for robotic rehabilitation may provide different training strategies depending on the type and severity of the patient's impairment. These can be divided into passive, active, assistive, or resistive [42]. In general, the devices can offer more than one type of training.

In passive training, the force/motion is generated by the robot alone to perform the exercise. The advantage of this training is that patients with minimal muscle activity can receive therapy. For instance, through repetition of a movement, ROM can often be maintained with muscles and joint structures (e.g. ligaments) repeatedly stretched, ultimately maintaining their physiological length. Such movement reduces contractures at joints, which can finally be very useful to caregivers making a notable difference to the ease of transfers (e.g. sitting in a wheelchair to lying in bed). Examples of devices using passive training are Innowalk [114] and Intellistretch [115].

Table 6 Lower limb exoskeleton rehabilitation robots

System (year)	Treated part of the body	DOFs	Actuator	Type of rehabilitation	Type of training	HCI input	Paediatric disease (design for or treated condition)	Paediatric design	Stage of the device
Lokomat (Hokoma, Switzerland) (2007) [203, 204]	Hip/knee	4	DC Motors	Physical therapy	Passive/ active/ assistive/	Impedance	Neurological	Yes	Clinical trial/ commercial (FDA)
HAL (Cyberdyne, Japan) (2007) [91, 129]	Hip/ knee/ ankle	6	DC Motors	Physical therapy/ assistance	Assistive	Footswitch EMG	CP	Yes	Clinical trial/ commercial (FDA)
HWA (Honda, Japan) (2007) [205, 206]	Hip	2	DC Motors	Physical therapy/ assistance	Assistive	Movement	CP	No	Clinical trial/ commercial
University of Verona (2011) [207]	Hip	2	Pneumatic	Assistance	Assistive	Footswitch	CP	Yes	Feasibility study
Ekso-GT (ekso Bionics, USA) (2012) [127, 208]	Hip/knee	4	DC motors	Physical therapy	Passive/ assistive	Hip movement	ABI	No	Clinical trial/ commercial (FDA)
PediAnklebot (2015) [75, 118]	Ankle	2 active + 1 passive	DC motors	Physical therapy	Active/ assistive	Impedance	Neurological	Yes	Clinical trial
Walkbot K (P&S Mechanics, South Korea) (2016) [209, 210]	Hip/ knee/ ankle	6	AC motors	Physical therapy	Passive/ assistive/ active	Impedance	Physical disabled	Yes	Clinical trial/ commercial (FDA)
Robogait (Bama teknoloji, Turkey) (2017) [211, 212]	Hip/knee	4	Electric motors	Physical therapy	Assistive	Force	Physical disabled	No	Clinical trial/ commercial
WAKE-Up (2017) [17, 213]	Knee/ ankle	4	SEA	Assistance	Assistive	Footswitch	CP	Yes	Feasibility study
Universidad Pontificia Bolivariana (2017) [214]	Hip/knee	4	DC motors	Physical therapy	Passive	–	Physical disabled	Yes	Prototype
CPWalker (2017) [92, 154]	Hip/knee	4	DC motors	Physical therapy	Passive/ active/ assistive	Impedance/ EEG/LRF	Neurological	Yes	Clinical trial
Rehabilitation Institute of Chicago (2017) [94, 215]	Ankle	1	DC motor	Physical therapy	Passive/ assistive/ resistive/ active	Torque/ position	ABI	No	Clinical trial

Table 6 (continued)

System (year)	Treated part of the body	DOFs	Actuator	Type of rehabilitation	Type of training	HCI input	Paediatric disease (design for or treated condition)	Paediatric design	Stage of the device
ATLAS (2017) [146, 167, 216]	Hip/knee/ankle	10	SEA	Assistance	Active/assistive/passive	Footswitch/position/force	SMA, SCI	Yes	Clinical trial
P.REX (2017) [95, 100]	Knee	1	DC motor	Physical therapy/assistance	Assistive	Footswitch/position/torque	CP	Yes	Clinical trial
University of Arizona ankle (2018) [73]	Ankle	1	DC motors/cable driven	Physical therapy	Assistive/resistive	Footswitch/torque	CP	Yes	Clinical trial
Tsukuba University (2018) [74]	Knee	2	Electric brake	Assistance	Assistive	Footswitch	CP	Yes	Feasibility study
Los Olivos University (2018) [217]	Hip/knee	4	DC motors	Assistance	Assistive	Joystick	DMD	Yes	Prototype
P-Legs (2019) [71]	Hip/knee/ankle	6	DC motors	Physical therapy/assistance	Passive/assistive	Impedance	Neurological	Yes	Prototype
ExRoLEG (2019) [218]	Knee	2	Linear actuators	Physical therapy/assistance	Assistive	EMG/limit switch	CP	Yes	Prototype
Cleveland State University (2019) [176, 219]	Hip/knee	4	DC motors	Physical therapy/assistance	Assistive	Position velocities	CP	Yes	Prototype
ExoRoboWalker (2019) [220]	Hip/knee/ankle	6	DC motors	Physical therapy	Passive		CP	Yes	Prototype
Indian Institute of Technology Guwahati (2020) [49]	Hip/knee/ankle	6	DC motors	Physical therapy	Passive		Physical disabled	Yes	Prototype
Instituto Politécnico Nacional (2020) [221]	Hip/knee/ankle	6	DC motors	Physical therapy	Assistive	EMG	Physical disabled	Yes	Prototype

In the active training mode, the patient's muscle can still generate activity on the affected limb. The robot does not help, making the patients perform the exercise by themselves at least partially. The active mode provides data concerning torques and the ROM produced, allowing assessments before and after therapy/surgery. For instance, Kinarm [116] and Lokomat [117] are devices that can perform active training.

For assistive or active-assistive training, the muscles of the affected body part can still be activated. Therefore, the patient can at least partially perform the exercise or

Table 7 End-effectors rehabilitation robots for upper and lower limbs

System (year)	Treated part of the body	DOFs	Actuator	Type of rehabilitation	Type of training	HCI input	Paediatric disease (design for or treated)	Paediatric design	Stage of the device
KPT Cycla (Kinetec, France) (2010)(96)	Upper: shoulder/elbow Lower: hip/knee	2	Electrical motor	Physical therapy	Passive/active	–	DMD	No	Clinical trial/commercial (discontinued)

movement without the robot. The assistance will be triggered after a particular event is detected through an HCI, allowing the patients to move further with the robot's help. Assistive training is relevant as it involves the active participation of the children. Moreover, it improves the physiological responses needed to maintain and increase muscle strength and length, ultimately leading to improved ROM, in which the muscles provide some of the torque required. Due to these advantages, many designers have produced devices that use this training mode. Examples are Pedianklebot [118] and the wrist-robot [119].

As the name implies, the robot applies a force opposing the desired movement in resistive training, making the task more challenging. Resistive training is used to enhance muscle strength in the treated limb. This type of training was employed in the ankle device developed by the University of Arizona [120] and the upper limb end-effector NJIT-RAVR [121].

Human–computer interface (HCI)

The term HCI refers to methodologies to identify the user's intent to move in the desired direction from different input sources and translate this intention into a command for the robot to move to facilitate the appropriate actions [122]. The designers who report upon the use of an HCI have primarily developed assistive training. Two main types of HCI inputs were identified: those associated with physical interactions and physiological signals [123]. In this aspect, the devices can rely upon only one signal as the input source or use two or more signals as input to start the desired movement.

The main physical interactions used on HCIs to control such robots are Impedance/admittance, body-powered control, and gait phases detectors. Impedance and

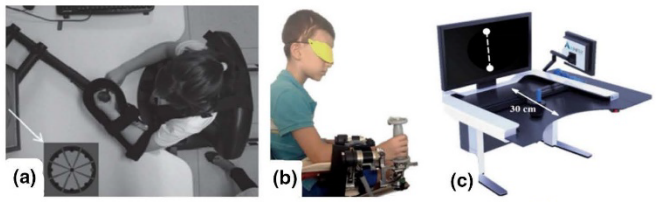

Fig. 2 Picture of upper limb end-effectors rehabilitation robots: **a** Inmotion2/Mitmanus [79], **b** wrist robot [80], **c** REAPlan [81]

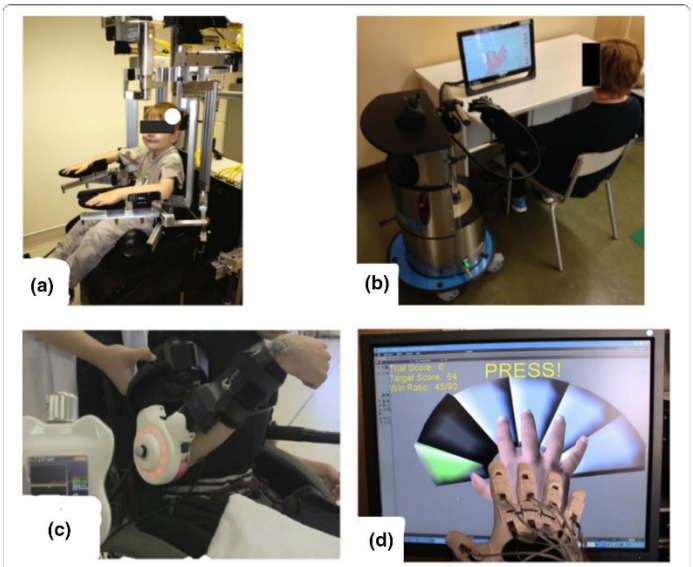

Fig. 3 Picture of upper limb exoskeletons rehabilitation robots **a** KINARM [82], **b** GLOREHA [83], **c** HAL single joint [84], and **d** PneuGlove [85]

admittance control are the two most commonly used HCI. They are based on the relation between position and force rather than controlling either force or position explicitly. Impedance control accepts position or velocity as the input and outputs force or torque, and admittance is the opposite of impedance. Hence, force or torque are inputs, and velocity or position the outputs. This method could provide a natural, comfortable, and safe touch interface [122]. Some examples of devices that used this HCI are the NJIT-RAVR [124] and Rehaptic [125] upper limb robots that employed admittance control or the robots for upper and lower limb Inmotion2 [126] and Pedianklebot [118] that applied impedance control.

When the children cannot generate an intention to move with the treated limb, body-powered control is applied. It consists of using the movement of a different body part as the trigger signal to initiate the rehabilitation robot. The main drawback of this approach is that it is hard to control many degrees of freedom due to the activation system's simplicity. An example of this HCI is the Ekso robot, where the activation was made by moving one's body weight laterally and then forward to trigger the assistance [127].

In assisted gait, a favoured approach for HCI is the use of gait phase detection. This technique identifies the different gait phases (heel strike, midstance, toe-off, and the swing phase) to apply forces to assist the children's movement depending on the gait phase. Robots usually perform gait segmentation using inertial measurement units (IMUs) to detect angular velocities of the shank and/or the thigh, or footswitches

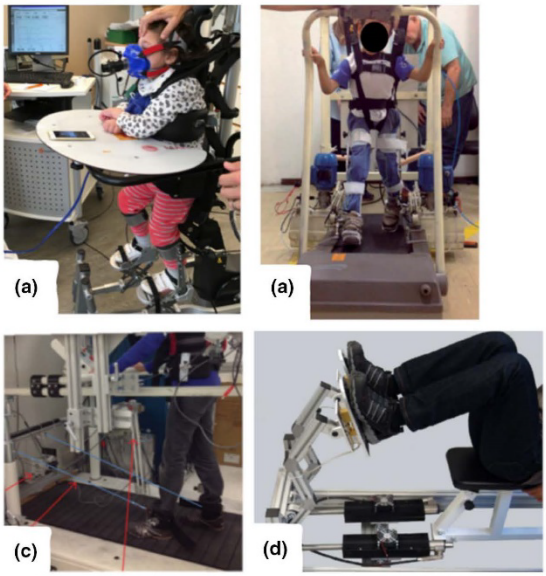

Fig. 4 Picture of lower limb end-effectors rehabilitation robots: **a** Innowalk [86], **b** UFMG [87], **c** 3DCaLI [88], **d** Leg Press [89]. Reprinted from Biomedical Signal Processing and Control, Vol. 38, F. Chrif et al., Control design for a lower-limb paediatric therapy device using linear motor technology, Page 121, Copyright (2017), with permission from Elsevier

to detect the foot's ground reaction forces while the child is walking [128]. The main advantage is that splitting the gait cycle into discrete phases provides enhanced consistency and robustness to an inherently variable process and allows lower-level controllers' implementation within each phase. The problem is that gait detection should be characterised for every target group, as the physical disability modifies the gait pattern [100]. An example of this type of system is the P.REX exoskeleton which utilised a combination of the footswitch and IMUs to detect the different gait phases to provide different levels of assistance within each phase [100].

Alternatively, for HCI based on physiological signals, Electromyograms (EMG) that measure electrical activity in the muscles and electroencephalograms (EEG), which measure electrical activity in the brain, are the main signals used. They are widely utilised because they can be obtained using non-invasive techniques without the need for medical intervention.

Concerning electromyograms, the primary type is surface electromyography (sEMG), a non-invasive and easy-to-configure procedure in which adhesive electrodes are placed on the skin above the muscle of interest. The benefit of using the EMG signal is that it allows detection of the user's intent before the movement occurs. The electrical activity can be detected even if it is insufficient to generate movement of a joint. However, sEMG

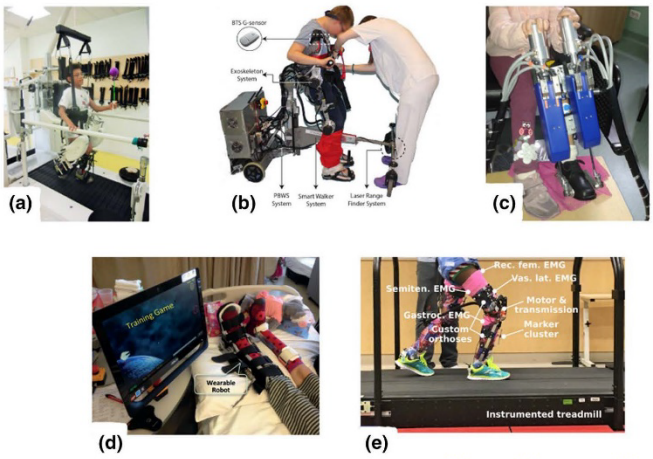

Fig. 5 Picture of lower limb exoskeletons rehabilitation robots: **a** Lokomat [90], **b** HAL [91], **c** CPWalker [92], **d** PediAnklebot [93], **e** wearable ankle rehabilitation robot developed by the Rehabilitation Institute of Chicago [94], **f** P.REX [95]

can suffer from contamination of the signal by electromagnetic interference, skin perspiration, movement of electrodes and crosstalk artefacts. Also, for each muscle group of interest, a single EMG channel only shows the activation of that group. So, to perform an activity where many muscles fibres are recruited, it is necessary to use multichannel sEMG. Some examples of this technology in paediatric rehabilitation robots are the lower limb exoskeleton HAL [129] and the device for upper elbow rehabilitation of the San Juan National University [130].

The electroencephalogram (EEG) signal is recorded using many small surface electrodes, often configured in a bathing like cap placed over the scalp that detects the underlying electrical signals. The main advantage of the EEG signal is that the physical disability level does not limit it. Even if the patient has lost all their ability to move the

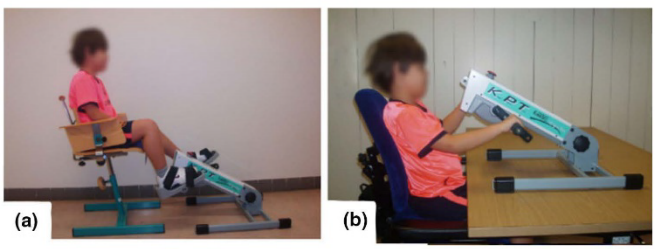

Fig. 6 Picture of KPT Cycla [96] an end-effectors rehabilitation robot for both **a** lower and **b** upper limbs

limb required for a task, the brain activity thought to be related to the intent to activate the muscles can be recorded. There are two main disadvantages to this system. Firstly, it is unsuitable for children with brain damage as they cannot generate standard brain patterns for limb activation. Secondly, the EEG signal has greater variability within it than the EMG signal, and it is also easily affected by changes in the patient's mood and attention. Examples of the EEG signal use are the CP walker that used this signal as a part of its HCI to help children with a physical disability move their legs [120] and the Exohand-2 that used the EEG signal to interact with the exoskeleton [131].

Treated conditions

The majority of studies and devices were for children with neurological conditions (np = 183, 89%), CP being the most studied condition (np = 129, 63%). In contrast, other neurological disorders included ABI and strokes. Significantly few researchers investigated other conditions such as neuromuscular diseases (np = 15, 8%) and traumatic injuries to limbs and the spine (np = 6, 3%). The results obtained from the studies that perform clinical trials or a feasibility study suggests that robotic rehabilitation could benefit children with physical disabilities.

Neurological disorders

Concerning CP, there was evidence of improvement in physical disability using assisted rehabilitation robots. The benefits include an increase in muscle activity [120, 132], endurance for physical activities [133, 134], improvements of balance [114], walking speed [134, 135], the strength of the muscles [136, 137], ROM of the joints [84, 138], upper limb kinematics [139], and manual dexterity [33, 140].

For paediatric ABI, there were reports in the improvement of the walking ability [141], improvement of the lower limb motor performance [94], increase in the ROM of the wrist joint and force increase in the hand [142], improvement in motor function, and gait pattern [143, 144].

In children who suffer a stroke, three studies used rehabilitation robots while performing physical therapy. Marini et al. [119] demonstrated an improvement in wrist motion after the robotic therapy, and Bützer et al. [26] showed the possibility of using a wearable hand exoskeleton to assist children during task-oriented training could be helpful for rehabilitation therapies or assist children during ADLs.

Neuromuscular diseases

The neuromuscular disease presented a different scenario than neurological disorder due to the degeneration of their muscles as the disease progresses, making hard the use of rehabilitation robot due to stiffness in the robot's joints, which can harm children's weak muscles. Hence they require compliant actuation [145, 146]. Jansen et al. [145] found that robotic rehabilitation therapy on upper and lower limbs help prevent functional deterioration in children with DMD. Meanwhile, Ganguly et al. [147], Garcia et al. [148] and Sanz-Merodio et al. [146] showed an improvement in walking ability in children with SMA with the assistance of ATLAS, and the exoskeleton was designed to provide Robotic-assisted gait training for children with SMA. Moreover, Koo et al.

[149] reported improved arm mobility in children with DMD while using a robotic arm device.

Traumatic injuries

Even if traumatic injuries are common in the paediatric population, robot rehabilitation has not been applied widely in injuries that differ from those at the head. Only scarce information was found related to these conditions. A study of hands robotic rehabilitation was found, highlighting the possibility of using robotic devices to treat burns [150]. Additionally, a study observed a significant improvement in the arm movement and elbowed angle after physical therapy using an upper-limb exoskeleton for 3 months in children that suffer a car accident [130]. Finally, another case reported improving walking ability after robotic-assisted gait training in a girl with SCI [151].

Discussion

It is possible to see that various novel rehabilitation robots have become available to rehabilitation professionals and clients in recent years. And this trend will continue as is possible to incorporate them in activity programs aimed at improving independent function [34–37] where they offer advantages over the traditional rehabilitation therapies, as they reduced the required effort of therapists during the exercises of the therapies, allowed massed practice in children with substantial limitations and provide information of the patient. Furthermore, they have the potential to be used as assistive devices to aid functional performance for users when they are worn. These possibilities will lead to a new variety of ways for assessment and intervention impacting users' abilities, task demands, or the environment to promote functional performance and participation.

The findings of this review indicate that the design and development of robotic technologies for the physical rehabilitation of children is in a preliminary stage of development, as many of the devices were designed for adult patients. However, there is a trend toward creating robots specifically for children [17, 26, 57, 148]. Yet less has been done to prove the benefits and constraints of such a system.

Traditionally, rehabilitation robot designers have focused solely on improving physical function [58], which can lead to rejection of the devices as not all the needs of children with disabilities are considered. Thus, to ensure successful adoption of the technology, the rehabilitation robots should cover these needs of the children. Hence, stakeholders' cooperation is essential through their integration within the design and production process by providing feedback. Designers can use this feedback to validate that the robot meets the stakeholder's needs. However, the fulfilment of these needs has strong relationships to the chosen technology, mainly the type of robot, the actuator, the training strategy and the HCI. Thus, it is essential to know the advantages and disadvantages of the technology.

Type of robot

When it comes to the type of robot, we can see a trend to migrate from end-effector to exoskeletons. However, most of the devices that had performed clinical trials were end-effector robots designed for adults. This relation could be because the end-effector robot

works on the distal part of the limb, guiding the children limb through a movement [152]. This property is helpful in the case of operability as it does not require adaptation to match the children limb's size, making it easy to be used by a diverse group of children. Furthermore, the bulky frames over the patient limbs are avoided, helping to reduce the weight that the children need to handle. These advantages come with the problem of the systems requiring bulky and heavy external structures, reducing the device's portability, constraining its use to medical facilities or specific spaces inside a building. Thus, limiting the amount of therapy that the children can have [153]. Additionally, the activity is restricted to a workspace constraining the number of possible movements [40], which could reduce motivation.

On the other hand, exoskeletons work in parallel to the patient limb to perform the activity. Hence, they can be portable devices with the possibility to provide assistive help during activities of ADLs and robotic-assisted rehabilitation therapy in a single device [26]. This advantage will help to provide free movement to enhance the subject's motivation and autonomously practise their movement training for longer periods [17, 154]. Furthermore, as technology advance, this freedom in mobility will help to increase the participation of children with physical disabilities in different social activities [155]. However, as the technology moves from clinical facilities to open spaces and robots interact more closely with the children, designers will face notable challenges (e.g. the irregularities of the surfaces on which one walks and how the robot reacts to perturbations outdoors environment). Consequently, the requirements of weight, comfort, safety, portability and social acceptability for the exoskeletons will be harder to achieve.

Actuators

The paediatric robotic rehabilitation technology is moving from end-effectors to exoskeletons due to their versatility to be used as a rehabilitation tool or an assistive device [26]. Consequently, actuation technology starts to be a critical part of the design as it negatively influences the weight and the size of the robot.

For the end-effectors robots, actuators are not as critical as with the exoskeletons because they could be placed in external structures. This advantage makes it possible to use bulky and heavy actuators like electric motors. However, using electric motors is hard to achieve compliance that is an important property to increase safety as it is needed to avoid opposing forces that can injure the children. In end-effector robots, compliance was achieved using sensors and a control strategy [146] or using a soft material like the Bowden cables [103].

On the other hand, for exoskeletons, the robot design requirements are hard to enhance with the currently used technology. The actuation system components such as motor and rigid elements are designed for industrial applications not to interact with and to be worn by children. However, they are still the standard as they have the advantages of efficiency, are easy to control, and are readably available in the market. Therefore, the choice of the actuation system is crucial to improve the weight, portability and safety of the exoskeleton.

The first exoskeletons relied on electric motors with rigid transmissions, making them bulky and heavy, reducing their compliance as they generate high resistive torque from the metallic links of the exoskeleton. Therefore, making it difficult to move and less safe

Table 8 General summary of advantages and drawbacks of each actuation technology

Actuation technology	Advantages	Drawbacks
Electric motors	High precision Easy to control Readably available in the market	Not compliant Large size Heavy Noisy
SEA	High precision Easy to control Compliant Better force control	Large size Heavy Complex structure
Bowden cable	Modularity Simple architecture Easy to reconfigure Low weight on the distal part of the limb	Unidirectional Difficult to model and control
Pneumatic	Lightweight Compliant Have high power density Fast actuation Low cost Easy to manufacture in different shapes and sizes	Poor portability because they require external components Difficult to model and control

can cause non-desirable inertial movements [156, 157]. Furthermore, they require external structures to manage the weight of the exoskeleton.

As the rehabilitation robots move from rehabilitation therapies inside a medical facility to assist the children during ADLs, new actuation technology is needed. This challenge led to using SEA actuators and cable transmission since they have the advantage of been intrinsically complaints as they incorporate soft materials, making the device safer.

Using Bowden cables in the transmissions brings other advantages like simple architecture, low weight on the limb's distal part, and easy to reconfigure. This last advantage is significant in paediatric rehabilitation as it allows to change the motor easily depending on the abilities and size of the children [26, 73], even though they present some disadvantages because they become unidirectional and difficult to model and control. Instead, in the case of SEAs, which still require rigid links, they were highlighted on the use for children with neuromuscular diseases, as some children are not only weak on the affected joint but the entire body. Thus the exoskeleton must hold the children, but at the same time being compliant to avoid inertial forces that can harm the weak muscles of the children [146].

Another type of actuator used on the robots was the pneumatic. Their attributes of low weight and easy-to-manufacture actuators of different shapes and sizes [158, 159] make them a desirable technology in this field. They are easy to adapt to children with various conditions. However, their main constraint is that they are typically connected to external mechanisms like compressors and pumps cumbersome and noisy. Thus, reducing their portability and appealing making them impractical to use outside clinical facilities.

In Table 8, the advantages and disadvantages of the current actuator technology are presented. It is possible to notice that there is no perfect actuator technology, so more research in this area is needed. Moreover, in the future will be interesting to see devices that use different soft actuators technologies that are inherent compliant and lightweight, such as the already mention SEAs, pneumatic, and Bowden cables. But also new technologies that are under research to be used on rehabilitation robots, like shape

memory alloys [160], dielectric elastomer [161], or twisted and coiled polymers actuators [162], as they will reduce the overall weight and increase the compliance. Furthermore, this new technology can be manufactured in different sizes and shapes [163] that could be easily adapted to robots for children of varying height and ability conditions.

Training strategy

In the case of the training strategy, there is no best strategy, but it rather depends on many factors like the abilities and disease that the children have. For example, passive training is suitable for patients with limited mobility; however, when the children are able to generate movements, it tends to decrease children's participation during the exercise, thus reducing the efficiency of the training [164]. That is why most of the research on the training strategy is centred on assistive training, where the children's participation is needed. This engagement with the therapy increases the motivation of the children to perform the activities, enhancing the benefits from the therapy [165]. Another advantage of assistive training is that it is used together with video games to increase children's motivation and social interaction [166]. In addition, this strategy is required for assistive devices. It needs to provide the required intensity to generate the movement safely, efficiently, and reliably, depending on the applied force by the user [167]. However, there is no clear which is the best strategy to provide assistive movement, where some examples of different assistive strategies are guidance force, path control, and locomotion strategy [57, 154, 165, 166].

Alternatively, some researchers suggest that resistive training could be more beneficial for rehabilitation therapy than an assistive force, as it increases the engagement of the children, which can help drive motor learning [120, 168]. Hence, further research is required on the optimal training strategy to increase the benefits from the rehabilitation therapies.

Human–computer interface

The HCIs are essential in developing robotic rehabilitation robots, as they are the medium for the interaction between the children and the robot, impacting the functioning of the actuators and training strategies directly. Thus, HICs are a crucial factor for safety and motivation needs, as it is how the children "communicate" their intention to the robot. Consequently, If the HCI is complex to use, it could lead to the rejection of the device [52]. Furthermore, for safety reasons, the HCI must detect the trigger signal properly and discern between intended movements and involuntary movements, as it can generate undesirable responses [41, 169]. For instance, in the case of CP patients presenting increased muscle tone, rapidly occurring muscle spasms, and severe jerks, which can be considered as a deviation of pattern, causing the robot to apply undesired forces to correct for it or turn off the device suddenly [170].

Consequently, selecting the best HCI for every case needs to be evaluated depending on the capabilities of the children. For example, it could be challenging for patients with advanced muscular dystrophy to use EMG and admittance/impedance interfaces as their muscles progressively deteriorate, turning unable to activate the muscles to generate a

movement or a detectable signal [149, 171]. On the other hand, EEG could lead to a better motor function recovery for children with CP as it integrates the central nervous system into rehabilitation therapy [154]. However, this technology could be hard to implement in patients with a cognitive deficit, requiring concentration [131, 172]. For HCIs, it would be interesting to see more devices using physiological signals as they can also evaluate the efficiency of the therapy [154], novel approaches of body-powered control to address children with limited mobility of limbs [173], and devices that integrate different HCI strategies to make the system more robust and adaptable [71, 167, 174].

Treated condition

To better understand how the technology can positively impact children's lives, it is essential to analyse how the rehabilitation robot's technology has addressed the different paediatric conditions that can generate physical disability. Because, even if they share in common the deterioration of the musculoskeletal system, each one of the conditions presents certain specific characteristics that need to be considered.

Most of the research has focused on children with neurological conditions, particularly children with CP. However, it seems likely that many of the designed robots that currently work with neurological conditions could also be utilised in traumatic injury scenarios, especially because they have been designed for rehabilitation therapies that can improve common problems across both neurological and traumatic injuries like ROM deficits and a lack of ability to generate muscle force [80, 150]. Contrarily, neuromuscular diseases present a different scenario than neurological disorders and traumatic injuries as the diseases are progressive, making it hard to obtain a permanent improvement on the children skills. Thus, the designs have been focused on design devices capable of assisting with exercise and helping with the ADLs to maintain specific abilities (e.g. walking) for a longer period of time [122, 155].

Unfortunately, the outcomes proving the efficiency of rehabilitation robot in children is still scarce, as the pieces of evidence are low and weak. Hence, the information coming from these studies should be asses carefully, as there are very few randomised controlled trials, with small sample sizes and variability in children's ability, outcomes measures, treatment protocols, and used devices [31, 65]. Thus, to better understand if the designed robots fulfil the paediatric needs properly by improving their quality of life and physical ability, more studies and robots designed especially for them are needed. Furthermore, more studies with children presenting different conditions from neurological ones are needed, as it can be noticed that the treated condition impacts the requirements design of the rehabilitation robot.

Limitations

It was apparent that some studies were conducted with participants from a wide range of ages; therefore, it was difficult to target all the articles that include paediatric participants. Another problem was the upper bound on the paediatric population's age as some papers with the term young adults included paediatric participants.

Conclusion

While robotic rehabilitation is gaining momentum with increasing numbers of devices being produced for adults, there is a lack of well-designed and effective products available for children. Early examples of robots have often been created by scaling downsize to meet the smaller stature of children. Few robots have been specifically designed and produced, with children being the focus of the project/program. It is apparent that children have special needs, and these need to be incorporated into designs early in the development program. And even if the fulfilment of these needs is closely related to the chosen structural and technological components like the actuator, training strategy and HCI, they go beyond them. Consideration must also be given to the aesthetics that appeal to children and the need for the robot's structure to be as unobtrusive as possible. Without such needs being met, no matter how effective the robot works from an engineering perspective, it will not be utilised well by the child.

It is apparent that there is still a lack of understanding of what the most effective therapy is to improve function and quality of life in specific paediatric conditions (e.g. CP or Stroke). Nevertheless, common impairments (e.g. ROM, strength) must be addressed across numerous clinical conditions if patients improve function in everyday tasks. Hence, there is much opportunity for robots to play a role in assisting paediatric rehabilitation. A much more difficult goal to achieve is the development of robots to assist children. At the same time, they do function-related tasks like walking, sitting, lying, and assisting when the child moves from one posture to another. This demand increased complexity throughout the various engineering systems of the robot. After that, a further challenge lies in the robot being able to assist indoors within a relatively safe environment and outdoors where the "lay of the land" is notably different and less predictable. Hence, exploring new technologies to actuate the system and detect children's intentions when they want to move is necessary.

Abbreviations

WHO: World Health Organization; FDA: US Food and Drug Administration; CP: Cerebral palsy; ABI: Acquired brain injury; DMD: Duchenne muscular dystrophy; SMA: Spinal muscular atrophy; SCI: Spinal cord injury; np: Number of papers; ROM: Range of motion; ADL: Activities of daily life; HCI: Human–computer interface; EMG: Electromyography; EEG: Electroencephalogram; LRF: Laser range finder; DOF: Degree of freedom; AC: Alternate current; DC: Direct current; SEA: Serial elastic actuator.

Acknowledgements

Not applicable

Authors' contributions

AG reviewed the literature, wrote the manuscript, and prepared the illustrations. LG, JK, PM contributed to the basic concept of the paper and critically revised the draft paper. All authors read and approved the manuscript.

Funding

Not applicable.

Availability of data and materials

Not applicable.

Declarations

Ethics approval and consent to participate

Not applicable

Consent for publication

Not applicable

Competing interests
The authors declare that they have no competing interests.

Author details
[1]BioDesign Lab, School of Engineering, Computer and Mathematical Sciences, Auckland University of Technology, Auckland, New Zealand. [2]Health and Rehabilitation Research Institute, Auckland University of Technology, Auckland, New Zealand.

Received: 20 April 2021 Accepted: 6 August 2021
Published online: 06 September 2021

References

1. Hall ML, Lobo MA. Design and development of the first exoskeletal garment to enhance arm mobility for children with movement impairments. Assist Technol. 2018;30(5):251–8.
2. Graham HK, Rosenbaum P, Paneth N, Dan B, Lin JP, Damiano DL, et al. Cerebral palsy. Nat Rev Dis Primers. 2016;2:15082.
3. Tsze DS, Valente JH. Pediatric stroke: a review. Emerg Med Int. 2011;2011: 734506.
4. Beretta E, Cesareo A, Biffi E, Schafer C, Galbiati S, Strazzer S. Rehabilitation of upper limb in children with acquired brain injury: a preliminary comparative study. J Healthc Eng. 2018;2018: 4208492.
5. Ryder S, Leadley RM, Armstrong N, Westwood M, de Kock S, Butt T, et al. The burden, epidemiology, costs and treatment for Duchenne muscular dystrophy: an evidence review. Orphanet J Rare Dis. 2017;12(1):79.
6. Robinson MT, Estupinan D. Neuromuscular diseases. In: Creutzfeldt CJ, Kluger BM, Holloway RG, editors. Neuropalliative care. Cham: Springer; 2019. p. 101–15.
7. Thurman DJ. The epidemiology of traumatic brain injury in children and youths: a review of research since 1990. J Child Neurol. 2016;31(1):20–7.
8. Umraw N, Chan Y, Gomez M, Cartotto RC, Fish JS. Effective hand function assessment after burn injuries. J Burn Care Res. 2004;25(1):134–9; discussion 28.
9. Case LE, Apkon SD, Eagle M, Gulyas A, Juel L, Matthews D, et al. Rehabilitation management of the patient with Duchenne muscular dystrophy. Pediatrics. 2018;142(Supplement 2):S17–33.
10. Falzarano V, Marini F, Morasso P, Zenzeri J. Devices and protocols for upper limb robot-assisted rehabilitation of children with neuromotor disorders. Appl Sci. 2019;9(13):2689.
11. Beretta E, Storm FA, Strazzer S, Frascarelli F, Petrarca M, Colazza A, et al. Effect of robot-assisted gait training in a large population of children with motor impairment due to cerebral palsy or acquired brain injury. Arch Phys Med Rehabil. 2020;101(1):106–12.
12. Roberts G, Howard K, Spittle AJ, Brown NC, Anderson PJ, Doyle LW. Rates of early intervention services in very preterm children with developmental disabilities at age 2 years. J Paediatr Child Health. 2008;44(5):276–80.
13. MEDICINE COPE. Management of pediatric trauma. Pediatrics. 2016;138(2):e20161569.
14. McDonald CM, Mercuri E. Evidence-based care in Duchenne muscular dystrophy. Lancet Neurol. 2018;17(5):389–91.
15. Lerner ZF, Harvey TA, Lawson JL. A battery-powered ankle exoskeleton improves gait mechanics in a feasibility study of individuals with cerebral palsy. Ann Biomed Eng. 2019;47(6):1345–56.
16. Abresch RT, Han JJ, Carter GT. Rehabilitation management of neuromuscular disease: the role of exercise training. J Clin Neuromuscul Dis. 2009;11(1):7–21.
17. Patane F, Rossi S, Del Sette F, Taborri J, Cappa P. WAKE-Up exoskeleton to assist children with cerebral palsy: design and preliminary evaluation in level walking. IEEE Trans Neural Syst Rehabil Eng. 2017;25(7):906–16.
18. Shi B, Chen X, Yue Z, Yin S, Weng Q, Zhang X, et al. Wearable ankle robots in post-stroke rehabilitation of gait: a systematic review. Front Neurorobot. 2019;13:63.
19. Low K, editor. Robot-assisted gait rehabilitation: from exoskeletons to gait systems. 2011 Defense Science Research Conference and Expo (DSR); 2011: IEEE.
20. Shishehgar M, Kerr D, Blake J. A systematic review of research into how robotic technology can help older people. Smart Health. 2018;7:1–18.
21. Khan A, Anwar Y, editors. Robots in healthcare: a survey. Science and information conference. Springer; 2019.
22. Martinez-Martin E, Costa A, Cazorla M. PHAROS 2.0—A PHysical assistant RObot system improved. Sensors. 2019;19(20):4531.
23. Lippross S, Jünemann K-P, Osmonov D, Peh S, Alkatout I, Finn J, et al. Robot assisted spinal surgery—a technical report on the use of DaVinci in orthopaedics. J Orthop. 2020;19:50–3.
24. Ona ED, Cano-de la Cuerda R, Sanchez-Herrera P, Balaguer C, Jardon A. A review of robotics in neurorehabilitation: towards an automated process for upper limb. J Healthc Eng. 2018;2018:9758939.
25. SPARC ER. Robotics 2020 Multi-Annual Roadmap for Robotics in Europe, Call 2 ICT24–Horizon 2020. Initial Release B. 2015;15(01):2014.
26. Bützer T, Dittli J, Lieber J, van Hedel HJ, Meyer-Heim A, Lambercy O, et al., editors. PEXO—a pediatric whole hand exoskeleton for grasping assistance in task-oriented training. 2019 IEEE 16th International Conference on Rehabilitation Robotics (ICORR); 2019: IEEE.
27. Shahid T, Gouwanda D, Nurzaman SG, Gopalai AA. Moving toward soft robotics: a decade review of the design of hand exoskeletons. Biomimetics. 2018. https://doi.org/10.3390/biomimetics3030017.
28. Maciejasz P, Eschweiler J, Gerlach-Hahn K, Jansen-Troy A, Leonhardt S. A survey on robotic devices for upper limb rehabilitation. J Neuroeng Rehabil. 2014;11(1):3.
29. del Carmen S-V, Gonzalez-Vargas J, Torricelli D, Moreno JC, Pons JL. Compliant lower limb exoskeletons: a comprehensive review on mechanical design principles. J Neuroeng Rehabil. 2019;16(1):55.

30. Narayan J, Kalita B, Dwivedy SK. Development of robot-based upper limb devices for rehabilitation purposes: a systematic review. Augment Hum Res. 2021;6(1):1–33.
31. Carvalho I, Pinto SM, das Virgens Chagas D, dos Santos JLP, de Sousa Oliveira T, Batista LA. Robotic gait training for individuals with cerebral palsy: a systematic review and meta-analysis. Arch Phys Med Rehabil. 2017;98(11):2332–44.
32. Cook A, Encarnação P, Adams K. Robots: assistive technologies for play, learning and cognitive development. Technol Disabil. 2010;22(3):127–45.
33. Kuo F, Lee H, Hsiao H, Lin J. Robotic-assisted hand therapy for improvement of hand function in children with cerebral palsy: a case series study. Eur J Phys Rehabil Med. 2020. https://doi.org/10.23736/S1973-9087.20.05926-2.
34. Zhang X, Yue Z, Wang J. Robotics in lower-limb rehabilitation after stroke. Behav Neurol. 2017;2017:3731802.
35. Fasoli SE, Ladenheim B, Mast J, Krebs HI. New horizons for robot-assisted therapy in pediatrics. Am J Phys Med Rehabil. 2012;91(11 Suppl 3):S280–9.
36. Hawe RL, Kuczynski AM, Kirton A, Dukelow SP. Assessment of bilateral motor skills and visuospatial attention in children with perinatal stroke using a robotic object hitting task. J Neuroeng Rehabil. 2020;17(1):1–12.
37. Mehrholz J, Thomas S, Werner C, Kugler J, Pohl M, Elsner B. Electromechanical-assisted training for walking after stroke. Cochrane Database Syst Rev. 2017;5: CD006185.
38. Martelli F, Rossi S, Frascarelli F, Germanotta M, Petrarca M, Castelli E, et al., editors. Estimation of multivariable dynamic ankle impedance after botulinum toxin injection in children with cerebral palsy. 2016 IEEE international symposium on medical measurements and applications (MeMeA); 2016: IEEE.
39. Alvarez-Perez MG, Garcia-Murillo MA, Cervantes-Sanchez JJ. Robot-assisted ankle rehabilitation: a review. Disabil Rehabil Assist Technol. 2019. https://doi.org/10.1080/17483107.2019.1578424.
40. McDaid AJ. Design, analysis, and multicriteria optimization of an overground pediatric robotic gait trainer. IEEE/ASME Trans Mechatron. 2017;22(4):1674–84.
41. He Y, Eguren D, Luu TP, Contreras-Vidal JL. Risk management and regulations for lower limb medical exoskeletons: a review. Med Devices Evid Res. 2017;10:89–107.
42. Chu CY, Patterson RM. Soft robotic devices for hand rehabilitation and assistance: a narrative review. J Neuroeng Rehabil. 2018;15(1):9.
43. Veale AJ, Xie SQ. Towards compliant and wearable robotic orthoses: a review of current and emerging actuator technologies. Med Eng Phys. 2016;38(4):317–25.
44. Kapsalyamov A, Hussain S, Jamwal PK. State-of-the-art assistive powered upper limb exoskeletons for elderly. IEEE Access. 2020;8:178991–9001.
45. Yan T, Cempini M, Oddo CM, Vitiello N. Review of assistive strategies in powered lower-limb orthoses and exoskeletons. Robot Auton Syst. 2015;64:120–36.
46. Maalej B, Medhaffar H, Chemori A, Derbel N, editors. A fuzzy sliding mode controller for reducing torques applied to a rehabilitation robot. 2020 17th International multi-conference on systems, signals & devices (SSD); 2020: IEEE.
47. Jribi R, Maalej B, Derbel N. Exoskeletons control via computed torque for lower limb rehabilitation. New trends in robot control. Springer; 2020. p. 131–51.
48. Chen J, Damiano DL, Lerner ZF, Bulea TC, editors. Validating model-based prediction of biological knee moment during walking with an exoskeleton in crouch gait: potential application for exoskeleton control. 2019 IEEE 16th international conference on rehabilitation robotics (ICORR); 2019: IEEE.
49. Narayan J, Dwivedy SK. Towards neuro-fuzzy compensated pid control of lower extremity exoskeleton system for passive gait rehabilitation. IETE J Res. 2020:1–18.
50. Zeng X, Zhu G, Zhang M, Xie SQ. Reviewing clinical effectiveness of active training strategies of platform-based ankle rehabilitation robots. J Healthc Eng. 2018;2018:2858294.
51. Plaza A, Hernandez M, Puyuelo G, Garces E, Garcia E. Lower-limb medical and rehabilitation exoskeletons: a review of the current designs. IEEE Rev Biomed Eng. 2021. https://doi.org/10.1109/RBME.2021.3078001.
52. Fosch-Villaronga E, Čartolovni A, Pierce RL. Promoting inclusiveness in exoskeleton robotics: addressing challenges for pediatric access. Paladyn, J Behav Robot. 2020;11(1):327–39.
53. Onis MD, Onyango AW, Borghi E, Siyam A, Nishida C, Siekmann J. Development of a WHO growth reference for school-aged children and adolescents. Bull World Health Organ. 2007;85:660–7.
54. Keller U, Klamroth V, van Hedel HJ, Riener R, editors. ChARMin: a robot for pediatric arm rehabilitation. 2013 IEEE International conference on robotics and automation; 2013: IEEE.
55. Ganley KJ, Powers CM. Gait kinematics and kinetics of 7-year-old children: a comparison to adults using age-specific anthropometric data. Gait Posture. 2005;21(2):141–5.
56. Borenstein J, Wagner AR, Howard A. Overtrust of pediatric health-care robots: a preliminary survey of parent perspectives. IEEE Robot Autom Mag. 2018;25(1):46–54.
57. Keller U, van Hedel HJA, Klamroth-Marganska V, Riener R. ChARMin: the first actuated exoskeleton robot for pediatric arm rehabilitation. IEEE/ASME Trans Mechatron. 2016;21(5):2201–13.
58. Lobo MA, Hall ML, Greenspan B, Rohloff P, Prosser LA, Smith BA. Wearables for pediatric rehabilitation: how to optimally design and use products to meet the needs of users. Phys Ther. 2019;99(6):647–57.
59. Wessels R, Dijcks B, Soede M, Gelderblom G, De Witte L. Non-use of provided assistive technology devices, a literature overview. Technol Disabil. 2003;15(4):231–8.
60. Liberati A, Altman DG, Tetzlaff J, Mulrow C, Gøtzsche PC, Ioannidis JP, et al. The PRISMA statement for reporting systematic reviews and meta-analyses of studies that evaluate health care interventions: explanation and elaboration. J Clin Epidemiol. 2009;62(10):e1–34.
61. Meyer-Heim A, van Hedel HJ, editors. Robot-assisted and computer-enhanced therapies for children with cerebral palsy: current state and clinical implementation. Semin Pediatr Neurol; 2013. https://doi.org/10.1016/j.spen.2013.06.006.

62. Bayon C, Raya R. Robotic therapies for children with cerebral palsy: a systematic review. Transl Biomed. 2016. https://doi.org/10.21767/2172-0479.100044.
63. Vova JA, Eggebrecht EM. Utilizing functional electrical stimulation and exoskeletons in pediatrics: a closer look at their roles in gait and functional changes in cerebral palsy. Curr Phys Med Rehabil Rep. 2019;7(2):57–66.
64. Zwicker JG, Mayson TA. Effectiveness of treadmill training in children with motor impairments: an overview of systematic reviews. Pediatr Phys Ther. 2010;22(4):361–77.
65. Chen Y-P, Howard AM. Effects of robotic therapy on upper-extremity function in children with cerebral palsy: a systematic review. Dev Neurorehabil. 2016;19(1):64–71.
66. Mahamud F, Anuar A, editors. Usage of robotic rehabilitation technology for lower limbs therapy of children with cerebral palsy-a review. 2014 IEEE international symposium on robotics and manufacturing automation (ROMA); 2014: IEEE.
67. Donenberg JG, Fetters L, Johnson R. The effects of locomotor training in children with spinal cord injury: a systematic review. Dev Neurorehabil. 2019;22(4):272–87.
68. Andrew I, Batavia J, Guy SH. Toward the development of consumer-based criteria for the evaluation of assistive devices. J Rehabil Res Dev. 1990;27(4):425.
69. Weightman APH, Preston N, Holt R, Allsop M, Levesley M, Bhakta B. Engaging children in healthcare technology design: developing rehabilitation technology for children with cerebral palsy. J Eng Des. 2009;21(5):579–600.
70. Organization WH. International classification of functioning, disability, and health: children & youth version: ICF-CY: World Health Organization; 2007.
71. Eguren D, Cestari M, Luu TP, Kilicarslan A, Steele A, Contreras-Vidal JL, editors. Design of a customizable, modular pediatric exoskeleton for rehabilitation and mobility. 2019 IEEE international conference on systems, man and cybernetics (SMC); 2019: IEEE.
72. Rossi S, Colazza A, Petrarca M, Castelli E, Cappa P, Krebs HI. Feasibility study of a wearable exoskeleton for children: is the gait altered by adding masses on lower limbs? PLoS ONE. 2013. https://doi.org/10.1371/journal.pone.0073139.
73. Lerner ZF, Gasparri GM, Bair MO, Lawson JL, Luque J, Harvey TA, et al. An untethered ankle exoskeleton improves walking economy in a pilot study of individuals with cerebral palsy. IEEE Trans Neural Syst Rehabil Eng. 2018;26(10):1985–93.
74. Yamada T, Kadone H, Shimizu Y, Suzuki K, editors. An exoskeleton brake unit for children with crouch gait supporting the knee joint during stance. 2018 International symposium on micro-nanomechatronics and human science (MHS); 2018: IEEE.
75. Michmizos KP, Krebs HI. Pediatric robotic rehabilitation: Current knowledge and future trends in treating children with sensorimotor impairments. NeuroRehabilitation. 2017;41(1):69–76.
76. Hall ML, Orzada BT. Expressive prostheses: meaning and significance. Fash Pract. 2013;5(1):9–32.
77. Schuler T, Brütsch K, Müller R, van Hedel HJ, Meyer-Heim A. Virtual realities as motivational tools for robotic assisted gait training in children: a surface electromyography study. NeuroRehabilitation. 2011;28(4):401–11.
78. Bulea TC, Lerner ZF, Gravunder AJ, Damiano DL, editors. Exergaming with a pediatric exoskeleton: facilitating rehabilitation and research in children with cerebral palsy. 2017 International Conference on Rehabilitation Robotics (ICORR); 2017: IEEE.
79. Frascarelli F, Masia L, Di Rosa G, Petrarca M, Cappa P, Castelli E. Robot-mediated and clinical scales evaluation after upper limb botulinum toxin type A injection in children with hemiplegia. J Rehabil Med. 2009;41(12):988–94.
80. Marini F, Squeri V, Morasso P, Campus C, Konczak J, Masia L. Robot-aided developmental assessment of wrist proprioception in children. J Neuroeng Rehabil. 2017;14(1):3.
81. Dehem S, Gilliaux M, Lejeune T, Detrembleur C, Galinski D, Sapin J, et al. Assessment of upper limb spasticity in stroke patients using the robotic device REAplan. J Rehabil Med. 2017;49(7):565–71.
82. Kuczynski AM, Kirton A, Semrau JA, Dukelow SP. Bilateral reaching deficits after unilateral perinatal ischemic stroke: a population-based case-control study. J Neuroeng Rehabil. 2018;15(1):77.
83. Varalta V, Picelli A, Fonte C, Montemezzi G, La Marchina E, Smania N. Effects of contralesional robot-assisted hand training in patients with unilateral spatial neglect following stroke: a case series study. J Neuroeng Rehabil. 2014;11(1):160.
84. Shimizu Y, Kadone H, Kubota S, Ueno T, Sankai Y, Hada Y, et al. Voluntary elbow extension-flexion using single joint hybrid assistive limb (HAL) for patients of spastic cerebral palsy: two cases report. Front Neurol. 2019;10:2.
85. Thielbar KO, Lord TJ, Fischer HC, Lazzaro EC, Barth KC, Stoykov ME, et al. Training finger individuation with a mechatronic-virtual reality system leads to improved fine motor control post-stroke. J Neuroeng Rehabil. 2014;11(1):171.
86. Tornberg AB, Lauruschkus K. Non-ambulatory children with cerebral palsy: effects of four months of static and dynamic standing exercise on passive range of motion and spasticity in the hip. PeerJ. 2020;8: e8561.
87. Volpini M, Bartenbach V, Pinotti M, Riener R. Clinical evaluation of a low-cost robot for use in physiotherapy and gait training. J Rehabil Assist Technol Eng. 2017;4: 2055668316688410.
88. Wu M, Kim J, Arora P, Gaebler-Spira DJ, Zhang Y. Kinematic and EMG responses to pelvis and leg assistance force during treadmill walking in children with cerebral palsy. Neural Plast. 2016;2016:5020348.
89. Chrif F, Nef T, Lungarella M, Dravid R, Hunt KJ. Control design for a lower-limb paediatric therapy device using linear motor technology. Biomed Signal Process Control. 2017;38:119–27.
90. Ricklin S, Meyer-Heim A, van Hedel HJA. Dual-task training of children with neuromotor disorders during robot-assisted gait therapy: prerequisites of patients and influence on leg muscle activity. J Neuroeng Rehabil. 2018;15(1):82.
91. Nakagawa S, Mutsuzaki H, Mataki Y, Endo Y, Matsuda M, Yoshikawa K, et al. Newly developed hybrid assistive limb for pediatric patients with cerebral palsy: a case report. J Phys Ther Sci. 2019;31(8):702–7.
92. Aycardi LF, Cifuentes CA, Munera M, Bayon C, Ramirez O, Lerma S, et al. Evaluation of biomechanical gait parameters of patients with cerebral palsy at three different levels of gait assistance using the CPWalker. J Neuroeng Rehabil. 2019;16(1):15.

93. Germanotta M, Taborri J, Rossi S, Frascarelli F, Palermo E, Cappa P, et al. Spasticity measurement based on tonic stretch reflex threshold in children with cerebral palsy using the PediAnklebot. Front Hum Neurosci. 2017;11:277.
94. Chen K, Xiong B, Ren Y, Dvorkin AY, Gaebler-Spira D, Sisung CE, et al. Ankle passive and active movement training in children with acute brain injury using a wearable robot. J Rehabil Med. 2018;50(1):30–6.
95. Lerner ZF, Damiano DL, Bulea TC. The effects of exoskeleton assisted knee extension on lower-extremity gait kinematics, kinetics, and muscle activity in children with cerebral palsy. Sci Rep. 2017;7(1):1–12.
96. Jansen M, de Groot IJ, van Alfen N, Geurts AC. Physical training in boys with Duchenne muscular dystrophy: the protocol of the no use is disuse study. BMC Pediatr. 2010;10(1):55.
97. Wu M, Landry JM. Toward flexible assistance for locomotor training: design and clinical testing of a cable-driven robot for stroke, spinal cord injury, and cerebral palsy. In: Reinkensmeyer DJ, Dietz V, editors. Neurorehabilitation technology. Cham: Springer; 2016. p. 435–59.
98. Krebs HI, Michmizos KP, Monterosso L, Mast J, editors. Pediatric anklebot: pilot clinical trial. 2016 6th IEEE international conference on biomedical robotics and biomechatronics (BioRob); 2016: IEEE.
99. Keller U, Riener R, editors. Design of the pediatric arm rehabilitation robot ChARMin. 5th IEEE RAS/EMBS international conference on biomedical robotics and biomechatronics; 2014: IEEE.
100. Lerner ZF, Damiano DL, Park HS, Gravunder AJ, Bulea TC. A robotic exoskeleton for treatment of crouch gait in children with cerebral palsy: design and initial application. IEEE Trans Neural Syst Rehabil Eng. 2017;25(6):650–9.
101. Gasparri GM, Bair MO, Libby RP, Lerner ZF, editors. Verification of a robotic ankle exoskeleton control scheme for gait assistance in individuals with cerebral palsy. 2018 IEEE/RSJ international conference on intelligent robots and systems (IROS); 2018: IEEE.
102. Kang J, Martelli D, Vashista V, Martinez-Hernandez I, Kim H, Agrawal SK. Robot-driven downward pelvic pull to improve crouch gait in children with cerebral palsy. Sci Robot. 2017;2(8): eaan2634.
103. Vashista V, Jin X, Agrawal SK, editors. Active tethered pelvic assist device (a-tpad) to study force adaptation in human walking. 2014 IEEE international conference on robotics and automation (ICRA); 2014: IEEE.
104. Xiong H, Diao X. A review of cable-driven rehabilitation devices. Disabil Rehabil Assist Technol. 2020;15(8):885–97.
105. Cestari M, Sanz-Merodio D, Garcia E. A new and versatile adjustable rigidity actuator with add-on locking mechanism (ARES-XL). Actuators. 2018;7(1):1.
106. Sanz-Merodio D, Cestari M, Arevalo JC, Garcia E, editors. A lower-limb exoskeleton for gait assistance in quadriplegia. 2012 IEEE international conference on robotics and biomimetics (ROBIO); 2012.
107. Borboni A, Mor M, Faglia R. Gloreha—hand robotic rehabilitation: design, mechanical model, and experiments. J Dyn Syst Meas Control. 2016;138(11).
108. Mirvakili SM, Hunter IW. Artificial muscles: mechanisms, applications, and challenges. Adv. Mater. 2018;30(6):1704407.
109. Zhang J, Sheng J, ONeill CT, Walsh CJ, Wood RJ, Ryu JH, et al. Robotic artificial muscles: current progress and future perspectives. IEEE transactions on robotics. 2019.
110. Wirekoh J, Valle L, Pol N, Park YL. Sensorized, flat, pneumatic artificial muscle embedded with biomimetic microfluidic sensors for proprioceptive feedback. Soft Robot. 2019;6(6):768–77.
111. Ugurlu B, Forni P, Doppmann C, Sariyildiz E, Morimoto J. Stable control of force, position, and stiffness for robot joints powered via pneumatic muscles. IEEE Trans Industr Inf. 2019;15(12):6270–9.
112. Cioi D, Kale A, Burdea G, Engsberg J, Janes W, Ross S, editors. Ankle control and strength training for children with cerebral palsy using the Rutgers Ankle CP. 2011 IEEE international conference on rehabilitation robotics; 2011: IEEE.
113. McCall JV, Ludovice MC, Blaylock JA, Kamper DG, editors. A platform for rehabilitation of finger individuation in children with hemiplegic cerebral palsy. 2019 IEEE 16th international conference on rehabilitation robotics (ICORR); 2019: IEEE.
114. Yazici M, Livanelioglu A, Gucuyener K, Tekin L, Sumer E, Yakut Y. Effects of robotic rehabilitation on walking and balance in pediatric patients with hemiparetic cerebral palsy. Gait Posture. 2019;70:397–402.
115. Wu YN, Hwang M, Ren Y, Gaebler-Spira D, Zhang LQ. Combined passive stretching and active movement rehabilitation of lower-limb impairments in children with cerebral palsy using a portable robot. Neurorehabil Neural Repair. 2011;25(4):378–85.
116. Kuczynski AM, Carlson HL, Lebel C, Hodge JA, Dukelow SP, Semrau JA, et al. Sensory tractography and robot-quantified proprioception in hemiparetic children with perinatal stroke. Hum Brain Mapp. 2017;38(5):2424–40.
117. Cherni Y, Girardin-Vignola G, Ballaz L, Begon M. Reliability of maximum isometric hip and knee torque measurements in children with cerebral palsy using a paediatric exoskeleton–Lokomat. Neurophysiol Clin. 2019;49(4):335–42.
118. Michmizos KP, Rossi S, Castelli E, Cappa P, Krebs HI. Robot-aided neurorehabilitation: a pediatric robot for ankle rehabilitation. IEEE Trans Neural Syst Rehabil Eng. 2015;23(6):1056–67.
119. Marini F, Hughes CML, Squeri V, Doglio L, Moretti P, Morasso P, et al. Robotic wrist training after stroke: adaptive modulation of assistance in pediatric rehabilitation. Robot Auton Syst. 2017;91:169–78.
120. Conner BC, Luque J, Lerner ZF. Adaptive ankle resistance from a wearable robotic device to improve muscle recruitment in cerebral palsy. Ann Biomed Eng. 2020;48(4):1309–21.
121. Qiu Q, Adamovich S, Saleh S, Lafond I, Merians AS, Fluet GG, editors. A comparison of motor adaptations to robotically facilitated upper extremity task practice demonstrated by children with cerebral palsy and adults with stroke. 2011 IEEE international conference on rehabilitation robotics; 2011: IEEE.
122. Nizamis K, Stienen AHA, Kamper DG, Keller T, Plettenburg DH, Rouse EJ, et al. Transferrable expertise from bionic arms to robotic exoskeletons: perspectives for stroke and duchenne muscular dystrophy. IEEE Trans Med Robot Bionics. 2019;1(2):88–96.
123. Chandrasiri M, Ranaweera R, Gopura R, editors. Development of a surface muscle pressure monitoring system for wearable robotic devices. 2019 Moratuwa engineering research conference (MERCon); 2019: IEEE.
124. Qiu Q, Ramirez DA, Saleh S, Fluet GG, Parikh HD, Kelly D, et al. The New Jersey Institute of Technology Robot-Assisted Virtual Rehabilitation (NJIT-RAVR) system for children with cerebral palsy: a feasibility study. J Neuroeng Rehabil. 2009;6:40.

125. Zhu TL, Klein J, Dual SA, Leong TC, Burdet E, editors. reachMAN2: a compact rehabilitation robot to train reaching and manipulation. 2014 IEEE/RSJ international conference on intelligent robots and systems; 2014: IEEE.
126. Krebs HI, Hogan N, Aisen ML, Volpe BT. Robot-aided neurorehabilitation. IEEE Trans Rehabil Eng. 1998;6(1):75–87.
127. Molteni F, Gasperini G, Gaffuri M, Colombo M, Giovanzana C, Lorenzon C, et al. Wearable robotic exoskeleton for overground gait training in sub-acute and chronic hemiparetic stroke patients: preliminary results. Eur J Phys Rehabil Med. 2017;53(5):676–84.
128. Taborri J, Rossi S, Palermo E, Cappa P, editors. A HMM distributed classifier to control robotic knee module of an active orthosis. 2015 IEEE international conference on rehabilitation robotics (ICORR); 2015: IEEE.
129. Suzuki K, Mito G, Kawamoto H, Hasegawa Y, Sankai Y. Intention-based walking support for paraplegia patients with Robot Suit HAL. Adv Robot. 2007;21(12):1441–69.
130. Lopez NM, de Diego N, Hernandez R, Perez E, Ensinck G, Valentinuzzi ME. Customized device for pediatric upper limb rehabilitation in obstetric brachial palsy. Am J Phys Med Rehabil. 2014;93(3):263–6.
131. Bobrov P, Biryukova E, Polyaev B, Lajsheva O, Usachjova E, Sokolova A, et al. Rehabilitation of patients with cerebral palsy using hand exoskeleton controlled by brain–computer interface. Bull Russ State Med Univ. 2020. https://doi.org/10.24075/brsmu.2020.047.
132. Bulea TC, Lerner ZF, Damiano DL, editors. Repeatability of EMG activity during exoskeleton assisted walking in children with cerebral palsy: implications for real time adaptable control. 2018 40th Annual international conference of the IEEE engineering in medicine and biology society (EMBC); 2018: IEEE.
133. Digiacomo F, Tamburin S, Tebaldi S, Pezzani M, Tagliaferro M, Casale R, et al. Improvement of motor performance in children with cerebral palsy treated with exoskeleton robotic training: a retrospective explorative analysis. Restor Neurol Neurosci. 2019;37(3):239–44.
134. Wu M, Kim J, Arora P, Gaebler-Spira DJ, Zhang Y. Effects of the integration of dynamic weight shifting training into treadmill training on walking function of children with cerebral palsy: a randomized controlled study. Am J Phys Med Rehabil. 2017;96(11):765–72.
135. Lee SJ, Jin D, Kang SH, Gaebler-Spira D, Zhang LQ. Combined ankle/knee stretching and pivoting stepping training for children with cerebral palsy. IEEE Trans Neural Syst Rehabil Eng. 2019;27(9):1743–52.
136. Bayon C, Martin-Lorenzo T, Moral-Saiz B, Ramirez O, Perez-Somarriba A, Lerma-Lara S, et al. A robot-based gait training therapy for pediatric population with cerebral palsy: goal setting, proposal and preliminary clinical implementation. J Neuroeng Rehabil. 2018;15(1):69.
137. Burdea GC, Cioi D, Kale A, Janes WE, Ross SA, Engsberg JR. Robotics and gaming to improve ankle strength, motor control, and function in children with cerebral palsy—a case study series. IEEE Trans Neural Syst Rehabil Eng. 2013;21(2):165–73.
138. Druzbicki M, Rusek W, Snela S, Dudek J, Szczepanik M, Zak E, et al. Functional effects of robotic-assisted locomotor treadmill thearapy in children with cerebral palsy. J Rehabil Med. 2013;45(4):358–63.
139. Gilliaux M, Renders A, Dispa D, Holvoet D, Sapin J, Dehez B, et al. Upper limb robot-assisted therapy in cerebral palsy: a single-blind randomized controlled trial. Neurorehabil Neural Repair. 2015;29(2):183–92.
140. Fasoli SE, Fragala-Pinkham M, Hughes R, Krebs HI, Hogan N, Stein J. Robotic therapy and botulinum toxin type A: a novel intervention approach for cerebral palsy. Am J Phys Med Rehabil. 2008;87(12):1022–6.
141. Beretta E, Molteni E, Biffi E, Morganti R, Avantaggiato P, Strazzer S. Robotically-driven orthoses exert proximal-to-distal differential recovery on the lower limbs in children with hemiplegia, early after acquired brain injury. Eur J Paediatr Neurol. 2018;22(4):652–61.
142. Marini F, Squeri V, Cappello L, Morasso P, Riva A, Doglio L, et al., editors. Adaptive wrist robot training in pediatric rehabilitation. 2015 IEEE international conference on rehabilitation robotics (ICORR); 2015: IEEE.
143. Molteni E, Beretta E, Altomonte D, Formica F, Strazzer S, editors. Combined robotic-aided gait training and 3D gait analysis provide objective treatment and assessment of gait in children and adolescents with Acquired Hemiplegia. 2015 37th Annual international conference of the IEEE Engineering in Medicine And Biology Society (EMBC); 2015: IEEE.
144. Beretta E, Romei M, Molteni E, Avantaggiato P, Strazzer S. Combined robotic-aided gait training and physical therapy improve functional abilities and hip kinematics during gait in children and adolescents with acquired brain injury. Brain Inj. 2015;29(7–8):955–62.
145. Jansen M, van Alfen N, Geurts AC, de Groot IJ. Assisted bicycle training delays functional deterioration in boys with Duchenne muscular dystrophy: the randomized controlled trial "no use is disuse." Neurorehabil Neural Repair. 2013;27(9):816–27.
146. Sanz-Merodio D, Puyuelo G, Ganguly A, Garces E, Goñi A, Garcia E. EXOtrainer project clinical evaluation of gait training with exoskeleton in children with spinal muscular atrophy. Advances in robotics research: from lab to market: Springer; 2020. p. 211–27.
147. Ganguly A, Sanz-Merodio D, Puyuelo G, Goñi A, Garces E, Garcia E, editors. Wearable pediatric gait exoskeleton-a feasibility study. 2018 IEEE/RSJ international conference on intelligent robots and systems (IROS); 2018: IEEE.
148. Garcia E, Sancho J, Sanz-Merodio D, Prieto M, editors. Atlas 2020: the pediatric gait exoskeleton project. human-centric robotics-proceedings of the 20th international conference clawar 2017; 2017: World Scientific.
149. Koo B, Montes J, Gamarnik V, Yeager K, Marra J, Dunaway S, et al., editors. Design and evaluation of a hybrid passive and active gravity neutral orthosis (GNO). 2009 Annual international conference of the IEEE engineering in medicine and biology society; 2009: IEEE.
150. Samhan AF, Abdelhalim NM, Elnaggar RK. Effects of interactive robot-enhanced hand rehabilitation in treatment of paediatric hand-burns: a randomized, controlled trial with 3-months follow-up. Burns. 2020;46(6):1347–55.
151. Hornby TG, Zemon DH, Campbell D. Robotic-assisted, body-weight–supported treadmill training in individuals following motor incomplete spinal cord injury. Phys Ther. 2005;85(1):52–66.
152. Chaparro-Rico BD, Cafolla D, Ceccarelli M, Castillo-Castaneda E. NURSE-2 DoF device for arm motion guidance: kinematic, dynamic, and FEM analysis. Appl Sci. 2020;10(6):2139.

153. Cleary K, Monfaredi R, Salvador T, Talari HF, Coley C, Kovelman S, et al., editors. Pedbothome: robotically-assisted ankle rehabilitation system for children with cerebral palsy. 2019 IEEE 16th international conference on rehabilitation robotics (ICORR); 2019: IEEE.
154. Bayón C, Ramírez O, Serrano JI, Castillo MDD, Pérez-Somarriba A, Belda-Lois JM, et al. Development and evaluation of a novel robotic platform for gait rehabilitation in patients with cerebral palsy: CPWalker. Robot Auton Syst. 2017;91:101–14.
155. Kapeller A, Nagenborg MH, Nizamis K. Wearable robotic exoskeletons: a socio-philosophical perspective on Duchenne muscular dystrophy research. Paladyn, J Behav Robot. 2020;11(1):404–13.
156. Zhu H, Doan J, Stence C, Lv G, Elery T, Gregg R, editors. Design and validation of a torque dense, highly back-drivable powered knee-ankle orthosis. 2017 IEEE international conference on robotics and automation (ICRA); 2017: IEEE.
157. Krishnan C, Ranganathan R, Dhaher YY, Rymer WZ. A pilot study on the feasibility of robot-aided leg motor training to facilitate active participation. PLoS ONE. 2013;8(10): e77370.
158. Heung HL, Tang ZQ, Shi XQ, Tong KY, Li Z. Soft rehabilitation actuator with integrated post-stroke finger spasticity evaluation. Front Bioeng Biotechnol. 2020;8:111.
159. Yang HD, Cooper M, Akbas T, Schumm L, Orzel D, Walsh CJ, editors. A soft inflatable wearable robot for hip abductor assistance: design and preliminary assessment. 2020 8th IEEE RAS/EMBS international conference for biomedical robotics and biomechatronics (BioRob): IEEE.
160. Copaci D, Martín F, Moreno L, Blanco D. SMA based elbow exoskeleton for rehabilitation therapy and patient evaluation. IEEE Access. 2019;7:31473–84.
161. Behboodi A, DeSantis C, Lubsen J, Lee S, editors. A mechanized pediatric elbow joint powered by a de-based artificial skeletal muscle. 2020 42nd annual international conference of the IEEE Engineering in Medicine & Biology Society (EMBC); 2020: IEEE.
162. Saharan L, de Andrade MJ, Saleem W, Baughman RH, Tadesse Y. iGrab: hand orthosis powered by twisted and coiled polymer muscles. Smart Mater Struct. 2017;26(10): 105048.
163. Chu W-S, Lee K-T, Song S-H, Han M-W, Lee J-Y, Kim H-S, et al. Review of biomimetic underwater robots using smart actuators. Int J Precis Eng Manuf. 2012;13(7):1281–92.
164. Aurich-Schuler T, Grob F, van Hedel HJA, Labruyere R. Can Lokomat therapy with children and adolescents be improved? An adaptive clinical pilot trial comparing guidance force, path control, and FreeD. J Neuroeng Rehabil. 2017;14(1):76.
165. Aurich-Schuler T, Labruyère R. An increase in kinematic freedom in the lokomat is related to the ability to elicit a physiological muscle activity pattern: a secondary data analysis investigating differences between guidance force, path control, and FreeD. Front Robot AI. 2019;6:109.
166. Gallagher J, Preston N, Holt R, Mon-Williams M, Levesley M, Weightman A, editors. Assessment of upper limb movement with an autonomous robotic device in a school environment for children with Cerebral Palsy. 2015 IEEE international conference on rehabilitation robotics (ICORR); 2015: IEEE.
167. Sanz-Merodio D, Sancho J, Pérez M, García E. Control architecture of the ATLAS 2020 lower-limb active orthosis. In: Advances in cooperative robotics. World Scientific; 2017. p. 860–8.
168. Wu M, Kim J, Gaebler-Spira DJ, Schmit BD, Arora P. Robotic resistance treadmill training improves locomotor function in children with cerebral palsy: a randomized controlled pilot study. Arch Phys Med Rehabil. 2017;98(11):2126–33.
169. Elias A, Frizera A, Bastos TF, Valadão C, editors. Robotic walkers from a clinical point of view: feature-based classification and proposal of the UFES Walker. 2012 ISSNIP biosignals and biorobotics conference: biosignals and robotics for better and safer living (BRC); 2012: IEEE.
170. Aurich-Schuler T, Warken B, Graser JV, Ulrich T, Borggraefe I, Heinen F, et al. Practical recommendations for robot-assisted treadmill therapy (lokomat) in children with cerebral palsy: indications, goal setting, and clinical implementation within the WHO-ICF framework. Neuropediatrics. 2015;46(4):248–60.
171. Rinaldi M, Petrarca M, Romano A, Vasco G, D'Anna C, Schmid M, et al., editors. EMG-based indicators of muscular co-activation during gait in children with duchenne muscular dystrophy. 2019 41st Annual international conference of the IEEE Engineering in Medicine and Biology Society (EMBC); 2019: IEEE.
172. Larina N, Nacharova M, Korsunskaya L, Vlasenko S, Pavlenko V. Changes in EEG patterns in the α-frequency band following BCI-based therapy in children with cerebral palsy. Bull Russ State Med Univ. 2020;(4):41–6.
173. Struijk LNA, Bentsen B, Gaihede M, Lontis ER. Error-free text typing performance of an inductive intra-oral tongue computer interface for severely disabled individuals. IEEE Trans Neural Syst Rehabil Eng. 2017;25(11):2094–104.
174. Johansen D, Popovic DB, Dosen S, Struijk LNA. Hybrid tongue-myoelectric control improves functional use of a robotic hand prosthesis. IEEE Trans Biomed Eng. 2021;68(6):2011–20.
175. Aubin PM, Sallum H, Walsh C, Stirling L, Correia A, editors. A pediatric robotic thumb exoskeleton for at-home rehabilitation: the Isolated Orthosis for Thumb Actuation (IOTA). 2013 IEEE 13th International conference on rehabilitation robotics (ICORR); 2013: IEEE.
176. Laubscher CA, Sawicki JT, editors. Gait guidance control for damping of unnatural motion in a powered pediatric lower-limb orthosis. 2019 IEEE 16th international conference on rehabilitation robotics (ICORR); 2019: IEEE.
177. Sancho-Perez J, Perez M, Garcia E, Sanz-Merodio D, Plaza A, Cestari M. Mechanical description of ATLAS 2020, A 10-DOF paediatric exoskeleton. Advances in cooperative robotics. World Scientific; 2017. p. 814–22.
178. Ladenheim B, Altenburger P, Cardinal R, Monterroso L, Dierks T, Mast J, et al. The effect of random or sequential presentation of targets during robot-assisted therapy on children. NeuroRehabilitation. 2013;33(1):25–31.
179. Masia L, Casadio M, Giannoni P, Sandini G, Morasso P. Performance adaptive training control strategy for recovering wrist movements in stroke patients: a preliminary, feasibility study. J Neuroeng Rehabil. 2009;6:44.

180. Fluet GG, Qiu Q, Saleh S, Ramirez D, Adamovich S, Kelly D, et al., editors. Robot-assisted virtual rehabilitation (NJIT-RAVR) system for children with upper extremity hemiplegia. 2009 virtual rehabilitation international conference; 2009: IEEE.
181. Sale P, Lombardi V, Franceschini M. Hand robotics rehabilitation: feasibility and preliminary results of a robotic treatment in patients with hemiparesis. Stroke Res Treat. 2012;2012:820931.
182. Gilliaux M, Lejeune T, Detrembleur C, Sapin J, Dehez B, Stoquart G. A robotic device as a sensitive quantitative tool to assess upper limb impairments in stroke patients: a preliminary prospective cohort study. J Rehabil Med. 2012;44(3):210–7.
183. Koenig A, Keller U, Pfluger K, Meyer-Heim A, Riener R, editors. PASCAL: Pediatric arm support robot for combined arm and leg training. 2012 4th IEEE RAS & EMBS international conference on biomedical robotics and biomechatronics (BioRob); 2012: IEEE.
184. Keller U, Rauter G, Riener R, editors. Assist-as-needed path control for the PASCAL rehabilitation robot. 2013 IEEE 13th international conference on rehabilitation robotics (ICORR); 2013: IEEE.
185. Tong LZ, Ong HT, Tan JX, Lin J, Burdet E, Ge S, et al., editors. Pediatric rehabilitation with the reachMAN's modular handle. 2015 37th Annual international conference of the IEEE engineering in medicine and biology society (EMBC); 2015: IEEE.
186. Scott SH. Apparatus for measuring and perturbing shoulder and elbow joint positions and torques during reaching. J Neurosci Methods. 1999;89(2):119–27.
187. Holley D, Johnson M, Harris G, Beardsley S, editors. A modular low-clearance wrist orthosis for improving wrist motion in children with cerebral palsy. 2014 36th Annual international conference of the IEEE engineering in medicine and biology society; 2014: IEEE.
188. Hesse S, Uhlenbrock D. A mechanized gait trainer for restoration of gait. J Rehabil Res Dev. 2000;37(6):701–8.
189. Smania N, Bonetti P, Gandolfi M, Cosentino A, Waldner A, Hesse S, et al. Improved gait after repetitive locomotor training in children with cerebral palsy. Am J Phys Med Rehabil. 2011;90(2):137–49.
190. Muraki S, Ehara Y, Yamasaki M. Cardiovascular responses at the onset of passive leg cycle exercise in paraplegics with spinal cord injury. Eur J Appl Physiol. 2000;81(4):271–4.
191. Damiano DL, Stanley CJ, Ohlrich L, Alter KE. Task-specific and functional effects of speed-focused elliptical or motor-assisted cycle training in children with bilateral cerebral palsy: randomized clinical trial. Neurorehabil Neural Repair. 2017;31(8):736–45.
192. Zhang LQ, Chung SG, Bai Z, Xu D, van Rey EM, Rogers MW, et al. Intelligent stretching of ankle joints with contracture/spasticity. IEEE Trans Neural Syst Rehabil Eng. 2002;10(3):149–57.
193. Chen K, Wu YN, Ren Y, Liu L, Gaebler-Spira D, Tankard K, et al. Home-based versus laboratory-based robotic ankle training for children with cerebral palsy: a pilot randomized comparative trial. Arch Phys Med Rehabil. 2016;97(8):1237–43.
194. Schmidt-Lucke C, Kaferle J, Rydh Berner BM, Ahlborg L, Hansen HM, Skjellvik Tollefsen U, et al. Effect of assisted walking-movement in patients with genetic and acquired neuromuscular disorders with the motorised Innowalk device: an international case study meta-analysis. PeerJ. 2019;7: e7098.
195. Wang F-C, Yu C-H, Chou T-Y. Design and implementation of robust controllers for a gait trainer. Proc Inst Mech Eng [H]. 2009;223(6):687–96.
196. Wu M, Hornby TG, Landry JM, Roth H, Schmit BD. A cable-driven locomotor training system for restoration of gait in human SCI. Gait Posture. 2011;33(2):256–60.
197. Nelson CA, Burnfield JM, Shu Y, Buster TW, Taylor AP, Graham A. Modified elliptical machine motor-drive design for assistive gait rehabilitation. J Med Devices. 2011. https://doi.org/10.1115/1.4003693.
198. Burnfield JM, Buster TW, Pfeifer CM, Irons SL, Cesar GM, Nelson CA. Adapted motor-assisted elliptical for rehabilitation of children with physical disabilities. J Med Devices. 2019; https://doi.org/10.1115/1.4041588.
199. Girone M, Burdea G, Bouzit M, editors. The Rutgers ankle orthopedic rehabilitation interface. Proceedings of the ASME haptics symposium; 1999: DSC.
200. Ren Y, Lee SJ, Park HS, Zhang LQ. A pivoting elliptical training system for improving pivoting neuromuscular control and rehabilitating musculoskeletal injuries. IEEE Trans Neural Syst Rehabil Eng. 2013;21(5):860–8.
201. Monfaredi R, Evans S, Coley C, Silverman A, Jain A, Wilson E, et al., editors. Robotically assisted ankle rehabilitation for pediatrics. 2016 6th IEEE international conference on biomedical robotics and biomechatronics (BioRob); 2016: IEEE.
202. Park EJ, Kang J, Su H, Stegall P, Miranda DL, Hsu W-H, et al., editors. Design and preliminary evaluation of a multi-robotic system with pelvic and hip assistance for pediatric gait rehabilitation. 2017 International conference on rehabilitation robotics (ICORR); 2017: IEEE.
203. B. Maalej, R. Jribi, N. Ayadi, F. Abdelhedi, N. Derbel. On a robotic application for rehabilitation systems dedicated to kids affected by cerebral palsy. 2018 15th International multi-conference on systems, signals & devices (SSD). 2018:414–9.
204. Meyer-Heim A, Borggraefe I, Ammann-Reiffer C, Berweck S, Sennhauser F, Colombo G, et al. Feasibility of robotic-assisted locomotor training in children with central gait impairment. Dev Med Child Neurol. 2007;49(12):900–6.
205. Kawasaki S, Ohata K, Yoshida T, Yokoyama A, Yamada S. Gait improvements by assisting hip movements with the robot in children with cerebral palsy: a pilot randomized controlled trial. J Neuroeng Rehabil. 2020;17(1):1–8.
206. Tanaka N, Matsushita S, Sonoda Y, Maruta Y, Fujitaka Y, Sato M, et al. Effect of stride management assist gait training for poststroke hemiplegia: a single center, open-label, randomized controlled trial. J Stroke Cerebrovasc Dis. 2019;28(2):477–86.
207. Smania N, Gandolfi M, Marconi V, Calanca A, Geroin C, Piazza S, et al. Applicability of a new robotic walking aid in a patient with cerebral palsy. Eur J Phys Rehabil Med. 2011;147(2):135–40.
208. Karunakaran KK, Ehrenberg N, Cheng J, Nolan KJ, editors. Effects of robotic exoskeleton gait training on an adolescent with brain injury. 2019 41st Annual international conference of the IEEE engineering in medicine and biology society (EMBC); 2019: IEEE.

209. Lee DR, Shin YK, Park J-H, You JH. Concurrent validity and test-retest reliability of the walkbot-K system for robotic gait training. J Mech Med Biol. 2016;16(08):1640029.
210. Jin LH, Yang S-S, Choi JY, Sohn MK. The effect of robot-assisted gait training on locomotor function and functional capability for daily activities in children with cerebral palsy: a single-blinded, randomized cross-over trial. Brain Sci. 2020;10(11):801.
211. Erbil D, Tugba G, Murat TH, Melike A, Merve A, Cagla K, et al. Effects of robot-assisted gait training in chronic stroke patients treated by botulinum toxin-a: a pivotal study. Physiotherapy Res Int. 2018;23(3): e1718.
212. Sucuoglu H. Effects of robot-assisted gait training alongside conventional therapy on the development of walking in children with cerebral palsy. J Pediatr Rehabil Med. 2020;13(2):127–35.
213. Mileti I, Taborri J, Rossi S, Petrarca M, Patanè F, Cappa P, editors. Evaluation of the effects on stride-to-stride variability and gait asymmetry in children with cerebral palsy wearing the WAKE-up ankle module. 2016 IEEE International symposium on medical measurements and applications (MeMeA); 2016: IEEE.
214. Cornejo JL, Santana JF, Salinas SA, editors. Exoskeleton for gait rehabilitation of children: conceptual design. 2017 International conference on rehabilitation robotics (ICORR); 2017: IEEE.
215. Ren Y, Wu YN, Yang CY, Xu T, Harvey RL, Zhang LQ. Developing a wearable ankle rehabilitation robotic device for in-bed acute stroke rehabilitation. IEEE Trans Neural Syst Rehabil Eng. 2017;25(6):589–96.
216. Sanz-Merodio D, Perez M, Prieto M, Sancho J, Garcia E, editors. Result of clinical trials with children with spinal muscular atrophy using the atlas 2020 Lower-limb active orthosis2017: World Scientific; 2017.
217. Medina-De-La-Cruz M, Mujaico-Mariano A, Tirado-Mendoza G, editors. Implementation of a mechanical-electronic system for children from 7 to 11 years old with Duchenne muscular dystrophy. 2018 IEEE XXV international conference on electronics, electrical engineering and computing (INTERCON); 2018: IEEE.
218. Adib MAHM, Han SY, Ramani PR, You LJ, Yan LM, Sahat IM, et al., editors. Restoration of kids leg function using exoskeleton robotic leg (ExRoLEG) device. Proceedings of the 10th national technical seminar on underwater system technology 2018; 2019: Springer.
219. Laubscher CA, Farris RJ, Sawicki JT, editors. Design and preliminary evaluation of a powered pediatric lower limb orthosis. ASME 2017 international design engineering technical conferences and computers and information in engineering conference; 2017: American Society of Mechanical Engineers Digital Collection.
220. Andrade RM, Sapienza S, Bonato P, editors. Development of a "transparent operation mode" for a lower-limb exoskeleton designed for children with cerebral palsy. 2019 IEEE 16th international conference on rehabilitation robotics (ICORR); 2019: IEEE.
221. Pérez-San Lázaro R, Salgado I, Chairez I. Adaptive sliding-mode controller of a lower limb mobile exoskeleton for active rehabilitation. ISA Trans. 2020. https://doi.org/10.1016/j.isatra.2020.10.008.

Publisher's Note

Paper 2:

REVIEW

ADVANCED INTELLIGENT SYSTEMS Open Access

www.advintellsyst.com

Soft Wearable Rehabilitation Robots with Artificial Muscles based on Smart Materials: A Review

Alberto Gonzalez-Vazquez, Lorenzo Garcia, Jeff Kilby, and Peter McNair*

Wearables robots have gained attention for the rehabilitation of people with physical disabilities. However, the current technology relies on heavy and bulky actuation components, making it hard to use outside clinical settings. Artificial muscles based on smart materials are trending for soft wearable rehabilitation robots as they present advantages of compliance, are lightweight, and do not require external components. Nevertheless, they present challenges that remain unresolved, preventing widespread adoption. This work reviews the current state of soft wearable rehabilitation robots with artificial muscles based on smart materials (AMSMs). A literature search is conducted utilizing Web of Science and Scopus. Based on the inclusion–exclusion criteria, 15 devices are found using four different smart materials. This study attempts to provide an insight into the distinct biomechanical requirements, the use of smart materials, their limitations, their designs, and possible future research directions, which can provide helpful guidance on the implementation and development of advanced soft wearable rehabilitation robots with AMSMs.

1. Introduction

During the past decade, wearable devices such as exoskeletons have gained popularity[1] in different fields, such as the military,[2] industry,[3] and rehabilitation.[4] In the latter, rehabilitation exoskeletons are used to restore or maintain the functionality and mobility of people with physical disabilities.[5] These are receiving greater attention as the number of people with disabilities affecting physical performance will increase in the following decades as the population ages and individuals live longer with noncommunicable conditions (e.g., cerebral palsy, stroke, acquired brain injuries, and muscular dystrophies).[6–8]

Most current exoskeletons use electric motors and rigid links to realize actuation and often have heavy and bulky designs that are difficult to safely wear outside clinical facilities.[9] Hence, researchers in this area are working to develop soft wearable rehabilitation robots (SWRRs), featuring soft actuators that are agreeable to the users as they have increased compliance, adaptability, comfort, safety, and less weight.[10–12]

Currently, SWRR relies mainly upon two soft robotic technologies, cable-driven and fluidic actuators. For a cable-driven system, the wire is embedded into clothes or tubes and attached to an anchor point. The other side of the wire is connected to an electric motor to generate the desired movement and force by pulling the cable[13,14] (**Figure 1**a). Alternatively, in fluidic actuation (Hydraulic/Pneumatic), a pressurized fluid is inserted into a chamber made of highly deformable material to generate a displacement[11,15,16] (Figure 1b). However, these require large and heavy external pumps and valves to compress the fluid.[17] Unfortunately, cable-driven and fluidic actuation need cumbersome components (e.g., electric motors, pumps, and valves) to work, compromising the portability of the systems when used in daily life.[18]

Therefore, in recent years, research has been committed to developing new actuator technologies that can overcome the drawbacks of the current actuators used in SWRR. These technologies include artificial muscles based on smart materials (AMSMs). AMSMs are soft actuators composed primarily of material with a low Young's modulus similar to that of soft biological materials (10^4–10^9 Pa) that can sense and directly convert physical stimulus (e.g., light, electrical, heat) into physical displacement.[19–23] Some examples of smart materials are shape-memory alloy (SMA),[24] dielectric elastomer actuators (DEAs),[25] ionic polymer–metal composites (IPMC),[26] shape-memory polymers (SMPs),[27] and twisted and coiled polymer actuators (TCPs).[28] Due to their inherent properties and manufacturing processes, AMSM can be fabricated in various shapes, allowing them to be embedded into flexible and deformable wearable devices.[29–32] Furthermore, it is possible to fabricate robots with a relatively small weight and volume as they present a power density comparable to the skeletal muscles.[33]

Nevertheless, AMSMs for rehabilitation robots are still at the early stage of development. Some drawbacks specific to every

A. Gonzalez-Vazquez, L. Garcia, J. Kilby
BioDesign Lab
School of Engineering
Computer and Mathematical Sciences
Auckland University of Technology
Auckland 1010, New Zealand
E-mail: lorenzo.garcia@aut.ac.nz

P. McNair
Health and Rehabilitation Research Institute
Auckland University of Technology
Auckland 1010, New Zealand

The ORCID identification number(s) for the author(s) of this article can be found under https://doi.org/10.1002/aisy.202200159.

DOI: 10.1002/aisy.202200159

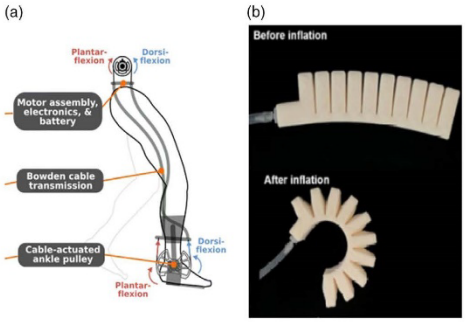

Figure 1. a) Ankle foot orthosis cable-driven system schematic providing plantar-flexion and dorsiflexion assistance. Reproduced with permission.[14] Copyright 2019, Springer Nature. b) Pneumatic actuator before and after inflation. Reproduced with permission.[16] Copyright 2020, IEEE.

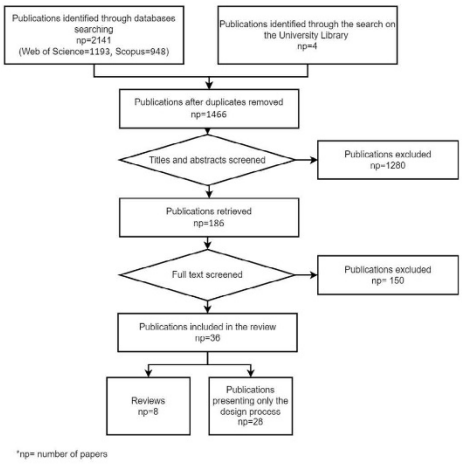

Figure 2. Literature search flow diagram.

smart material (e.g., low speed in SMA and TCPs and low force generation in DEAs and ionic polymer–metal composites) need to be tackled if they are to become widespread technology utilized in SWRR.[33,34]

The purpose of this article was to review soft wearable rehabilitation robots (SWRR) incorporating AMSM; seeks to: a) identify the biomechanical requirements for these robots; b) identify the different AMSM technologies utilized; b) identify the AMSM limitations for these robots; c) describe the AMSM enhancement design techniques; d) discuss future trends for development in the field of SWRR based on AMSM.

2. Findings

Based on the keywords, 2141 publications were found, with 1193 publications from Web of Science, 948 publications from Scopus, and 4 from a search on the university library.

First, a check was made for duplicated publications. Thereafter, the abstracts of 1466 publications were screened, and 186 titles were selected for full-text reading. After carefully applying the exclusion criteria to the fully read articles, 36 publications were selected. Among the chosen publications, 8 were reviews, and 28 discussed the development and characteristics of the device (**Figure 2** shows a flow diagram that illustrates the process of the selection of the articles).

Six of the eight reviews were focused on compliant actuators for rehabilitation systems and partially included AMSM as part of their scope. Peng et al.[20] focused on soft robots for rehabilitation and nursing care, but most of the analysis was centered on soft robots driven by electric motors and pneumatics. Shahid et al.[15] investigated the soft robotic devices designed for hand rehabilitation, where one device based on AMSM was included. Veale et al.[18] analyzed the current technology on compliant actuators, addressing the potential of new smart materials to be used in wearable exoskeletons. Zhu et al.[23] looked at the developments in soft wearable robots, covering the diverse application of AMSM where rehabilitation robots were included. Bardi et al.[36] researched SWRR for the upper limb, where a section of devices using SMA was included. Finally, Aliseichik et al.[37] went through different artificial muscle technologies, including sections related to SMA and electroactive polymers (EAPs). Two reviews focused on specific smart materials, namely the SMA (Nematollahi et al.[38]) or DEA and plasticized polyvinyl chloride gel (PVC) (Dong et al.[39]) in rehabilitation robots. The difference between the previous review articles and this work is that the earlier articles only partially covered the SWRR based on AMSM, as their scope was more related to soft actuators in general without a focused analysis of AMSM.

Within the 28 focused articles, 4 different types of AMSM technologies were found. Moreover, 17 SWRRs were noticed, 11 systems were designed for the upper limb, especially for treating the wrist and fingers, 5 for the lower limb, and 1 for the face.

3. Discussion

This section is divided into five parts. The first part (3.1) discusses the different biomechanical requirements used in the design of the SWRR. The second part (3.2) presents the different AMSMs and the SWRR that use each technology. The next part (3.3) focuses on the challenges that the SWRR faces. Followed by a part that (3.4) is concerned with how the robot's design can enhance the AMSM properties. Finally in (3.5), future developments are discussed.

3.1. Biomechanical Considerations

During the past decade, wearable exoskeletons have gained popularity[1] in different fields like military, industrial, and

rehabilitation.[3] Each of these fields has different applications and purposes, sometimes with partial overlap. Military exoskeletons are intended to enhance the physical capabilities and increase the mobility of soldiers during load carriage.[40] Industrial exoskeletons focus on augmentation and reinforcing a worker's performance to increase productivity and lower the risk of injury.[3] In contrast, the rehabilitation exoskeleton's purpose is to restore the functionality and mobility of people with a physical disability and whose functional performance is often severely affected.[5]

Moreover, another difference between military and industrial robots compared to rehabilitation robots is the range of populations they cover. For instance, military and industrial systems are mainly focused on healthy adults as beneficiaries. Concerning rehabilitation robots, there is a vast spectrum within the target population requiring different amounts of assistance, from children to the elderly,[41,42] different levels of disabilities,[43] and different types of diseases.[44]

This variability in the target population has led to a different specification for each group as SWRR based on AMSM are in a developmental stage and still present limitations compared to traditional robots.[18,20] Because of this, it is essential to appreciate the biomechanical requirements to develop a helpful SWRR. Furthermore, it will be valuable to understand the advantages and limitations of each AMSM.

Different biomechanical parameters can severely restrict the range of SWRRs that could be utilized in rehabilitation. These parameters are the degree of freedom (DOF) (number of planes of motion, e.g., flexion, extension supination, pronation at the elbow joint), range of motion (ROM), frequency (the maximum frequency that the actuator can be excited continuously), angular velocity (maximum during functional activity), the torque produced, device/system weight, and control scheme.[45] These parameters change depending on the joint, as each of them moves limbs with different mass and lengths, often with different moments of inertia, and is used to perform different activities. In **Table 1–8**, the biomechanical parameters of the biological joints and the SWRRs are presented to allow easy comparison between them.

3.1.1. DOF

In respect of planes of motion, most robot DOFs vary from one to three, depending on the joint. Only three devices have covered all the DOFs observed in human joints. Of note, more DOFs are apparent in robots for the upper limb. This could be explained by the upper limb activities of daily life (ADL) often requiring greater ranges of motion in multiple planes to perform different tasks like grasping and reaching.[46] In contrast, during many gait activities, the requirement for a larger ROM is predominantly in the sagittal plane.[47]

3.1.2. ROM

For ROM, two different values could be considered, the overall ROM and the ROM required to meet the demands of most tasks. The overall ROM is the maximum value that a joint can reach in a plane. In contrast, the activity ROM is the ROM needed to perform a specific activity, which can be much less than the whole ROM of the joint (Table 1–7).

Therefore, in SWRR development, it is essential to know the ROM requirements for the tasks to be assisted.[46,47] As the AMSM is starting the developmental phase, it is reasonable to focus on specific and uncomplicated tasks.[48] With this in mind, it may be easier to develop simple robots that can achieve the practical demands of the patient.[49] For example, consider the hip joint in the sagittal plane during flexion–extension movement. The full ROM is from ≈120° flexion to ≈20° extension. Yet, during walking, the required range would be ≈40° flexion to 11° extension.

3.1.3. Joint Forces and Torques

For AMSM to generate the ROM sufficient to undertake tasks often performed in daily living, it must be able to generate sufficient forces/torques. These forces need to overcome those associated with gravity and the inertia of the limb being moved. In most research in this area, the reported value was torque.

Table 1. Shoulder Soft Wearable Robots Biomechanical Properties.

Research group	Material	DOF	ROM [°]	Torque/Force	Frequency	Angular velocity [° s $^{-1}$]	Control strategy	Weight [kg]
Human Body[37,51,139,140]	Skeletal muscle	3	Typical values −60 to 180 Extension/ Flexion 0 to 180 Adduction/ Abduction	Minimum to lift the patient's limb against gravity 79.9 Nm Flexion 74.9 Nm Extension 73 Abduction 76.4 Adduction	Typical values <20 Hz	Typical values >50	N/A	N/A
			ADLs −18.3 to 62.3 Extension/ Flexion −14 to 133.6 Adduction/ Abduction	ADLs 9.6 Extension/Flexion 10.05 Adduction/ Abduction	ADLs ≈1.1 Hz	ADLs 100 Extension/ Flexion 171.5 Adduction/ Abduction		
KAIST[100]	SMA (spring)	1	90 Abduction	10.1 Nm	N/A	18	N/A	0.675 Wearable assembly

Table 2. Elbow soft wearable Robots Biomechanical Properties.

Research group	Material	DOF	ROM [°]	Torque/Force	Frequency	Angular velocity [° s^{-1}]	Control strategy	Weight [kg]
Human Body[34,46,50–52,141]	Skeletal muscle	3	Typical values 0 to 150 Flexion/ Extension −120 to 120 Pronation/ Supination	Minimum to lift the patient's limb against gravity ≈3.5 Nm Flexion/ Extension ≈1.85 Nm Pronation/ Supination	Typical values <20 Hz	Typical values >50	N/A	N/A
			ADLs >81 Flexion/Extension −13 to 53 Pronation/ Supination	ADLs ≈3.7 Nm Flexion/ Extension ≈0.04 Nm Pronation/ Supination	ADLs ≈1.25 Hz	ADLs <135 Flexion/Extension <486 Pronation/Supination		
University of Delaware[a)][60]	DEA	1	19.5	1 N (applied) weight applied to the arm	N/A	16.2	Pulse train	N/A
Carlos III University of Madrid[52]	SMA	2	0 to 120 Flexion/ Extension −50 to 50 Pronation/ Supination	3.5 Nm Flexion/ Extension 1 Nm Pronation/ Supination	100° at 0.2 rad s^{-1} (0.0318 Hz)	N/A	BPID	<1 (2.9 with power supply)
KAIST[97]	SMA (spring)	2	60 to 150 Flexion −27.6 to 27.6 Pronation/ Supination	3.2 Nm Flexion/ Extension 0.5 Nm Pronation/ Supination	N/A	Full movement in 10 s	Step signal	1.55 Wearable assembly
Korea Institute of Machinery and Materials[101]	SMA (spring)	1	Strain of 26.1% (47 mm contraction)	80 N	N/A	Full movement in ≈5 s (With a cooling system and an agonist–antagonist configuration)	Step signal	0.57 Total

[a)]Biomechanical Properties based on children 2 years old.

Table 3. Wrist soft wearable Robots Biomechanical Properties.

Research group	Material	DOF	ROM [°]	Torque/Force	Frequency	Angular velocity [° s^{-1}]	Control strategy	Weight [kg]
Human Body[34,46,50,51,142]	Skeletal muscle	2	Typical values −38 to 40 Flexion/ Extension −38 to 28 Ulnar deviation/Radial deviation	Minimum to lift the patient's limb against gravity 1.43 Nm Flexion/Extension 1.43 Nm Ulnar deviation/ Radial deviation	Typical values <20 Hz	Typical values >50	N/A	N/A
			ADLs −38 to 40 Flexion/ Extension −38 to 28 Ulnar deviation/Radial deviation	ADLs ≈0.2 Nm Flexion/ Extension ≈0.3 Nm Ulnar deviation/ Radial deviation	ADLs 1–5 Hz	ADLs <232 Flexion/Extension <203 Ulnar deviation/ Radial deviation		
MENRVA[87]	TCP	1	N/A	0.3 Nm	≈13 N at 0.1 Hz	N/A	PID	N/A
Carlos III University of Madrid[94]	SMA	2	80 Flexion/Extension −45 to 45 Ulnar deviation/ Radial deviation	0.5 Nm in both directions	50° at < 0.04 Hz Extension 40° at ≈0.04 Hz Ulnar deviation/Radial deviation	N/A	BPID	0.960 Total
KAIST[98]	SMA (spring)	2	−33.8 to 30.4 Flexion/ Extension 21.4 to 15.4 Ulnar deviation/Radial deviation	1.32 Nm Extension 0.61 Nm Flexion 0.90 Nm Radial deviation 0.62 Nm Ulnar deviation	80° at 0.5 Hz	N/A	Step signal	0.151 Wearable assembly (Whole device ≈1)

Table 4. Hand (fingers) soft wearable Robots Biomechanical Properties.

Research group	Material	DOF	ROM [°]	Torque/Force	Frequency	Angular velocity [$^\circ s^{-1}$]	Control strategy	Weight [kg]
Human Body[34,143,144]	Skeletal muscle	3 DOF Each finger	Typical values Index finger DIP = 70 PIP = 100 MCP = 90	Pinch of 1.4 N to 31.4 N	Typical values <20 Hz ADLs >1 Hz	Typical values >50	N/A	N/A
University of Pisa[68]	DEA	1	N/A	1 N	N/A	N/A	Step signal	N/A
Bio-robotics and Smart Systems Laboratory[59]	TCP	3 DOF Each finger	Index finger DIP − 11 PIP − 21 MCP = 41	2 N	N/A	Full movement in 25 s (Pulsed 2 s)	Step signal/ Pulsed actuation	≈0.1 Wearable assembly
Universidad Iberoamericana[82]	TCP	1	N/A	3 N	N/A	N/A	Step signal	N/A

Table 5. Hip soft wearable Robots Biomechanical Properties.

Research group	Material	DOF	ROM [°]	Torque/Force	Frequency	Angular velocity [° s $^{-1}$]	Control strategy	Weight [kg]
Human Body[34,145–148]	Skeletal muscle	3	Typical values −122 to 22 Flexion/ Extension −44 to 26 Abduction/ Adduction −33 to 34 Median rotation/Lateral rotation	Minimum torque to lift the patient's limb against gravity 80 Nm (120° flexion) ≈10 Nm (40° Flexion)	Typical values <20 Hz	Typical values >50	N/A	N/A
			ADLs −37.8 to 10.5 Flexion/ Extension −9.7 to 6.9 Adduction/ Abduction −1.0 to 11.2 Median rotation/Lateral rotation	Walking 80 Nm Flexion 65 Nm Extension 111 Nm Abduction 68 Nm Adduction 13 Nm Internal rotation 18.35 Nm External rotation	ADLs > 1.05 Hz	Walking <115 Extension <195 Flexion		
Zhejiang University of Technology[81]	PVC	1	N/A	≈70 Nm Flexion	N/A	N/A	State machine	0.6 Wearable assembly and 0.8 for the controller and the battery

However, for the hand, some devices have been developed to replicate/generate the force required for grasping and pinch activities. In the case of facial expressions, as with the finger joint, it is not measured on torque but the force that muscles generate in a direction to generate facial expressions.

Regarding torques, as with ROM, two different values are most often considered by developers. First, torque levels occur during ADLs and the minimum torque that would move the limb against gravity. Interestingly, the ADLs torques are similar or less for many activities in the upper limbs than the passive torques. For example, considering the wrist in ADLs, the necessary torques were less than 1 Nm in all directions, but in the case of torque required to move it against gravity, they were in the order of 1.5 Nm.[50–52] In contrast, in the lower limb, some muscles need to activate to a sufficient level to carry the person's body weight in the stance phase of gait activities and, at the same time, generate appropriate torque to produce the joint motion required for the gait activity being performed. For instance, the bigger discrepancy occurs during ankle plantarflexion, where a peak torque above 100 Nm is required, while for passive movement, the required torque is around 5 Nm.[53,54]

Table 6. Knee soft wearable Robots Biomechanical Properties.

Research group	Material	DOF	ROM [°]	Torque/Force	Frequency	Angular velocity [° s^{-1}]	Control strategy	Weight [kg]
Human Body[55,146,148,149]	Skeletal muscle	1	Typical values −134 to 1 Flexion/ Extension	Passive torque ≈50 Nm (≈50°)	Typical values <20 Hz	Typical values >50	N/A	N/A
			Walking −64.6 to 0 Flexion/ Extension	Walking 45.15 Nm	ADLs ≈1.15 Hz	Walking ≈360 Extension ≈300 Flexion		
Wyss Institute[a][93]	SMA (spring)	1	−34 to 0 Flexion	N/A	N/A	2.56	Step signal	N/A

[a]Biomechanical Properties based on children 4 years old.

Table 7. Ankle soft wearable Robots Biomechanical Properties.

Research group	Material	DOF	ROM [°]	Torque/Force	Frequency	Angular velocity [° s^{-1}]	Control strategy	Weight [kg]
Human Body[47,53–55,148]	Skeletal muscle	3	Typical values −55 to 20 Plantarflexion/ Dorsiflexion −23 to 12 Inversion/ Eversion	Passive torque ≈5 Nm (10°) Dorsiflexion ≈5 Nm (30°) Plantarflexion	Typical values <20 Hz	Typical values >50	N/A	N/A
			Walking −20 to 10 Plantarflexion/ Dorsiflexion	Walking Plantarflexion ≈110 Nm	ADLs ≈1.75 Hz	Walking ≈310 Plantarflexion ≈190 Dorsiflexion		
CNR Institute for Energetics and Interphases at Lecco[89,150]	SMA	1	−5 to 20 Plantarflexion/ Dorsiflexion	15 N with a lever arm of 10 cm (Torque = 1.5 Nm)	N/A	N/A	Square pulse	N/A
State Key Laboratory of Mechanism System and Vibration[85]	SMA	1	−16 to 16 Plantarflexion/ Dorsiflexion	10.9 Nm	16° at 1 Hz	N/A	SBH Feedforward + PID	N/A
Ajou University[91,92]	SMA	1	20 Plantarflexion	1 Nm	N/A	100 contraction	Step signal	0.428 g Without power supply

Table 8. Facial soft wearable Robots Biomechanical Properties.

Research group	Material	DOF	Displacement	Torque/ Force	Frequency	Angular velocity [° s^{-1}]	Control strategy	Weight [kg]
Human Body[151]	Skeletal muscle	N/A	N/A	1.1–3.5 N	N/A	N/A	N/A	N/A
Artificial Intelligence Laboratory[88]	SMA	N/A	20 mm	N/A	N/A	N/A	Feedback controller	N/A

3.1.4. Frequency and Angular Velocity

Human movements are dynamic tasks, and therefore these are characterized by temporal parameters like angular velocity and frequency of the movements. Even if these are related to each other, these are different concepts, and ideally, both should be reported. Angular velocity is the rate of flexion and extension of a joint, while frequency is related to the maximum trackable sinusoidal frequency of the amplitude of the movement. It is possible to approximate the angular velocity from the frequency with the next formula.

$$\omega = \lambda * 2 * F \quad (1)$$

where ω is the angular velocity in $^\circ\,s^{-1}$, λ is the amplitude of the sinusoidal wave in °, and F is the frequency in Hz. In the case of the velocities, it is possible to notice that it varies depending on the extremity, from around $120^\circ\,s^{-1}$ in the case of the ankle to more than $400^\circ\,s^{-1}$ for the elbow (Table 1 and 7). However, in the case of the frequencies, they remain similar, around 1.5 Hz.[55] This could be related to the fact that speeds are not constant during the movement, while the frequencies are related to the median speed of a movement limited in a specific ROM. In the case of the SWRR, when the frequency is provided is essential to look at the amplitude to estimate how fast a device is.

3.1.5. Control Strategies

The control strategy is a crucial element during the design process of SWRR. The control strategy's objective is to track the device's trajectory[56] and/or forces[57] to plan the desired action to apply a stimulus to the actuator later to generate a movement. This process is similar to the motor control of the human body, where the central nervous system plans the movement base on sensory information and sends the command to drive the muscles.[58] From the founded devices, it is possible to identify mainly three different control strategies, pulses, state machines, and proportional–integral–derivative (PID) controllers.

The pulse strategy is an open-loop control strategy as the system's output depends on the input, but the input is independent of the output. This scheme consists of applying a pulse or steps to generate a certain level of force or displacement from the AMSM. However, there is no feedback. Thus, it is impossible to compensate for the influence of external stimuli.[59,60]

In the case of the state machine, the device can change between different states in response to an event. The simple state machine is an on–off switch that changes based on an external stimulus, such as the change between the gait swing and stance phases.[61]

PID is a closed-loop control mechanism employing feedback from the system output. The controller is continuously calculating an error value between the reference signal and the output and then applies a correction. PIDs are used to reject disturbances and to implement setpoint changes.[52]

3.1.6. Weight

The weight of the artificial muscle and overall device is critical to establishing its usability by patients. Excessive weight can negatively affect the motion of the limbs as significant weight generates inertial forces that increase energy consumption and could make it uncomfortable and unsafe for patients to use.[62] For instance, the threshold for an acceptable weight on the hand and forearm is around 400 to 500 g.[63] Furthermore, in the case of the lower limbs, a weight of 4 kg on foot doesn't seem to affect the gait kinematics. However, the net metabolic rate increased by 36%.[64]

3.2. Soft Wearable Rehabilitation Robots

While biomechanical considerations are the main factors to consider in the design of SWRR, the system's capabilities depend more on the functional properties of the AMSM that are inherited from the material used to fabricate them. In this section, the different systems are presented and arranged by the material used to manufacture them. In this section, the different systems are presented and arranged by the material used to manufacture them to understand the advantages and disadvantages of each AMSM technology applied to SWRR.

Table 1–8 present the material utilized, the system's weight, the control strategy, the ROM at the joint involved, frequency of motion, typical joint angular velocities, and the associated torques. These parameters are presented within subsections related to body parts upon which systems were designed.

3.2.1. DEAs

EAPs are polymers that can be stimulated to change their shape using electrical energy. One of the most common types of EAPs is DEA.[65] It consists of a compliant capacitor composed of a thin elastic dielectric film coated on both surfaces by compliant electrodes. When DC voltage is applied to the electrodes, both attract each other, increasing the pressure over the dielectric film (Maxwell pressure) due to the electrostatic force while reducing thickness and area expansion (**Figure 3**).[39,66] Maxwell pressure is related to the permittivity of the material and the strength of the applied electric field. The relation can be expressed as

$$P = \varepsilon_0 \varepsilon_m E^2 = \varepsilon_0 \varepsilon_m (V/d)^2 \quad (2)$$

where P is the Maxwell pressure, ε_0 is the vacuum permittivity, ε_m is the material permittivity, E is the electric field strength that depends on the applied voltage V, and the thickness of the film d.

DEAs in Wearables Devices: DEA actuators are one of the most studied AMSMs due to their properties that, in most cases, surpass those of the muscle, with strain approaching 200%, a high bandwidth up to the range of kilohertz, and high efficiency,[33,34,67] which are all desirable properties for SWRR. However, they have limitations when placed in robotic applications that interact with people. DEAs need high voltage, in the order of hundreds of volts, requires bulky and expensive electronics and are considered unsafe. Nevertheless, DEAs are challenging to produce in a compact size to generate appropriate amounts of power and force.[18,66]

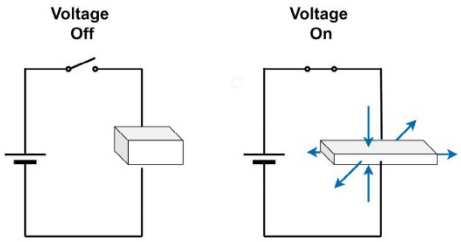

Figure 3. The working principle of the DEAs, when a voltage is applied, a Maxwell pressure is generated between the electrodes.

Two different research groups developed SWRR with this AMSM. Carpi et al.[68] developed a hand rehabilitation device based on folded DEAs to generate flexion and extension movements at the finger joints actively. The structure of the hand-split consists of a plastic-made wrist guard with support for the actuator in combination with an aluminum rod. Three folded DEAs actuators were connected to a miniature DC to high-voltage DC converter to provide the required high voltage. The converters were able to supply voltage in the range of 0–10 kV. With this configuration, the device could generate forces in a range of 1 N and a contraction of 7% to the original length using an input voltage ranging from 0 to 6 kV.

Behboodi et al.[60] designed a platform for pediatric rehabilitation to generate flexion and extension movements of the elbow joint (**Figure 4**). The device used a bundle of stacked DEAs,[66] with three parallel fibers consisting of 5 stacked DEAs in series.

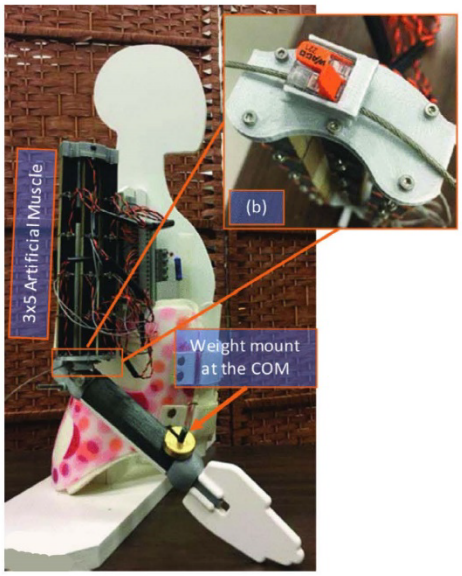

Figure 4. Example of a SWRR based on DEAs. Reproduced under the terms of the CC BY license.[60] Copyright 2020, IEEE.

The bundle of actuators was mounted on a mannequin resembling the elbow joint of a 2 years old child, and it was able to flex the elbow at 19.5° with an angular velocity of 16.2° s^{-1}. These results were obtained by applying a square signal with 1230 V amplitude.

3.2.2. PVC Gel Actuators

PVC gel actuators are EAPs similar to DEAs. PVC gels are produced by thermally or chemically melting PVC resins with liquid plasticizers. When PVC gel is placed between electrodes and an electric field is applied, a creeping deformation on the anode can be observed, and when the electric field is discharged, the PVC gel returns to its original shape[69,70] (**Figure 5**). The creep deformation can generate different types of deformation like bending, crawling, and linear contractions.[71]

Hashimoto et al.[72] developed an AMSM from PVC gel able to generate contractions. The PVC gel was sandwiched between a stainless mesh that acted as an anode, while a stainless foil served as a cathode. The cathode was located under the PVC gel, and the anode was above the gel. When the electric field is applied, the PVC gel creeps up the anode and moves into the mesh. The PVC electro-mechanical dynamics can be modeled as

$$\frac{\alpha}{T_\alpha s + 1} * \frac{1}{R_1 R_2 C s + R_1 + R_2} E(s) = \beta X(s) + F_{ext}(s) \quad (3)$$

where $X(s)$ and $F_{ext}(s)$ are the contraction strain and output stress, respectively. $E(s)$ is the applied electric field. The terms R_1, R_2, and C are the resistances and capacitance from an equivalent electric circuit. T_α is the time constant of the system. α and β are gains that can be determined from the experimental results.

PVC Gels in Wearable Devices: PVC gel actuators are a promising technology to be used as AMSM for SWRR, with their main advantages being relatively high actuation frequency (about 9 Hz), high strain (75%), low power consumption (2.9 μW mm^{-2}), and a very long life span (>5 million cycles). However, they require high voltages to work (≈3600 V), have low stress (0.6 MPa), and additionally, the electromechanical deformation mechanism is not fully understood, making it challenging to generate controlled joint movement.[61,71]

Only one SWRR has used this technology (**Figure 6**). Yi Li and Minoru Hashimoto are pioneers in using PVC gel actuators for wearable devices. In 2015, they presented their first prototype of a wearable system to assist in hip joint motion while walking.[73] Their latest development has been to upgrade the system with a new actuation unit.[61] The actuation unit had a length of

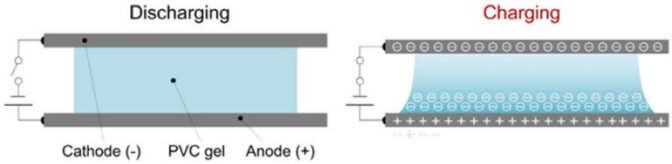

Figure 5. Deformation mechanism of polyvinyl chloride (PVC) gel when an electrical stimulus is applied. Reproduced under the terms of the CC BY license.[70] Copyright 2015, The Authors. Licensee InTech.

Figure 6. Example of an SWRR based on PVC gel actuator. Reproduced with permission.[138] Copyright 2016, IEEE.

200 mm, and to ensure appropriate fitting to the human body, it had a curved shape to mold more accurately to the body part. The whole device (for two legs) weighed 2 kg (0.6 per actuation unit + 0.8 kg for the control unit, including the battery). When the whole system was tested using a voltage of 400 V, the displacement of the assistive device was ≈16 mm (8%), the maximum output force was around 94 N, the response time was ≈56 ms, and the power consumption was around 1.6 W. The device was activated through a state machine controller strategy, switching the assistance on and off during the swinging and stance phase, respectively.

3.2.3. TCP Actuators

TCP actuators have emerged as a promising AMSM technology for SWRR. TCP actuators are constructed by continuously twisting polymer fibers or filaments (e.g., nylon fishing lines and sewing threads) until they form coils. The actuator works by converting a temperature change into strain or stress. In general, TCP actuators are driven by Joule heating (**Figure 7**a), adding a layer of a conductive material (e.g., silver) over the precursor fiber[74,75] or by embedding a resistance wire within the actuator[76,77] (Figure 7b). Consequently, the actuator can be modeled as an electrothermal–mechanical system. The electrothermal dynamics can be represented as a first-order linear system represented as[78,79]

$$C_{\text{th}}\frac{dT}{dt} = P(t) - \lambda(T - T_0) \tag{4}$$

where C_{th} and λ are the actuator's thermal mass and absolute thermal conductivity, respectively. T is the actuator's temperature, T_0 is the ambient temperature, and $P(t)$ is the electrical input applied at a specific time t. To quantify the speed of the dynamics, the time constant, $\tau = \frac{C_{\text{th}}}{\lambda}$ can be adopted. τ can be obtained by examining the actuators' rise and fall response and is equal to the average time the actuator takes to reach the 63% of a steady-state value given a step input under a steady-state condition.

In the case of the thermomechanical properties, this can be described as a spring–damper system with an added temperature-dependent term, which is expressed as

$$F = k(x - x_0) + b\dot{x} + c(T - T_0) \tag{5}$$

where x and x_0 are the loaded lengths and resting lengths of the actuator, respectively. K represents the stiffness, b is a damping term, and c denotes the thermal constant. Under steady conditions where $\dot{x} = 0$, the overall model can be obtained by combining (3) and (4).

$$F = k(x - x_0) + \frac{c}{\lambda}P \tag{6}$$

TCPs in Wearables Devices: TCPs are a recent discovery.[80] They have gained significant attention in the field of SWRR, with advantages such as high-power density (27 W g^{-1}) and stress (10 MPa), linear behavior, and a high strain (21%). In contrast, their main disadvantages are low efficiency (≈1%)[28,33,34] and the low frequencies (<3 Hz) at which they operate. Three promising examples of wearable devices based on TCPs were found.

The assistive wrist orthosis developed by Sutton et al.[81] used an arrangement of 16 TCPs wires made of silver-coated Nylon 6.6 sewing thread (**Figure 8**a). The splint prototype consisted of 3D-printed parts to mount the device on the arm and attachments for

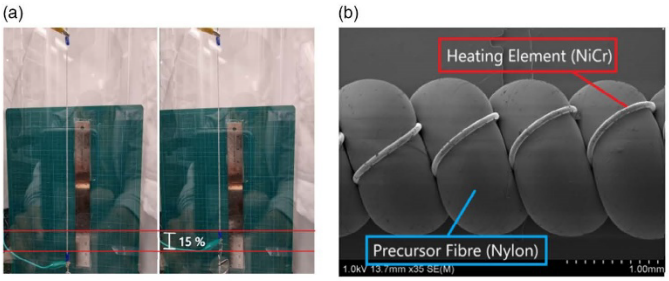

Figure 7. a) TCP actuator lifting a 1 kg load by 15% strain after heat is applied. b) Scanning electron microscope image of a nylon TCP actuator with a NiCr embedded wire as the heating element.

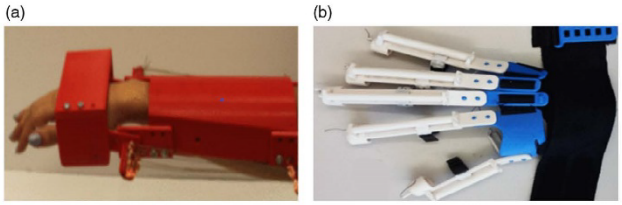

Figure 8. Examples of SWRR based on TCP are: a) MENRVA group SWRR for wrist. Reproduced with permission.[81] Copyright 2016, IEEE. b) Universidad Iberoamericana SWRR for hand. Reproduced with permission.[82] Copyright 2018, IEEE.

the nylon actuators. The device was designed to have one DOF and provide a torque of 0.3 Nm on the wrist joint in the flexion direction. The final prototype was able to produce torques around 0.32 Nm in 3.9 s. Using a PID controller, the system could track a 0.1 Hz with an amplitude of 10 N during actuation very closely, but during the relaxation time, the error increased due to the slow response time during the cooling down phase.

The group of Saharan et al.[59] designed iGrab, an ergonomic orthotic device powered by TCPs, to assist flexion and extension movement of the fingers. The prototype comprised 3D printed parts and sewn parts with artificial tendons routed from the fingers to the wrist using polytetrafluoroethylene (PTFE) pipes. The tendons were connected with a metallic ring to the TCPs mounted on a forearm bracelet. The TCP muscles were wrapped around frictionless pulleys to utilize long actuators. Furthermore, to improve energy consumption, the extension motion was facilitated with the help of rubber strips. When a 0.6 A step signal was applied to the TCPs, the fingers were able to reach their maximum displacement after 25 s (i.e., the index finger was able to move 40° for the MCP joint, 21° for the PIP joint, and 11° in the case of the DIP joint). The results were improved when a pulsed signal was used, reducing the actuation time from 25 s to less than 5 s.

Patiño et al.[82] also developed a wearable orthosis for hand rehabilitation movements, with a TCP actuator on each finger (Figure 8b). The exoskeleton is composed of two main parts fitted to the dorsum of the hand and the fingers. The dorsum of the hand was composed of five 3D printed plates, of which four are aligned with the fingers and one more adjustable plate that serves to fit the device to the user's hand. In the case of the fingers, each of them is composed of a silicone tube containing a TCP and a filament strain sensor. The TCP inside the finger structure could produce forces of around 3 N when a step input of 0.3 A was applied.

3.2.4. SMAs

SMAs are metallic materials that use the memory effect property to generate motion. The SMP is defined as the material's property to recover a previously described shape when an external stimulus is applied. Nickel–titanium (NiTi) alloys are the most popular SMAs, and they recover their original "memorized" shape after being deformed when heated above their transformation temperature.[38,83] SMA can be used as single fibers (**Figure 9a**) or as springs (Figure 9b) to generate linear displacement. SMA elements are generally heated through the Joule effect, where an electric current is applied to the SMA actuator. However, they present a high thermal hysteresis between the transition that occurs from martensite (low temperatures) to austenite (high temperatures) and the one occurring from austenite to martensite[84] (Figure 9c). When using a model is essential to take into consideration the nonlinear hysteresis properties of the material as the system's behavior in both phases is different.[85,86]

Zhang et al.[85] propose a sigmoid-based hysteresis (SBH) model for a single SMA fiber, where they introduce two different sigmoidal curves representing the major hysteresis properties.

$$y = \frac{k(\sigma,f)}{1+e^{-a_+(\sigma,f)[u-r_+(\sigma,f)]}} \quad \text{For } \dot{u} \geq 0 \tag{7}$$

$$y = \frac{k(\sigma,f)}{1+e^{-a_-(\sigma,f)[u-r_-(\sigma,f)]}} \quad \text{For } \dot{u} < 0 \tag{8}$$

where u is the input voltage, y is the output displacement. k represents maximum displacement. σ signifies the prestress applied to the fiber. f denotes the driving frequency. $a_{+/-}$ and $r_{+/-}$ represent curve slopes and voltage values at peak transformation of martensite to austenite and austenite to martensite. Besides, the hysteresis gap can be represented by $\Delta r(\sigma,f)$, which is defined as follows

$$\Delta r(\sigma,f) = r_+(\sigma,f) - r_-(\sigma,f) \tag{9}$$

To compensate for the minor hysteresis properties, two suitable scaling factors $\beta_{+/-}$ (where $\beta_{+/-} \in [0,1]$) are introduced. Hence Equation (7) and (8) can be rewritten as

$$y = \beta_+ \frac{k(\sigma,f)}{1+e^{-a_+(\sigma,f)[u-r_+(\sigma,f)]}} \quad \text{For } \dot{u} \geq 0 \tag{10}$$

$$y = \beta_- \frac{k(\sigma,f)}{1+e^{-a_-(\sigma,f)[u-r_-(\sigma,f)]}} + (1-\beta_-)k(\sigma,f) \quad \text{For } \dot{u} < 0 \tag{11}$$

For SMA springs, Koh[111] introduced a model derived by combining the conventional coil spring equation and a large deformation term for the austenite (12) and martensite (13) phases, respectively.

$$F_A = \frac{G_A d^4}{8D^3 n}\left(\frac{\cos^3\alpha_i}{\cos^2\alpha_{AF}(\cos^2\alpha_{AF} + \sin^2\alpha_{AF}/(1+\nu))}\right)\delta_A \tag{12}$$

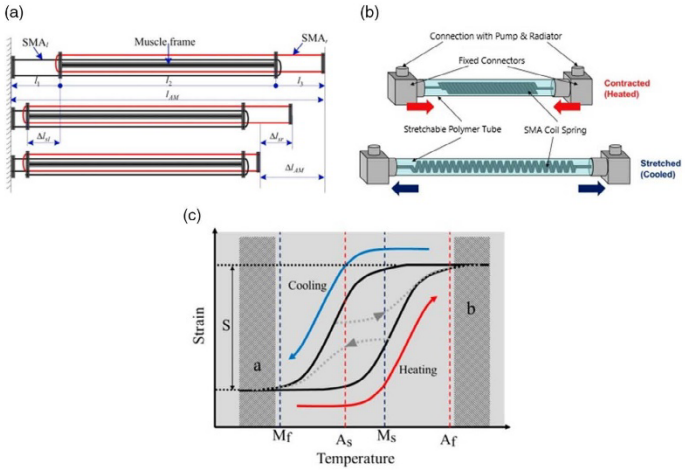

Figure 9. SMA actuators were functioning after and before applying joule heating. As: a) wires or b) springs. a) Reproduced with permission.[85] Copyright 2013, Elsevier. b) Reproduced under the terms of the CC BY license.[98] Copyright 2019, The Authors. Licensee MDPI. c) Temperature strain relationship of SMA actuators (As = Austenite start, Af = Austenite finish, Ms = Martensite start, Mf = Martensite finish). Reproduced under the terms of the CC BY license.[86] Copyright 2018, The Author. Licensee MDPI.

$$F_M = \frac{G_A d^4}{8D^3 n}\left(\frac{\cos^3\alpha_i}{\cos^2\alpha_{MF}(\cos^2\alpha_{MF} + \sin^2\alpha_{MF}/(1+\nu))}\right)\delta_M - \frac{\pi d^3}{8D} G_M \gamma_L \xi_{S\gamma} \quad (13)$$

where the material properties are: G the shear modulus, ν the Poisson's ratio, and γ_L the residual strain. Then the design parameters determined by the user are: d wire diameter, D the coil diameter, α_i initial pitch angle, and n the number of the coils. Lastly, the variables are F the force, $\xi_{S\gamma}$ the detwinned martensite volume fraction that changes with temperature and stress, δ the displacement, and αf the final pitch angle. Subscripts A and M denote the austenite and the martensite, respectively.

The deformation of the coil can be represented with δ, αf, γ. Although these variables are dependent variables, combining them complicates the equations. The pitch angle α_f is the term that describes the large deformation of the spring, δ is the original spring force–displacement, and γ is the shear strain for the detwinning term. Equations to describe the relationship of these three variables are provided so that they can be converted as needed. α_f can be converted to δ with Equation (14). Also, the final pitch angle can be converted to γ with Equation (15).

$$\delta = \frac{\pi n D}{\cos\alpha_i}(\sin\alpha_f - \sin\alpha_i) \quad (14)$$

$$\gamma = \frac{d}{D}\frac{\cos^2\alpha_i(\sin\alpha_f + \sin\alpha_i)}{\cos^2\alpha_f(\cos^2\alpha_f + \frac{\sin^2\alpha_i}{1+\nu})} \quad (15)$$

Furthermore, F can be converted to τ with Equation (16).

$$\tau = \frac{8DF}{\pi d^3} \quad (16)$$

The detwinned martensite volume fraction ($\xi_{S\gamma}$) is commonly a function of τ and temperature. However, to simplify the model $\xi_{S\gamma}$ is modified to be a function of γ as follows.

$$\xi_{S\gamma} = \frac{1}{2}\cos\left(\frac{\pi}{\gamma_s^{cr} - \gamma_f^{cr}}(\gamma - \gamma_f^{cr})\right) \quad (17)$$

where γ^{cr} is the critical strain for detwinning start (γ_s^{cr}) and finish γ_f^{cr}, which is the property of SMA.

In summarizing, Equation (12) and (14) are used to plot the force–displacement relationship for the full austenite phase, and Equation (13)–(15),(17) are used to plot the force–displacement relationship for the full martensite phase. Equation (14)–(16) are used to convert the force–displacement relationship into a shear stress and shear strain relationship.

SMAs in Wearables Devices: SMAs are superior to mammals' muscles and other AMSMs in terms of power density and stress, these being as high as 50 W g^{-1} and 200 MPa, respectively. Consequently, SMA actuators have been successfully used in automotive, aerospace, and biomedical fields.[87] However, they have limitations in respect of robotic rehabilitation, and these are low efficiency, a small strain range (up to 8%), and high thermal hysteresis making them difficult to control.[18,33,34] Nevertheless, SMA is the most used AMSM for rehabilitation robots, and it has been used within nine different devices.

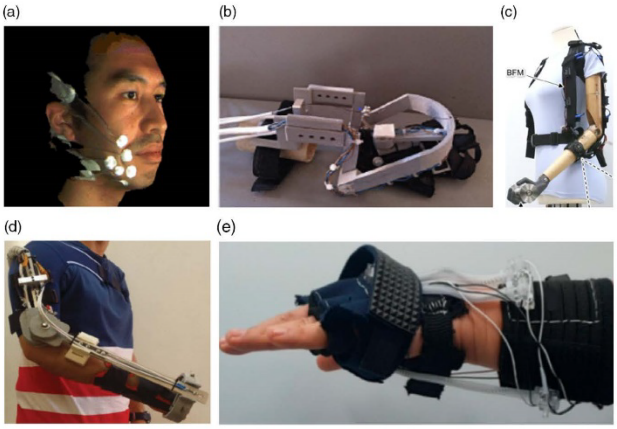

Figure 10. Examples of SMA-based SWRR. a) Artificial Intelligence Laboratory Smile recovery device. Reproduced with permission.[88] Copyright 2008, IEEE. b) Carlos III University of Madrid wrist device. Reproduced with permission.[94] Copyright 2018, IEEE. c) Korea Institute of Machinery and Materials elbow robot. Reproduced under the terms of the CC BY license.[101] Copyright 2022, The Authors, published by Springer Nature. d) Carlos III University of Madrid elbow SWRR. Reproduced under the terms of the CC BY license.[52] Copyright 2019, IEEE. e) KAIST Wrist SWRR. Reproduced under the terms of the CC BY license.[98] Copyright 2019, The Authors. Licensee MDPI.

Jayatilake et al.[88] investigated the ability of a device based on spring SMAs to help people with facial paralysis recover the ability to make facial expressions (**Figure 10**a). The device consisted of a wearable robotic external mask. The mask included six SMAs per side, and these were arranged in a specific position to replace or reproduce the face muscles' activity. The authors reported that it was possible to generate some facial expressions with a contraction of 20 mm, using a feedback controller. However, to create complex facial expressions, several SMAs are required.

Pittaccio et al.[89,90] developed SHADE, an ankle orthosis capable of providing active and passive exercise for the dorsiflexion movement. The system used an SMA wire mounted on an insulated aluminum cartridge with dimensions of 150 × 20 × 15 mm. Inside the cartridge, the wire was led back and forth between two arrays of ten mini-pulleys, making it possible to store a long wire within a limited space. The prototype consisted of two cartridges and two thermoplastic shells hinged at the ankle joint. Later, three adult patients tested the prototype. During these trials, the prototype provided passive dorsiflexion movements in the range of 0–23° to all the patients with speeds similar to the movement's natural speed. The control signal used during the experiments was a square signal with a current injection of 0.7 A for 7 s and a coiling phase of 30 s.

Zhang et al.[85] proposed using SMAs on an SWRR to assist the ankle dorsiflexion movement. To power the SWRR, an actuation unit composed of 2 × 250 mm SMA wires were developed. The system consisted of two parallel units and a bias spring mounted in two lightweight thermoplastic shells with articulated joints. To compensate for the hysteresis of the SMA, the prototype employed an SBH feedforward controller with a PID controller. With this control configuration, the system was tested by following a sinusoidal signal with a peak-to-peak value of 30° at 0.2 Hz and 16° at 1 Hz. The system tracked the signal with a maximum tracking error lower than 16% and the root-mean-square tracking error lower than 7.3% in both cases.

Regarding plantarflexion at the ankle joint, Koo et al.[91,92] produced a lower extremity SWRR using SMA wire. The system was light, silent, and flexible. A prototype was built using a multilayered structure consisting of functional fabrics, seam sealing tape, Velcro straps, Teflon tubes, and an SMA cable. The SMA was wrapped around the lower limb with both ends of the SMA anchored at the waist, and the middle part of the cable was attached to the ankle. The viability of the prototype was evaluated using an adult-like PVC mannequin. Joule heating was employed to activate the system, and when a 1 A current was applied, an angular displacement of around 20° (plantar flexion) within 0.2 s was achieved.

For the knee joint, Stirling et al.[93] investigated the use of spring SMA on an active soft orthotic (ASO) device. The ASO comprised four sets of actuators on the dorsal surface of the knee (to assist flexion) and one set on the frontal surface (to help extension). Each group of actuators consisted of four SMA springs with a length of 17.5 cm. The system was tested on a robotic leg resembling the size and mass of that of a 4 years old child. With the four sets of actuators activated through joule heating, the ASO flexed the knee by 34° in ≈25 s. The results were obtained after applying a step signal of 0.4 A to each set of actuators.

The Carlos III University of Madrid group has published a number of articles concerning SWRR actuated by SMA.[52,83,94–96] Recently, a wrist rehabilitation robot[94] was

designed to assist flexion, extension, ulnar deviation, and radial deviation movement (Figure 10b). The rehabilitation robot consisted of a 3D-printed mechanical structure sewn onto a glove. The device used three SMA wires, one for the extension movement and a pair to generate the ulnar/radial deviation movements. A sinusoidal signal with a frequency of 0.04 Hz and a ROM of −10° to 40° was used to test the flexion–extension and the radial–ulnar deviation movements. The SWRR was able to track the extension movement, but it could not follow the signal input during flexion due to the slow cooling process of SMA. In ulnar/radial deviation movement, it tracked the whole movement as it presented an agonist–antagonist structure, improving the performance compared to a single wire.

Another article from this research group concerned an elbow SWRR[52] (Figure 10d) that had two DOFs (flexion/extension and pronation/supination). Each DOF had a pair of antagonist SMA actuation units. The units utilized a set of SMA wires encapsulated inside a PTFE tube. The number of SMA wires inside the actuation unit differed according to the direction of the movement. In the case of the flexion–extension, the actuation units were configured with a bundle of three SMA wires 1.5 m in length for flexion and two for extension. For the pronation/supination movement, each direction was actuated by a single SMA wire with a length of 2 m. To test the device, a sinusoidal signal with an amplitude of 100° and a frequency of 0.2 rad s^{-1} was applied while performing a flexion–extension movement. The device could follow the pattern with an error of less than 4°. In both devices, to control the contraction of the SMA wires, they used a four-term bilinear-proportional–integral–derivative (BPID). The BPID controller is a combination of a standard linear PID controller cascaded with a bilinear compensator to counteract the hysteresis behavior of the SMA.

A group from the Korea Advanced Institute of Science and Technology (KAIST)[97–99] has designed SWRRs to assist patients who have difficulty moving the upper limb using SMA springs. The first SWRR they developed was a device to assist wrist movements[98,99] (Figure 10e). They chose to use single SMA springs to generate a high contraction strain. The SWRR consisted of a wearable fingerless glove worn on the hand and a wearable strap placed on the forearm. Five actuators were used to provide the required movements, three over the forearm and two under the forearm. A cooling system pumping mineral oil was employed to improve the speed of the SMA springs. The device could provide torques of 1.32, 0.61, and 0.90, and a 0.62 Nm for extension, flexion, radial deviation, and ulnar deviation movements. Regarding the ROM while the SWRR was worn, it was 33.8°, 30.4°, 21.4°, and 15.4° for flexion, extension, radial deviation, and ulnar deviation, respectively. To achieve a cycling performance of 0.5 Hz, a step signal of 4 A was applied to the SMA springs during the heating phase, while a step signal of 2.7 W was used for the pump during the cooling phase.

After the wrist device, the KAIST group developed two DOFs SWRR to assist during the elbow's flexion and pronation/supination movements.[97] The device used artificial muscle units composed of a bundle of four SMA springs inside of a coolant-based vessel containing mineral oil. The robot presents three different artificial muscle units attached to soft braces to mimic the motions of human muscles. One unit is used by itself to assist elbow flexion, while the other two are arranged in an agonist/antagonist structure to help with the forearm pronation/supination. The device was able to provide torques up to 3.2 Nm with a ROM in the range of 60° to 150° for flexion movement. Meanwhile, for the pronation/supination, the ROM was from −26.7° to 26.7° with a torque up to 0.5 Nm. The result from the forearm was obtained by applying a current of 1.5 A for 10 s in ambient temperature.

Finally, KAIST developed a four-bar linkage-based SWRR to assist with shoulder abduction.[100] An actuator was designed to generate the required forces using a bundle of 14 SMA springs. Each actuator produced an output force of 270 N when the actuator was stretched by up to 150%. The system consisted of a four-bar linkage-based supported hinge and an actuator unit. Where the four links are constructed by the arm, the torso, and two extra 100 and 200 mm connected linkages. Furthermore, the actuator was placed in the middle of the 200 mm link and the upper arm. With this configuration, the mechanism could produce assistive torque up to 10.1 Nm and a ROM of 90° during shoulder abduction. An electrical current of 1.5 A was supplied to each spring to activate the device. The effect of assistance was evaluated by measuring and analyzing the difference in the electromyography (EMG) activity between assisted and unassisted activity. However, there were no significant differences between the two conditions.

At the Korea Institute of Machinery and Materials, Park et al.[101,102] presented an SWRR made of fabric muscle with a cooling acceleration structure for elbow extension assistance (Figure 10c). The device is actuated by fabric muscle that consists of SMA spring bundles, conductive fabrics, cover fabrics, and electrical wiring. Furthermore, to improve the cooling rate of the fabric, two small fans are attached to each piece of fabric. The final exosuit consists of a shoulder anchor, forearm anchor, two overlapped biceps fabric muscles, one triceps fabric muscle, battery, and controller (with a total weight of 0.57 kg). The biceps fabric muscles were set on an agonists–antagonist configuration to improve the system's speed. Furthermore, when the fans were used, the system could contract 47 mm (26% strain) and generate a force of 80 N while flexing the elbow in 5 s. This was achieved by applying 10 A to the bicep's fabric for 3 s and fan cooling and activating the triceps fabric (10 A) for 3 s.

3.2.5. Other Smart Materials

While those materials presented earlier have been utilized for SWRR, there are other materials that had been highlighted as a possible option in previous articles,[37,103] like IPMC,[104] hydraulically amplified self-healing electrostatic (HASEL),[103] and SMP[105] that present attractive properties as they have been used in similar applications (grippers, robotic hands, or as compliance mechanism inside a rehabilitation robot). However, their current limitations prevent their use on SWRR.

IPMCs are EAPs made by coating a thin sheet of ionic polymer with metal electrodes. When an external electric field is applied, ions of the same charge begin to move from the anode to the cathode. As a result, the system undergoes a fast-bending deformation, followed by a slow relaxation[106,107] (**Figure 11a**). They have compelling advantages, such as efficiency, low working voltage (1–5 V), high working frequency up to 100 Hz, and

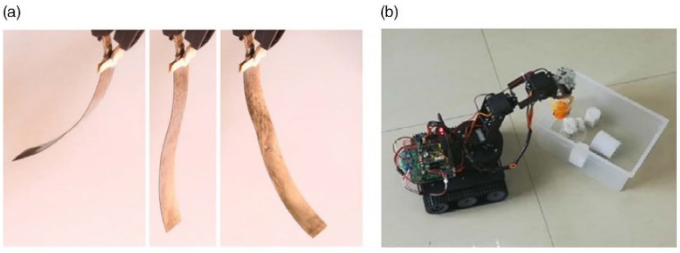

Figure 11. a) IPMC actuator bending in response to an electrical input with opposite polarities (left and right) and at rest (middle). Reproduced under the terms of the CC BY license.[107] Copyright 2019, The Authors. Licensee MDPI. b) Air-operating IPMC soft gripper assembled with a mobile mechanical arm. Reproduced with permission.[110] Copyright 2020, IOP.

considerable strain up to 40%. Nevertheless, they present some problems, such as relaxation under direct current (DC) voltage, low power density (0.02 W g^{-1}), and solvent evaporation that complicate their use in not watery environments.[33,108,109] He et al.[110] developed a microgripper using an air-operating IPMC actuator with consecutive channels. However, under this environment, the actuator by itself was only able to produce a strain of 0.44% and a force of 12.06 mN at 1 Hz using 5 V input which is lower than what skeletal muscles can generate. Nevertheless, the actuator proved its functionality operating on air, as it was used on a microgripper (0.14 g) that was able to pick up and transfer a nut (0.656 g) 4.69 times its own weight (Figure 11b).

Recently introduced HASEL actuators are fabricated from dielectric liquids filling pouches made of polymer films and partially covered by electrodes[111] (**Figure 12a**). HASEL actuators behave similarly to DEAs. They generate a Maxwell pressure when high voltage is applied, increasing the volume of the pouches and decreasing the length of the actuator.[112] Their main advantages for rehabilitation devices are their high linear strain (over 24%) and high bandwidth (126 Hz). Nevertheless, as with the DEAs, their main limitations are low stress (<1 MPa) and the high voltage (in the range of kV) required to drive them.[113] To understand the advantages and disadvantages of the HASEL actuator in rehabilitation robots, Yoder et al.[114] compared the HASEL actuator with DC motors, activating the Bebionic v2 Prosthetic hand (Figure 12b). In this comparison, the HASEL actuator surpassed the speed (HASEL = 1,587° s^{-1}, Motor = 150° s^{-1}) and the energy consumption (HASEL = 0.94 mW, Motor = 9,200 mW) of the motor. The ROM attained was similar in both cases (HASEL = 77.17°, DC Motor = 85°). However, the force provided by the HASEL actuator was lower than the generated by the motor (HASEL = 0.91 N, DC Motor = 13 N) and below that required to perform daily life activities (Table 4).

Like SMA, SMP can recover a predetermined shape after certain stimuli are applied, such as light, moisture, electricity, and heat[115,116] (**Figure 13a**). Due to their versatility of activation to different stimuli and the possibility of being produced from biodegradable materials, SMPs have been used in different

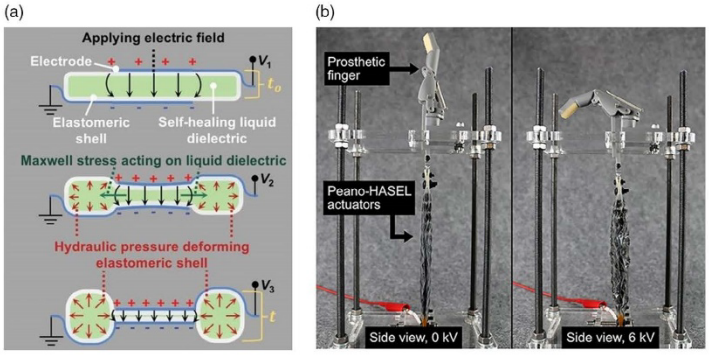

Figure 12. a) HASEL actuator schematic shown at three different applied voltages (where V1 < V2 < V3). Reproduced with permission.[111] Copyright 2018, The American Association for the Advancement of Science. b) An array of Peano-HASEL actuators driving a custom prosthetic finger. Reproduced under the terms of the CC BY license.[114] Copyright 2020, The Authors.

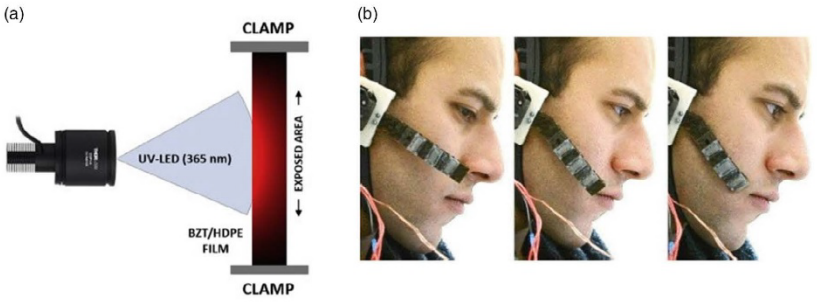

Figure 13. a) Photothermal effect originates from the thermal energy produced by a BZT/HDPE film after exposure to a UV light. Reproduced with permission.[116] Copyright 2020, Elsevier. b) Experiments using a single robot finger for performing the initial reconfiguration utilizing an SMP. Reproduced with permission.[105] Copyright 2017, IEEE.

biomedical applications such as drug delivery, self-tightening sutures, stents, and cellular surgery.[117] However, in the field of rehabilitation robotics, even though they have a high strain, which is a desirable feature (>10%), they are still not used because they present the problem of low stress (1–3 MPa) and slow recovery response (<1 Hz).[33] An example of the incorporation of this technology into the rehabilitation setup is the soft facial rehabilitation robot developed by Firouzeh et al.[105] They incorporate SMPs into a soft robot actuated by a cable-driven system to improve the compliance of the system. The prototype had five points of actuation, and each of them incorporated an SMP to control the stiffness (Figure 13b). The multiple DOFs presented by the robot allowed for initial reconfiguration and activation of different movement patterns depending on the needs of each patient and training. Nevertheless, the switch between different training positions was time consuming (≈10 s) due to the slow transition of the SMP.

3.3. SWRR Based on AMSM Limitations

AMSMs have outstanding flexibility and are lightweight, making them a promising choice to power the next generation of compliant rehabilitation robots. However, the use of these materials is still at the early stage of development, and the devices employing them have fundamental limitations that prevent their successful application.

Most of the robots utilizing AMSM were unable to generate the ROM to perform ADLs. For instance, this problem is related to the limited strain that most AMSM can produce, which is under the skeletal muscle's typical strain (20%). Another requirement that is influenced by the actuator's strain is torque. As the displacement generated by the actuators is linear, and the robots require angular displacements, making the necessary structures to transform linear to angular displacements can lead to a loss of force in the transition. Nevertheless, the main factor in producing the desired torque is the force generated by the AMSM. Concerning the required torque, most of the devices could produce the necessary torque to move the limb against gravity, except for the elbow developed by Behboodi et al.[60] Therefore, most of the evaluated AMSM can generate enough force to be used on wearable robots, except for DEAs that can't deliver high forces with small actuators.

The biggest obstacle for devices based on AMSM seems to be the actuation speed, as most of the reported frequencies and angular velocities were far from the required for ADLs (Table 1–8). However, a possible option would be to use them for rehabilitation therapies where the required speeds to perform the exercises are slower, usually under 100° s^{-1} and frequencies below 0.2 Hz.[118–121] This limitation could also be related to the mathematical models that explain the actuation principles of the AMSM. As the different technologies suffer from different problems like nonlinearity, hysteresis, and electromechanical instability that are difficult to model. The mathematical models are necessary to develop robust control strategies required for high-performance applications.[71,84,122] Hence, most of the evaluated devices used open-loop control schemes toggling between two different predefined levels to alter the length of the AMSM.

Generally, it is possible to categorize the current AMSM for SWRR into two categories: EAPs (DEAs and PVC gels) and thermally activated actuators (SMAs and TCPs). These two groups of actuators translate their limitation into the SWRR. The EAPs present a high actuation speed but low forces (high angular velocity/frequency but low torques). Contrary to the thermally activated actuator that shows low speeds but high forces (low angular velocities/frequency but high torques). Furthermore, the strain seems to be a general limitation (restrict ROM). Nevertheless, these constraints could be lessened with a proper design of the SWRR, as will be explored in the next section.

3.4. Artificial Muscles Enhancements Techniques

Although some SWRRs have initially demonstrated their potential as an assistant rehabilitation tool, all of them have been used in experimental setups in the laboratory environment only. New materials vary in their ability to meet the biomechanical requirements to be useful in the clinical setting. However, SWRRs made of AMSM show great potential for rehabilitation, thanks to their inherent compliance and lightweight. Currently,

an AMSM covering all the essential characteristics to behave like the skeletal muscles does not exist (Table 9). However, some of the deficiencies in smart materials can be remedied through the SWRR design.

Table 9. Comparison of artificial muscles Properties.

Device	Actuator technology	Strain [%]	Force [N]	Stress [MPa]	Frequency [Hz]	Size (Length and area or diameter)
Human Body[114]	Skeletal Muscles	20	N/A	0.1	20 Maximum	N/A
Korea Institute of Machinery and Materials[101] (2022)	SMA (spring)	50	0.2	N/A	23.4 s	L: 26 mm D_{SMA}: 0.08 mm D_{Spring}: 0.44 mm
KAIST[100] (2022)	SMA (spring)	N/A	19.28	N/A	N/A	L: N/A D_{SMA}: 0.5 mm D_{Spring}: 2 mm
University of Delaware[60,66] (2020)	DEA	5	10	0.0346	<100	L: 39 mm A: 17 × 17 mm
University of Pisa[68] (2008)	DEA	N/A	0.33	0.000982	N/A	L: 85 mm A: 16 × 21 mm
Zhejiang University of Technology[61] (2017)	PVC	10	80	0.080	9	L: 200 mm A: 0.001 m^2
Universidad Iberoamericana[87] (2018)	TCP	10	5.4	1.1	≈0.02	L: N/A D: 2.5 mm
Bio-robotics and Smart Systems Laboratory[59] (2017)	TCP	16	3	2	≈0.04	L: 380 mm D: 1.35 mm
MENRVA Group[81] (2016)	TCP	15.	0.9	N/A	0.1	N/A
KAIST[97] (2022)	SMA (spring)	90 mm contraction	11.67	N/A	N/A	L: 120 mm (unstreched) D_{SMA}: 0.5 mm D_{Spring}: 2 mm
Ajou University[92] (2020)	SMA	5	10.5	594	≈1	L: 800 mm D: 0.15 mm
Carlos III University of Madrid[52] (2019)	SMA	4	35.6	181.3	≈0.046 rad s (0.007)	L: 1.5 m Flexion/Extension L: 2 m Pronation/Supination D: 0.5 mm
KAIST[98] (2019)	SMA (spring)	33	10	2	0.5 (cooling system with mineral oil)	L: 150 mm D_{SMA}: 0.5 mm D_{Spring}: 2.5 mm
Carlos III University of Madrid[91] (2018)	SMA	5	35.6	181.3	≈0.04	L: 2.2 m Flexion L: 1.7 m Ulnar/Radial deviation D: 0.5 mm
State Key Laboratory of Mechanism System and Vibration[95] (2013)	SMA	10	13.72	280	> 0.1 (Free convection) 5 (Cooling system with water)	L: 220 mm D: 0.25 mm
Wyss Institute[93] (2011)	SMA (spring)	≈66	5	11	≈0.02	L: 175 mm D_{SMA}: 0.25 mm $D_{InnerSpring}$: 0.51 mm
CNR Institute for Energetics and Interphases at Lecco[89] (2009)	SMA	≈3	10	203	≈0.025	L: 2.5 m D: 0.25 mm
Artificial Intelligence Laboratory[88] (2008)	SMA	20 mm contraction	N/A	N/A	N/A	N/A

The required torque depends on two different aspects, the generated force and the lever arm. In the case of force, SMA is the best material to generate forces, unlike DEAs, which struggle to generate high forces. To overcome this limitation, the most used strategy is to employ bundles of actuators that generate the required force.[52,68,81,100] An alternative to increase the torque is to use a larger lever arm. Nevertheless, this strategy presents the drawback that the lever arm length negatively influences the ROM generated by the AMSMs linear displacement.[61,85] The relation of torque and linear displacement with relation to the lever arm could be expressed as

$$\begin{cases} \Delta l = a \sin \Delta\theta \\ T = Fa \end{cases} \tag{18}$$

where Δl is the required linear displacement of the AMSM, a the lever arm, $\Delta\theta$ angular displacement of the joint, T torque, and F is the force.

The linear displacement is related to the strain of the AM. This is another aspect that limits the use of AMSM, as they usually have decreased strain compared to skeletal muscles (<20%). However, thanks to their flexibility and softness, it is possible to place long actuators in small spaces, allowing the device to attain the required displacement without impacting the actuator's performance.[59,89] For SMA, another option to increase the strain is to fabricate springs made of single wires, similar to TCP, when coiled around a mandrel, with the disadvantage of reducing the generated force.[93,123]

In the case of the speed of the motion, it is mainly related to the frequency of the AMSM. DEAs and PVC gel actuators surpassed the frequencies observed in skeletal muscles. In contrast, TCP and SMA actuators experience frequency as the main limitation. The lower frequency of this technology is related to the slow cooling time of the actuators. To improve the speed of the system, actuators with small diameters with lower thermal mass could be utilized as they cool faster.[80,92] Alternatively, one could use external cooling systems,[99,124] but they introduce two issues: increases in weight and power consumption of the device.

In general, to improve the performance of the actuators is necessary to implement closed-loop control strategies that allow the system to provide faster, accurate, and efficient responses.[52,59,78] Applying these closed-loop control strategies usually requires different sensors to read external variables like position and force. Nevertheless, one of the advantages of AMSM is that they present self-sensing properties, allowing for more compact designs as they can be used as sensors and actuators simultaneously.[125–127]

3.5. Summary and Future Developments

The majority of exoskeletons are heavy and bulky, which may cause earlier fatigue or damage to the weak muscles of people with physical disabilities.[9,128] AMSMs have emerged as a solution for this problem thanks to their properties of compliance and lightweight. Nevertheless, they require high voltages and present high-power consumption, making necessary the use of cumbersome equipment such as batteries and high-voltage amplifiers, which are the main contributors to the final weight of the device. Furthermore, power consumption and high voltages are problematic from other perspectives. They can limit the device's use time as well as its autonomy. In some instances, tethering to a power supply may be required,[59] and in the case of the voltages, it may pose a safety risk to the users. However, energy storage and energy transmission are continually being developed, with improvements in the energy density[129,130] and miniaturization of batteries,[131–133] as well as downsized electronic systems,[114] which will ultimately lead to the implementation of SWWR based on AMSM being feasible in the early future.

A specific problem for the thermal base AMSM (SMA and TCP) is the temperatures that they can reach. To generate the maximum force/displacement, they generate temperatures over the pain threshold of humans (44 °C at the dermal/epidermal interface of the skin).[59,134] For this reason, it is still necessary to research design and materials that help to incorporate the artificial muscles seamlessly into the SWRR that can insulate the actuator from the users allowing for comfortable use.[91,135]

AMSM actuators have some properties exceeding those of the skeletal muscles (e.g., SMA generates higher output stress, and DEAs can work at higher frequencies than skeletal muscle). However, currently, there is no AMSM that can integrate all the properties needed to achieve the body's musculoskeletal movement (e.g., AMSM still has a lower strain). Furthermore, there is still a lack of mathematical models that can represent all the physical transformations that the actuators present.[71,84,122] Hence, research on new theoretical models and manufacturing processes that permit or use different compounds to improve the performance of AMSM is still needed.

Based on the data concerning biomechanical requirements related to human movement and the current capability of existing devices (Table 1–8), it is still challenging to use AMSM in SWRR. Nevertheless, using them could be feasible if a proper control strategy is implemented and the assistive task is specific and simple.[59,85] An example is assisting ankle dorsiflexion through the swing phase of gait to help people with "foot drop".[136] This task is in only one plane of motion, does not require fast movement nor high forces given the mass of the foot, and the ROM required is relatively small. Another possibility to start exploring the use of AMSM is to integrate them into hybrid devices with two or more actuation technologies. For instance, it is possible to find devices where the primary actuator generates the forces, and the movements are electric motors, with a smart material to add compliance to the device.[105]

4. Conclusion

It can be concluded that AMSMs are promising actuators to be used in SWRR. However, a better understanding of the minimum biomechanical requirements is necessary to design solutions that can provide a reasonable level of assistance to specific tasks. It seems logical to address relatively simple tasks first before moving toward more complex multifaceted movements that may require high forces and high angular velocities of joint motion with rapid acceleration and decelerations. There is applicability waiting to improve the quality of life of the elderly as well as younger individuals with diseases and

injuries that have left them notably disabled due to muscle weakness.

5. Limitations

The sources analyzed in regard to AMSM are limited to their relationship with SWRR. Therefore, it is not representative of the whole cohort of AMSM currently available for other applications.

In contrast, as this work mainly focuses on the functionality and the gap in the technology of SWRR based on AMSM, artificial muscles for rehabilitation with better performance could exist.

6. Experimental Section

An in-depth literature search was performed, following the search strategy of the Preferred Reporting Items for Systematic Reviews and Meta-Analyses (PRISMA) guidelines.[137] The literature search utilized Scopus and Web of Science databases, using the combination of the following keywords: (Artificial Muscle*) OR (actuat* AND (complian* OR elastic* OR soft)) and (robot* OR wearable OR "active ortho*" OR "active prosthe" OR exoskeleton) and (rehab* OR assistance) not pneumatic*. To make our search as complete as possible, a search through the university library databases was also conducted.

To eliminate areas not linked sufficiently with the aims, articles in the following areas were excluded: a) Non-actuated compliant systems; b) Non-wearable systems; c) Solutions where the soft actuator relies on electric motors or fluidic systems (e.g., pneumatic and hydraulic) as the source of force generation; d) Studies that did not report any mechanical information on the robot; e) Studies not related to either assistance or rehabilitation.

Acknowledgements

This work was partially supported by "Consejo Nacional de Ciencica y Tecnologia" of Mexico (no. 739850).

Conflict of Interest

The authors declare no conflict of interest.

Keywords

artificial muscles, rehabilitation, smart materials, soft robots, wearables

Received: June 8, 2022
Revised: September 6, 2022
Published online:

[1] D. J. Reinkensmeyer, *J. Neuroeng. Rehabil.* **2019**, *16*, 144.
[2] A. Zoss, H. Kazerooni, A. Chu, in *2005 IEEE/RSJ Int. Conf. on Intelligent Robots and Systems*, IEEE, Piscataway, NJ **2005**, pp. 3465–3472.
[3] J. Howard, V. V. Murashov, B. D. Lowe, M. L. Lu, *Am. J. Ind. Med.* **2020**, *63*, 201.
[4] M. Kuroda, S. Nakagawa, H. Mutsuzaki, Y. Mataki, K. Yoshikawa, K. Takahashi, T. Nakayama, N. Iwasaki, *Brain Dev.* **2020**, *42*, 468.
[5] P. Maciejasz, J. Eschweiler, K. Gerlach-Hahn, A. Jansen-Troy, S. Leonhardt, *J. Neuroeng. Rehabil.* **2014**, *11*, 3.
[6] R. Lee, *J. Econ. Perspect.* **2003**, *17*, 167.
[7] Organization, W. H., The global burden of disease: 2004 update, **2008**.
[8] M. Shishehgar, D. Kerr, J. Blake, *Smart Health* **2018**, *7*, 1.
[9] Y. He, D. Eguren, T. P. Luu, J. L. Contreras-Vidal, *Med. Devices Evidence Res.* **2017**, *10*, 89.
[10] Z. F. Lerner, G. M. Gasparri, M. O. Bair, J. L. Lawson, J. Luque, T. A. Harvey, A. T. Lerner, *IEEE Trans. Neural Syst. Rehabil. Eng.* **2018**, *26*, 1985.
[11] R. A. Bos, K. Nizamis, B. F. J. M. Koopman, J. L. Herder, M. Sartori, D. H. Plettenburg, *IEEE Trans. Neural Syst. Rehabil. Eng.* **2020**, *28*, 258.
[12] J. Sancho-Perez, M. Pérez, E. García, D. Sanz-Merodio, A. Plaza, M. Cestari, *Advances in Cooperative Robotics*, World Scientific, Singapore **2017**, pp. 814–822.
[13] T. Bützer, J. Dittli, J. Lieber, H. J. van Hedel, A. Meyer-Heim, O. Lambercy, R. Gassert, 2019 *IEEE 16th Inter. Conf. on Rehabilitation Robotics (ICORR)*, IEEE, Piscataway, NJ **2019**, pp. 108–114.
[14] Z. F. Lerner, T. A. Harvey, J. L. Lawson, *Ann. Biomed. Eng.* **2019**, *47*, 1345.
[15] A. Borboni, M. Mor, R. Faglia, *J. Dyn. Syst. Meas. Contr.* **2016**, *138*.
[16] B. W. Ang, C.-H. Yeow, *IEEE Rob. Autom. Lett.* **2020**, *5*, 3731.
[17] R. S. Araujo, C. R. Silva, S. P. Netto, E. Morya, F. L. Brasil, *Front. Neurosci.* **2021**, *15*.
[18] A. J. Veale, S. Q. Xie, *Med. Eng. Phys.* **2016**, *38*, 317.
[19] D. Rus, M. T. Tolley, *Nature* **2015**, *521*, 467.
[20] Z. Peng, J. Huang, *Appl. Sci.* **2019**, *9*, 3102.
[21] M. Bengisu, M. Ferrara, *Materials that Move: Smart Materials, Intelligent Design*, Springer, Berlin **2018**.
[22] S. Bahl, H. Nagar, I. Singh, S. Sehgal, *Mater. Today: Proc.* **2020**, *28*, 1302.
[23] M. Zhu, S. Biswas, S. I. Dinulescu, N. Kastor, E. W. Hawkes, Y. Visell, *Proc. IEEE* **2022**, *110*, 246.
[24] H. Jin, E. Dong, M. Xu, C. Liu, G. Alici, Y. Jie, *Smart Mater. Struct.* **2016**, *25*, 085026.
[25] U. Gupta, L. Qin, Y. Wang, H. Godaba, J. Zhu, *Smart Mater. Struct.* **2019**, *28*, 103002.
[26] W. Peng, Y. Zhang, J. Gao, Y. Wang, Y. Chen, Y. Zhou, *Sens. Actuators A: Phys.* **2019**, *299*, 111613.
[27] Y. Zhang, L. Huang, H. Song, C. Ni, J. Wu, Q. Zhao, T. Xie, *ACS Appl. Mater. Interfaces* **2019**, *11*, 32408.
[28] C. S. Haines, M. D. Lima, N. Li, G. M. Spinks, J. Foroughi, J. D. W. Madden, S. H. Kim, S. Fang, M. Jung De Andrade, F. Göktepe, Ö. Göktepe, S. M. Mirvakili, S. Naficy, X. Lepró, J. Oh, M. E. Kozlov, S. J. Kim, X. Xu, B. J. Swedlove, G. G. Wallace, R. H. Baughman, *Science* **2014**, *343*, 868.
[29] W.-S. Chu, K.-T. Lee, S.-H. Song, M.-W. Han, J.-Y. Lee, H.-S. Kim, M.-S. Kim, Y.-J. Park, K.-J. Cho, S.-H. Ahn, *Int. J. Precis. Eng. Manuf.* **2012**, *13*, 1281.
[30] R. Granberry, J. Barry, B. Holschuh, J. Abel, *Adv. Mater. Technol.* **2021**, *6*, 2000825.
[31] V. Murphy, B. P. Edmonds, A. L. Trejos, *Actuators* **2021**, *10*, 37.
[32] J. Guo, C. Xiang, T. Helps, M. Taghavi, J. Rossiter, in *2018 IEEE Int. Conf. on Soft Robotics (RoboSoft)*, IEEE, Piscataway, NJ **2018**, pp. 339–343.
[33] J. Zhang, J. Sheng, C. T. O'Neill, C. J. Walsh, R. J. Wood, J.-H. Ryu, J. P. Desai, M. C. Yip, *IEEE Trans. Rob.* **2019**, *35*, 761.
[34] S. M. Mirvakili, I. W. Hunter, *Adv. Mater.* **2018**, *30*, 1704407.
[35] T. Shahid, D. Gouwanda, S. G. Nurzaman, A. A. Gopalai, *Biomimetics* **2018**, *3*, 17.
[36] E. Bardi, M. Gandolla, F. Braghin, F. Resta, A. L. G. Pedrocchi, E. Ambrosini, *J. NeuroEng. Rehabil.* **2022**, *19*.

[37] A. P. Aliseichik, D. A. Gribkov, A. R. Efimov, I. A. Orlov, V. E. Pavlovsky, A. V. Podoprosvetov, I. V. Khaidukova, *J. Comput. Syst. Sci. Int.* **2022**, *61*, 270.
[38] Nematollahi, M., Baghbaderani, K. S., Amerinatanzi, A., Zamanian, H. & Elahinia, M. *Application Of NiTi In Assistive And Rehabilitation Devices: A Review. Bioengineering*, Basel **2019**, p. 6, https://doi.org/10.3390/bioengineering6020037.
[39] T.-Y. Dong, X.-L. Zhang, T. Liu, *Front. Inf. Technol. Electron. Eng.* **2018**, *19*, 1303.
[40] K. L. Mudie, A. C. Boynton, T. Karakolis, M. P. O'Donovan, G. B. Kanagaki, H. P. Crowell, R. K. Begg, M. E. Lafiandra, D. C. Billing, *J. Sci. Med. Sport* **2018**, *21*, 1154.
[41] M. A. Lobo, M. L. Hall, B. Greenspan, P. Rohloff, L. A. Prosser, B. A. Smith, *Phys. Ther.* **2019**, *99*, 647.
[42] A. Kapsalyamov, S. Hussain, P. K. Jamwal, *IEEE Access* **2020**, *8*, 178991.
[43] S. Kawasaki, K. Ohata, T. Yoshida, A. Yokoyama, S. Yamada, *J. NeuroEng. Rehabil.* **2020**, *17*, 1.
[44] K. Nizamis, A. H. A. Stienen, D. G. Kamper, T. Keller, D. H. Plettenburg, E. J. Rouse, D. Farina, B. F. J. M. Koopman, M. Sartori, *IEEE Trans. Med. Rob. Bionics* **2019**, *1*, 88.
[45] M. Cenciarini, A. M. Dollar, in *2011 IEEE Int. Conference on Rehabilitation Robotics*, IEEE, Piscataway, NJ, pp. 1–6.
[46] D. H. Gates, L. S. Walters, J. Cowley, J. M. Wilken, L. Resnik, *Am. J. Occup. Ther.* **2016**, *70*, 7001350010p7001350011.
[47] C. L. Brockett, G. J. Chapman, *Orthop. Trauma* **2016**, *30*, 232.
[48] H. Tanaka, M. Yoshikawa, E. Oyama, Y. Wakita, Y. Matsumoto, *J. Rob.* **2013**, *2013*, 12.
[49] H. S. Nam, H. G. Seo, J.-H. Leigh, Y. J. Kim, S. Kim, M. S. Bang, *Appl. Sci.* **2019**, *9*, 2471.
[50] H. I. Krebs, B. T. Volpe, D. Williams, J. Celestino, S. K. Charles, D. Lynch, N. Hogan, , *IEEE Trans. Neural Syst. Rehabil. Eng.* **2007**, *15*, 327.
[51] J. Rosen, J. C. Perry, N. Manning, S. Burns, B. Hannaford, in *ICAR'05. Proc., 12th Int. Conf. on Advanced Robotics*, Seattle, WA 2005, pp. 532–539.
[52] D. Copaci, F. Martín, L. Moreno, D. Blanco, *IEEE Access* **2019**, *7*, 31473.
[53] K. J. Ganley, C. M. Powers, *Gait Posture* **2005**, *21*, 141.
[54] L.-Q. Zhang, S. G. Chung, S. G. Zhiqiang Bai, S. G. Dali Xu, E. M. T. Van Rey, M. W. Rogers, M. E. Johnson, E. J. Roth, *IEEE Trans. Neural Syst. Rehabil. Eng.* **2002**, *10*, 149.
[55] A. Proto, M. Penhaker, D. Bibbo, D. Vala, S. Conforto, M. Schmid, *Sensors* **2016**, *16*, 524.
[56] C. A. Laubscher, J. T. Sawicki, in *2019 IEEE 16th Int. Conf. on Rehabilitation Robotics (ICORR)*, IEEE, Piscataway, NJ **2019**, pp. 676–681.
[57] R. Vicario, A. Calanca, E. Dimo, N. Murr, M. Meneghetti, R. Ferro, E. Sartori, T. Boaventura, *The 14th PErvasive Technologies Related to Assistive Environments Conf.*, Corfu, Greece **2021**, pp. 359–364.
[58] D. M. Wolpert, *Trends Cognit. Sci.* **1997**, *1*, 209.
[59] L. Saharan, M. J. de Andrade, W. Saleem, R. H. Baughman, Y. Tadesse, *Smart Mater. Struct.* **2017**, *26*, 105048.
[60] A. Behboodi, C. DeSantis, J. Lubsen, S. Lee, in *2020 42nd Annual Int. Conf. of the IEEE Engineering in Medicine & Biology Society (EMBC)*, IEEE, Piscataway, NJ **2020**,pp. 4930–4935.
[61] Y. Li, M. Hashimoto, *Smart Mater. Struct.* **2017**, *26*, 125003.
[62] A. Gonzalez, L. Garcia, J. Kilby, P. McNair, *BioMed. Eng. OnLine* **2021**, *20*.
[63] C. J. Nycz, T. Butzer, O. Lambercy, J. Arata, G. S. Fischer, R. Gassert, *IEEE Rob. Autom. Lett.* **2016**, *1*, 976.
[64] R. C. Browning, J. R. Modica, R. Kram, A. Goswami, *Med. Sci. Sports Exercise* **2007**, *39*, 515.
[65] Y. Bar-Cohen, Y. Bar-Cohen, *Electroactive polymer (EAP) actuators as artificial muscles: Reality, potential, and challenges*, Vol. *136*, SPIE Press, Bellingham, WA **2004**.
[66] A. Behboodi, S. Lee, in *2019 IEEE 16th Int. Conf. on Rehabilitation Robotics (ICORR)*, IEEE, Piscataway, NJ **2019**, pp. 499–505.
[67] B. Shi, X. Chen, Z. Yue, S. Yin, Q. Weng, X. Zhang, J. Wang, W. Wen, *Front. Neurorob.* **2019**, *13*, 63.
[68] F. Carpi, A. Mannini, D. De Rossi, in *Electroactive Polymer Actuators and Devices (EAPAD)*, International Society for Optics and Photonic, **2008**, p. 692705.
[69] Y. Li, M. Hashimoto, *Sens. Actuators A: Phys.* **2015**, *233*, 246.
[70] Y. Li, Y. Maeda, M. Hashimoto, *Int. J. Adv. Rob. Syst.* **2015**, *12*, 175.
[71] Y. Li, M. Guo, Y. Li, *J. Mater. Chem. C* **2019**, *7*, 12991.
[72] M. Yamano, N. Ogawa, M. Hashimoto, M. Takasaki, T. Hirai, in *2008 IEEE Int. Conf. on Robotics and Biomimetics*, IEEE, Piscataway, NJ **2008**, pp. 745–750.
[73] Y. Li, M. Hashimoto, in *2015 IEEE Int. Conf. on Robotics and Automation (ICRA)*, IEEE, Piscataway, NJ **2015**, pp. 2920–2925.
[74] S. M. Mirvakili, A. Rafie Ravandi, I. W. Hunter, C. S. Haines, N. Li, J. Foroughi, S. Naficy, G. M. Spinks, R. H. Baughman, J. D. W. Madden, Simple and strong: twisted silver painted nylon artificial muscle actuated by Joule heating, Vol. 9056, SPIE, **2014**.
[75] S. Y. Yang, K. Kim, J. U. Ko, S. Seo, S. T. Hwang, J. H. Park, H. S. Jung, Y. J. Gong, J. W. Suk, H. Rodrigue, *Soft Rob.* **2022**.
[76] S. A. Horton, P. Dumond, *IEEE/ASME Trans. Mechatron.* **2019**, *24*, 2130.
[77] Y. Almubarak, M. Schmutz, M. Perez, S. Shah, Y. Tadesse, Kraken: A wirelessly controlled octopus-like hybrid robot utilizing stepper motors and fishing line artificial muscle for grasping underwater, **2021**.
[78] M. C. Yip, G. Niemeyer, *IEEE Trans. Rob.* **2017**, *33*, 689.
[79] A. Simeonov, T. Henderson, Z. Lan, G. Sundar, A. Factor, J. Zhang, M. Yip, *IEEE Rob. Autom. Lett.* **2018**, *3*, 1671.
[80] C. S. Haines, G. Niemeyer, in *2018 IEEE/RSJ Int. Conf. on Intelligent Robots and Systems (IROS)*, IEEE, Piscataway, NJ **2018**, pp. 6980–6985.
[81] L. Sutton, H. Moein, A. Rafiee, J. D. Madden, C. Menon, in *2016 6th IEEE Inter. Conf. on Biomedical Robotics and Biomechatronics (BioRob)*, IEEE, Piscataway, NJ **2016**, pp. 1074–1079.
[82] A. G. Patiño, A. Ferrone, C. G. D. Gastélum, C. Menon, in *2018 IEEE 9th Annual Information Technology, Electronics and Mobile Communication Conf. (IEMCON)*., IEEE, Piscataway, NJ **2018**, pp. 620–625.
[83] D. Copaci, E. Cano, L. Moreno, D. Blanco, *Appl. Bionics Biomech.* **2017**, *2017*, 1605101.
[84] Á. Villoslada, N. Escudero, F. Martín, A. Flores, C. Rivera, M. Collado, L. Moreno, *Sens. Actuators A: Phys.* **2015**, *236*, 257.
[85] J. Zhang, Y. Yin, J. Zhu, *Sens. Actuators A: Phys.* **2013**, *201*, 264.
[86] J.-S. Koh, *Materials* **2018**, *11*, 2324.
[87] J. M. Jani, M. Leary, A. Subic, M. A. Gibson, *Mater. Des.* **2014**, *56*, 1078.
[88] D. Jayatilake, A. Gruebler, K. Suzuki, in *2008 4th Int. Conf. on Information and Automation for Sustainability*, Colombo, Sri Lanka **2008**, pp. 395–400.
[89] S. Pittaccio, S. Viscuso, M. Rossini, L. Magoni, S. Pirovano, E. Villa, S. Besseghini, F. Molteni, *J. Mater. Eng. Perform.* **2009**, *18*, 824.
[90] S. Pittaccio, F. Zappasodi, S. Viscuso, F. Mastrolilli, M. Ercolani, F. Passarelli, F. Molteni, S. Besseghini, P. M. Rossini, F. Tecchio, *Hum. Brain Mapp.* **2011**, *32*, 60.
[91] S. H. Koo, Y. B. Lee, C. Kim, G. Kim, G. Lee, J.-S. Koh, *Int. J. Clothing Sci. Technol.* **2020**, *33*, 513.

[92] C. Kim, G. Kim, Y. Lee, G. Lee, S. Han, D. Kang, S. H. Koo, J.-S. Koh, *Smart Mater. Struct.* **2020**, *29*, 055003.
[93] L. Stirling, C.-H. Yu, J. Miller, E. Hawkes, R. Wood, E. Goldfield, R. Nagpal, *J. Mater. Eng. Perform.* **2011**, *20*, 658.
[94] D. Serrano, D. S. Copaci, L. Moreno, D. Blanco, in *2018 IEEE/RSJ Int. Conf. on Intelligent Robots and Systems (IROS)*, IEEE, Piscataway, NJ **2018**, pp. 2318–2323.
[95] D. Copaci, D. Blanco, L. Moreno, in *Proc. of the Joint Workshop on Wearable Robotics and Assistive Devices, Inter. Conf. on Intelligent Robots and Systems (IROS 2016)*, Daejeon, Korea **2016**, pp. 9–14.
[96] A. Villoslada, A. Flores, D. Copaci, D. Blanco, L. Moreno, *Rob. Auton. Syst.* **2015**, *73*, 91.
[97] J. Jeong, K. Hyeon, S.-Y. Jang, C. Chung, S. Hussain, S.-Y. Ahn, S.-K. Bok, K.-U. Kyung, *IEEE Rob. Autom. Lett.* **2022**, *7*, 6028.
[98] J. Jeong, I. B. Yasir, J. Han, C. H. Park, S.-K. Bok, K.-U. Kyung, *Appl. Sci.* **2019**, *9*, 4025.
[99] J. Jeong, K. Hyeon, J. Han, C. H. Park, S.-Y. Ahn, S.-K. Bok, K.-U. Kyung, *IEEE/ASME Trans. Mechatron.* **2021**, *27*, 1046.
[100] K. Hyeon, J. Jeong, C. Chung, M. Cho, S. Hussain, K.-U. Kyung, *IEEE Rob. Autom. Lett.* **2022**, *7*, 10635.
[101] S. J. Park, K. Choi, H. Rodrigue, C. H. Park, *Sci. Rep.* **2022**, *12*.
[102] S. J. Park, C. H. Park, *Sci. Rep.* **2019**, *9*.
[103] A. Behboodi, J. F. Alesi, S. C. Lee, *Soft Robotics In Rehabilitation*, Elsevier, Amsterdam **2021**, pp. 241–258.
[104] A. Washington, J. Neubauer, K. J. Kim, *Soft Robotics In Rehabilitation*, Elsevier, Amsterdam **2021**, pp. 89–110.
[105] A. Firouzeh, J. Paik, in *2017 IEEE/RSJ Int. Conf. on Intelligent Robots and Systems (IROS)*, IEEE, Piscataway, NJ **2017**, pp. 306–313.
[106] T. Mirfakhrai, J. D. W. Madden, R. H. Baughman, *Mater. Today* **2007**, *10*, 30.
[107] W. Mohdisa, A. Hunt, S. H. HosseinNia, *Sensors* **2019**, *19*, 3967.
[108] S. M. Mirvakili, I. W. Hunter, *Adv. Mater.* **2018**, *30*, 1704407.
[109] M. Hao, Y. Wang, Z. Zhu, Q. He, D. Zhu, M. Luo, *Front. Rob. AI* **2019**, *6*, 129.
[110] Q. He, Z. Liu, G. Yin, Y. Yue, M. Yu, H. Li, K. Ji, X. Xu, Z. Dai, M. Chen, *Smart Mater. Struct.* **2020**, *29*, 045013.
[111] E. Acome, S. K. Mitchell, T. G. Morrissey, M. B. Emmett, C. Benjamin, M. King, M. Radakovitz, C. Keplinger, *Science* **2018**, *359*, 61.
[112] S. K. Mitchell, X. Wang, E. Acome, T. Martin, K. Ly, N. Kellaris, V. G. Venkata, C. Keplinger, *Adv. Sci.* **2019**, *6*, 1900178.
[113] N. Kellaris, P. Rothemund, Y. Zeng, S. K. Mitchell, G. M. Smith, K. Jayaram, C. Keplinger, *Adv. Sci.* **2021**, *8*, 2100916.
[114] Z. Yoder, N. Kellaris, C. Chase-Markopoulou, D. Ricken, S. K. Mitchell, M. B. Emmett, R. F. Weir, J. Segil, C. Keplinger, *Front. Rob. AI* **2020**, *7*, 181.
[115] H. Meng, J. Hu, *J. Intell. Mater. Syst. Struct.* **2010**, *21*, 859.
[116] M. R. A. Bhatti, E. Bilotti, H. Zhang, C. W. Bastiaansen, T. Peijs, *Polymer* **2020**, *207*, 122897.
[117] L. Sun, W. M. Huang, Z. Ding, Y. Zhao, C. C. Wang, H. Purnawali, C. Tang, *Mater. Des.* **2012**, *33*, 577.
[118] S.-H. Chen, W.-M. Lien, W.-W. Wang, G.-D. Lee, L.-C. Hsu, K.-W. Lee, S.-Y. Lin, C.-H. Lin, L.-C. Fu, J.-S. Lai, J.-J. Luh, W.-S. Chen, *IEEE Trans. Neural Syst. Rehabil. Eng.* **2016**, *24*, 1199.
[119] Y. N. Wu, M. Hwang, Y. Ren, D. Gaebler-Spira, L. Q. Zhang, *Neurorehabil. Neural Repair* **2011**, *25*, 378.
[120] R. Michnik, et al., *Information Technologies in Biomedicine*, Springer, Berlin **2008**, pp. 551–558.
[121] S. J. Bae, S. H. Jang, J. P. Seo, P. H. Chang, *Front. Hum. Neurosci.* **2017**, *11*.
[122] F. Karami, L. Wu, Y. Tadesse, *IEEE/ASME Trans. Mechatron.* **2020**, *26*, 300.
[123] T. Tsabedze, C. Mullen, R. Coulter, S. Wade, J. Zhang, in *2020 IEEE Int. Conf. on Robotics and Automation (ICRA)*, IEEE, Piscataway, NJ **2020**, pp. 5862–5868.
[124] B. P. Edmonds, A. L. Trejos, in *2019 IEEE 16th Inter. Conf. on Rehabilitation Robotics (ICORR)*, IEEE, Piscataway, NJ **2019**, pp. 368–373.
[125] K. Ly, N. Kellaris, D. McMorris, B. K. Johnson, E. Acome, V. Sundaram, M. Naris, J. S. Humbert, M. E. Rentschler, C. Keplinger, *Soft Rob.* **2020**, *8*, 637.
[126] D. Zhou, W. Zuo, X. Tang, J. Deng, Y. Liu, *Bioinspiration Biomimetics* **2021**, *16*, 045003.
[127] S. Wang, H. Huang, H. Huang, B. Li, K. Huang, *IEEE Rob. Autom. Lett.* **2021**, *6*, 2775.
[128] A. Plaza, M. Hernandez, G. Puyuelo, E. Garces, E. Garcia, *IEEE Rev. Biomed. Eng.* **2021**.
[129] L. Ma, N. Li, C. Long, B. Dong, D. Fang, Z. Liu, Y. Zhao, X. Li, J. Fan, S. Chen, S. Zhang, C. Zhi, *Adv. Funct. Mater.* **2019**, *29*, 1906142.
[130] B. Zhu, X. Wang, P. Yao, J. Li, J. Zhu, *Chem. Sci.* **2019**, *10*, 7132.
[131] M. Synodis, J. Pikul, S. A. B. Allen, M. Allen, in *2019 20th Int. Conf. on Solid-State Sensors, Actuators and Microsystems & Eurosensors XXXIII (TRANSDUCERS & EUROSENSORS XXXIII)*, Berlin, Germany **2019**, pp. 789–792.
[132] B. He, Q. Zhang, L. Li, J. Sun, P. Man, Z. Zhou, Q. Li, J. Guo, L. Xie, C. Li, X. Wang, J. Zhao, T. Zhang, Y. Yao, *J. Mater. Chem. A* **2018**, *6*, 14594.
[133] Q. Liu, G. Zhang, N. Chen, X. Feng, C. Wang, J. Wang, X. Jin, L. Qu, *Adv. Funct. Mater.* **2020**, *30*, 2002086.
[134] J. Lawrence, J. Bull, *Eng. Med.* **1976**, *5*, 61.
[135] J. Berzowska, M. Coelho, in *Ninth IEEE Int. Symp. on Wearable Computers (ISWC'05)*., IEEE, Piscataway, NJ, pp. 82–85.
[136] F. Alnajjar, R. Zaier, S. Khalid, M. Gochoo, *Expert Rev. Med. Dev.* **2020**, *18*, 31.
[137] A. Liberati, D. G. Altman, J. Tetzlaff, C. Mulrow, P. C. Gøtzsche, J. P. A. Ioannidis, M. Clarke, P. J. Devereaux, J. Kleijnen, D. Moher, *J. Clin. Epidemiol.* **2009**, *62*, e1.
[138] Y. Li, M. Hashimoto, in *2016 6th IEEE Inter. Conf. on Biomedical Robotics and Biomechatronics (BioRob)*, IEEE, Piscataway, NJ **2016**, pp. 686–691.
[139] P. Dehail, D. Gagnon, L. Noreau, S. Nadeau, *Spinal Cord* **2008**, *46*, 552.
[140] M. R. Gross, *Anatomical Kinesiology*, Jones & Bartlett Learning, Burlington MA **2020**.
[141] H. Shaaban, C. Pereira, R. Williams, V. Lees, *J. Hand Surg.* **2008**, *33*, 3.
[142] K. A. Mann, F. W. Wernere, A. K. Palmer, *J. Orthopaedic Res.* **1989**, *7*, 304.
[143] A. P. Tjahyono, K. C. Aw, H. Devaraj, W. Surendra, E. Haemmerle, J. Travas-Sejdic, *Ind. Rob. Int. J.* **2013**, *40*, 251.
[144] N. Smaby, M. E. Johanson, B. Baker, D. E. Kenney, W. M. Murray, V. R. Hentz, *J. Rehabil. Res. Dev.* **2004**, *41*, 215.
[145] L. E. Diamond, T. V. Wrigley, K. L. Bennell, R. S. Hinman, J. O'Donnell, P. W. Hodges, *Gait Posture* **2016**, *43*, 198.
[146] N. B. Reese, W. D. Bandy, *Joint Range of Motion and Muscle Length Testing-E-Book*, Elsevier Health Sciences **2016**.
[147] T. B. Palmer, N. D. Jenkins, J. T. Cramer, *J. Sports Sci.* **2013**, *31*, 867.
[148] B. F. Mentiplay, M. Banky, R. A. Clark, M. B. Kahn, G. Williams, *Gait Posture* **2018**, *65*, 190.
[149] S. R. Freitas, J. R. Vaz, P. M. Bruno, M. J. Valamatos, P. Mil-Homens, *Physiol. Meas.* **2013**, *34*, 1483.
[150] S. Pittaccio, S. Viscuso, E. Beretta, A. C. Turconi, S. Strazzer, *Prosthet. Orthot. Int.* **2010**, *34*, 305.
[151] J. G. Neely, R. G. Pomerantz, *Laryngoscope* **2002**, *112*, 1562.

Alberto Gonzalez-Vazquez received a B.S. degree in electronic engineering from Instituto Tecnologico de Morelia and an M.S. degree in biomedical engineering from Politecnico di Milano. He is currently a Ph.D. student at Auckland University of Technology, New Zealand. His research interests include wearables, artificial muscles, and soft robots applied to rehabilitation.

Lorenzo Garcia. BioDesign engineer and academic within the Mechanical Engineering Department at Auckland University of Technology (AUT), New Zealand, holds a B.S. in applied physics, a B.E. in mechanical engineering, and a Ph.D. in biomedical engineering. He is the theme leader in Biomechanics and Biomechatronics Design within the BioDesign Lab Institute. He develops three research lines: Rehabilitation and assistive technologies; tools for trauma and orthopedic medicine, and bio-inspired devices for health care and conservation of nature.

Jeff Kilby. I am presently a senior lecturer in electrical and electronic engineering at Auckland University of Technology (AUT), Auckland, New Zealand. My postgraduate qualifications include a Ph.D. titled "Development of a New Multi-channel Electrode and Signal Processing for Surface Electromyography Signals Feature Extraction" and an M.Eng. (Hons) titled "Wavelet Analysis and Classification of Surface Electromyography Signals", both awarded by AUT. My primary research activity is in biomedical instrumentation and feedback, signal processing, and wireless sensor technology related to surface electromyography. An active member in the following research institutes: Biodesign Lab and Health and Rehabilitation Research Centre at AUT.

Paper 3:

2021 43rd Annual International Conference of the
IEEE Engineering in Medicine & Biology Society (EMBC)
Oct 31 - Nov 4, 2021. Virtual Conference

Artificial muscles performance based on TCP-NiCr actuators

Alberto Gonzalez, *EMBS IEEE Student Member*, Lorenzo García *IEEE Member*,
Jeff Kilby *EMBS IEEE Member* and Harsimran Singh.

***Abstract*—In the past years, artificial muscles (and or soft-actuators) have gained attention to be used in rehabilitation robots due to their inherent compliance. Twisted and coiled polymers (TCP) artificial muscles are one of the prominent alternatives. A recently introduced method to activate the TCP is to use an embedded metallic wire. This work analyses the strain and the response time of TCP actuators with different Nichrome (NiCr) wire diameters.**

***Clinical Relevance*— This work constitutes a preliminary guideline to design TCP-NiCr artificial muscles for rehabilitation or assistive soft robotics devices.**

I. INTRODUCTION

In the last decade, exoskeletons have gain interest in the field of healthcare. Current exoskeletons rely on cumbersome elements, making it challenging to overcome adaptability, comfort and safety problems. Consequently, researchers started to pay attention to more compliant components such as artificial muscles and soft-actuators.

TCPs are artificial muscles fabricated by inserting a twist in precursor fibre while attaching a dead weight at the end until it forms a coil structure, followed by heat treatment. TCPs are thermally driven with high power to weight ratio, high stress, a considerable strain, low hysteresis [1].

So, to activate the TCP, the most used strategy is Joule heating. Recently the use of metallic embedded resistance wire into the TCP is gaining attention. However, this method can affect the actuators' performance, changing the strain in a wide range (from 5.5% to 40% [2]-[4]). The main goal of this study is to evaluate the strain and response time of TCP-NiCr.

II. METHODS

10 cm length TCPs were fabricated using a monofilament Nylon fishing line as the precursor fibre (BURNSCO®) with a diameter of 440 μm. The nylon fibres were twisted and coiled along with a NiCr wire, using a weight of 250g (≈ 20 MPa). The NiCr wire was also suspended from the motor shaft but only straightened using a small weight (≈ 1.2 MPa). Five different diameters (0.06 mm to 0.16 mm) of NiCr wires were used for the experiments.

Each actuator was hanging above a laser displacement sensor (0d80 15p850, Sick Optex®), with a weight of 250g attach to one end. A square signal of 90 seconds on (0.15 W/cm) and 90 seconds off was applied on all the tests to activate the actuators.

All authors are with the BioDesign Lab, School of Engineering, Computer and Mathematical Sciences, Auckland University of Technology, Auckland, New Zealand (e-mail: alberto.gonzalez.vazquez@aut.ac.nz, lorenzo.garcia@aut.ac.nz, jeffrey.kilby@aut.ac.nz, xrq1622@autuni.ac.nz). The corresponding author is A. Gonzalez

III. RESULTS

The relationships between strain and diameter, and response time and diameter; for the five different samples are plotted in Fig. 1. The behaviour in both cases appears to be linear, except for an anomaly at 0.08 mm. This anomaly could be related to the applied tension to the NiCr wire, as in the case of the 0.08 mm, the stress was slighter higher (<0.1 MPa).

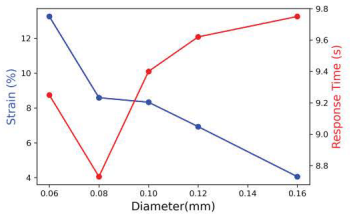

Figure 1. Strain and response time of TCP actuators fabricated with different NiCr wire diameters.

IV. DISCUSSION & CONCLUSION

This work provides pilot guidance to design TCP actuators with metallic embedded wires. However, to better understand the effect of the metallic wire, an evaluation of the impact caused by different precursor fibre sizes is needed. Another essential aspect that required further investigation is the applied tension on the NiCr, as it seems to impact how the wire wraps around the fibre. In conclusion, this study provides highlights on how to tune the desired strain on TCP-NiCr actuators, which is the main parameter to generate motion in artificial muscles for wearable rehabilitation robots.

REFERENCES

[1] C. S. Haines *et al.*, "Artificial muscles from fishing line and sewing thread," *science,* vol. 343, no. 6173, pp. 868-872, 2014.

[2] S. Liu, X. Tang, D. Zhou, and Y. Liu, "Fascicular module of nylon twisted actuators with large force and variable stiffness,", *Sensors and Actuators A: Physical,* vol. 315, Nov 1 2020.

[3] L. Wu, I. Chauhan, and Y. Tadesse, "A Novel Soft Actuator for the Musculoskeletal System", *Advanced Materials Technologies,* vol. 3, no. 5, May 2018, doi: 10.1002/admt.201700359.

[4] J. B. Chossat, D. K. Y. Chen, Y. L. Park, and P. B. Shull, "Soft Wearable Skin-Stretch Device for Haptic Feedback using Twisted and Coiled Polymer Actuators," *IEEE Trans Haptics,* Sep 24 2019, doi: 10.1109/TOH.2019.2943154.

978-1-7281-1178-0/21/$31.00 ©2021 IEEE

Paper 4:

Smart Materials and Structures

PAPER • OPEN ACCESS

Improved performance in temperature and speed of TCP artificial muscles for soft wearables robots by length modification

To cite this article: Alberto Gonzalez-Vazquez *et al* 2023 *Smart Mater. Struct.* **32** 085002

OPEN ACCESS
IOP Publishing
Smart Materials and Structures
Smart Mater. Struct. 32 (2023) 085002 (13pp)
https://doi.org/10.1088/1361-665X/acded6

Improved performance in temperature and speed of TCP artificial muscles for soft wearables robots by length modification

Alberto Gonzalez-Vazquez, Lorenzo García* and Jeff Kilby

BioDesign Lab, School of Engineering, Computer and Mathematical Sciences, Auckland University of Technology, 1010 Auckland, New Zealand

E-mail: lorenzo.garcia@aut.ac.nz

Received 9 February 2023, revised 29 May 2023
Accepted for publication 15 June 2023
Published 26 June 2023

Abstract

Artificial muscles provide a unique solution for wearable rehabilitation robots (WRRs) because they are compliant, compact, and lightweight. Twisted and coiled polymer actuators (TCPs) are artificial muscles from thermally activated polymer fibres. They present high power density, linearity, stress and strain compared to other artificial muscles. Nevertheless, as TCPs require heat to start, their main barrier for widespread use in WRRs are their slow reaction times and the high temperatures they reach. Previous studies have analysed different parameters, like fibre material, fibre diameter, and various cooling systems, to improve TCP frequency response and working temperature. Nevertheless, the length of the actuator has not been explored as a possible parameter to enhance the actuation performance in this regard. This work focuses on studying the behaviour of TCPs with different lengths and how the performance in frequency response and temperature can be improved using the length as a primary parameter, as they are critical for wearable robots. First, a characterisation of the TCPs was performed. Then, a method to improve frequency response, based on offsets on long actuators was implemented and validated using a chirp signal. The experimental results show that the mechanical characteristics are similar regardless of the actuator's length. They reached a strain of 10% with a power of 0.16 W cm^{-1}. However, the electrothermal properties changed as the power needed to increase temperature was higher when the actuator was enlarged. Therefore, an improvement in the required temperature was found, able to reduce the temperature with the same frequency response. Regarding the technique to enhance the speed of the actuator, it was possible to increase the frequency by 0.0006 Hz for each mm applied as an offset. Hence, the frequency response for the same displacement was increased linearly as the actuator was elongated.

* Author to whom any correspondence should be addressed.

Supplementary material for this article is available online

Keywords: artificial muscles, twisted and coiled polymer actuators, wearable devices, rehabilitation robots

(Some figures may appear in colour only in the online journal)

1. Introduction

People with a physical disability caused by conditions like cerebral palsy, stroke, muscular dystrophy, or ageing; face reduced quality of life due to limited mobility and independence [1]. The standard rehabilitation therapies used to manage the musculoskeletal system's deterioration and improve or maintain physical ability, include physiotherapy [2]. These therapies often involve intensive stretching and strengthening exercises facilitated by the physiotherapist to improve motor skills [3]. These interventions are often highly labour-intensive and challenging to perform [4].

During the last decade, wearable rehabilitation robots (WRRs) have gained popularity in rehabilitation [5]. WRRs are expected to improve the outcomes of rehabilitation therapies as they allow for mass practice with reduced intervention of the physiotherapists and help people during daily life activities [6]. However, most current WRRs use electric motors and rigid links to actuate them and often have heavy and bulky designs that are difficult to wear outside clinical facilities safely [7]. Consequently, researchers started to develop soft wearable rehabilitation robots (SWRR) through the use of more compliant elements such as artificial muscles [8] like shape memory alloys [1], dielectric elastomer [9], pneumatic [10], and twisted and coiled polymer actuators (TCPs).

TCPs are artificial muscles fabricated by inserting a twist in precursor polymer fibre while attaching a dead weight at the end until it forms a coil structure, followed by heat treatment [11]. To activate the TCPs is necessary to use an external source of heat as they are made of plastic thread. One option is to utilise joule heating by applying an electric current through a conductive heating element embedded into a TCP, such as metallic wires (e.g. Nichrome wires). This method presents the advantage of making the actuators electrically controllable [12, 13]. In comparison to other artificial muscles, TCPs stand out due to their high power density (27 W g^{-1}), high stress (10 MPa), large strain (21%), and linear behaviour with low hysteresis [14]. Nevertheless, they suffer from low frequencies (<1 Hz) and high temperatures (>65 °C), all critical aspects for SWRR [14–16].

For SWRR applications, there are biomechanical considerations that need to be fulfilled, like torque/force, range of motion/displacement, and velocity/frequency [17, 18]. Due to their advantages, TCPs have gained attention in the SWRR area, as they present high forces and strains. However, they still require improvements in their overall performance as it is still not optimum for the SWRR applications. The main drawbacks are the frequency response and the working temperature.

To overcome these drawbacks, researchers have investigated how different TCPs parameters and techniques impact the actuators' frequency response and working temperature to be used on SWRRs. Hiraoka *et al* [19] used hard linear low-density polyethene fibres to improve the operating temperature. Haines and Niemeyer [20] demonstrated that the response time depends on the fibre diameter. Yip and Niemeyer [21] used a closed-loop control strategy to improve the speed of the fibres during the heating phase. Edmonds and Trejos [22] showed how an active cooling system can increase the maximum frequency where the TCPs can work.

Even if length is one of the primary parameters to consider when designing an application, there is no literature exploring the use of length to improve the response time and temperature of the TCPs. Therefore, this article explores how different lengths impact the actuator's temperature and response time behaviour. Furthermore, a new methodology is presented to improve the TCP frequency response based on the actuator's length without using external cooling systems.

This work is divided into four parts: the first one, section 2, aims to investigate the length impact on the TCPs behaviour by using TCPs of three different lengths (75, 180 and 295 mm) in isotonic contraction (i.e. the muscle contract generating a displacement). The second part, section 3, implements a methodology to improve the frequency response and manage the operational temperature base on the length of the actuator and a PID displacement control. Then, Section 4 discusses the advantages of longer fibres in wearables rehabilitation robots. Finally, a conclusion is presented in section 5.

2. Actuator characterisation

An isotonic contraction test was applied to the TCPs to characterise the actuators and understand their properties in force, strain, response time and temperature, as they are the main requirements for SWRR.

2.1. Materials and methods

The TCP actuators to be analysed were fabricated similarly to the process described by Chossat *et al* [23]. 1.25 m Nylon fishing line was used as the precursor fibre (Trilene Big Game fishing line 50 lb) with a diameter of 700 μm. The nylon fibres were twisted and coiled along with a 36 AWG (127 μm) Nickel-Chromium 80 (NiCr) wire (Fogslord). One side of the nylon fibre was fixed at the end of the output shaft of a NEMA17 (T-Trees Technology) motor. The other end is on a slider weighing 800 g (≈20 MPa). The NiCr wire was also

Figure 1. TCP actuators, (a) Initial actuator, (b) actuators of different sizes with spade electric terminals.

suspended from the motor shaft but only straightened using a small weight of 1.6 g (≈1.2 MPa) and was left free to untwist. The fibres were twisted and coiled at a slow speed of 250 rpm [24]. The embedded NiCr wire generated joule heating for the annealing phase. The annealing process involves applying five consecutive five-minute-long periods with an annealing current of 240 mA each. Between every period, a cooling phase of 1 min was used.

After this process, TCPs with an average length of 330 mm were obtained (figure 1(a)). They were manually trimmed into three sizes of approximately one-quarter, two-quarters, and three-quarters of the initial measurement. They resulted in actuators with a length of 75 mm, 165 mm, and 250 mm. Then the outcoming actuators were clamped with insulated male spade electric terminals, reducing the functional area by 10 mm as each electrical terminal required 5 mm to be crimped (figure 1(b)). The final active lengths of the TCPs were 65 mm, 155 mm and 240 mm with resistance values of 25 Ω, 59 Ω and 92 Ω respectively, meaning that all of them present a resistivity $\rho \approx 0.38\ \Omega\ \mathrm{mm}^{-1}$. The relation between length and resistance can be described with a linear approximation:

$$R = 0.38281 \times L - 0.0305 \quad (1)$$

where R is the resistance (in ohms), and L is the actuator's length (in mm).

Three TCP actuators of each size were manufactured, following the mentioned method. All the samples fabricated for the study were tested using a custom-made experimental test bench. The experimental setup consists of a displacement sensor (Sick Optex 0d80 15p850) connected to a current sensor (Texas Instruments INA269), an Arduino NANO connected to the computer, and a transistor (Vishay Siliconix IRF540) to control the voltage coming from the power supply. The actuator was hanging above the sensor, weighing 700 g. Furthermore, the temperature and the power to activate the TCP were measured using an NTC thermistor (5K3A1, TE Connectivity) and an extra current sensor (Texas Instruments INA269).

A square signal of 150 s on and 150 s off was applied to obtain the strain and power relation. The 150 s was chosen to give enough time to the system to reach a stable condition. The experiment was repeated for different current levels ranging from 160 mA to 220 mA with increments of 20 mA. After applying the load (700 g), the actuator's length was 75 mm, 180 mm and 295 mm. The loaded lengths were the ones used in the results section. Throughout

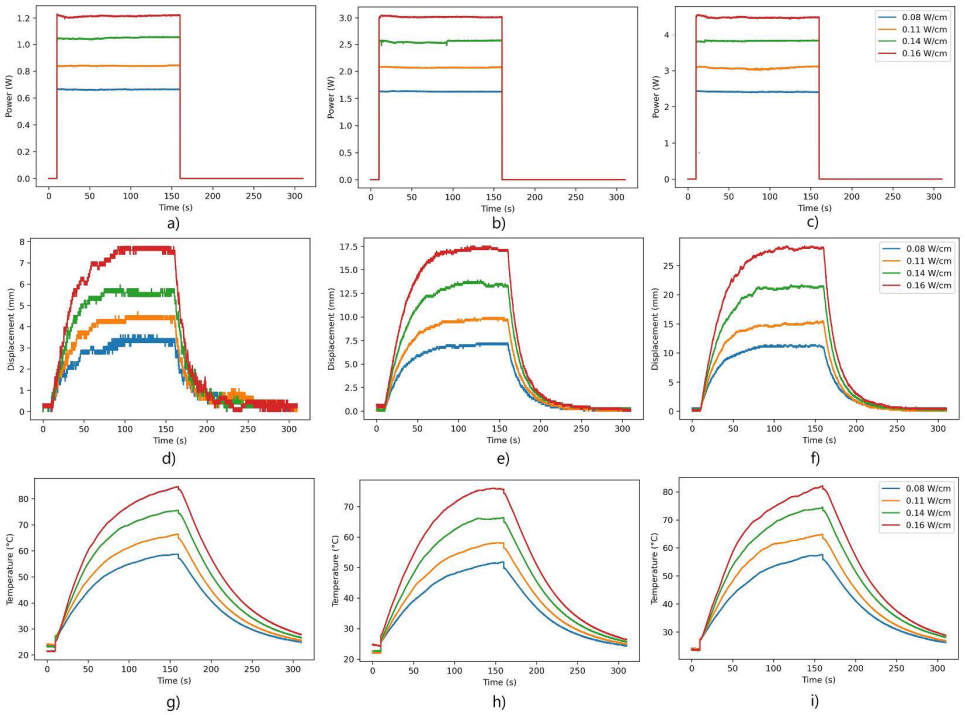

Figure 2. Power consumed by the actuators during the isotonic contraction tests (a) 75 mm, (b) 180 mm, (c) 295 mm. Resultant contraction from the actuator during the isotonic contraction test (d) 75 mm, (e) 180 mm, (f) 295 mm. Reached temperatures from the actuator during the isotonic contraction test (g) 75 mm, (h) 180 mm, (i) 295 mm.

the trial, the TCA temperatures, power consumed, and the weight distance from the sensor were logged into a computer using an Arduino NANO with a sampling time of 50 ms. This test was performed for every actuator of different sizes.

2.2. Results

After performing all of the trials for each different size, the resulting power, displacement, and temperature values were obtained (figure 2). The power consumption was derived from the applied current and the resistance values of the different actuators. When full power was applied to the actuators (1.2 W, 2.8 W and 4.5 W, respectively), the maximum achieved displacements were 7.12 mm, 17.1 mm, and 28.9 mm for the 75 mm, 180 mm, and 295 mm, respectively. The maximum strain of all the TCP of different sizes was ≈10% of the initial length. Regarding the temperature (figures 2(g)–(i)), the maximum average temperatures obtained were 81.26 °C, 80.36 °C, and 76.83 °C for the 75 mm, 180 mm, and 295 mm TCP actuators, respectively.

Other interesting information that can be obtained from the data is the rise (τ_r) and fall (τ_f) response times of the actuators. This is the average time the actuator takes to reach 63% of a steady-state value given a step input. For the 75 mm actuators, $\tau_r = 17.98\,s$ and $\tau_f = 14.51\,s$. In the case of the 180 mm actuators, the τ_r and τ_f were 22.59 s and 16.10 s, respectively. Finally, for the 295 mm actuators, the τ_r and τ_f were 23.58 s and 16.49 s.

The stroke and power levels were calculated for each set of actuators. Then, a linear regression was applied to the mean values of each set of actuators to determine a linear model. In figure 3(a), the linear relation between the applied power in W and the generated stroke can be seen. From this relation, it is possible to observe that, independently of the length of the actuator, the applied power will generate the same amount of stroke. This relation can be represented as ($R^2 = 0.9708$):

$$D = 6.1033 \times P - 1.6426 \quad (2)$$

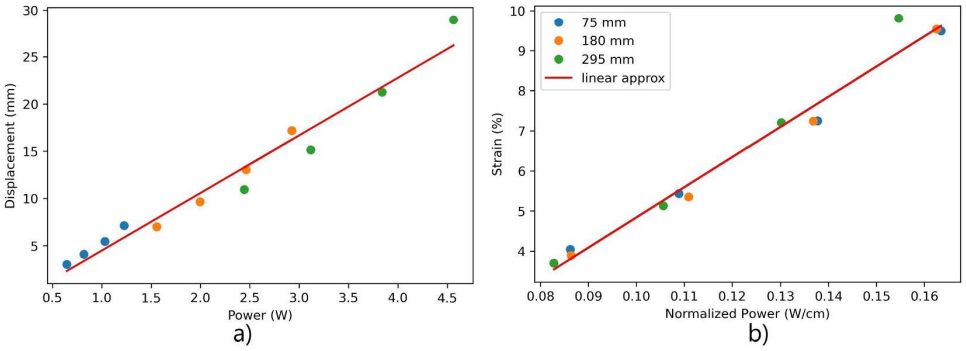

Figure 3. Maximum displacement relation with respect to power, with overlaid linear regression, (b) normalised to TCP length relation.

where D is the generated stroke in mm, and P is the required power in watts.

Furthermore, the idea remains that the relationship between the stroke and the applied power is independent of the actuator length. The TCP length normalised the stroke and the power during the experiments (figure 3(b)), and the following linear relation was obtained ($R^2 = 0.9821$):

$$S = 75.2979 \times NP - 2.692. \tag{3}$$

In this case, S is the strain of the actuator, and NP is the normalised power (W cm^{-1}). The strain of the system is the relation between the initial length (L) of the actuator and the generated stroke (ΔL) when activated, expressed in % as follows:

$$S = \frac{\Delta L}{L} \times 100. \tag{4}$$

Regarding the temperature, a linear trend was found between the temperature and the applied normalised power ($R^2 = 0.9624$):

$$T = 326.9759 \times NP + 27.0464 \tag{5}$$

where T is the temperature in °C and NP is the normalised power. Finally, a linear relation was found between temperature and strain ($R^2 = 0.9296$):

$$S = 0.2204 \times T - 8.257. \tag{6}$$

With the observed relation (equation (3)), it is possible to witness that independently of any unit of length, the strain stay the same due to the asymmetric thermal expansion of polymer monofilaments [11]. Nevertheless, when it comes to the thermal properties, they will change with the length of the actuator [25]. The central values on the electrothermal relation (equation (7)) are dependent on the length (thermal resistance (R_{th}) and thermal capacitance (C_{th})) (figure 4(a)). The dependency on length could be seen in equations (8) and (9) as it forms part of the surface area and volume; respectively

$$C_{th}\frac{\mathrm{d}T(t)}{\mathrm{d}t} = P(t) - \frac{(T_{tcp}(t) - T_{\infty})}{R_{th}} \tag{7}$$

where C_{th} is the thermal capacitance, P is the applied power, R_{th} is the thermal resistance, T_{tcp} is the surface temperature of the TCP and T_{∞} the ambient temperature

$$R_{th} = \frac{1}{A_{tcp}x\left(h + \varepsilon_{tcp} \times \sigma \times (T_{tcp} + T_{\infty}) \times \left(T_{tcp}^2 + T_{\infty}^2\right)\right)} \tag{8}$$

R_{th} can be calculated using the surface area A_{tca}, the thermal convection coefficient h, the emissivity ε_{tcp}, the Stefan Boltzmann's constant σ, and the temperatures generated by the TCP T_{tcp} and the environmental temperature T_{∞}. Moreover A_{tca} can be calculated with:

$$A_{tcp} = 2\pi rL + 2\pi r^2. \tag{9}$$

Being the r the radius of the TCP cross sectional area and the actuator length L

$$C_{th} = \rho x c x v. \tag{10}$$

Finally, C_{th} is obtained multiplying the ρ density, the specific heat capacity c and the volume of the sample v.

It is possible to see the advantages of implementing long actuators into WRR. It is feasible to obtain the same stroke using the same amount of power from a more extended actuator rather than a small actuator's full stroke range and reduce the generated temperature from the TCP actuator (figures 4(b)–(d)) without increasing the time. The main disadvantage of the actuator's increases in length, is the R_{th} decrease as the surface area increase (equation (8)). The change in R_{th} will cause an increase in power consumption to generate the

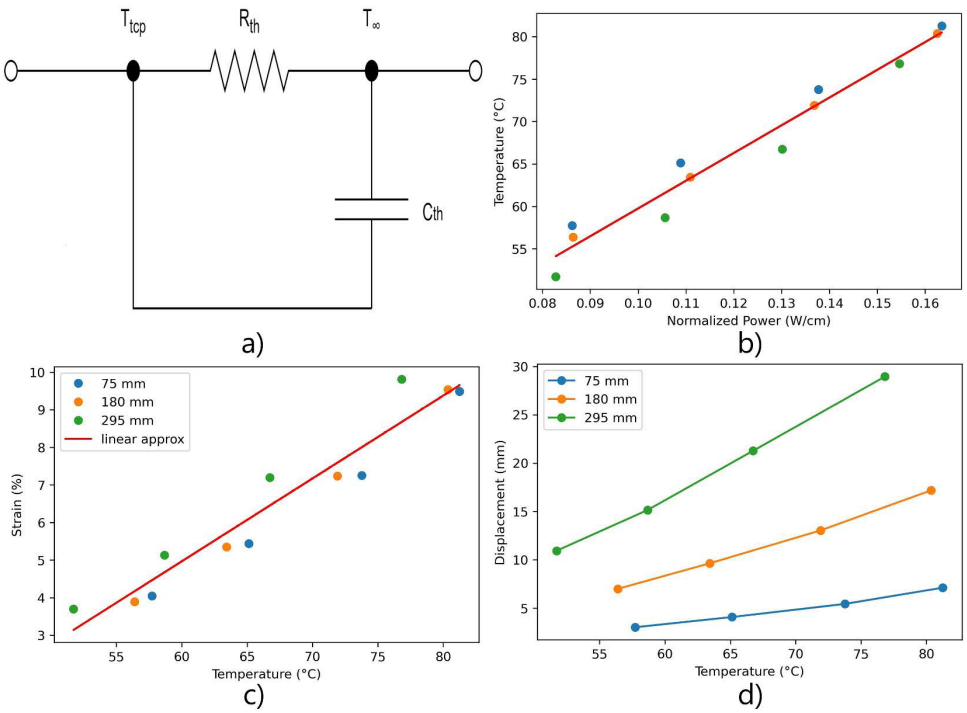

Figure 4. (a) Simplified thermal model of the TCP, consisting of the thermal capacitance C_{th}, the thermal resistance R_{th}, the TCP surface temperature T_{tcp} and the ambient temperature T_∞. Temperature relations during the isotonic contraction test. (b) Temperature against the normalised power, and (c) strain versus temperature. (d) Generated displacement with the three different lengths against the temperature.

same temperature (equation (7)). Nevertheless, the response time will remain similar:

$$\tau = C_{th} x R_{th} \tag{11}$$

where is possible to notice from equations (8) and (9) that the increased and decreased values of C_{th} and R_{th} will change in the same linear manner with the length of the actuator.

3. Displacement control implementation

In the previous section, the characterisation of the TCP actuators was performed. Furthermore, the advantage of a reduction in temperature using longer actuators was found. However, one of the main disadvantages of TCPs is the low frequencies at which they can work (<1 Hz). A strategy to increase the response time could be to briefly apply a pulsed signal with high power peaks [12, 26]. However, the continuation of a high-power pulse will produce an overheating of the actuator, causing it to break or burn out [27]. Hence, a control strategy should be applied to avoid overheating the actuator and work under safety actuation ranges. However, this strategy can only be used during the rising time but not during the falling time, as TCPs are unidirectionally actuated. A popular approach to reducing the response time during the falling time is to implement a cooling system, decreasing the overall response time, with the constraint of requiring external equipment like pumps or fans [21, 22].

This section investigates a method to improve the actuation speed but using long actuators. From the isotonic test in the previous section, it could be seen that length impacts the actuation temperature, as it is possible to obtain a more significant displacement with a lower temperature. Furthermore, Cho *et al* [28] show that the falling time in the temperature of the TCPs depends on how different the final temperature is from the starting temperature. Moreover, Tang *et al* [29] proposed to constrain the range of the activation to improve the speed of a crawling robot. Considering the previous concepts, a method combining both approaches is presented and analysed on how the actuator length could benefit from them and increase the frequency without needing an external cooling system. The technique consists of actuating a specific

Table 1. Frequency domain transfer functions for the power–stroke relationships $G_{PD}(s)$ with one or non-zero for each actuator size.

Actuator size (mm)	G_{PD} (no zero)	Accuracy	G_{PD} (1 zero)	Accuracy
75	$\frac{0.2815}{s^3+4.295s^2+1.232s+0.4748}$	94.8%	$\frac{5.947s+3.119}{s^3+55.48s^2+13.73s+0.5228}$	96.47%
180	$\frac{0.0003572}{s^3+0.162s^2+0.0061s+5.77e^{-5}}$	93.82%	$\frac{1.326s+0.1758}{s^3+7.25s^2+0.8503s+0.02774}$	98.98%
295	$\frac{0.0003575}{s^3+0.1514s^2+0.00643s+5.55e^{-5}}$	97.85%	$\frac{14.53s+2.132}{s^3+89.27s^2+11.24s+0.3366}$	98.93%

displacement using different displacement offsets on the actuators. As the actuator lengthens is possible to add more offsets, which will change the actuation range in temperatures, increasing the actuation speed as the cooling time is reduced.

3.1. Materials and methods

After characterising, in section 2, the strain production of the actuator in an open-loop system, a closed-loop control scheme to operate the displacement output of the actuator is provided. Two different experiments were performed to test the response of the controlled system. First, a step signal was used to analyse the response time while heating, and later a chirp signal was used to analyse the system's frequency response on the proposed control method based on the actuator length.

The test bench was the same as in the characterisation experiments (section 2), with two differences. The sensor reading the current across the TCP was removed due to the higher power values needed to activate the actuator when the PID controller is on. Instead of using the MOSFET as a digital on-off switch, a power pulse width modulation (PWM) strategy was implemented (100 ms cycle time). It allows the usage of high-power signals controlled by the microcontroller. The power was constrained to 0.86 W cm^{-1}, equal to 6.5 W, 16.4 W, and 25.5 W for the 75 mm, 190 mm and 295 mm, respectively. The maximum applied power was chosen due to limitations with the power supply at full power.

3.2. System identification

The controller was constructed based on the stroke characterisation experiment results, which generated a time-domain relationship between stroke output and the input power. The input signal was the maximum applied power for each actuator size, and the output signal was the generated displacement. Later, the curves' pairs were input into the System Identification Toolbox in MATLAB, which derived the power–displacement transfer functions G_{PD} (s) for each actuator length (table 1). The proposed model by Yip and Niemeyer [21] was used as the initial guess to find the order of the transfer function. In this work, the model was divided into a temperature-force relation, a power–force relation, and a force-movement relation.

First, a temperature–force relation was modelled as a spring and damper model with the addition of a linear temperature-dependent term:

$$f(t) = k(x - x_0) + b\dot{x} + c(T(t) - T_0) \tag{12}$$

where f is the force of the system, k is the spring constant, b is the damping coefficient, c is the thermal constant, x is the position, x_0 is the initial position and $\dot{x}$ is the speed.

When the wires are held in isometric tension, the force can be modelled by:

$$f(t) = c(T(t) - T_0). \tag{13}$$

To obtain the power-force relation, equation (13) is combined with the thermoelectric model of the actuators (equation (7)):

$$\frac{F(s)}{P(s)} = \frac{c}{C_{th}s + \frac{1}{R_{th}}}. \tag{14}$$

Then to obtain the force–displacement relation can be modelled as a second-order mass-spring-damper system:

$$f = m\frac{d^2x}{dt^2} + b\frac{dx}{dt} + k(x - x_0). \tag{15}$$

That will result in the following transfer function:

$$\frac{X(s)}{F(s)} = \frac{1}{ms^2 + bs + k}. \tag{16}$$

Finally, combining equations (14) and (16), a third-order system of the following form is obtained:

$$\frac{X(s)}{P(s)} = \frac{A}{Bs^3 + Cs^2 + Ds + E}. \tag{17}$$

A, B, C, D, and E are values derived from the model constants.

The initial estimation of the system was a third-order transfer function with no zeros. However, it was noticed that adding a zero increased the system's accuracy (table 1). Hence the used models were those with one zero.

3.3. Control strategy

When using the transfer functions, a proportional-integral-derivative (PID) controller was tuned using the Control system toolbox in MATLAB. Then the closed loop with the PID controller system was simulated in MATLAB/Simulink. In particular, special care was taken to minimise the overshoot, settling error of the controller, and the necessary power to activate the system, as errors of that nature would result in an incorrect application of force to the user, which could cause harm.

Applying the maximum power, the speed to achieve the highest contraction (10% of the initial length) was 7.5 s.

Table 2. PID controller values.

Actuator length (mm)	Speed (s)	KP	KI	KD
75	7.5	1.394	0.082 67	0
180	7.5	1.309	0.079 55	0
295	7.5	1.484	0.083 65	0
295	1	12.05	4.408	0

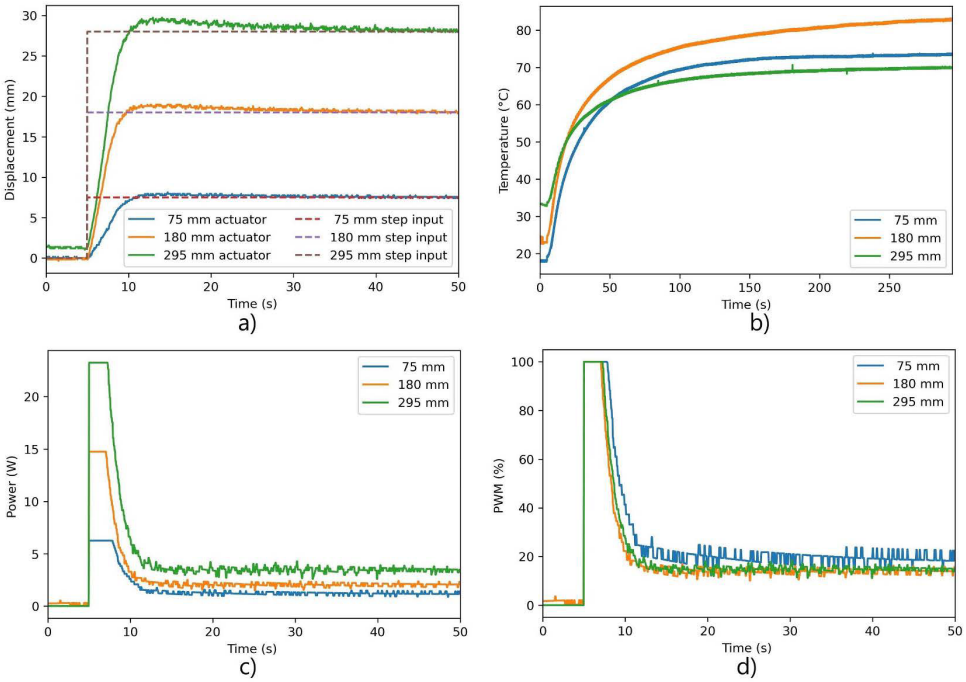

Figure 5. (a) Step response and (b) temperature from different sizes of TCPs when the PID controller strategy is applied. PWM control signal expressed (c) in consumed power and (d) in % of the PWM.

However, the values for a reaction time of 1 s equivalent to a frequency of 1 Hz were also investigated and applied in the chirp test. As most activities of daily life (ADLs) frequencies are around 1 Hz [30, 31]. According to table 2, the PID values are similar for all the different lengths. The values obtained for the 295 mm model were used, as this model was the best of the 3 cases obtaining accuracies over 83% when fitting to the data.

After the closed-loop controller was tuned, it was implemented on an Arduino NANO microcontroller. Two different tests were performed. First, a step input test was applied to determine their performance in controlling the actuator, and then a chirp test was used to test the bandwidth of the actuator.

3.4. Results

3.4.1. Step response. The step response was applied to the full stroke (a strain of 10%). Figure 5(a) shows the position reference and the output when a step signal was applied for the different actuator sizes. It can be observed that the output follows the reference, but the system presents an underdamped response. The time from 0% to 10% of the initial length was less than 10 s. Contraction time can be minimised by changing the controller gains, but an aggressive control signal will increase the peak power required to produce the change.

Nevertheless, the falling time was the same as the open-loop system and depended on the convective air to cool down

the system. From figure 5(c), it is possible to notice the difference between the required power to make a fast movement and the power to maintain a steady state. In the case of the steady-state power, once the actuator reaches a steady-state, the consumed power is similar to the power required on the open-loop system (approx. 1.2 W, 2.13 W and 3.1 W for the 75 mm, 180 mm and 295 mm, respectively). The consumed power was calculated as a function of the percentage of the duty cycle on the PWM. figure 5(d) shows the percentage of the PWM duty cycle, and it can be noticed that the PWM values are similar for all the sizes. Finally, figure 5(b) shows the reached temperatures during the experiments. They were comparable to those obtained during the open-loop experiments, with the difference of a faster temperature increase at the beginning due to the higher applied energy. Interestingly, in any case, the temperature surpassed 70 °C–80 °C, which were the maximum temperatures before the actuator failed.

3.4.2. Chirp response. The benchmarking for the actuator speed using the proposed variable length method was performed by applying a linear chirp signal [32]. It consists of a sinusoidal sweep signal that varies its frequency over time, which can be expressed as follow:

$$chirp\,(t) = \mathbf{A}\sin\left[2\pi\left(\frac{c}{2}t^2 + f_0 t\right)\right] \tag{18}$$

where f_0 is the final frequency, **A** is the amplitude of the sinewave, and c is the chirp rate, described by:

$$c = \frac{f_e - f_0}{T} \tag{19}$$

where f_e is the final frequency, and T is the time it takes to sweep from f_0 to f_e.

The sinewave amplitude was 6 mm for testing, making the base displacement 1 mm–7 mm. This was chosen to use the whole stroke of the 75 mm actuator. From here, offsets of 60 mm were applied to the longer actuators. Hence, in the case of the 180 mm, experiments with a maximum displacement of 7, 13 and 19 mm were performed. Moreover, with the 290 mm, a maximum displacement of 25 mm was added.

The initial chirp frequency was 0.01 Hz. This frequency was chosen as it is lower than 0.05 Hz, which is the inverse of the response time of the actuator ($\tau_f = 23.58$ s). Furthermore, the final frequency is equal to 0.1 Hz, near the maximum frequency of the controller speed of 7.5 s (0.133 Hz). In the case of the final frequency, it was chosen to be lower than the inverse of the maximum rate with the controller, as the controller only works in the contraction direction, making it slow when cooling down. The maximum working frequency for each TCP was established when the actuator lost −3 dB in amplitude (when the active actuator range was reduced by half) in the frequency analysis of the output signal.

As with the previous experiments, the behaviour of the lower range in the 180 mm and 290 mm actuators was similar to using a 75 mm (except the maximum temperature), and the same applies to the 180 mm to with the 290 mm, meaning that the linear behaviour of different lengths is still valid. Due to these similarities, figure 6 presents only the result of the 290 mm TCP at various levels.

After analysing the data of the 190 mm TCP, there was a slight difference between the 120 and 180 mm offset, and neither reached the −3 dB in amplitude (figures 6(a) and (b)). Furthermore, during the test, the maximum power was only applied at the beginning of the test to reach the offset. After that, the used power was less than half of the maximum power (figure 6(c)). Hence, a new chirp was used, but this time with a maximum frequency of 1 Hz, PID values were changed to those that allowed the actuator for 1 s reaction times (table 2). In the case of the temperature, as the speed increases, it reaches temperatures as if a step signal were applied. This is because the system cannot respond to those frequencies and starts behaving like a DC voltage signal (figure 6(d)).

Table 3 shows the maximum temperature reached during the test, the frequency at −3 dB, and the peak power consumption at this frequency for each actuator and offset.

After increasing the chirp frequency and the PID controller, the difference between 120 and 180 mm offset increases. Both reach the mark of −3 dB in amplitude at different frequencies, 0.11 and 0.15 Hz, respectively (figures 7(a) and (b)). It is possible to appreciate how the response time of the actuator change as the offset is increased in both time (figure 7(a)) and frequency domains (figure 7(b)). In this case, as the speed increases, the maximum power starts to be used during the activation time to achieve the actuation at the high frequencies (1 Hz). Nevertheless, during relaxation times, the cooling process is slow. This slow cooling process is what sets the frequency. The temperature was not pictured for the 1 s PID as the temperature tends to be a constant similar to that achieved during the step test.

When the reached frequencies (F) are compared to the given offset a linear relation was found ($R^2 = 0.9809$):

$$F = 0.0006 \times Offset + 0.0477. \tag{20}$$

For every mm increased as an offset a gain of 0.0006 Hz is obtained. In the proposed example, the initial frequency of the 6 mm displacement was 0.051 Hz, and it improved to 0.15 Hz with the 295 mm actuator (approximately three times faster). The change in the frequency is due to the displacement range used. The relation is independently of the length of the actuator, it can be seen the trend of the 180 mm and 295 mm actuator are similar for the first two offsets. Furthermore, the maximum temperature was almost the same for the faster test on the 295 mm than in the case of the 75 mm, providing an advantage as it is possible to reduce the temperature with the same or better performance in speed. However, the consumed power will increase (figure 7(c)) as higher frequencies require more significant offsets.

4. Discussion

This work presents the properties of long TCP actuators to increase the bandwidth and reduce the working temperature to explore their use on WRR.

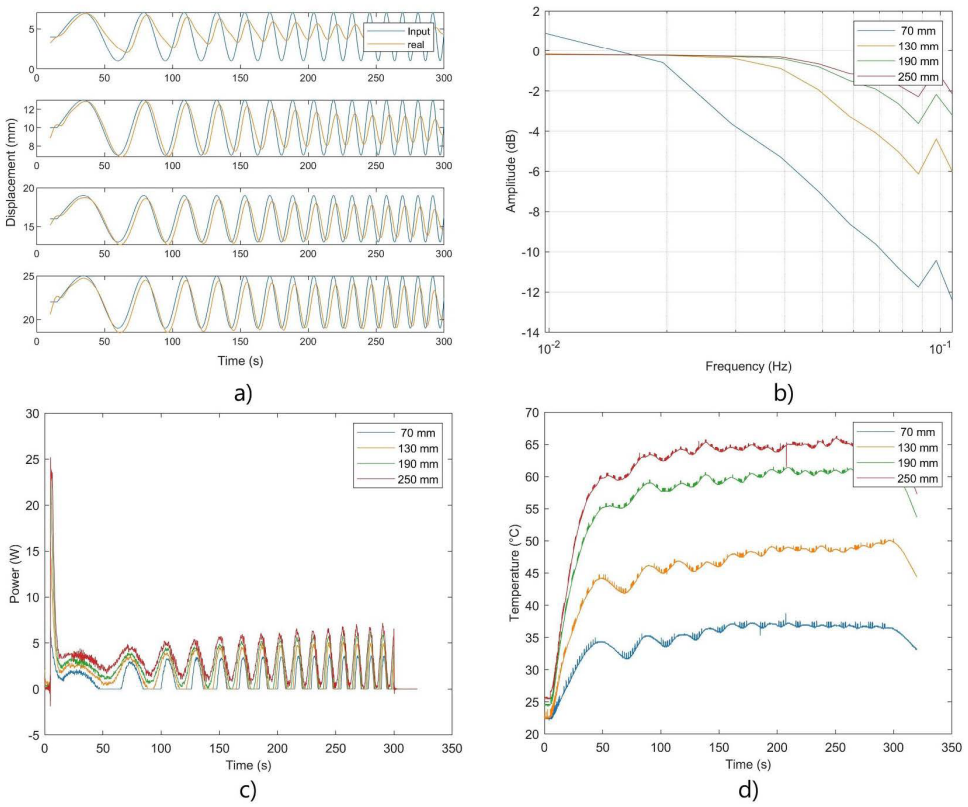

Figure 6. (a) Position response with chirp signal reference (0.01–0.1 Hz) to different offsets on the 295 mm TCP with a 7.5 s response time PID controller. (b) Magnitude Bode plot for the 295 mm with different offsets. (c) Power consumption corresponds to the chirp test response (0.01–0.1 Hz). (d) Reached temperatures during the chirp test.

Table 3. Maximum values of the 1 Hz Chirp Test.

Actuator (offset)	Maximum temperature (°C)	Frequency at −3 dB (Hz)	Power at −3 dB (W)
75 mm	72.74	0.051	4.0
180 mm	45.5	0.046	4.16
180 mm (60 mm)	60.35	0.09	7.63
180 mm (120 mm)	71.4	0.127	10.15
295 mm	40.03	0.043	4.27
295 mm (60 mm)	52.17	0.082	7.78
295 mm (120 mm)	63.23	0.11	10.19
295 mm (180 mm)	71.07	0.15	13.64

From the result of the characterisation test, the length does not affect the maximum stroke that an actuator can generate, as all the different sizes presented a strain of ≈10% of the initial length. Furthermore, the mechanical properties are maintained, and a linear relationship was found between the applied power and the achieved stroke.

Another advantage is the temperature reduction to generate a particular stroke as the actuator length increases.

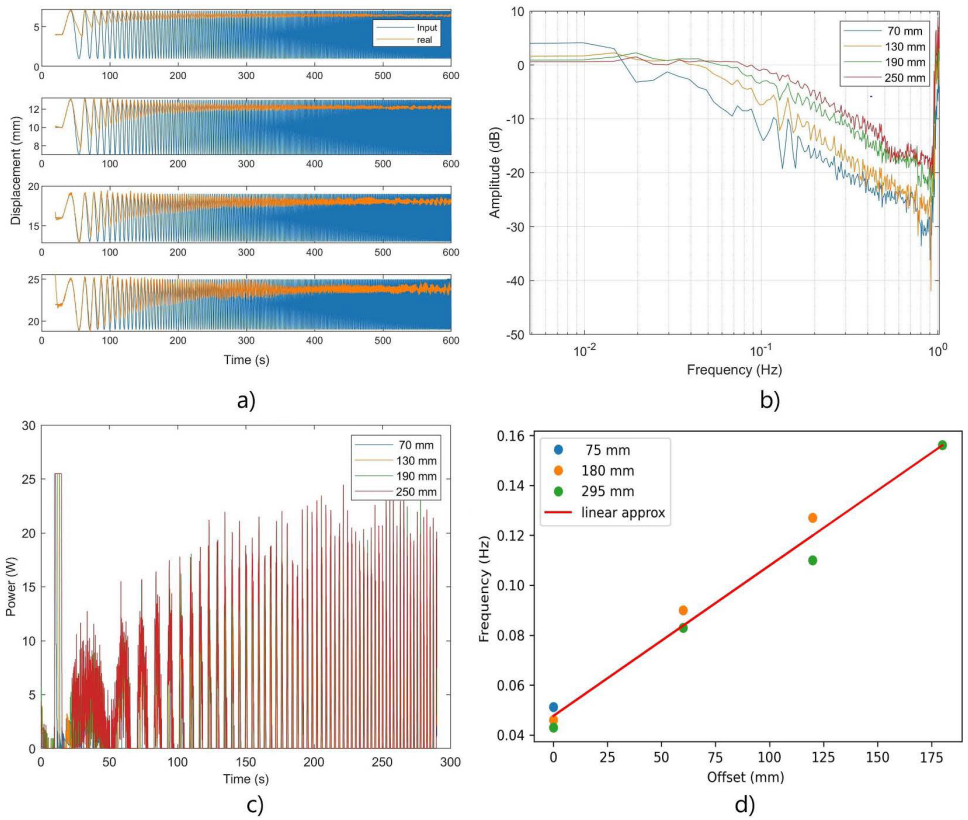

Figure 7. (a) Position response with chirp signal reference (0.01–1 Hz) to different offsets on the 295 mm TCP with a 1 s response time PID controller. (b) Magnitude Bode plot for the 295 mm with different offsets. (c) Power consumption for the 295 mm with different offsets (0.01–0.5 Hz). (d) Linear relationship between offset increment and frequency increment.

This advantage is a crucial design feature for SWRR using thermally activated actuators, as the temperature for the pain threshold of humans is 44 °C at the dermal/epidermal interface of the skin [16]. Meanwhile, if the actuator is activated at its full range, it can reach a temperature above 70° C (figure 4(b)).

For example, in the case of a wrist SWRR, which requires a range of motion of 40° extension and 38° flexion during ADLs, a stroke of ≈23 mm is needed [22]. From the used actuators, the most similar to get this length with the maximum stroke will be 180 mm; at its maximum stroke ≈18 mm, the temperature is ≈82°. In contrast, if the 295 mm actuator is used to obtain the same displacement, the temperature will be ≈62°. And it can be reduced more if a longer actuator were to be used. Furthermore, space should not be a constraint. Like shape memory alloys [33], TCP actuators could be wrapped around pulleys [16, 34] to utilise longer muscle lengths allowing larger strokes.

Regarding the speed of the actuators, during open-loop activation, there is no difference between the different lengths of actuators as the time response is similar, independently of the length. In the case of the fabricated actuators, it was around 20 s. Nevertheless, reaching high contraction speeds independently of the length is possible with a correct closed-loop control strategy and high-power values. Furthermore, as the electromechanical model is similar for all the lengths, using the same PID controller is possible.

As noticed from previous research [21, 22], the problem with the TCP actuators is the cooling time to recover the initial length, which is found during the isotonic contraction tests. The typical method to improve the speed is to reduce the TCP

diameter with the disadvantage of reducing the force or using a cooling system that will increase the system's complexity. In this work, a different strategy is proposed for single TCP actuators. The proposed approach uses actuators to produce more significant contractions than the required ones. It is possible to provide offsets and use different activation regions to improve the closed-loop bandwidth for the whole movement and not only the contraction [13]. Using offsets equal to the required contraction, it was found that the base bandwidth increases linearly by 0.0006 Hz. In the case of the used actuators, the bandwidth improves from 0.051 Hz to 0.15 Hz without requiring any external cooling system and keeping the output force. However, if speed is the main objective, it could use thinner TCP actuators. For instance, if an offset of 1 m is used, the final frequency will be 0.6477 Hz. This frequency improvement could be useful for physical rehabilitation therapy and low frequency ADLs, as the minimum frequency for these activities is 0.5 Hz [26, 35].

Considering that contraction speeds depend on the controller and the applied power, another option to improve the system's speed is using agonist and antagonist fibres that allow the system to actuate in two different directions. Their main disadvantage is that they accumulate heat, preventing the actuators' recovery and making them unable to finish the whole pattern after three cycles [1]. The use of long actuators could also benefit this structure. It will be possible to obtain the same displacement as with a smaller actuator but with the advantage of reducing the temperature. It will be harder to saturate the actuators, and it will be possible to go for higher frequencies. Moreover, as noticed from both the isotonic and the closed-loop controllers' experiments, the consumed power is related to the produced stroke rather than the length of the actuator, so in theory, the power consumption will not increase if the activation frequencies are the same. Nevertheless, research on the variable stiffness actuator and stiffness control algorithm is missing to implement a system of this characteristic.

5. Conclusion

The work in this paper presents the study on the usage of longer TCP actuators to improve the frequency and temperature characteristics of the TCP actuators, where it was found that the strain is independent of the length. However, electrothermal properties change with the length. As a result, the activation temperature to obtain displacement can be reduced with longer actuators. Furthermore, a new strategy to increase TCP actuators' speed without external cooling systems is presented. The model takes into consideration the advantages of long actuator fibres. This was done by estimating an electromechanical system model through an isotonic contraction test. The model was invariant on the length, meaning that the actuators behave similarly independently of the size. Then a PID controller was implemented to control the displacement of the actuator, in the case of the contraction is dependent on the applied power. However, it was found that the cooling time can also be improved by varying the activation section of the used actuator, so having long actuators can improve linear movement by increasing its length. Furthermore, the temperature generated by the TCP fibres is reduced by increasing length.

Data availability statement

All data that support the findings of this study are included within the article (and any supplementary files).

ORCID iDs

Alberto Gonzalez-Vazquez https://orcid.org/0000-0001-6514-7888
Lorenzo García https://orcid.org/0000-0002-1122-497X

References

[1] Copaci D, Martín F, Moreno L and Blanco D 2019 SMA based elbow exoskeleton for rehabilitation therapy and patient evaluation *IEEE Access* **7** 31473–84
[2] Lerner Z F, Harvey T A and Lawson J L 2019 A battery-powered ankle exoskeleton improves gait mechanics in a feasibility study of individuals with cerebral palsy *Ann. Biomed. Eng.* **47** 1345–56
[3] Graham H K *et al* 2016 Cerebral palsy *Nat. Rev. Dis. Primers* **2** 15082
[4] Patane F, Rossi S, Del Sette F, Taborri J and Cappa P 2017 WAKE-up exoskeleton to assist children with cerebral palsy: design and preliminary evaluation in level walking *IEEE Trans. Neural. Syst. Rehabil. Eng.* **25** 906–16
[5] Reinkensmeyer D J 2019 JNER at 15 years: analysis of the state of neuroengineering and rehabilitation *J. Neuroeng. Rehabil.* **16** 144
[6] Bützer T, Dittli J, Lieber J, van Hedel H J, Meyer-Heim A and Lambercy O (eds) 2019 PEXO-A pediatric whole hand exoskeleton for grasping assistance in task-oriented training *2019 IEEE 16th Int. Conf. on Rehabilitation Robotics (ICORR)* (IEEE)
[7] He Y, Eguren D, Luu T P and Contreras-Vidal J L 2017 Risk management and regulations for lower limb medical exoskeletons: a review *Med. Devices: Evid. Res.* **10** 89–107
[8] Veale A J and Xie S Q 2016 Towards compliant and wearable robotic orthoses: a review of current and emerging actuator technologies *Med. Eng. Phys.* **38** 317–25
[9] Behboodi A, DeSantis C, Lubsen J and Lee S (eds) 2020 A mechanized pediatric elbow joint powered by a de-based artificial skeletal muscle *2020 42nd Annual Int. Conf. IEEE Engineering in Medicine & Biology Society (EMBC)* (IEEE)
[10] Ugurlu B, Forni P, Doppmann C, Sariyildiz E and Morimoto J 2019 Stable control of force, position, and stiffness for robot joints powered via pneumatic muscles *IEEE Trans. Ind. Inform.* **15** 6270–9
[11] Haines C S *et al* 2014 Artificial muscles from fishing line and sewing thread *Science* **343** 868–72
[12] Wu L, Chauhan I and Tadesse Y 2018 A novel soft actuator for the musculoskeletal system *Adv. Mater. Technol.* **3** 1700359
[13] Tang X, Li K, Liu Y, Zhou D and Zhao J 2019 A soft crawling robot driven by single twisted and coiled actuator *Sens. Actuators* A **291** 80–86

[14] Zhang J, Sheng J, ONeill C T, Walsh C J, Wood R J, Ryu J H, Desai J P and Yip M C 2019 Robotic artificial muscles: current progress and future perspectives *IEEE Trans. on Robotics* **35** 761–81
[15] Hyeon K, Jeong J, Chung C, Cho M, Hussain S and Kyung K-U 2022 Design of a wearable mechanism with shape memory alloy (SMA)-based artificial muscle for assisting with shoulder abduction *IEEE Robot. Autom. Lett.* **7** 10635–42
[16] Saharan L, de Andrade M J, Saleem W, Baughman R H and Tadesse Y 2017 iGrab: hand orthosis powered by twisted and coiled polymer muscles *Smart Mater. Struct.* **26** 105048
[17] Cenciarini M and Dollar A M (eds) 2011 Biomechanical considerations in the design of lower limb exoskeletons *2011 IEEE Int. Conf. on Rehabilitation Robotics* (IEEE)
[18] Gonzalez-Vazquez A, Garcia L, Kilby J and McNair P 2023 Soft wearable rehabilitation robots with artificial muscles based on smart materials: a review *Adv. Intell. Syst.* **5** 2200159
[19] Hiraoka M, Nakamura K, Arase H, Asai K, Kaneko Y, John S W, Tagashira K and Omote A 2016 Power-efficient low-temperature woven coiled fibre actuator for wearable applications *Sci. Rep.* **6** 36358
[20] Haines C S and Niemeyer G (eds) 2018 Closed-loop temperature control of nylon artificial muscles *2018 IEEE/RSJ Int. Conf. on Intelligent Robots and Systems (IROS)* (IEEE)
[21] Yip M C and Niemeyer G 2017 On the control and properties of supercoiled polymer artificial muscles *IEEE Trans. Robot.* **33** 689–99
[22] Edmonds B P and Trejos A L (eds) 2020 Frequency response analysis of actively cooled nylon twisted coiled actuators for use in wrist rehabilitation devices *2020 8th IEEE RAS/EMBS Int. Conf. for Biomedical Robotics and Biomechatronics (Biorob)* (IEEE)
[23] Chossat J B, Chen D K Y, Park Y L and Shull P B 2019 Soft wearable skin-stretch device for haptic feedback using twisted and coiled polymer actuators *IEEE Trans. Haptics* **12** 521–32
[24] Saharan L and Tadesse Y (eds) 2016 Fabrication parameters and performance relationship of twisted and coiled polymer muscles *ASME 2016 Int. Mechanical Engineering Congress and Exposition* (American Society of Mechanical Engineers Digital Collection)
[25] Edmonds B P, DeGroot C T and Trejos A L 2020 Thermal modeling and characterization of twisted coiled actuators for upper limb wearable devices *IEEE/ASME Trans. Mechatron.* **26** 966–77
[26] Murphy V, Edmonds B P and Trejos A L 2021 Characterisation and control of a woven biomimetic actuator for wearable neurorehabilitative devices *Actuators* **10** 37
[27] Patiño A G, Ferrone A, Gastélum C G D and Menon C (eds) 2018 A novel biomedical technology based on the use of artificial muscles to assist with hand functions *2018 IEEE 9th Annual Information Technology, Electronics and Mobile Communication Conf. (IEMCON)* (IEEE)
[28] Cho K H, Song M-G, Jung H, Yang S Y, Moon H, Koo J C and Choi H R (eds) 2016 Fabrication and modeling of temperature-controllable artificial muscle actuator *2016 6th IEEE Int. Conf. on Biomedical Robotics and Biomechatronics (Biorob)* (IEEE)
[29] Tang X, Li K, Chen W, Zhou D, Liu S, Zhao J and Liu Y 2019 Temperature self-sensing and closed-loop position control of twisted and coiled actuator *Sens. Actuators* A **285** 319–28
[30] Proto A, Penhaker M, Bibbo D, Vala D, Conforto S and Schmid M 2016 Measurements of generated energy/electrical quantities from locomotion activities using piezoelectric wearable sensors for body motion energy harvesting *Sensors* **16** 524
[31] Mann K A, Werner F W and Palmer A K 1989 Frequency spectrum analysis of wrist motion for activities of daily living *J. Orthop. Res.* **7** 304–6
[32] Vicario R, Calanca A, Dimo E, Murr N, Meneghetti M, Ferro R, Sartori E and Boaventura T (eds) 2021 Benchmarking force control algorithms *The 14th Pervasive Technologies Related to Assistive Environments Conf. (Corfu, Greece)*
[33] Pittaccio S, Viscuso S, Rossini M, Magoni L, Pirovano S, Villa E, Besseghini S and Molteni F 2009 SHADE: a shape-memory-activated device promoting ankle dorsiflexion *J. Mater. Eng. Perform.* **18** 824–30
[34] Hope J and McDaid A 2017 Development of wearable wrist and forearm exoskeleton with shape memory alloy actuators *J. Intell. Robot. Syst.* **86** 397
[35] Jeong J, Hyeon K, Han J, Park C H, Ahn S-Y, Bok S-K and Kyung K-U 2021 Wrist assisting soft wearable robot with stretchable coolant vessel integrated SMA muscle *IEEE/ASME Trans. Mechatron.* **27** 1046–58

Paper 5:

Smart Materials and Structures

PAPER • OPEN ACCESS

Paediatric ankle rehabilitation system based on twisted and coiled polymer actuators

To cite this article: Alberto Gonzalez-Vazquez *et al* 2024 *Smart Mater. Struct.* **33** 075009

OPEN ACCESS
IOP Publishing
Smart Materials and Structures
Smart Mater. Struct. 33 (2024) 075009 (14pp)
https://doi.org/10.1088/1361-665X/ad50b0

Paediatric ankle rehabilitation system based on twisted and coiled polymer actuators

Alberto Gonzalez-Vazquez, Lorenzo Garcia* and Jeff Kilby

School of Engineering, Computer and Mathematical Sciences, Auckland University of Technology, Auckland, New Zealand

E-mail: lorenzo.garcia@aut.ac.nz

Received 15 December 2023, revised 16 May 2024
Accepted for publication 27 May 2024
Published 6 June 2024

Abstract

Rehabilitation is crucial for children with physical disabilities arising from various conditions. Traditional exoskeletons, reliant on electric motors and rigid components, making them cumbersome, heavy, and unsuitable for use outside clinical facilities. To overcome these, researchers are turning to soft wearable rehabilitation robots (SWRRs) with artificial muscles based on smart materials like twisted and coiled polymer actuators (TCPs). TCPs offer enhanced compliance, adaptability, comfort, safety, and reduced weight—critical for paediatric use. Despite facing challenges like low operating frequencies and high temperatures, TCPs are explored as potential artificial muscles for SWRRs, due to their advantages on the force they can generate, the strain and a linear behaviour. This study details a proof of concept for a paediatric rehabilitation system for ankles based on TCPs, including the actuator characterization, mechanical design, control strategy, and human-computer-interface (HCI). The resulting device achieved a 1.4 Nm torque, a 10° range of motion in dorsiflexion within 5 s, and integrated electromyographic HCI. This research marks a promising step towards innovative, soft wearable rehabilitation solutions for children with physical disabilities.

Supplementary material for this article is available online

Keywords: artificial muscles, exoskeletons, soft robotic, twisted and coiled polymer actuator, rehabilitation

1. Introduction

Ongoing paediatric physical disabilities can result from various causes, including neurological conditions like Cerebral Palsy [1], strokes [2], acquired brain injuries [3], neuromuscular diseases such as Duchenne muscular dystrophy [4] and spinal muscular atrophy [5], as well as traumatic injuries. Children with physical disabilities often face limitations in performing daily activities independently, which can impede their typical development. Mobility and exploration are crucial aspects of a child's development, contributing to cognitive, physical, social, and emotional growth [6].

Rehabilitation plays a vital role in assisting these children in recovering or maintaining functionality, enabling them to interact with their environment, and ultimately improving their quality of life and autonomy [7]. Rehabilitation exoskeletons have gained significant attention for their potential to address mobility challenges in individuals with physical disabilities. They offer advantages such as enabling extensive

* Author to whom any correspondence should be addressed.

practice for children with substantial disabilities, reducing the effort required from therapists during exercises, and providing a quantitative assessment of the patient's motor function [8].

However, most existing rehabilitation exoskeletons rely on electric motors and rigid components for their functionality. Unfortunately, these designs are often cumbersome, heavy, and unsuitable for use outside clinical facilities [9]. To overcome these limitations, researchers are now focusing on developing soft wearable rehabilitation robots (SWRRs) that incorporate artificial muscles based on smart materials (AMSMs). AMSM provides increased compliance, adaptability, comfort, safety, and reduced weight [10].

Due to this advantages they are interesting to be used in paediatric devices as the main characteristics that differentiate them from the adults version are safety, operability, weight and motivation [11]. Safety can be improved thanks to the compliance of the materials [12]. And the weight can be reduce drastically preventing abnormal movements pattern and increase energy consumption [13, 14]. Due to this advantages they are interesting to be used in paediatric devices as the main characteristics that differentiate them from the adults version are safety, operability, weight and motivation [11]. Safety can be improved thanks to the compliance of the materials [12]. And the weight can be reduce drastically preventing abnormal movements pattern and increase energy consumption [13, 14].

AMSMs are soft actuators composed primarily of material with a low Young's modulus like that of soft biological materials (10^4–10^9 Pa) that can sense and directly convert physical stimulus (e.g. light, electrical, heat) into physical displacement [15–17].

Shape memory alloys (SMAs) [18] and dielectric elastomer actuators (DEAs) [19] are indeed promising AMSM solutions for SWRR. However, they each have limitations that hinder their widespread use in this context.

DEAS present desirable characteristics with strain reaching 200%, a high bandwidth up to the range of kHz and high efficiency [20–22]. However, DEAs need high voltage, in the order of hundreds of volts, requires bulky and expensive electronics. Moreover, DEAs are challenging to produce in a compact size to generate appropriate amounts of power and force [23, 24].

SMAs present the advantages of power density and stress, these being as high as 50 W g^{-1} and 200 MPa, respectively [22, 25]. These advantages have made them the most popular option on SWRR prototypes [10]. However, they have limitations to be used on SWRR, as they have low efficiency, a small strain range (up to 8%) and high thermal hysteresis making them difficult to control [20, 22, 23]. SMAs present the advantages of power density and stress, these being as high as 50 W g^{-1} and 200 MPa, respectively [22, 25]. These advantages have made them the most popular option on SWRR prototypes [10]. However, they have limitations to be used on SWRR, as they have low efficiency, a small strain range (up to 8%) and high thermal hysteresis making them difficult to control [20, 22, 23].

Another noteworthy type of AMSM is the twisted and coiled polymer actuator (TCP). TCPs are created by twisting precursor polymer fibres and applying heat treatment [26]. To activate TCPs, an external heat source, such as metallic wires, is employed to induce joule heating, thereby enabling precise electrical control. TCPs offer several advantages, including high power density (27 W g^{-1}), stress (10 MPa), strain capacity (21%), and linear behaviour with minimal hysteresis. However, they do face certain limitations, such as low operating frequencies (<1 Hz), low power efficiency (<1.32%) and high operating temperatures (>80 °C) [20, 22, 27]. Due to their advantages three promising examples of wearable devices based on TCPs were founded:

Sutton *et al* [28] developed an assistive wrist orthosis with a single degree of freedom. This device employed 16 TCP) actuators made of silver-coated Nylon 6.6 sewing thread. It generated a torque of 0.3 Nm to the wrist joint in the flexion direction within 3.9 s. They implemented a proportional–integral–derivative (PID) controller to accurately follow a 0.1 Hz sinusoidal signal with a 10 N amplitude. The prototype was able to track the movement during activation but encountered challenges with slow response times during the relaxation phase.

IGrab [27], an ergonomic orthotic device to assist in finger flexion and extension movements, was designed by Saharan *et al*. The device featured a combination of 3D-printed components and sewn parts, including artificial tendons routed from the fingers to the wrist. The finger tendons were linked to TCP actuators, which were mounted on a forearm bracelet. Frictionless pulleys optimised TCP actuation, and rubber strips enhanced energy efficiency. When applying a 0.6 A step signal, the fingers reached their maximum displacements within 25 s (i.e. the index finger was able to move 40° for the metacarpophalangeal joint, 21° for the proximal interphalangeal joint, and 11° in the case of the distal interphalangeal joint), with further improvements observed when using pulsed signals, reducing actuation time to under 5 s.

Patiño *et al* [29] developed a wearable orthotic device for hand rehabilitation featuring individual TCP actuators for each finger. The orthosis consisted of two main components: one fitted to the dorsum of the hand and another for the fingers. Each finger incorporated a silicone tube housing a TCP and a filament strain sensor. The TCP actuators within the finger structure could generate forces of approximately 3 N when a 0.3 A step input was applied.

The orthotic devices mentioned demonstrate the application of TCPs in hand and wrist rehabilitation. However, there is a notable absence of studies exploring the feasibility of TCP utilization in the lower limb or paediatric systems. Moreover, previous literature has extensively investigated TCP as an actuation type and its mechanical design (inherent to the explored joint). Nevertheless, other critical components remain insufficiently explored in these works. These unexplored parameters may include considerations related to control strategy and human-computer interface (HCI), which are crucial for successfully developing and implementing paediatric SWRR systems [11, 30] (figure 1).

This paper explores the feasibility of TCPs as artificial muscles to drive SWRRs for children with physical disabilities. It highlights the advantages and the current limitations of TCPs on SWRR. The paper presents the design process of

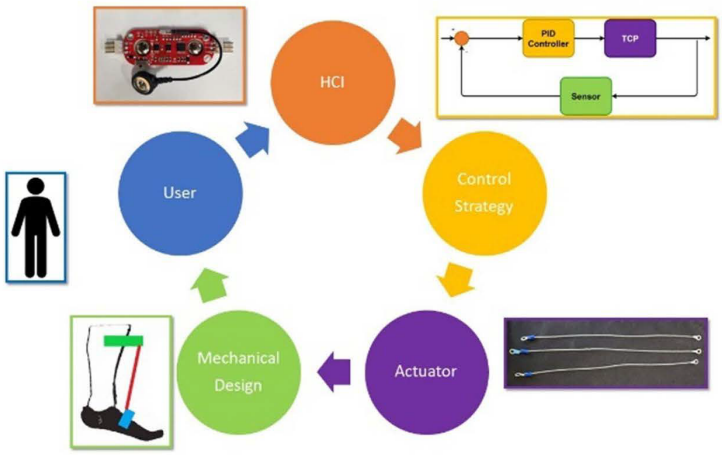

Figure 1. SWRR components.

a prototype for paediatric ankle SWRRs based on TCPs covering the main parameters of SWRRs being the actuator characterization, the mechanical design based on the biomechanical requirements for paediatric ankle dorsiflexion, the implementation of a control strategy that is merged with an HCI, with this covering the essential parameters that require a paediatric SWRR.

2. Design of the device and methods

This section presents a description of the TCP manufacturing process and its behaviour. Then, the biomechanical structure of the ankle and a dummy based on it are given as they are required to design and test the SWRR. Later, the design process of the SWRR is presented. Finally, the behaviour of the prototype and a mathematical model are shown.

2.1. TCPs manufacturing

The TCP actuators were fabricated using the process similar to Chossat *et al* [31]. A 1.5 m Nylon fishing line as the precursor fibre (EDGE Mono trace 80 LB) with a diameter of 840 μm. The nylon fibres were twisted and coiled alongside a 36 AWG (127 μm) Nickel–Chromium 80 (NiCr) wire (Fogslord). One end of the nylon fibre was firmly attached to the output shaft of a NEMA17 motor, while the other end was connected to a slider carrying a 1000 g weight (17.68 MPa, value according with: Force (1 Kg*9.8 m s^{-2})/ Fibre Cross Sectional Area (π^{*}(420 $\times$ 10^{-4} m)^{2})). The NiCr wire was also suspended from the motor shaft but was only weighted with 1.6 g (1.2 MPa) to maintain it in a straightened state. The nylon fibres were twisted and coiled at a slow rotation speed of 250 RPM. The twisting and coiling process was stopped manually once the precursor fibre was fully coiled.

Table 1. TCP manufacturing parameters.

Parameter	Value
Precursor fibre material	Nylon
Precursor fibre diameter (mm)	0.84
Precursor fibre length (mm)	1500
Precursor fibre tension (g MPa^{-1})	1000/17.68
Resistance wire material	Nichrome 80
Resistance wire diameter (AWG μm^{-1})	36/127
Resistance wire length (mm)	1670
Resistance wire tension (g MPa^{-1})	1.6/1.2
RPM	250
Motor turns	726 $\pm$ 6
TCP after coiling length (mm)	375 $\pm$ 5
TCP after annealing length (mm)	440 $\pm$ 5
Annealing current (mA)	240
TCP resistance (Ω)	137.1 $\pm$ 7.8
TCP DIAMETER (MM)	1.97 $\pm$ 0.04

For the annealing process, the embedded NiCr wire was employed to produce Joule heating. This annealing process consisted of five consecutive five-minute periods, each applying an annealing current of 240 mA. A 1 min cooling phase was inserted between each annealing period. After this treatment, TCPs with an average length of 44 cm and a diameter of 1.97 $\pm$ 0.04 mm were produced, the measurement were taken with a digital calliper (Duratool). The resulting actuators were trimmed to 39.5 cm and clamped with insulated male spade electric terminals. Each electrical terminal required 5 mm for crimping, which led to a 10 mm reduction in the functional area. Table 1 depict the main manufacturing parameters of the fabricated TCPs.

To test the fabricated samples, a custom-made experimental test bench was utilised to measure force and displacement

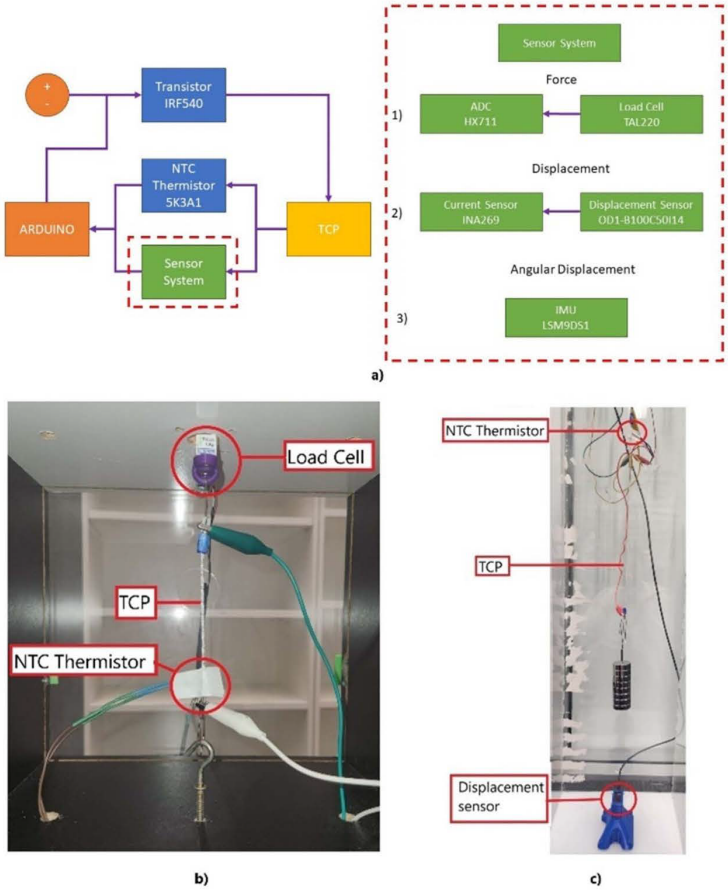

Figure 2. (a) Test bench block diagram for (1) force, (2) displacement and (3) angular displacement test. (b) Force test bench. (c) Displacement test bench.

(figure 2(a)). In both cases, an Arduino NANO served as the data acquisition system. A transistor (Vishay Siliconix IRF540) regulated the voltage from the power supply, while an NTC thermistor (TE Connectivity, 5K3A1) was employed to monitor the temperature of the TCP.

In the force test (figure 2(b)), one end of the actuator was fastened to a fixed hook, and the other end was connected to a 10 Kg load cell (TAL220). This load cell was interfaced with the Arduino through an analogue-to-digital converter (Avia semiconductor, HX711). For the displacement test (figure 2(c)), the actuator was suspended with a weight above a laser displacement sensor (Sick OD mini OD1-B100C50I14), which was connected to a current sensor (Texas Instruments INA269) interfacing with the Arduino. The calibration process for the sensor can be found in the supplementary information (Calibration Procedures).

Both force and displacement tests applied a square signal of 2400 s on and 240 s off to observe the strain and power relationship. The 240 s duration was chosen to allow the system to reach a stable condition. Experiments were repeated at different power levels ranging from 160 mA to 240 mA with the applied current incrementing by 20 mA.

Throughout the experiments, data on TCA temperatures, power consumption, and the weight distance from the sensor were continuously recorded using an Arduino NANO with a sampling time of 50 ms. In the case of the displacement test, various weight values ranging from 600 g to 1000 g were employed to assess the actuator's performance. Each test

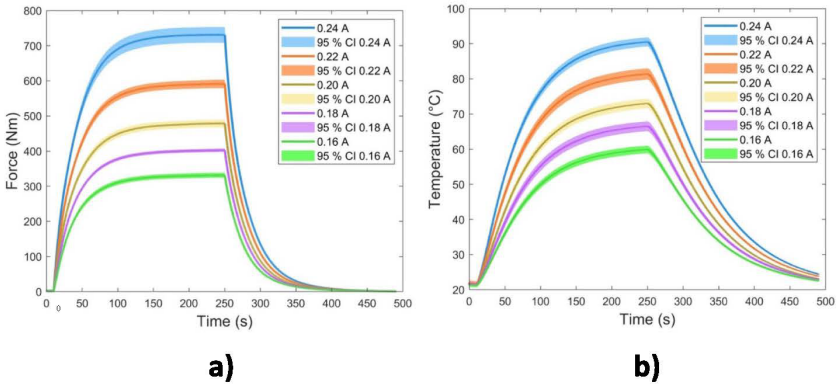

Figure 3. Force power relationship (a) and temperature power relationship during the isotonic force test. Confident intervals (CI) included.

(force and strain) was performed using 5 different actuators, each one used 4 times, for 20 trials per test.

2.2. TCP behaviour

Characterising the performance of the manufactured actuators is essential to determine their suitability for the SWRR requirements. In these tests using TCPs as linear actuators, two primary parameters of interest are force and strain, which will later be converted into torque and range of motion (ROM). The mean of the last 50 samples before turning off the applied power was averaged to calculate the maximum in both tests. This average represents the system's steady state after the step signal was applied. Then, from the 20 maximum values, the mean and standard deviation of the maximum force, temperature, displacement, and strain were obtained.

Figure 3 displays the results obtained from the force test. The TCP actuator's maximum force output is 7.9 ± 0.5 N (807.9 ± 57.6 g) when a current of 240 mA is applied. However, it is important to note that when considering the prestress of the fibre (0.7 ± 0.2 N or 76.8 ± 21.2 g), the maximum change in force is 7.1 ± 0.4 N (730.0 ± 46.3 g) (figure 3(a)). To assess the response times for heating (τ_h) and cooling (τ_c), the analysis focused on the average time required for the actuator to reach 63% of a steady-state value after a step input. The analysis results indicate that the average τ_h is 31.42 ± 1.02 s, and τ_c is 28.2 ± 0.4 s. At the highest applied power level, the generated temperature reached 78.35 °C ± 2.07 °C (figure 3(b)).

In contrast, the results from the displacement test highlight the noticeable impact of pre-strain (generated by the weights) on the actuator's length, causing it to contract from 386.0 ± 3.7 mm to 380.2 ± 3.7 mm, 373.88 ± 4.08 mm, 365.3 ± 4.8 mm, 357.9 ± 5.3 mm. This pre-strain has a direct effect on the actuator's contraction. When a current of 240 mA was applied with different loads, the maximum displacements were as follows 38.7 ± 1.9 mm, 39.8 ± 0.8 mm, 40.4 ± 2.1 mm, 43.5 ± 2.4 mm, 44.5 ± 1.1 mm for weights of 1000 g, 900 g, 800 g, 700 g, and 600 g, respectively (figure 4(a)). Nevertheless, when the final elongation is considered, the strain can be obtained using the following formula:

$$S = \frac{\Delta L}{L} X 100. \tag{1}$$

Here, strain (S) represents the relationship between the initial length (L) of the actuator and the resulting stroke (ΔL) when activated, expressed as a percentage. Analysing the strain data, the results were as follows: 10.02% ± 0.45%, 10.4% ± 0.1%, 10.9% ± 0.6%, 11.7% ± 0.7%, 12.3% ± 0.3% for weights of 1000 g, 900 g, 800 g, 700 g, and 600 g, respectively (figure 4(b)). It is noteworthy that these strain values align with the findings from the maximum force analysis, where the maximum generated force was observed at 7.1 N (730.0 ± 46.3 g). After this point is possible to see a fall in the displacement and strain. The average response times (τ_h) and (τ_c) are measured at 39.2 ± 1.3 s and 20.6 ± 0.5 s, respectively.

2.3. Ankle biomechanics

The ankle, characterised by its intricate anatomy, comprises the tibiotalar joint and the transverse tarsal joint, collectively affording a broad spectrum of multidirectional motion. Critical motions within the ankle joint complex encompass plantar- and dorsiflexion, occurring predominantly in the sagittal plane, as well as ab-/adduction in the transverse plane and inversion-eversion in the frontal plane. Combinations of rotations across the subtalar and tibiotalar joints generate three-dimensional motions called supination and pronation [32, 33].

However, it is worth mentioning that the majority of ankle movement primarily occurs within the sagittal plane, with plantar and dorsiflexion being predominantly governed by the

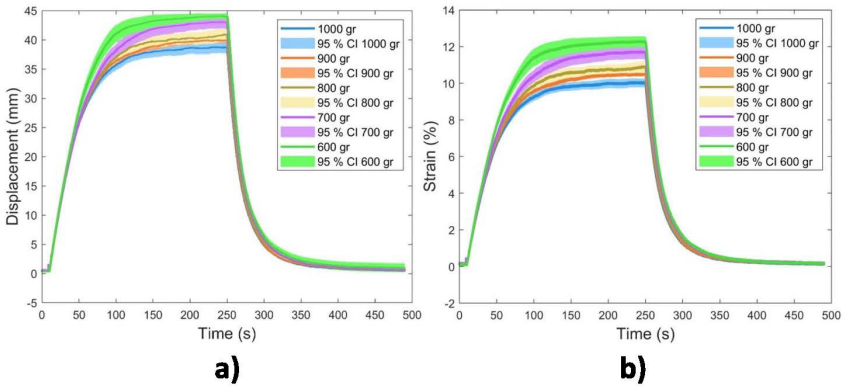

Figure 4. (a) Displacement-weight relationship and (b) strain-weight relationship. Confident intervals (CI) included.

tibiotalar joint. The total ankle ROM in the sagittal plane typically spans from 65° to 75°, encompassing 25° to 30° of dorsiflexion and 40° to 45° of plantarflexion. Nevertheless, during activities like walking, the required ROM in the sagittal plane is considerably reduced to approximately 25°. In this context, adult ankles generally move from 20° of plantar flexion to 10° of dorsiflexion, while children exhibit a range of 5° dorsiflexion. Regarding ankle stiffness, which pertains to the mechanical resistance to passive movement, achieving 10° of dorsiflexion necessitates 6.21 Nm of torque for adults, whereas children require 1.5 Nm [34, 35].

The plantar-dorsiflexion movement within a 66° range is commonly observed during daily activities such as walking, climbing stairs, etc. These activities typically occur at a frequency of around 1.75 Hz. However, it is important to note that during rehabilitation sessions, these movements are often executed at much lower frequencies, usually falling below 0.2 Hz [10, 36, 37].

2.4. Dummy testing platform

For conducting trials on the paediatric ankle SWRR, a mannequin designed to replicate the lower limb proportions of an average 10 year-old child was employed. Accurate measurements for the leg were derived from the World Health Organization's (WHO) child growth standards [38] and the anthropometric data provided by Winters [39]. These references guided the determination of limb dimensions, resulting in a crus length (knee to ankle) of 40 cm, foot length and width of 22 cm and 7 cm respectively. Thet total foot weight 300 g. The used dummy is shown in figure 5.

To assess the exoskeleton's response to various torques, diverse weights were added to the foot, situated 10 cm from the ankle's centre of rotation. The weights ranged from 500 g to 3000 g, incremented in 500 g intervals. This weight variation corresponded to a torque spectrum from 3 Nm to 0.5 Nm.

2.5. Paediatric ankle SWRR design

The SWRR consisted of two 3D-printed braces that wrapped around the top part of the crus brace (CB) and the second one on top of the foot instep brace (FIB), figure 5. The FIB was positioned 5 cm away from the centre of rotation of the ankle. Both braces use Velcro to maintain the position over the mannequin. Furthermore, the braces are divided into two different parts: the brace and the lid. This design allowed the connection of the TCPs in series using copper tape between both parts as the electrical connection. The computer-aided design (CAD) model of both braces is displayed in figure 5. The entire device weight was 300 g (without a power supply or battery), making each brace weight 150 g.

On figure 6 an ankle model is showed. P1 is the point at where the TCPs are connected to FIB, P2 is the point where the TCP is connected to CB and $P0$ the point at the centre of rotation with coordinate (0,0). The coordinate of $P1$ (X_{p1}, Y_{p1}) is:

$$X_{p1} = r\cos\theta_1, Y_{p1} = r\sin\theta_1 \tag{2}$$

Then L_{Tcp} can be written as:

$$L_{Tcp} = \sqrt{(L_H - X_{p1})^2 + (L_V + Y_{p1})^2}. \tag{3}$$

And θ_2:

$$\theta_2 = \tan^{-1}\left(\frac{L_V + Y_{p1}}{L_H - X_{p1}}\right) \tag{4}$$

where r is the radius between the centre of rotation and $P1$, θ_1 is the angle of the foot during dorsiflexion, θ_2 is the angle between the TCPS and the braces, L_V is the distance between $P1$ and $P2$ when $\theta_1 = 0$, L_H is the distance between the centre of rotation and the connection of the TCP on CB (x axis). Finally, L_{Tcp} is the length of the TCPs.

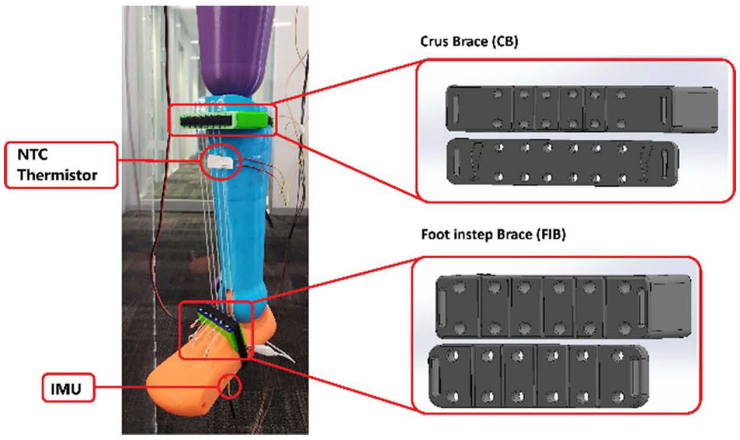

Figure 5. Paediatric leg dummy and CAD design of the SWRR braces.

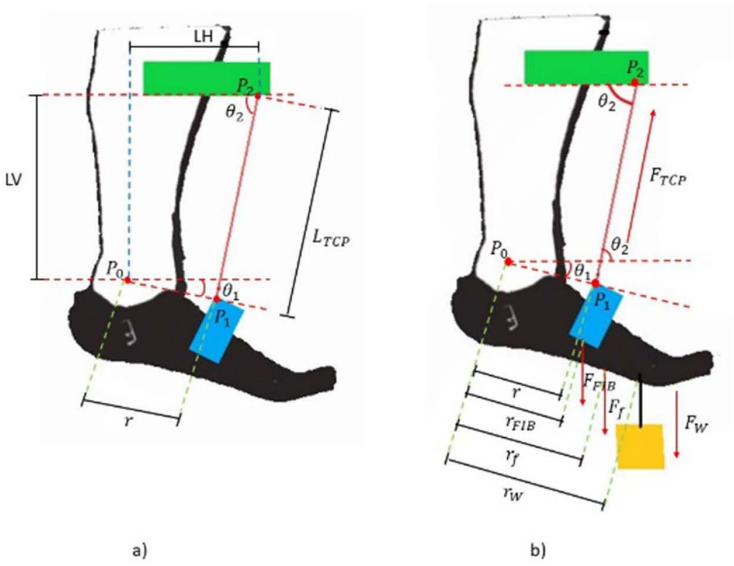

Figure 6. Free body diagram for (a) displacement and (b) forces acting on the dummy.

In the case of the generated Torque (T), the system can be evaluated as follows:

$$T = F_{\mathrm{TCP}} x \sin\theta_2 x r x \cos\theta_1 - F_w x r_w x \cos\theta_1 - F_f x r_f x \cos\theta_1 - F_{\mathrm{FIB}} x r_{\mathrm{FIB}} x \cos\theta_1 \quad (5)$$

where F_W is the force generated by the weight used on the experiments, r_W the distance of the weight to the centre of rotation, F_f is the force generated by the weight of the foot and r_f is the foot centre of gravity, F_{FIB} is the force generated by the weight of the FIB and r_{FIB} the distance of the weight to the centre of rotation, F_{TCP} is the force generated by the TCPs.

With the mechanical model of the SWRR, the behaviour of the TCP and the requirements given in section 2.3. Then The SWRR was designed to provide dorsiflexion movement of children with the following characteristics: (i) being able to

provide an angular displacement of 10° in the plantarflexion direction, (ii) providing a torque of 1.5 Nm. Hence, five TCPs of 30 cm, when unloaded, were used for this. The number of fibres was constrained to five as the biggest challenge for TCPs is the speed. Keeping in mind that the width of the leg was 7 cm, a gap of 12 mm was left to prevent heat crosstalk and improve the cooling time [40]. Furthermore, this study is centred on reaching frequencies that can be used in a rehabilitation set-up of 0.2 Hz. Hence, a PID controller was developed to achieve the desired angular displacement in 5 s (section 3).

2.6. SWRR test

The performance assessment of the paediatric ankle SWRR was carried out using the testing setup described in section 2.4. The electronic components used were nearly identical to those employed in the force and displacement tests for the unit TCP. These components included an Arduino, a MOSFET, and a thermistor. However, a key distinction lies in the sensor utilised to record angular displacement (figure 2). To fulfil this purpose, a 9-degree-of-freedom Inertial Measurement Unit (IMU), was employed (LSM9DS1, STMicroelectronics).

Both testing procedures followed the application of a square signal, consisting of 180 s on and 180 s off, to establish the strain-power relationship. The selection of the 180 s duration allowed sufficient time for the system to reach a stable equilibrium. The experiments were conducted across various current levels, spanning from 160 mA to 240 mA (incrementally adjusted by increasing the current in 20 mA steps), encompassing all the different TCP actuators. Throughout the test, data about TCA (Thermally Activated Contractile) temperatures, power consumption, and the angular displacement of the foot were recorded and stored on a computer, with the data acquisition performed using an Arduino NANO at a sampling rate of 50 ms. The testing protocol encompassed a range of torque conditions, spanning from 0.5 Nm to 3.0 Nm in 0.5 Nm increments. In addition to the torque generated by the load, it is essential to account for the total negative torque produced by the combined weight of the foot and the FIB (300 g from the dummy and 150 g from FIB), which amounts to approximately 0.4 Nm. Each test was conducted four times utilizing the identical set of actuators. The mean of the last 50 samples before deactivating the applied power was computed to determine the maximum in both tests. This average reflects the system's steady state following the application of the step signal. Subsequently, from the 4 maximum values obtained, the mean and standard deviation of the maximum angular displacement, and temperature were calculated.

The results depicted in figure 7(a) sows the effect of the load on the TCPs fibres, stretching the fibres decreasing the initial starting point to −15, −27°, −33°, −37.5°, −40° and −42.5° respectively to the applied torque of 0.5 Nm, 1 Nm, 1.5 Nm, 2 Nm, 2.5 Nm, and 3 Nm. After removing this offset figure 7(b) illustrate that the maximum ROM was attained under a 1.0 Nm load. These findings align with the design objectives, as they are closest to the specified 1.5 Nm torque requirement, registering at around 1.4 Nm. The resulting angular displacement was of 25.1° ± 0.3°. The observed behaviour resembled that of the linear displacement of the TCP; as the load increased, displacement decreased, and elongation increased (indicated by a shift to a higher negative angle in the starting position). Conversely, when the load was too low (e.g. 0.5 Nm), the device experienced saturation. The relation between the input power and displacement can be seen as a linear relation. For example, the linear equation for the 1.0 Nm load will be equal to:

$$\alpha = 0.1916\,(\mathrm{mA}) - 20.397 \tag{6}$$

where α is the angular displacement in degrees, furthermore the R^2 if the linear equation is 0.9896 and a RMSE of 0.556.

The values for τ_h and τ_c ranged between 19 and 30 s (figure 7(c)). Additionally, the relationship between input power and temperature resembled that of the single fibre configuration, having its maximum temperature at 83.7 °C ± 0.2 °C when the 240 mA was applied (figure 7(d)).

2.7. SWRR model

After acquiring experimental data from the SWRR prototype, a computer model was developed by establishing a connection between ROM and input power. For this purpose, the 1.0 Nm load scenario was selected, as it closely approximated to the required torque of 1.5 Nm when the weight of the foot is taken into account and offered the most significant ROM (25°, sufficient for full dorsiflexion). The input signal comprised the applied power, while the output signal represented the resulting angular displacement. This dataset was then processed using the System Identification Toolbox in MATLAB. The Toolbox produced a power-angular displacement transfer function denoted as TFPD(s). The best model was as follows:

$$\mathrm{TFDP}\,(s) = \frac{0.01406s + 0.000249}{s^4 + 0.6203s^3 + 0.0327s^2 + 0.0003954}. \tag{7}$$

The model provides an accuracy of 92.83%.

3. Control strategy and results

Utilising the transfer function TFDP(s), a PID controller was tuned with the aid of the Control System Toolbox in MATLAB. Subsequently, a closed-loop system with the PID controller was simulated in MATLAB/Simulink. The simulation was focused on minimising potential issues such as overshoot, controller settling error, and power requirements, as any such errors could lead to the incorrect application of force to the user, potentially causing harm. To attain the desired maximum ROM of 10°, it took 5 s, corresponding to an inverse

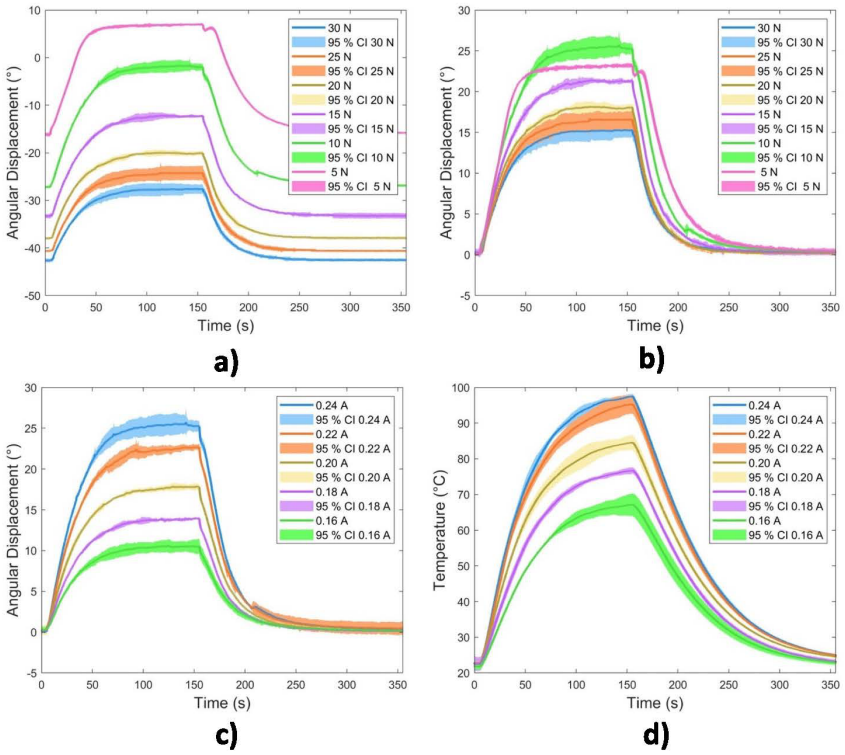

Figure 7. TCPs relations dummy test characteristics. (a) Angular displacement–torque relation when the maximum current of 240 mA is applied. (b) Angular displacement-power relation and (c) temperature-power relation when a torque of 1 Nm is applied. Confident intervals (CI) included.

of 0.2 Hz. The proportional, integral, and derivative components of the controller were configured as follows: $K\mathrm{p} = 17.14$, $K\mathrm{i} = 1.489$, $K\mathrm{d} = 33.84$.

After the closed-loop controller was tuned, it was implemented on an Arduino NANO microcontroller. A maximum power limit of 148 W was imposed, as determined by the capacity of the available power supply (60 V, 2.46 A). A pulse-width modulation strategy was employed to apply the requisite power. Three distinct tests were conducted: a step input test to evaluate the controller's performance, followed by a chirp test to assess the actuator's bandwidth. Lastly, an HRI was established using an electromyography (EMG) sensor MyoWare 1.0 (MyoWare) to capture muscle signals from the calf, demonstrating its potential as a control mechanism for the SWRR. Ag/AgCl electrodes were used, with bipolar electrodes situated on the belly of the tibialis anterior muscle and a reference electrode placed on the tibia. The EMG signal acquisition was performed with a 33 year-old male subject, using the same test bench employed for SWRR characterisation, now including the EMG sensor for the HRI test (as show in video S1).

3.1. Step signal

The reference signal for the step response was set at 10°, representing the ROM commonly observed during walking activities. In figure 8(a), the plot illustrates the position reference and the system's output when subjected to a step signal in the SWRR. The output closely tracks the reference signal; however, the system exhibits an overshoot response. It takes approximately 5 s to move from 0° to 10°. The power graph reveals that the controller initially requires the maximum available power of 148 W, which decreases to an average of 17 W (figure 8(b)).

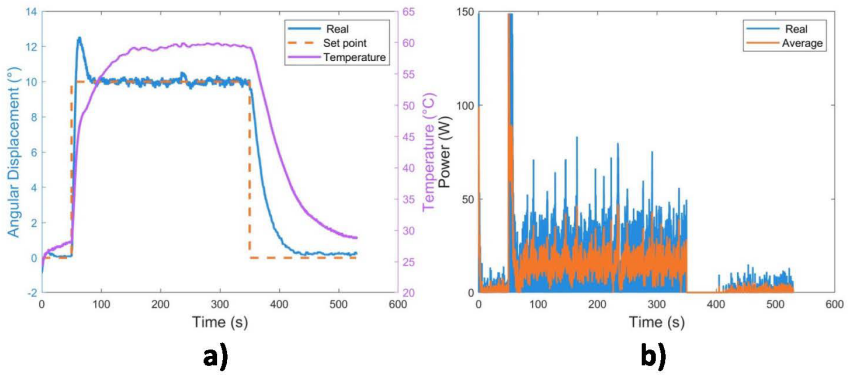

Figure 8. (a) Angular displacement and temperature of the SWRR after applying a step signal of 10° using a PID controller. (b) Power was applied to generate the 10° displacement.

Concerning temperature, it experiences a rapid rise initially but stabilises at 60 °C (figure 8(a)). Notably, the power and temperature values in the steady state closely resemble those observed during the open-loop test (with a step input of 180 mA).

3.2. Chirp signal

A chirp test was used to benchmark the working frequency of the whole system to understand its capabilities. A chirp signal consists of a sinusoidal sweep signal that varies its frequency over time, which can be expressed as follows:

$$\text{chirp}(t) = A\sin\left[2\pi\left(\frac{c}{2}t^2 + f_0 t\right)\right]. \tag{8}$$

Here f_0 is the final frequency, A is the amplitude of the sinewave, t is the time, and c is the chirp rate, described by:

$$c = \frac{f_e - f_0}{T_s} \tag{9}$$

where f_e is the final frequency, and T_s is the time it takes to sweep from f_0 to f_e.

The sinewave had an amplitude of 10°, aligning with the required displacement, covering from a baseline of 0° to 10°. The frequency range was from 0.001 Hz to 0.1 Hz (figure 9(a)). The cutoff frequency was identified when the magnitude decreased to −3 dB. During the test, the actuator reached the −3 dB threshold at a frequency of 0.025 Hz (figure 9(b)). Regarding temperature, the actuator maintained an average temperature of 53 °C, indicating that the TCP struggled to track the chirp signal precisely (figure 9(c)). The power response was distinct, as the system attempted to operate at that frequency by oscillating between maximum power and zero (figure 9(d)). To enhance response time without requiring an external cooling system, an offset of 10° was introduced on the ROM, operating within the 10°–20° range. With this adjustment, the working frequency improved to 0.034 Hz, which was 1.36 times faster. Nevertheless, it still fell short of the target of 0.2 Hz.

3.3. EMG HRI

The EMG signal was sampled at a frequency of 20 Hz, corresponding to the speed of the serial communication. Using the MyoWare 1.0 sensor, two types of signals were obtained: the EMG raw signal and the EMG envelope (EMGe) signal. The latter serves as an amplitude-modulated representation of the raw signal. To identify muscle activation, a threshold of 150 mV was set for the EMGe signal, preventing errors coming from movement artefacts. The activation pattern remained active for 8 s to achieve the 10° movement, followed by 90 s to allow the system to cool down and return to the starting position, following a similar approach to Pittaccio *et al* [36].

From the graphical representations, it is evident that the system is triggered when the EMG envelope surpasses the 150 mV threshold (figures 10(a) and (c)). This activation prompts the utilisation of the entire power output, which relaxes over 90 s (figure 10(b)). These observations confirm that the SWRR device responds effectively to the EMG signal.

4. Discussion and conclusion

This study explored the proof of concept for a SWRR system using TCP AMSM. The research included an actuator characterisation and the design process to meet biomechanical requirements. The resulting device is lightweight, flexible, and compact, meeting the minimum biomechanical needs of children with physical disabilities. This includes achieving a 10° ROM within 5 s, a torque of 1.5 Nm and an HRI. However, several improvements are needed before this technology can be applied in rehabilitation settings.

The study's results indicate that the behaviour of single fibres is similar to the multifibre approach integrated in the

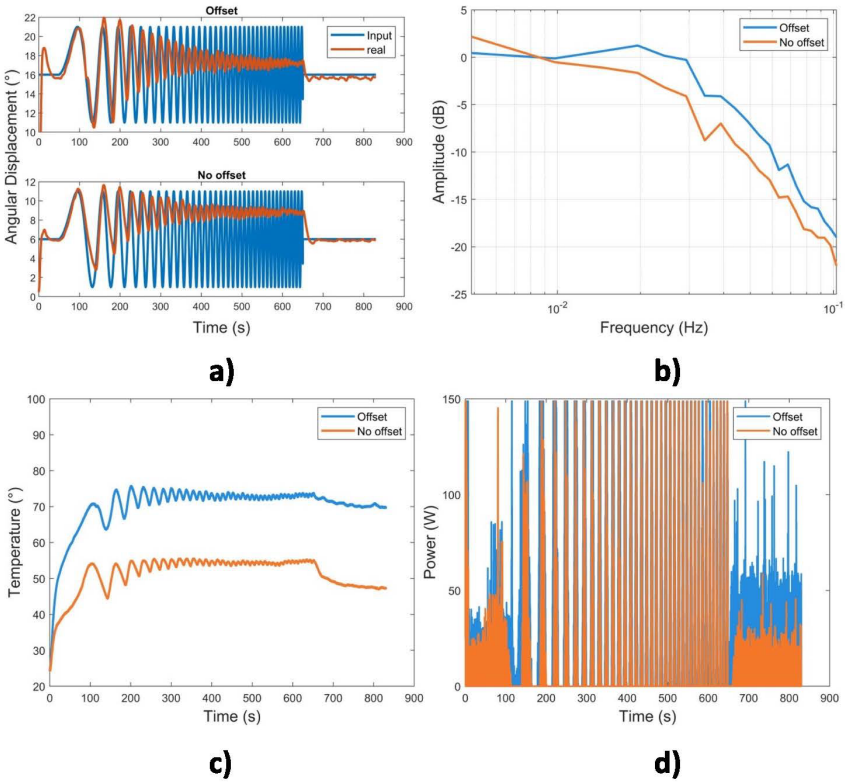

Figure 9. Chirp test results. (a) angular displacement of the SWRR following the chirp signal. (b) Magnitude decay in dB through frequency. (c) TCP temperature. (d) Power used by the SWRR.

SWRR. With differences in displacement and force as they translate into angular displacement and Torque. These differences are due to the mechanical design, and there's a trade-off between torque and displacement, as they are inversely proportional.

Despite the challenges, the technology appears highly adaptable, and many approaches can be taken to improve the performance. To enhance torque, incorporating additional fibres, as seen in previous TCP studies, is a viable direction [40, 41]. In this study, that approach was followed to get the required torque, as a single fibre would be insufficient to generate the necessary force.

Using longer actuators can significantly improve ROM, as this study shows. While the initial design requirement was a 10° ROM, the longer actuators enabled an impressive 25.18° ROM, effectively covering the full dorsiflexion range. This approach offers an additional advantage, as previously emphasised by Gonzalez *et al* [42], which is the reduction in temperature. This temperature control is vital for ensuring the device's safety during use. It is worth noting that the pain threshold for human skin at the dermal/epidermal layer is approximately 44 °C [27]. In this context, when considering the 10° ROM, the temperature was 65 °C lower compared to the temperatures reached when the actuator operated at its maximum stroke, which often exceeded 90 °C. Nonetheless, if the device is intended for use with children, the incorporation of an insulation layer, such as Polytetrafluoroethylene, is advisable to ensure optimal comfort and safety [43].

Nevertheless, coming from equations (2) and (5), the variation of r affect the linear displacement need to generate an angular displacement and the toque in an inverse manner. Is possible to improve this factor by tunning these distances, in the case of the study the r was chosen to be as small as possible because is the technology is envisioned to be used as a fabric that will be incorporated in clothes like socks.

The primary challenge associated with this technology pertains to its reaction time. However, this initial disadvantage could be solved by dividing this problem into two

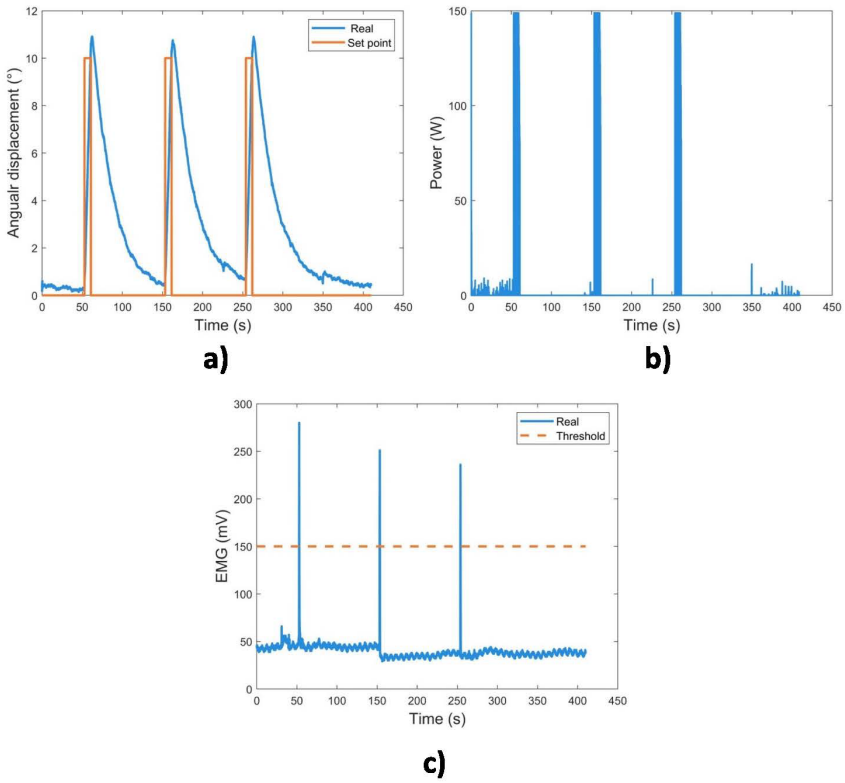

Figure 10. (a) Angular displacement generated after the EMG threshold was surpassed. (b) Power consumption of the SWRR during the EMG activation. (c) An EMG signal is used to trigger the SWRR.

distinct aspects due to the actuator's unidirectional nature, where applying power triggers contraction but cannot control elongation.

On one side, accelerating the contraction time necessitates increased applied power, leading to higher temperatures more quickly. The critical constraint lies in the need to carefully regulate this applied power to prevent heat-induced damage to the actuator. The research demonstrated that implementing the suggested control strategy allowed faster speeds without harming the actuator, preventing the fibre from overheating and burning [29]. Nevertheless, this approach demands substantial power levels to achieve rapid responses, often exceeding 100 Watts. This power requirement poses a challenge given the limitations of current battery technology. Nonetheless, advancements in energy storage and transmission are ongoing, promising improvements in energy density and battery miniaturisation [44–46].

On the other hand, addressing the relaxation phase poses a more complex challenge. This research sought to optimise the device's cooling process without external systems, relying on convective airflow. These optimisations involved creating sufficient spacing between each actuator to prevent heat transfer between individual fibres [40]. Regrettably, this consideration is counterproductive in the design as it limits the number of fibres used in the SWRR to produce higher torques.

Additionally, it was experimented with operating within an optimal temperature range, introducing an offset from the initial working point (from 0° to 10°) to achieve a faster movement previously investigated by Gonzalez *et al* [42]. This approach increased the frequency by 1.36 times. However, it did not significantly improve due to the actuator's considerably slower natural frequency than the required frequencies (0.02 Hz in TCP versus 1 Hz in walking activity).

Two potential alternatives come to light to address this issue. The first is incorporating a cooling system, as seen in numerous TCP research studies [47, 48]. The second option involves adopting agonist–antagonist muscle systems [43, 49]. However, it is important to note that these approaches entail

increased system complexity, requiring additional components that expand the system's size and weight. Furthermore, it necessitates more sophisticated control strategies to activate each component as needed.

Finally, another crucial facet of SWRR technology is the HCI. To demonstrate the device's feasibility, a straightforward EMG HCI was implemented, showcasing the technology's capabilities. This approach allowed system activation to be controlled based on the user's intent through muscle activation, a pivotal component of rehabilitation therapy that enhances user engagement. Looking ahead, it would be compelling to explore the incorporation of various wearable sensor technologies in conjunction with TCP technology to create SWRR devices that can seamlessly integrate into the daily lives of children. This advancement holds the promise of substantially improving their overall quality of life.

This study presents innovative components to design paediatric ankle SWRRs. These elements provide solutions to specific issues of traditional exoskeletons (weight and compliance) and can be translated to develop SWRR for different purposes. Nevertheless, as discussed, the technology still needs to be improved for its widespread adoption in rehabilitation settings. Additionally, it is essential to collaborate closely with human users to understand better and address any technology shortcomings.

Data availability statement

All data that support the findings of this study are included within the article (and any supplementary files).

Acknowledgments

This work was partially supported by 'Consejo Nacional de Ciencia y Tecnologia' of Mexico (No. 739850). A G V thanks Nick Van Der Geest for her help in the CAD design of the Braces.

Conflict of interest

The authors declare no conflict of interest.

Limitations

The current device was not tested on paediatric patients due to ethical limitations. Hence, the performance shown in the study could change when applied to paediatric patients.

In the case of the used metric from the biomechanical requirements, all the analysed metrics were the minimum requirements for all the attributes. However, it recognised the need for additional refinement before clinical use. This research is proof of concept of the technology aimed to explore its strengths and limitations, emphasising the ongoing work required for its potential widespread clinical implementation.

Ethics declaration

The authors declare that the research was compliant with the New Zealand code of ethics.

ORCID iDs

Alberto Gonzalez-Vazquez https://orcid.org/0000-0001-6514-7888
Lorenzo Garcia https://orcid.org/0000-0002-1122-497X

References

[1] Chen D, Huang M, Yin Y, Gui D, Gu Y, Zhuang T, Chen C and Huo K 2022 Risk factors of cerebral palsy in children: a systematic review and meta-analysis *Trans. Pediatr.* **11** 556
[2] Abgottspon S, Thaqi Q, Steiner L, Slavova N, Grunt S, Steinlin M and Everts R 2022 Effect of age at pediatric stroke on long-term cognitive outcome *Neurology* **98** e721–9
[3] Ryan J L, Zhou C, Levac D E, Fehlings D L, Beal D S, Hung R and Wright F V 2023 Gross motor change after inpatient rehabilitation for children with acquired brain injury: a 10-year retrospective review *Dev. Med. Child Neurol.* **65** 953–60
[4] Vandekerckhove I *et al* 2022 Longitudinal alterations in gait features in growing children with Duchenne muscular dystrophy *Front. Hum. Neurosci.* **16** 861136
[5] Scheijmans F E *et al* 2022 Population-based assessment of nusinersen efficacy in children with spinal muscular atrophy: a 3-year follow-up study *Brain Commun.* **4** fcac269
[6] Hall M L and Lobo M A 2018 Design and development of the first exoskeletal garment to enhance arm mobility for children with movement impairments *Assist. Technol.* **30** 251–8
[7] Gmelig Meyling C, Verschuren O, Rentinck I R, Engelbert R H and Gorter J W 2022 Physical rehabilitation interventions in children with acquired brain injury: a scoping review *Dev. Med. Child Neurol.* **64** 40–48
[8] Hawe R L, Kuczynski A M, Kirton A and Dukelow S P 2020 Assessment of bilateral motor skills and visuospatial attention in children with perinatal stroke using a robotic object hitting task *J. Neuroeng. Rehabil.* **17** 1–12
[9] Eguren D, Cestari M, Luu T P, Kilicarslan A, Steele A and Contreras-Vidal J L 2019 Design of a customizable, modular pediatric exoskeleton for rehabilitation and mobility *2019 IEEE Int. Conf. on Systems, Man and Cybernetics (SMC)* (IEEE) pp 2411–6
[10] Gonzalez-Vazquez A, Garcia L, Kilby J and McNair P 2023 Soft wearable rehabilitation robots with artificial muscles based on smart materials: a review *Adv. Intell. Syst.* **5** 2200159
[11] Gonzalez A, Garcia L, Kilby J and McNair P 2021 Robotic devices for paediatric rehabilitation: a review of design features *Biomed. Eng. Online* **20** 1–33
[12] Patane F, Rossi S, Del Sette F, Taborri J and Cappa P 2017 WAKE-Up exoskeleton to assist children with cerebral palsy: design and preliminary evaluation in level walking *IEEE Trans. Neural Syst. Rehabil. Eng.* **25** 906–16
[13] Rossi S, Colazza A, Petrarca M, Castelli E, Cappa P and Krebs H I 2013 Feasibility study of a wearable exoskeleton for children: is the gait altered by adding masses on lower limbs? *PLoS One* **8** e73139
[14] Lerner Z F, Gasparri G M, Bair M O, Lawson J L, Luque J, Harvey T A and Lerner A T 2018 An untethered ankle exoskeleton improves walking economy in a pilot study of

individuals with cerebral palsy *IEEE Trans. Neural Syst. Rehabil. Eng.* **26** 1985–93
[15] Rus D and Tolley M T 2015 Design, fabrication and control of soft robots *Nature* **521** 467–75
[16] Bahl S, Nagar H, Singh I and Sehgal S 2020 Smart materials types, properties and applications: a review *Mater. Today Proc.* **28** 1302–6
[17] Bengisu M and Ferrara M 2018 *Materials that Move: Smart Materials, Intelligent Design* (Springer)
[18] Nematollahi M, Baghbaderani K S, Amerinatanzi A, Zamanian H and Elahinia M 2019 Application of NiTi in assistive and rehabilitation devices: a review *Bioengineering* **6** 37
[19] Dong T-Y, Zhang X-L and Liu T 2018 Artificial muscles for wearable assistance and rehabilitation *Front. Inf. Technol. Electron. Eng.* **19** 1303–15
[20] Mirvakili S M and Hunter I W 2018 Artificial muscles: mechanisms, applications, and challenges *Adv. Mater.* **30** 1704407
[21] Shi B, Chen X, Yue Z, Yin S, Weng Q, Zhang X, Wang J and Wen W 2019 Wearable ankle robots in post-stroke rehabilitation of gait: a systematic review *Front. Neurorobot.* **13** 63
[22] Zhang J, Sheng J, O'Neill C T, Walsh C J, Wood R J, Ryu J-H, Desai J P and Yip M C 2019 Robotic artificial muscles: current progress and future perspectives *IEEE Trans. Robot.* **35** 761–81
[23] Veale A J and Xie S Q 2016 Towards compliant and wearable robotic orthoses: a review of current and emerging actuator technologies *Med. Eng. Phys.* **38** 317–25
[24] Behboodi A and Lee S 2019 Benchmarking of a commercially available stacked dielectric elastomer as an alternative actuator for rehabilitation robotic exoskeletons *2019 IEEE 16th Int. Conf. on Rehabilitation Robotics (ICORR)* (IEEE) pp 499–505
[25] Jani J M, Leary M, Subic A and Gibson M A 2014 A review of shape memory alloy research, applications and opportunities *Mater. Des.* **56** 1078–113
[26] Haines C S *et al* 2014 Artificial muscles from fishing line and sewing thread *Science* **343** 868–72
[27] Saharan L, de Andrade M J, Saleem W, Baughman R H and Tadesse Y 2017 iGrab: hand orthosis powered by twisted and coiled polymer muscles *Smart Mater. Struct.* **26** 105048
[28] Sutton L, Moein H, Rafiee A, Madden J D and Menon C 2016 Design of an assistive wrist orthosis using conductive nylon actuators *2016 6th IEEE Int. Conf. on Biomedical Robotics and Biomechatronics (Biorob)* (IEEE) pp 1074–9
[29] Patiño A G, Ferrone A, Gastélum C G D and Menon C 2018 A novel biomedical technology based on the use of artificial muscles to assist with hand functions *2018 IEEE 9th Annual Information Technology, Electronics and Mobile Communication Conf. (IEMCON)* (IEEE) pp 620–5
[30] Sarajchi M, Al-Hares M and Sirlantzis K 2021 Wearable lower-limb exoskeleton for children with cerebral palsy: a systematic review of mechanical design, actuation type, control strategy, and clinical evaluation *IEEE Trans. Neural Syst. Rehabil. Eng.* **29** 2695–720
[31] Chossat J B, Chen D K Y, Park Y L and Shull P B 2019 Soft wearable skin-stretch device for haptic feedback using twisted and coiled polymer actuators *IEEE Trans. Haptics* **24** 521–32
[32] Brockett C L and Chapman G J 2016 Biomechanics of the ankle *Orthop. Trauma* **30** 232–8
[33] Alvarez-Perez M G, Garcia-Murillo M A and Cervantes-Sanchez J J 2019 Robot-assisted ankle rehabilitation: a review *Disability Rehabil. Assist. Technol.* **15** 1–15
[34] Peng Q, Park H-S, Shah P, Wilson N, Ren Y, Wu Y-N, Liu J, Gaebler-Spira D J and Zhang L-Q 2011 Quantitative evaluations of ankle spasticity and stiffness in neurological disorders using manual spasticity evaluator *J. Rehabil. Res. Dev.* **48** 473
[35] Chung S G, Van Rey E, Bai Z, Roth E J and Zhang L-Q 2004 Biomechanic changes in passive properties of hemiplegic ankles with spastic hypertonia *Arch. Phys. Med. Rehabil.* **85** 1638–46
[36] Pittaccio S, Viscuso S, Rossini M, Magoni L, Pirovano S, Villa E, Besseghini S and Molteni F 2009 SHADE: a shape-memory-activated device promoting ankle dorsiflexion *J. Mater. Eng. Perform.* **18** 824–30
[37] Chen S-H *et al* 2016 Assistive control system for upper limb rehabilitation robot *IEEE Trans. Neural Syst. Rehabil. Eng.* **24** 1199–209
[38] Organization W H 2020 Growth reference 5–19 years (available at: www.who.int/growthref/en/)
[39] Winter D A 2009 *Biomechanics and Motor Control of Human Movement* (Wiley)
[40] Haines C S and Niemeyer G Closed-loop temperature control of nylon artificial muscles 2018 *2018 IEEE/RSJ Int. Conf. on Intelligent Robots and Systems (IROS)* (IEEE) pp 6980–5
[41] Murphy V, Edmonds B P and Trejos A L 2021 Characterisation and control of a woven biomimetic actuator for wearable neurorehabilitative devices *Actuators* **10** 37
[42] Gonzalez A, Garcia L and Kilby J 2023 Improved performance in temperature and speed of TCP artificial muscles for soft wearables robots by length modification *Smart Mater. Struct.* **32** 085002
[43] Copaci D, Martín F, Moreno L and Blanco D 2019 SMA based elbow exoskeleton for rehabilitation therapy and patient evaluation *IEEE Access* **7** 31473–84
[44] Subasinghage K, Gunawardane N, Kularatna N and Moradian M 2022 Modern supercapacitors technologies and their applicability in mature electrical engineering applications *Energies* **15** 7752
[45] Ma L *et al* 2019 Achieving both high voltage and high capacity in aqueous zinc-ion battery for record high energy density *Adv. Funct. Mater.* **29** 1906142
[46] Liu Q, Zhang G, Chen N, Feng X, Wang C, Wang J, Jin X and Qu L 2020 The first flexible dual-ion microbattery demonstrates superior capacity and ultrahigh energy density: small and powerful *Adv. Funct. Mater.* **30** 2002086
[47] Edmonds B P and Trejos A L 2019 Design of an active cooling system for thermally activated soft actuators *2019 IEEE 16th Int. Conf. on Rehabilitation Robotics (ICORR)* (IEEE) pp 368–73
[48] Yip M C and Niemeyer G 2017 On the control and properties of supercoiled polymer artificial muscles *IEEE Trans. Robot.* **33** 689–99
[49] Park S J, Choi K, Rodrigue H and Park C H 2022 Fabric muscle with a cooling acceleration structure for upper limb assistance soft exosuits *Sci. Rep.* **12** 1–13

Appendix B: Supplementary Information

Supplementary information (Calibration procedures) for:

Paediatric Ankle Rehabilitation System based on twisted and coiled polymer actuators.

Authors: Alberto Gonzalez-Vazquez[1], Lorenzo Garcia[1*], Jeff Kilby[1].

1 School of Engineering, Computer and Mathematical Sciences, Auckland University of Technology, Auckland, New Zealand.
*Corresponding Author lorenzo.garcia@aut.ac.nz

Sensor Calibration Procedures:

The following supplementary material document contains the calibration procedure for the sensors use in "Paediatric Ankle Rehabilitation System based on twisted and coiled polymer actuators."

10 Kg Load Cell (TAL220).

The TAL220 load Cell have a capacity of 10 KG. The load cell was interface to an Arduino through an analogue-to-digital converter (Avia semiconductor, HX711). To calibrate the load cell measurement of 3 different weights were taken (0 grams, 500 grams and 1000 grams). Each measurement was taken 5 times and then averaged. With these 3 points as the TAL220 present a linear behaviour in the relation voltage to weight it was possible to obtain the following equation:

$$Weight = 0.0047 * voltage + 557.62$$

Laser Displacement Sensor (Sick OD mini OD1-B100C50I14)

The Sick OD mini OD1-B100C50I14 have a range of 50 mm to 150 mm with a linearity of $\pm 100\mu m$. The sensor was interface with an Arduino using a current sensor (Texas Instruments INA269). The process to calibrate the displacement senor was using a 3d printed structure with a stair shape to have different levels with different distances. The height of each step was 6 mm. The structure had 3 different steps. Measuring each of the steps 5 times and then averaged a relation between current and distance was obtained:

$$Distance = 5.3066 * current\_mA - 22.327$$

Temperature Sensor NTC thermistor (TE Connectivity, 5K3A1)

The NTC thermistor 5K3A1 is a analogue temperature sensor. Its resistance change as the temperature change. The thermistor was put in a voltage divider arrange with a resistance of 1 KΩ. With this arrangement is possible to obtain the resistance value with the following equation:

$$RThermistor = 1000 * (1023.0 / Voltage - 1.0)$$

Using the values provide by the datasheet relating resistance to temperature a logarithmic equation was fit:

$$Temperature_{Thermistor} = -29.12 * \log(RThermistor) + 269.81;$$

Finally, the sensor data was compared to a reference thermometer Fluke 1523. 3 different measures steady state temperatures were taken, temperature inside a fridge, ambient temperature and boiling water. After comparing the temperatures, the data from the thermistor was fit to the temperature of the reference thermometer using the following relation:

$$Temperature_{calibrated} = Temperature_{Thermistor} * 0.7827 + 7.5701$$

Digital Calliper Duratool

The calibration of the Duratool Digital Calliper was perform measuring a 2 mm Mitotuyo gage block. 20 measurements were taken with an accuracy of 0.001 mm.

Inertial Measurement Unit (LSM9DS1)

Gyroscope

The gyroscope inside the LSM9DS1, was calibrating by removing the bias out of the readings. To remove the bias the sensor was left in a static position for 5 seconds. The 3 different axes (x,y,z) reads are taken at the same time. Then all the readings were average to obtain an average and it was subtracted from the readings.

Magnetometer

The magnetometer was calibrated following the tutorial from Adafruit (https://learn.adafruit.com/how-to-fuse-motion-sensor-data-into-ahrs-orientation-euler-quaternions/magnetic-calibration-with-motioncal).